Anglia Ruskin University

AN INVESTIGATION INTO THE ANALYSIS OF INNOVATIVE SLIT REINFORCED CONCRETE SHAFTS DESIGN IN ELEVATED WATER TANKS IN SEISMIC REGIONS

FILIP GURKALO

A Thesis in partial fulfilment of the requirements of Anglia Ruskin University for the degree of a Doctor of Philosophy

Submitted: January 2015

ANGLIA RUSKIN UNIVERSITY
ABSTRACT

FACULTY OF SCIENCE & TECHNOLOGY

DOCTOR OF PHILOSOPHY

AN INVESTIGATION INTO THE ANALYSIS OF INNOVATIVE SLIT REINFORCED CONCRETE SHAFTS DESIGN IN ELEVATED WATER TANKS IN SEISMIC REGIONS

FILIP GURKALO

January 2016

Elevated water tanks are used within water distribution facilities in order to provide storage and necessary pressure in water network systems. During the occurrence of a severe seismic event, the failure or severe damages in the reinforced concrete shaft could result in the total collapse of the structure.
In a reinforced concrete shaft, plastic hinge formation only occurs at the base of the shaft and nonlinear resources of the rest of the shaft remains unexploited. This research presents an innovative technique for the assembly of shafts for elevated water tanks, using the slits in the reinforced concrete shaft design, which reduces the stress concentration at the shaft base and distributes stresses uniformly along the height of the shaft.
The main aim of this study was to investigate the nonlinear seismic performance of the innovative RC slit shaft of the elevated water tanks by means of a finite element approach. The capacity spectrum and time history analyses were carried out to understand the nonlinear behaviour of the proposed support system.
The results revealed that the slit width in the reinforced concrete shaft directly affected the failure mode and stiffness of the elevated water tanks. It was concluded that, with an appropriate design, the conversion of a solid shaft into a slit shaft can significantly increase the ductility of a reinforced concrete shaft, but there would be a slight reduction in the lateral strength. Furthermore, the results revealed that crack propagation was more uniform along the height of the slit shafts in comparison to the solid shaft and the ductility of the shafts increases as the slits become wider. Conclusively, this study showed that introducing the slits in the shaft could result in a significant reduction in the seismic response values of the elevated water tank, resulting in an economical design of the shaft structure and the foundation system.

Key words: Elevated RC water tank, nonlinear, SAP2000, finite element analysis, seismic, earthquake, dynamic, modal, pushover, time-history, capacity spectrum

Acknowledgments

I would like to express my sincerest gratitude to a number of individuals who have provided me with support and help throughout writing this thesis.

First and foremost, my sincere gratitude to my supervision team, my former 1st supervisor and current advisor Dr Konstantinos Poutos, my 1st supervisor Dr Carlos Jimenez-Bescos, my 2nd supervisor Dr Yingang Du and my 3rd supervisor Dr Sunny Nwaubani who guided me throughout my thesis with their patience and knowledge. Above all and the most needed, they provided me encouragement and support in various ways. Working under their supervision has been a great opportunity in my life and I would like to show my greatest appreciation to them.

In my daily work I have been blessed with a friendly group of colleagues in the department of engineering and the built environment at Anglia Ruskin University. I offer my regards to all of them for supporting me in any respect during the completion of the project.

The financial support from Anglia Ruskin University in the form of a scholarship is greatly appreciated.

Last but not the least, my deepest gratitude goes to my parents and all relatives, for giving me unconditional love and support throughout my life.

Table of Contents

List of Figures

List of Tables

List of Appendices

List of Abbreviations

FE	Finite element
FEA	Finite element analysis
FEM	Finite element method
FSI	Fluid structure interaction
MDOF	Multy degree of freedom
RC	Reinforced concrete
SDOF	Single degree of freedom

Copyright

Chapter 1

Introduction

1.1 Overview

There are a large number of storage tanks around the world most of which are used as water storage facilities. These structures play an imperative role in municipal water supply and firefighting systems. Elevated water tanks are water storage facilities, which are installed on a supporting staging to provide necessary pressure for the water distribution system obtained by gravity instead of the implementation of a heavy pumping facility.

There are numerous elevated water tanks that are considered as indispensable facilities and are expected to be functional after the occurrence of a severe earthquake. Elevated water tanks rely on hydrostatic pressure produced by the elevation of water, hence are able to supply water even during power outages. This feature of elevated water tanks becomes more critical when a power outage occurs after a severe earthquake; therefore pumping systems are inoperable due to the dependency on electrical power.

Overall, the supporting structure of the elevated water tanks can be classified as reinforced concrete frame, steel frame, masonry shaft or a reinforced concrete shaft. In this thesis, the term “Elevated Water Tank” only refers to the last group, which is the tank, mounted on the reinforced concrete shaft and will be the subject of this research.

The elevated water tank, supported by the reinforced concrete (RC) shaft, commonly has two main configurations. The first type being the “Elevated Concrete Tank” (Figure 1.1.), where both the shaft and tank are constructed from reinforced concrete. However, the second type “Elevated Composite Steel-Concrete Tank” or simply a “composite elevated tank”, consists of a RC shaft and welded steel tank. The welded steel tank is mounted on top of the RC shaft. The lower section of the tank is cone shaped, whereas the upper part is cylindrical.

The features of the concrete elevated tanks such as size, dimensions and geometry are commonly referred to in this study, yet all the research results are also applicable

to the composite elevated tanks as well. However, this study has only focused on the RC shaft seismic response behaviour, which has similar properties for both types of elevated water tanks.

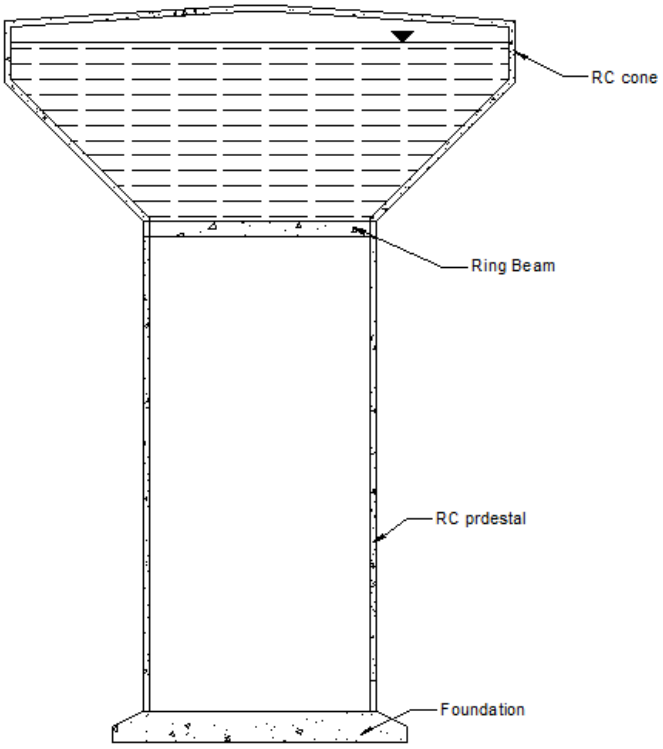

Figure 1.1. Configuration of concrete elevated water tank

Elevated water tanks are considered to be vital lifeline elements and are expected to remain functional after severe ground motions to serve, as a provider of potable water, as well as firefighting operations. The failure or malfunction of this essential infrastructure disrupts the emergency response and recovery after an earthquake has occurred.

However, elevated water tanks in the past have not performed up to expectations during earthquakes. The poor performance of these structures in many earthquakes have been documented in literature such as; Jabalpur 1997 (Rai, 2002), Chile 1960 (Steinbrugge, 1960), Bhuj 2001 (Rai, 2002) and Manjil Roudbar 1990 (Memari and Ahmadi, 1990). The extent of the damages range from minor cracks in the shaft up to complete collapse of the entire structure.

There are many grounds that could explain the undesirable performance of the structures. The configuration of these structures, resembles an inverse pendulum,

lack of redundancy, very heavy gravity load (compared to conventional structures) and poor construction detailing are among the major contributors.

There have been numerous studies carried out, regarding fluid-structure interaction and improvement of performance of water tanks. However, minimal study has been conducted on the investigation and improvement of the reinforced concrete shafts.

Unlike the majority of other structures that may have uniform load distribution during their lifetime, elevated water tanks experience significantly different gravity loads whilst working in the water system. When the tank is empty, the overall weight of the structure may drop to 25% of the full tank state (Ghatel, 2006). This change in the gravity load adds complexity to the seismic design of elevated water tanks. Furthermore, elevated water tanks do not have any load redistribution path that results in a lack of redundancy. During strong seismic event, even if the tank last without damages, heavy damages in the RC shaft could result in a total failure of the structure. During recent earthquakes a number of elevated water tanks have either collapsed or become non-functional as a result of the damages to the shaft due to low redundancy and poor ductility in thin reinforced concrete shafts.

The total energy transferred to the structure can be dissipated by two ways, damping energy and hysteretic energy. The only amount of dissipated energy due to the inelastic deformation is considered to damage the structure subjected to an earthquake. According to this criteria, collapse of a structure can be explained as a lack of ability to dissipate hysteretic energy through inelastic deformation (Terapathana, 2012). Furthermore, hysteretic energy is used as a design parameter among many researchers, Akiyama (1985), Leelataviwat, et al. (1999) and Estes (2003), for energy design. In RC structures, hysteretic energy is appropriate parameter due to the representing cumulative nonlinear responses such as cracking and plastic hinging of the ductile members.

Monolithic elevated water tanks have relatively high strength and stiffness, however they do not show ductile behaviour. Ductile behaviour in the RC shafts occurs by yielding of the flexural reinforcement at the shaft base through forming of plastic hinges (Rai, 2002).

In case of high intensity earthquakes, flexible support systems are preferred as they can receive large deformations. On the other hand, for low intensity earthquakes that

occur frequently, or for wind action; solid shafts should be considered, for the reason that they prevent large displacements.

Increasing a fundamental period far beyond the predominant period of the input motion can reduce the seismic response of the elevated tank model. This can be achieved by providing a soft slice within the shaft structure itself to produce some ductility and extend its fundamental period. In other words, the earthquake response of the structure can be reduced by providing a more flexible structural design, which can be developed by making changes in the configuration of the shaft.

The dissipation of the hysteric energy in the RC shaft elevated water tank is similar to shear wall system that generally occurs through the concentrated plastic hinge formation at the lower part of the wall, which is difficult to repair and ductility resources of the rest of the wall remains unexploited as shown in Figure 1.2(a).

Numerous investigations have been conducted to improve the ductility of shear walls subjected to seismic loads and some practical solutions were proposed. The researches aim was to reduce the energy concentration from the base of the wall and distribute it along whole height of the wall. In the early 1970s, an improved type of the shear wall called the slit shear wall was proposed by Muto (1973) to improve the shear wall performance against lateral forces. The slit wall showed the increase of the ductility and seismic energy dissipation due to slits and connectors between parts of the wall (Figure 1.2(b)). Further studies of other researches revealed an increase in the ductility and decrease in the stiffness within the slit shear walls in comparison to normal shear walls (Kwan, et al., 1999; Lu, et al., 2000; Jiang, et al., 2003).

However, no published research work has been identified that applies properties of slit walls to RC shafts in elevated water tanks. In the light of unpublished research findings it appears that the slit shaft provides an opportunity for a unique and original research study on the structural response of water tanks under seismic loading. The use of slits in RC shaft design could greatly improve the performance of RC shafts under seismic loading and the earthquake resistance of the elevated RC water tank.

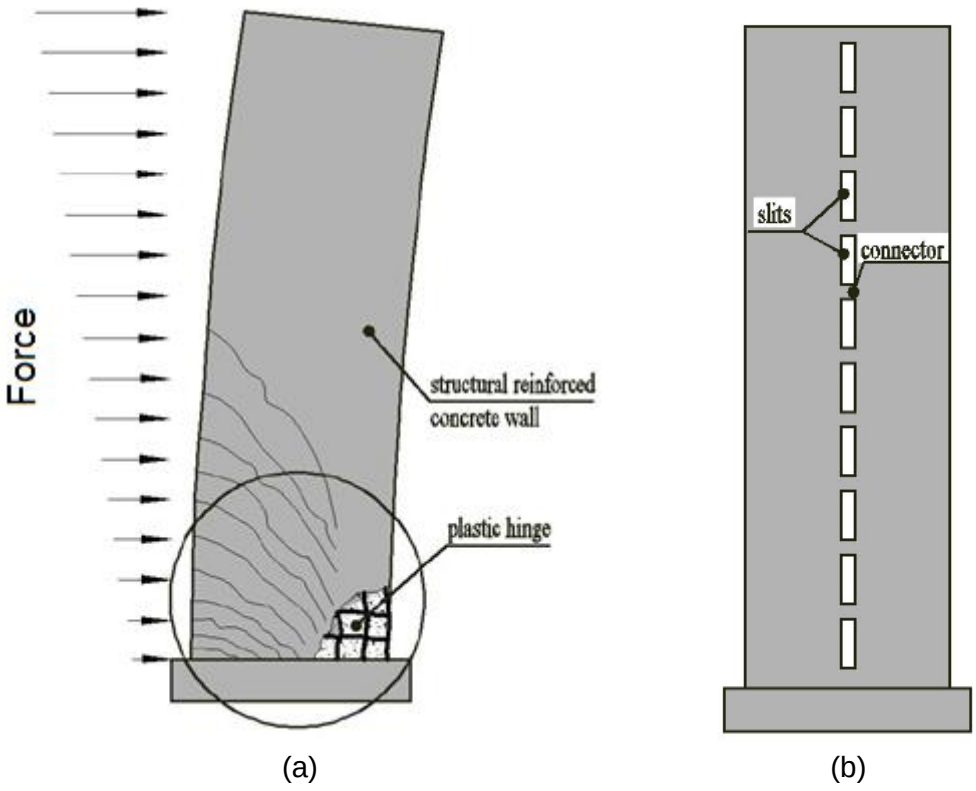

Figure 1.2. (a) Destruction of reinforced concrete walls at horizontal seismic action, (b) Reinforced concrete slit wall with shear connections (Baetu, 2011)

1.2 Gap in knowledge

This research presents an innovative system of assembling RC shafts for elevated water tanks using a slit wall technique (Figure 1.3). In this study, the researcher attempted to reduce the stress concentration at the shaft base and uniform distribute the stresses along the shaft height, which may lead to a decreased demand ductility capacity at the base. Therefore detailed analytical research study of the seismic response of the proposed slit shafts was undertaken to fill the gap in knowledge. This study aims to overcome the gap in knowledge and investigate various aspects of nonlinear response behaviour of proposed RC slit shafts by employing a finite element approach.

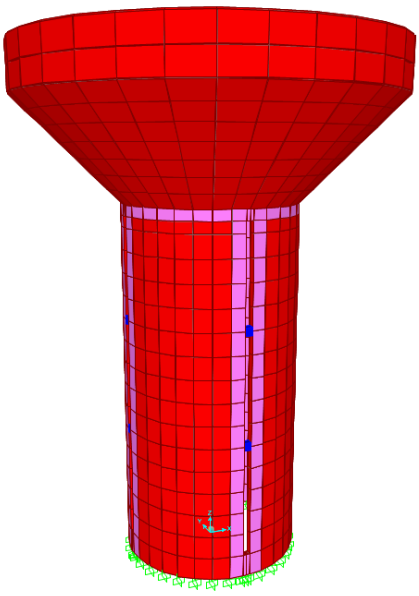

Figure 1.3. Reinforced concrete slit shaft elevated water tank

1.3 Research aim and objectives

The main aim of this study was to investigate the nonlinear seismic performance of the innovative RC slit shaft of the elevated water tanks by means of a finite element approach and compare results with those obtained from conventional RC solid shaft elevated water tanks.

Different types of analyses including modal, pushover, capacity spectrum and time history were performed using the general-purpose finite element software SAP2000. Through this research, a detailed parametric study was carried out on elevated water tanks. The slit width was assumed a main parameter used for the study.

In the study both static and dynamic methods were employed. In the first part, investigation of the dynamic behaviour of proposed elevated water tank models was conducted by modal analysis and fundamental periods of the models werefound.

In the second part of the research study, seismic performance of the proposed elevated water tanks was determined by spectrum capacity method. This method included both pushover analysis and response spectrums designed according to Eurocode 8. In addition, the effects of slit width on the nonlinear behaviour were studied and crack propagation in RC shafts were observed.

In the third part, the time history method was employed in order to determine a dynamic nonlinear response in the slit shaft elevated water tanks and validate the capacity spectrum method.

In summary, the main objectives of this research are as follows:

1) Perform a comprehensive literature review on the seismic response behaviour of elevated water tanks as well as the slit shear walls.
2) Develop finite element models of the RC solid shaft and slit shaft elevated water tanks that are capable of predicting the nonlinear response of reinforced concrete elements and corroborate them by comparing it to the studies reported in literature.
3) Investigate the dynamic behaviour of the proposed slit shaft elevated water tanks by conducted modal analysis.
4) Investigate the nonlinear response behaviour of proposed water tank models by capacity spectrum analysis and investigate stresses propagation patterns in RC slit shafts in order to determine stress localisation zones.
5) Investigate the nonlinear dynamic response behaviour of proposed water tank models by nonlinear time history analysis and compare the obtained results to pushover analysis results.
6) Determine the most efficient slit width for reinforced concrete elevated water tanks.

1.4 Thesis layout

This thesis consists of nine chapters. The first chapter includes the introduction, gap in knowledge, the scope, objectives and the outline of the thesis.

Chapter 2 presents a comprehensive literature review on seismic response of elevated water tanks. The performance of elevated water tanks during past earthquakes and previous research studies on seismic response of elevated water tanks and fluid-structure interaction were discussed within this chapter. In addition, a literature review on slit shear walls as well as an introduction to current codes and guidelines related to design and analysis of elevated water tanks is included.

Chapter 3 possesses the seismic analysis methods employed in this thesis for studying nonlinear static and dynamic response behaviour of RC shafts. The general equations and formulation for each analysis method was briefly reviewed in this

chapter. Response spectrum development, nonlinear static analysis, sources of nonlinearity in the structure's response and equations of transient dynamic analysis as well as modal analysis and Rayleigh damping were covered in this chapter. Finally, water modelling according to Eurocode 8 was discussed in this chapter.

Chapter 4 defines and verifies a finite element technique for modelling RC shafts. Mathematical models for constructing stress-strain curves of concrete and steel material were briefly described within this chapter. The chapter concludes with corroborating the proposed finite element model by comparing the finite element model to analytical results presented in the literature and design of finite element models.

In Chapter 5, the dynamic behaviour of the proposed elevated water tanks were investigated in a three-dimensional space by performing modal analysis. Impulsive and convective fundamental modes of proposed models were studied. The modal energy dissipation of proposed models was compared.

The seismic performance of elevated water tanks was investigated by performing pushover analysis in Chapter 6. The chapter continues with the evaluation of seismic performance by the capacity spectrum method for soil types A, B, C and D from EC-8. Finally performance of the models with slit shaft and solid shaft was compared. The chapter ends with analysing and determining the stress propagation patterns in the proposed slit RC shafts under lateral seismic loads and localisation of the compression stresses in slit shaft elevated water tanks.

Chapter 7 evaluates and verifies the capacity spectrum method by performing nonlinear time history analysis. Furthermore, the results of the nonlinear time history analysis of RC shafts, such as deformation, base shear and base moment versus time were presented and discussed in this chapter along with hysterics loops of models. Stress propagation patterns and stress localisation zones in the proposed RC shafts were determined and compared to pushover analysis results. The chapter continues with an investigation of the influence of earthquake intensity on the base compression stress localisation. In addition, the effect of various parameters such as water tank capacity and shaft dimensions are investigated on the dynamic response of proposed slit shaft elevated water tanks.

Finally, Chapter 8 and 9 provides a summary and conclusion of the study. The chapter also presents a number of recommendations for further studies and future works

Chapter 2

Literature Review

In this chapter an extensive literature review on dynamic response of liquid containing structures is presented. In Section 2.1 seismic performance of elevated water tanks under earthquake excitations is discussed. Section 2.2 reviews and summarises the available literature on seismic response of liquid storage tanks. The significant contributions made by previous researchers are also explained. Section 2.3 reviews the available literature on fluid structure interaction (FSI). The chapter continue with Section 2.4 that provides a literature review on slit shear walls. Finally, an overview on existing codes, standards, and guides used in design of liquid storage tanks provided in Section 2.5.

2.1 Earthquake damage to elevated water tanks

There are a number of reports that show inefficient and occasionally catastrophic seismic performance of elevated water tanks due to previous earthquakes in the literature. The damages were reported from minor cracks in RC shafts to severe damages and complete failure of elevated water tanks.

Severe damage levels and failures were observed in elevated water tanks during strong seismic events such as 1960 Chile (Steinbrugge and Cloough, 1960),1990 Manjil-Roudbar (Memari and Ahmadi, 1990), 1997 Jabalpur (Rai, D. et al, 2002), and 2001 Bhuj (Rai, D., 2002 and Dutta et al. (2009)) earthquakes. That is not acceptable because elevated water tanks should be designed to withstand strong earthquakes remaining functional in order to provide potable water and also supply water demand for possible firefighting operations.

During 1990 Manjil-Roudbar earthquake, a 1500 m^3 RC elevated water tank two-third full at the time of the earthqauek collapsed (Mehrain, 1990). The tank was 46 m height. The structure a RC shaft 6 m diameter, 25.5 m height and 0.3 m wall thickness. Figure 2.1 shows the remaining of this collapsed elevated water tank. The water distribution was disturbed for many weeks after the failure of this structure.

Figure 2.1 Collapsed 1500 m^3 elevated water tank in Manjil-Roudbar earthquake (Mehrain, 1990)

Another RC elevated water tank damaged in 1990 earthquake between the towns Rudbar and Majiil in Iran presented in Figure 2.2. The elevated water tank was 50m height with tank capacity of 2500m^3, shaft height – 25m, internal diameter – 7m and wall thickness – 0.5m. The tank was empty at the time of earthquake. The main damages, such as tension-flexural cracks were observed around openings in the RC shaft (Memari and Ahmadi, 1990).

In the 1997 Jabalpur earthquake, two concrete elevated water tanks supported on 20 meters tall shafts developed cracks near the base (Rai, 2002). The Gulaotal elevated water tank was full during the earthquake and suffered severe damages. This tank developed flexural-tension cracks along half its perimeter, as shown in Figure 2.3. The flexure-tension cracks in shafts appeared at the level of the first lift and a plane of weakness, at 1.4 m above the ground level.

Rai (2002) reported that numerous of RC elevated water tanks received severe damages at their RC shafts during the 2001 Bhuj earthquake. For most damaged water tanks, the tension – flexure cracks in shafts were observed up to one third the height of the shaft, as shown in Figure 2.4(a). These cracks were parallel to the ground and covered the entire perimeter of the shaft. The shaft heights were ranging from 10 to 20 meters and the wall thickness varied between 150mm to 200mm. Moreover, it has been reported that at least three of elevated water tanks collapsed. Figure 2.4(b) showed the collapsed 265kL water tank in Chobari village about 20km from the epicentre. The tank was approximately half full during the earthquake.

Figure 2.2. Damaged the 2500 m^3 water tank in Manjil-Roudbar earthquake (Mehrain, 1990);

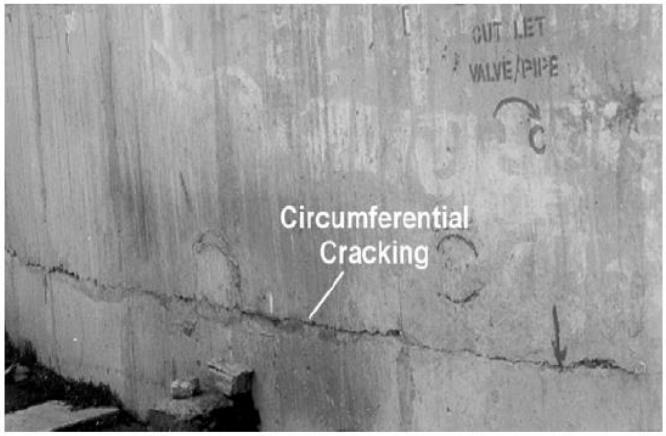

Figure 2.3 Horizontal flexural-tension cracking near the base of Gulaotal water tank damaged in 1997 Jabalpur earthquake (Rai, 2002)

(a) (b)

Figure 2.4 (a) Damaged 200 kL Bhachau water tank developed tension-flexural cracks in 2001 Bhuj 2001 earthquake (b) Collapsed 265 m3 water tank in 2001 Bhuj earthquake (Rai, 2004)

Failure of elevated water tanks depends on different parameters such as construction material, tank configuration, tank type, and supporting mechanism. Reported damage to elevated concrete water tanks during past earthquakes can be categorised as (Aware and Mathada, 2015):

1) Deformation, cracks and leakage in side shell
2) Failure of piping and other accessories connected to the tank because of the relative movement of the flexible shell
3) Damage to the supporting structure in elevated water tanks
4) Damage to the foundation system
5) Failure of supporting soil due to over-stressing

Elevated water tanks are very vulnerable to seismic excitations because of the concentrated large mass located at top of the shaft structure. As a result, strong lateral seismic motions may result in large tensile stresses on one side of the concrete shaft section which may eventually lead to severe cracking or even collapse of the concrete shaft. As mentioned before, many elevated tanks collapsed during the 1960 Chilean, 1997 Jabalpur and 2001 Bhuj earthquakes since insufficient reinforcement was provided in the shaft section.

2.2 Previous research on response of elevated water tanks

The number of research studies that investigated the seismic response of RC shafts of elevated water tanks is very limited. Although widespread research work on seismic response of liquid storage tanks began in 1960s, only a few research studies could be found that have analysed the seismic behaviour of the RC support systems individually.

Housner (1963) performed the first research to evaluate the seismic response behaviour of both ground and elevated water tanks subjected to lateral seismic loads. In this study, Housner proposed a useful idealisation for obtaining liquid dynamic response inside the tanks which has still being widely used in engineering practice. Many current codes and guidelines such as Eurocode 8 have adapted the original Housner's method only by applying a few adjustments.

According to Housner's proposed method the hydrodynamic response was separated into "impulsive" component, in which the liquid was assumed to be rigidly attached to the tank and moved in unison with the tank shell, and "convective" component, which was characterised by long-period oscillations and involved vertical displacement of the fluid free surface. The convective mode of vibration was assumed to be attached to the tank wall by springs with specific stiffness. Housner proposed that the impulsive and convective components were modelled using lumped masses. For the elevated water tank (Figure 2.4(a)), the impulsive mass (M_0) represented equivalents mass of a structure and impulsive mass of a water and the convective mass (M_C) represented convective mass. However, for the ground supported water tank (Figure 2.4(b)) the impulsive mass (M_I) and convective mass (M_C) were used. The Housner's method allowed engineers to carry out the seismic response analysis of elevated tanks using a two-mass idealisation.

Sonobe (1969) used a Housner's idealisation of two mass model in seismic analysis of elevated tanks. In this study, two models were investigated. The first model was a cylindrical tank model supported by a frame which had several levels of rigidity. The second model was a spherical tank of the same size. Free vibration and stationary vibration tests were conducted. Additionally, a vibration test under the input of pseudo 1940 El-Centro record was carried out on the cylindrical elevated tank model. Maximum displacement of the frame and maximum sloshing height of the stored water was measured and compared. Experimental results were in good agreement with

those obtained from the analytical solution using a simplified two mass system. In creating this equivalent model, the weight of the frame and dead water was assumed to be rigidly fastened to the tank, while the weight of free water was assumed to be attached to the tank by means of springs.

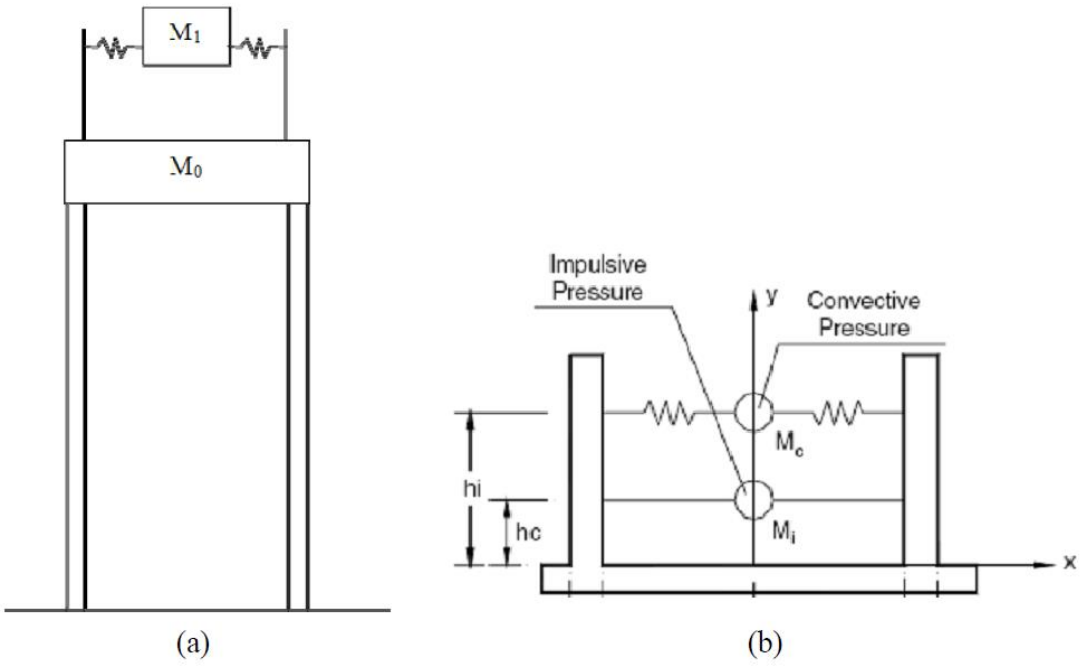

Figure 2.5 Equivalent dynamic system of liquid tanks (a) elevated water tank (b) Ground supported tank (Housner, 1964)

Shepherd (1972) also used the two mass system to represent the dynamic behaviour of elevated water tanks. The validity of the model was verified by comparing the analytical values with those of a simple dynamic test conducted on the RC elevated water tank. The equivalent water masses, the heights of attached masses, and the spring stiffness were calculated using Housner's formulation. The sloshing frequency of the water inside the tank was determined by hand shaking tests. The results of the study showed that the use of the two mass equivalent model would provide acceptable assessments of the fundamental frequencies of the elevated water tanks.

Haroun and Ellaithy (1985) presented an equivalent mechanical model for evaluating the dynamic response of elevated water tanks. Two types of staging were analysed, namely cross braced frame a RC shaft. The effect of tank wall flexibility and both rocking and translational motions of vessel were included in the study. Analyses indicated that the rocking component of vessel could have a significant effect on maximum shear and moment exerted at the top of the tank.

Vandepitte, et al. (1982) conducted an experimental research study on the stability of elevated conical tanks under hydrostatic loading. In this study, a finite element model capable to include both geometric and material nonlinearities for stability analysis of liquid-filled conical elevated tanks under hydrostatic loading was proposed. The effect of geometric imperfections on the stability of such structures was examined.

Memari and Ahmadi (1992) investigated the behaviour of two concrete elevated water tanks damaged in the 1990 Manjil-Roudbar earthquake. Finite element models of both structures were developed. The design load by standards and actual loads were compared and concluded that the current standard design loads were much higher than design loads in standards of the construction time. It was also concluded that the sloshing and P-Δ had a minor effect in concrete elevated tanks. The single degree of freedom model was also known to be inadequate in modelling elevated concrete water tanks and predominant mode of failure was indicated to be flexural.

El Damatty, et al. (1997B; 1997C) studied seismic behaviour of elevated conical steel tanks. In the study, a numerical FE model was developed using shell elements and the fluid was modelled using the coupled boundary-shell element technique. Only the impulsive component of the hydrodynamic pressure was considered. Tank models were classified as tall or broad according to their aspect ratio (the ratio of the tank radius to its height). The supporting structure was modelled as a linear spring. The effects of both material and geometric nonlinearities were included in the model. Modal and nonlinear time history analyses were carried out. It was concluded that elevated conical tanks, especially the tall tanks, were very sensitive to seismic excitations. The results also showed that the vertical ground motion contributes significantly to the dynamic instability of conical elevated tanks.

Joshi (2000) proposed an equivalent mechanical model for seismic analysis of rigid intze type tanks under horizontal seismic load by replacing with equivalent cylindrical tank model. Model parameters were evaluated for a wide spectrum of tank shapes and compared with those of the equivalent cylindrical tanks. Fluid pressure was calculated using linearized potential flow theory. The fluid was assumed inviscid and incompressible and the sloshing height was assumed to be small. Furthermore, in developing the mechanical model only first sloshing mode was taken into account. It was concluded that the associated errors due to the use of equivalent cylindrical tank model instead of the original intze tanks were negligible. As a result, for design

applications, the intze tank models could be replaced by the equivalent cylindrical models without loss of accuracy.

Rai (2002) studied the performance of elevated tanks damaged and collapsed in 2001 Bhuj earthquake. It was concluded that RC shaft type supporting structures extremely vulnerable to severe earthquake forces. Moreover, results showed that India codes underestimated design forces compare to the international building code (IBC) requirements. The main accent was made on the luck of redundancy in RC shafts. It was concluded that thin shaft were not able to dissipate the seismic energy due to lack of redundancy.

Rai, et al. (2004) carried out an analytical investigation and case study of RC shaft supported tanks. The study showed that shear demand was more for empty tank rather than when it was full. For studied tanks it was concluded that for all shaft aspect ratios of empty tank flexure strength governed the failure mode. However, for full tanks, shear mode was found to be governing in stiffer shafts and tension-flexure mode in more flexural shafts, having long fundamental period and large aspect ratio. Moreover, the damage patterns during previous earthquakes showed that for tanks with large aspect ratio which have long fundamental periods, flexural behaviour was more critical than shear under seismic loads.

Livaoglu and Dogangun (2004; 2005) proposed a method for seismic analysis of fluid-elevated tank-soil system considering interaction effects. The new method can be used for the frequency domain analysis. The method provided an estimation of the base shear and overturning moment, top lateral displacement of supporting system as well as wave height on the vessel. Results showed that sloshing response was not effected by soil properties. Moreover, it was concluded that softer soils increased roof displacement and reduced the base shear and overturning moment of the supporting system. The new method could lead to the economic design of the elevated water tanks.

A review of simplified seismic design procedures for elevated tanks carried out by Livaoglu and Dogangun (2006). 10 models were evaluated by using mechanical and finite-element approaches (Figure 2.6) including approach for the fluid–structure models, the massless foundation and soil–structure interaction. Soil types for this analysis were taken from Eurocode 8. It was concluded that single lumped-mass models could lead to underestimation of the base shear and the overturning moment. Other approaches showed acceptable assessment however the added mass

approach had an advantage of not using any fluid finite element. It was recommended that the distributed mass approach for seismic analysis of elevated tanks was used in general-purpose structural analyses programs (Figure 2.7). Additionally results showed that periods for convective modes were not remarkably different for any approach and soil type (Figure 2.8).

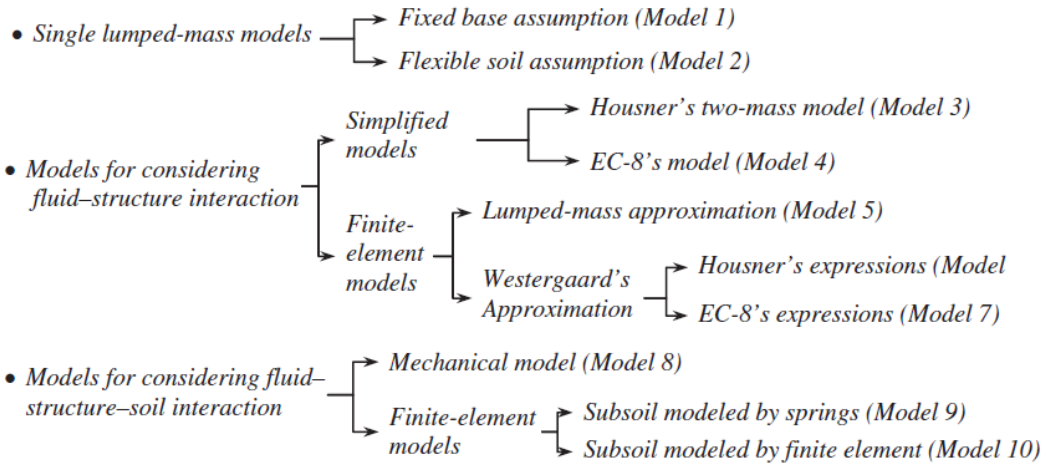

Figure 2.6. Mechanical and FE models (Livaoglu and Dogangun, 2006)

Livaoglu and Dogangun (2006) conducted seismic analyses of FE models of elevated tanks with circular frame and cylindrical shell supporting systems for different soil classes. The studies included soil classes from Turkish Earthquake Code (TEC), which included Z1, Z2, Z3 and Z4 soil classes from the softest (Z1) to the hardest (Z4) and Eurocode 8, which included A, B, C soil classes from the softest (A) to the hardest (C). The results showed that a ground type could considerably affect the magnitude of lateral displacement (Figure 2.9) and shear forces (Figure 2.10) for both frame and shaft support systems. It was also concluded that soft ground types were not appropriate for elevated water tanks construction in a view of performance of a support system.

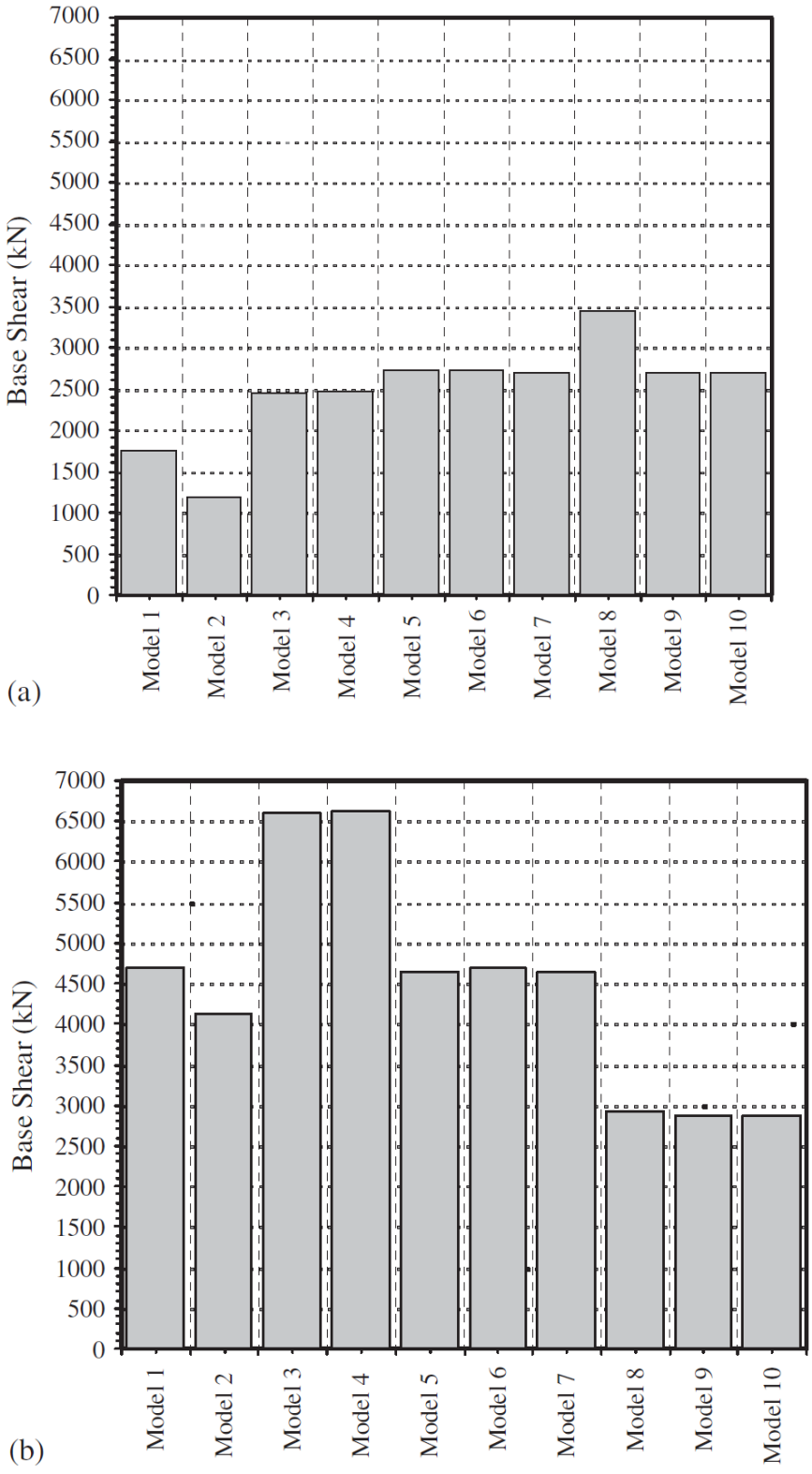

Figure 2.7. Base shears obtained for ten models considered for subsoil of (a) class A and (b) class D (Livaoglu and Dogangun, 2006)

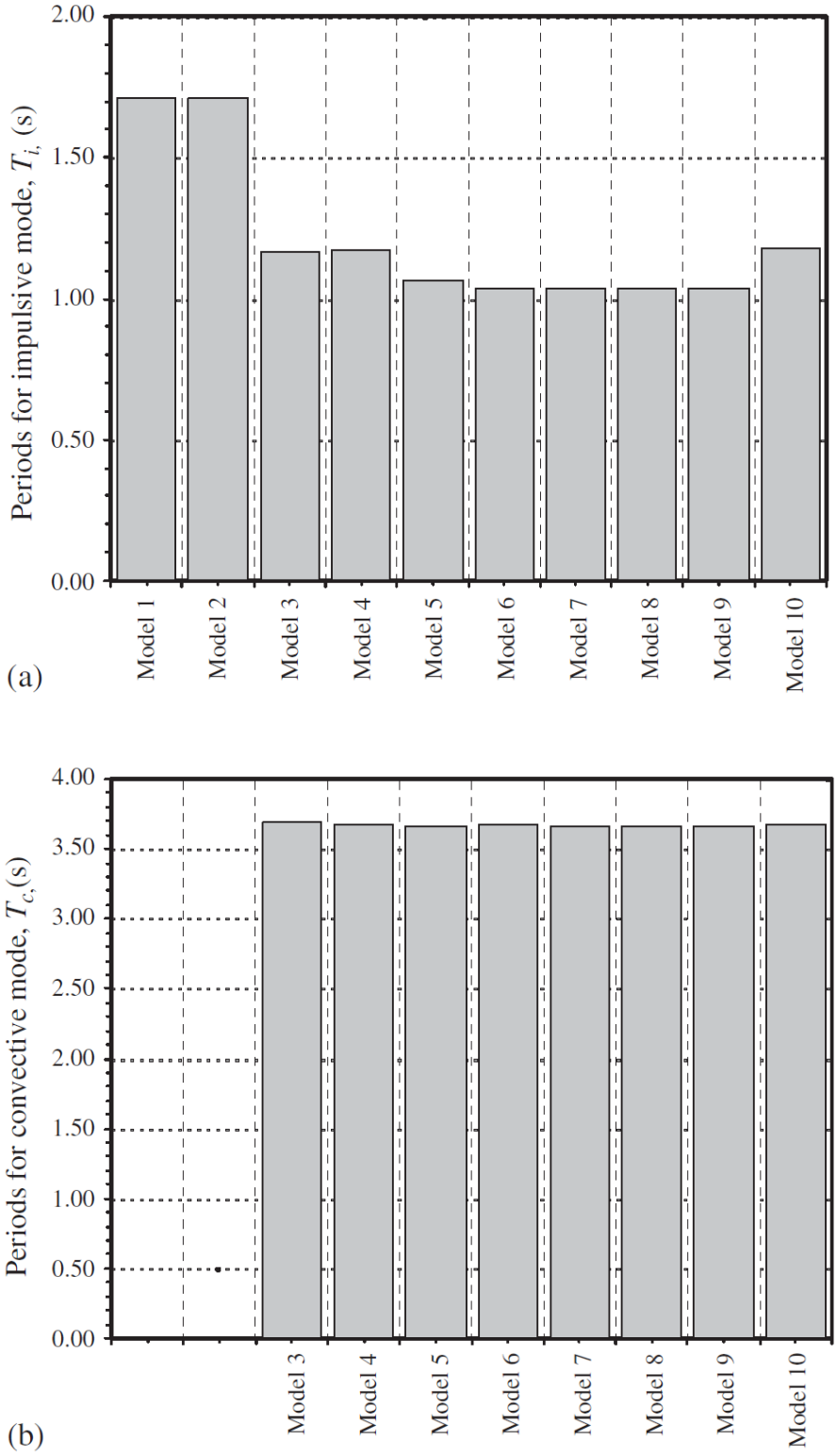

Figure 2.8. Periods for (a) impulsive mode and (b) convective mode obtained for ten models considered for subsoil of class A (Livaoglu and Dogangun, 2006)

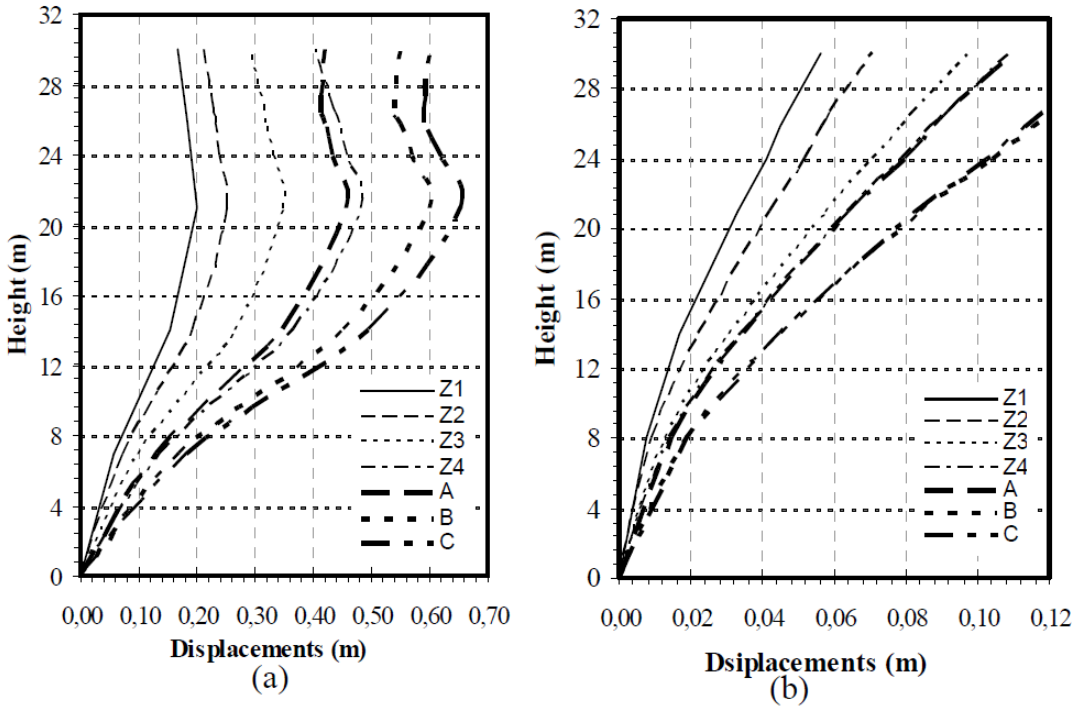

Figure 2.9. Displacement for subsoil classes (a) for frame supporting system and (b) shell supporting system (Livaoglu and Dogangun, 2006)

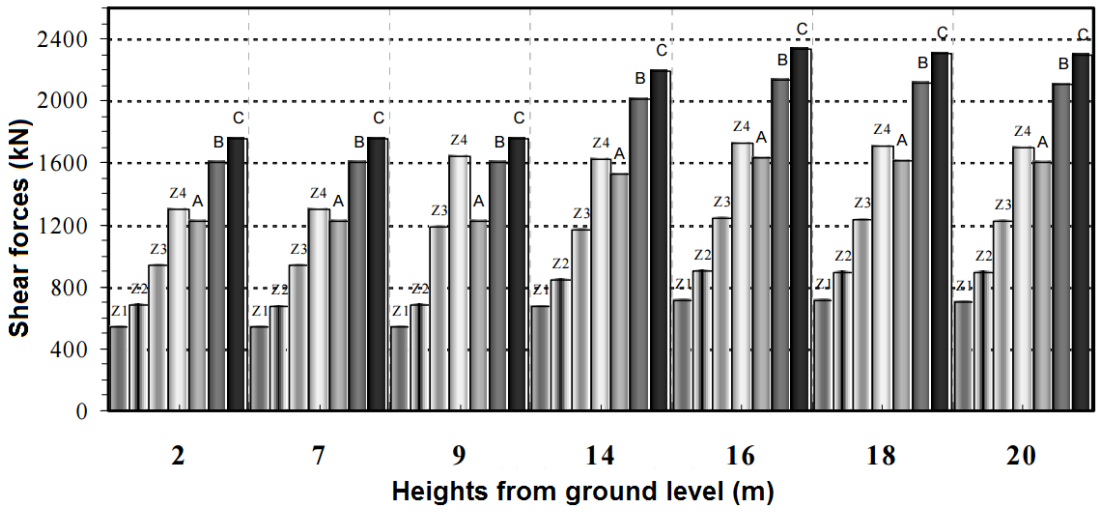

Figure 2.10. Shear forces for selected column-level obtained from seismic analysis of elevated water tank (Livaoglu and Dogangun, 2006).

In the other study, Livaoglu et al. (2008) analysed the effect of soil-structure interaction on the sloshing response of elevated cylindrical tanks using a finite element model. It was concluded that for soft soils, the foundation embedment has more influences on the system behaviour and that embedment was more pronounced in elevated tanks with shaft supporting than the frame supporting tanks.

Sweedan (2009), proposed an equivalent mechanical model for seismic forces in combined elevated tanks subjected to vertical earthquake excitation. The proposed simplified model was able to consider the flexibility of the tank wall. Two components, flexible and rigid, where developed to represent water. Parametric analyses were performed to evaluate the fundamental period and contribution of the stored liquid mass to the impulsive response by performing modal analyses.

Dutta, et al. (2009) conducted FE analytical and small scale experimental studies on the dynamic behaviour of RC elevated tanks. The soil structure interaction effect was included in the study. This study concluded that empty-tank condition governed by axil tension in the tank staging, white base shear was the major matter in full tank condition. Also it was concluded that fundamental period could be changed by soil-structure interaction. Moreover, the effect of soil-structure interaction considerably increased tension and compression forces in comparison to fixed support condition.

Nazari (2009) conducted a research to investigate the response modification factor of the elevated water tank based on ATC 19 (1995) method. A pushover analysis were conducted to examine the seismic response of an elevated water tank, designed according to the current practice. The response modification factor was determined to vary from 1.6 to 2.5 for different regions of Canada.

Shakib, et al. (2010) carried out investigation on the seismic nonlinear response of concrete elevated water tanks supported by moment resisting frame by using FE analysis. Three RC elevated water tanks were subjected to horizontal seismic excitations. It was concluded that the maximum response did not always occur in the full tanks for frame support elevated water tanks. The results also showed that the reduction of stiffness of the reinforced concrete frame staging resulted in the fundamental period increase. On the other hand, the increase of mass resulted in increase of the fundamental period.

Moslemi, et al. (2011) evaluated the performance of conical elevated tanks under seismic motions. Both free vibration and transient analysis were conducted to study fluid-structure interaction in elevated water tanks. The effects of liquid sloshing and tank wall flexibility were considered and fundamental modes were divided to impulsive and convective. The obtained results were also compared with those recommended by current practice. The objective of the study was responses were shear and overturning moment at the base of the shaft. It was concluded that modal FE analyses results were very close to those obtained from Housner's method (Figure 2.11).

Furthermore, the comparison of FE time history results to current practice showed that the current practice could estimate the dynamic response of elevated water tanks with reasonable accuracy.

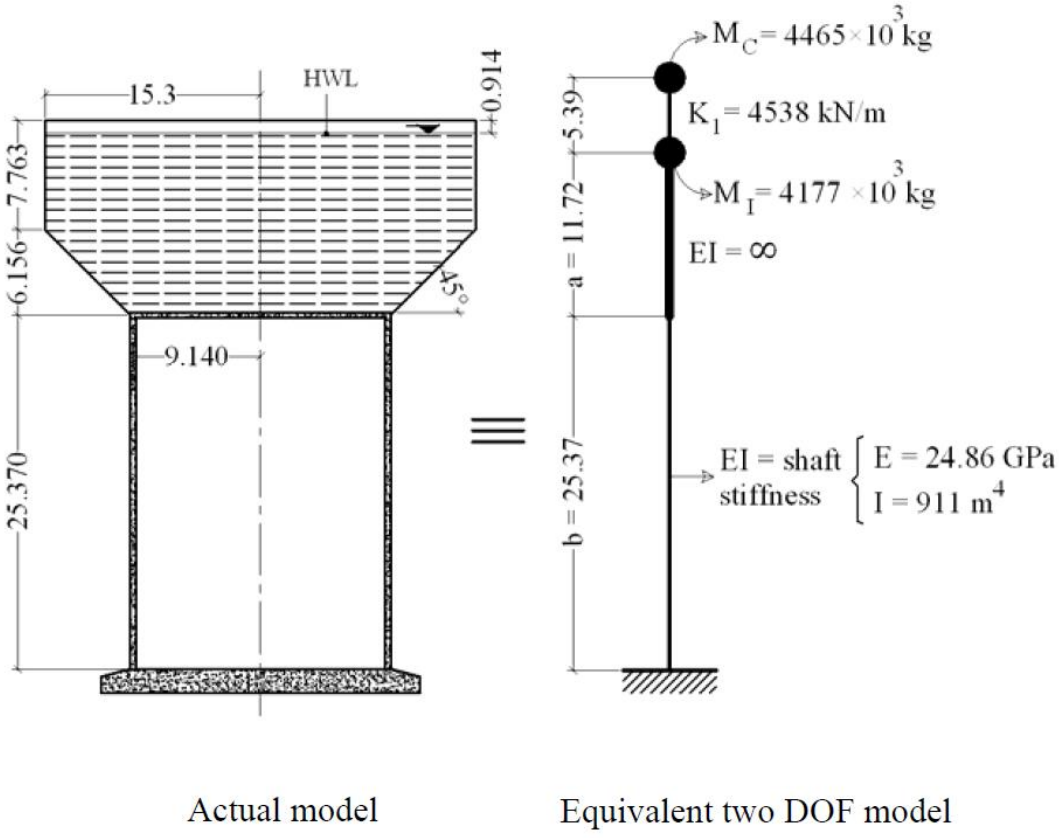

	Current practice			FE time history	Response ratio
	Impulsive	Convective	Total		
Base Shear (kN)	16 389	1 078	16 425	17 421	1.06
Base Moment (kNm)	607 834	45 794	609 557	646 940	1.06

Figure 2.11. Comparison of FE time history analysis with current practice (Moslemi, et al., 2011)

2.3 Fluid Structure interaction (FSI)

A fluid structure interaction (FSI) problem is defined as a problem where one or more deforming solids interact with an internal or surrounding fluid flow. FSI problems have been one of the biggest focus points for research within the field of computational engineering for the recent years. A reason for this is that the interaction between fluids and solids plays an important role in many different fields of engineering (Souli and Benson, 2010).

A vast majority of these applications often include large and complex structures in combination with a strong nonlinearity due to the non-stationary coupling as well as the inherent nonlinearities from the respective domains, especially from the fluid domain. This makes it almost impossible to use analytical methods to obtain accurate solutions for these problems and the possibility to perform laboratory experiments is often limited and expensive. Hence, numerical methods have to be employed to investigate the often complex interaction between fluids and solids (Hou, et. al., 2012).

As mentioned above, the research area of numerical methods for analysis FSI problems is an area where a lot of work is currently being performed, which has resulted in a large number of different approaches to the problem, depending on the intended field of application. Hence, one typical method may be very accurate for its proposed field of application, but it may neglect some effects that are important in another field of analysis, therefore, making it unsuitable for that field. Many of these methods are of course more or less related to each other and they can be classified with different aspects in mind.

2.3.1 Single degree of freedom

Single degree of freedom (SDOF) is a system which contributes only one displacement or rotation to describe the motion of a mass under a dynamic load. Elevated water tank is classified as single degree of freedom and simple structure. This is because the water tank or its reservoir is a mass of the structure especially when it full with water was supported by massless structure which is space structure under the water tank (Chopra, 2007)

The concept that enables analysis of elevated water tanks as a single lumped-mass model was suggested in the 1950s (Chandrasekaran and Krishna, 1954). Elevated tanks (Figure 2.14) and the SDOF model for this concept showed in Figure 2.12(e).

Two key points should be pointed out in this approach. The first point is related to the behaviour of the fluid. If the container is completely full and contained is closed, there no possibility for water sloshing, so an elevated tank can be treated as a single-degree-of-freedom system in such a case. When the container is not full and there is an opportunity of sloshing, the SDOF system cannot reproduce the real behaviour of water inside an elevated water tank.

The other point is related to the supporting structures. The main properties which have an influence on the seismic design are ductility and the capacity of absorbing energy by supporting staging of at elevated water tanks. In SDOF approach, it is assumed that the supporting structure has a uniform rigidity along the height. However, the elevated tanks can have different types of supporting structures, which could be in the form of a reinforced concrete shell (Figure 2.14(a)), a steel frame (Figure 2.14(b)), a reinforced concrete frame (Figure 2.14(c)) or a masonry shaft (Figure 2.14(d)) thus a cantilever of uniform rigidity along the height cannot represent all the supporting structure types. It can be concluded that SDOF system is the most suitable for the reinforced concrete shell or masonry supporting structures.

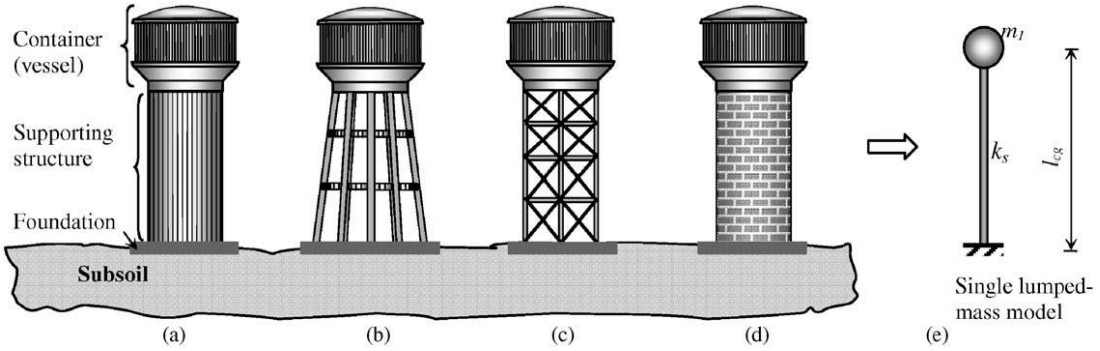

Figure 2.12. Elevated tanks and the single lumped-mass model: (a) the tank with reinforced concrete shaft supporting structure, (b) the tank with reinforced concrete frame supporting structure, (c) the tank with reinforced concrete frame with diagonal braces or steel frame supporting structure, (d) the tank with masonry shaft supporting structure, (e) single lumped-mass model. (Livaoglu and Dogangun, 2006)

2.3.2 Multi degree of freedom fluid-structure system idealisation

Normally most of the elevated tanks are not completely filled with liquid. Hence the seismic behaviours of elevated water storage tanks subjected to earthquakes can be represented by two fundamental modes of vibration. The first impulsive mode is related to the impulsive mass m_i that rigidly moves together with the tank structure

and the other convective mode related to the convective mass m_c corresponds to the liquid sloshing (Housner, 1963).

In Housner's (1963) approach, the two masses (m_i and m_c) are assumed to be uncoupled and the earthquake forces on the support are estimated by considering two separate single-degree-of-freedom systems: The convective mass m_c represents only sloshing and convective mass m_i consists of impulsive fluid mass, weight of container and some parts of the supporting structure (two-thirds of the supporting structure weight is recommended in Eurocode 8 and the total weight of the supporting structure is recommended by Priestley et al., (1986). This two-mass model suggested by Housner has been commonly used for seismic design of elevated tanks (Figure 2.13).

Eurocode-8 (2006) suggests two mass model, based on the work of Veletsos, et al. (1984) and Malhotra, et al. (2000) that is Housner's approach with certain modifications

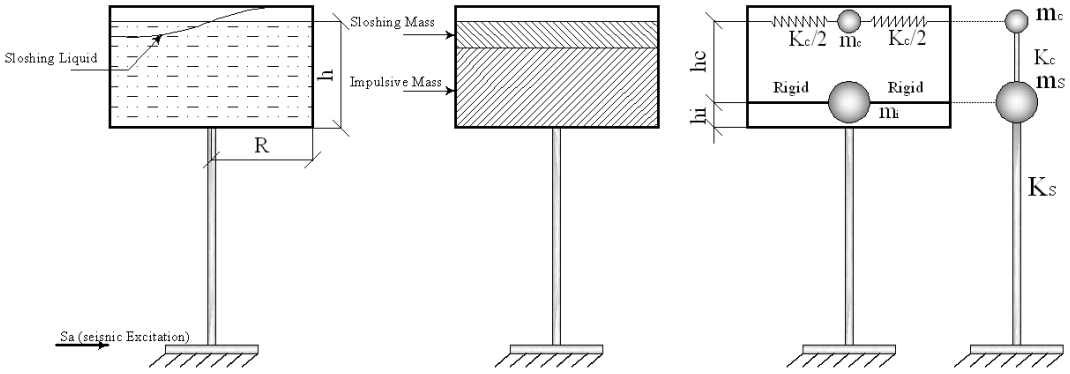

Figure 2.13.Two degree of freedom system (Gareane, et al., 2011)

Additional higher-mode convective masses may also be included (Chen and Barber, 1976; Bauer, 1964) for the ground-supported tanks. Haroun and Housner (1981) have also developed a three-mass model of ground-supported tanks that takes tank-wall flexibility into account. However, a single convective mass is generally used for the practical design of the elevated tanks (Haroun and Housner, 1981; Livaoglu and Dogangun, 2005) and higher modes of sloshing have negligible influence on the forces exerted on the container even if the fundamental period of the structure is in the vicinity of one of the fundamental periods of sloshing (Haroun and Ellaithy, 1985).

2.3.3 FSI model through finite element method (FEM)

The finite element method (FEM) is one of the most important developments in civil engineering. The FEM is applicable to wide range of problems from assemblage of one dimensional finite elements to a three dimensional complex problems. Using FEM linear and nonlinear behaviour of material can be developed. Moreover, static as well as dynamic analysis can be performed (Wilson, 2002; Chopra, 2007).

There are different approaches to investigate the fluid–structure interaction problems:

- added mass approach (Westergaard, 1931; Barton and Parker, 1987; Dogangun, et al., 1996a; Gareane, et al., 2011).
- Eulerian approach (Zienkiewicz and Bettes, 1978)
- Lagrangian approach (Wilson and Khalvati, 1983; Olson and Bathe, 1983; Dogangun et al., 1996b, 1997; Dogangun and Livaoglu, 2004)
- Eulerian–Lagrangian approach (Donea, et al.,1982).

The most widely used method in industry and researches and the simplest method of these is the added mass approach; while using the other approaches for analyses, special programs that include fluid elements or sophisticated formulations are necessary (Livaoglu and Dogangun, 2006).

2.3.3.1 Added mass approach

A complete dynamic analysis of a structure that is in contact with a fluid requires the hydrodynamic effects to be accounted during the analysis. The fluid must be incorporated within the idealized model for the problem.

In the added mass approach, a mass that is obtained by different techniques is added to the mass of the structure at the fluid–structure interface (Copra, 2007). For a system subjected to an earthquake excitation, the general equation of motion can be written as:

$$M\ddot{u} + C\dot{u} + K = -M\ddot{u}_g \qquad \textit{Equation 2.1}$$

Where:

M is the mass matrix,

C is the damping matrix,

K is the stiffness matrix,

g is the ground acceleration,

u is the relative displacement

$\dot{u}$ is the relative velocity

$\ddot{u}$ is the relative acceleration

If the added mass approach is used, the regulating equation changes in the following form:

$$M^*\ddot{u} + C\dot{u} + K = -M^*\ddot{u_g} \qquad \textit{Equation 2.2}$$

Where:

$M*$ is the total mass matrix consisting of the structural mass matrix M and added mass matrix (Ma).

In this approach, it is assumed that the added mass of Ma synchronously vibrates with the structure; therefore, only the mass matrix is increased to consider the fluid effect, whereas stiffness and damping matrices do not change.

2.3.3.2 Westergaard Model

Westergaard's method was originally developed for the dams but it can be applied to other hydraulic structure such as water tank under earthquake loads. In this method impulsive mass equally distributed along the tank wall:

$$m_{ai} = \left[\frac{7}{8}\rho\sqrt{h(h-y_i)}\right]A_i \qquad \textit{Equation 2.3}$$

Where:

m_{ai} is the mass of water

ρ is the mass density

h is the depth of water

A_i is the tributary area associated with node i

In the case of intze tank where the walls having sloped and curved contact surface, the Equation 2.4 should be compatible with the tank shape by assuming the pressure is still expressed by Westergaard's original parabolic shape (Figure 2.14). But the fact that the orientation of the pressure is normal to the face of the structure and its

magnitude is proportional to the total normal acceleration at the recognized point (Prajapati, et al., 2014). In general, the orientation of pressures in a 3-D surface varies from point to point; and if it is expressed in Cartesian coordinate components, it would produce added-mass terms associated with all three orthogonal axes. Following this description the generalized Westergaard added mass at any point i on the face of a 3-D structure is expressed by Kuo (1982) in the Equation 2.4.

$$m_{ai} = \alpha_i A_i \lambda_i^t \lambda_i = \alpha_i A_i \begin{bmatrix} \lambda_x^2 & & sym \\ \lambda_y \lambda_x & \lambda_y^2 & \\ \lambda_z \lambda_x & \lambda_z \lambda_y & \lambda_z^2 \end{bmatrix} \qquad \textit{Equation 2.4}$$

Where:

A_i is the tributary area associated with node i;

λ_i is the normal direction cosine (λ_x, λ_y, λ_z)

α_i is the Westergaard pressure coefficient.

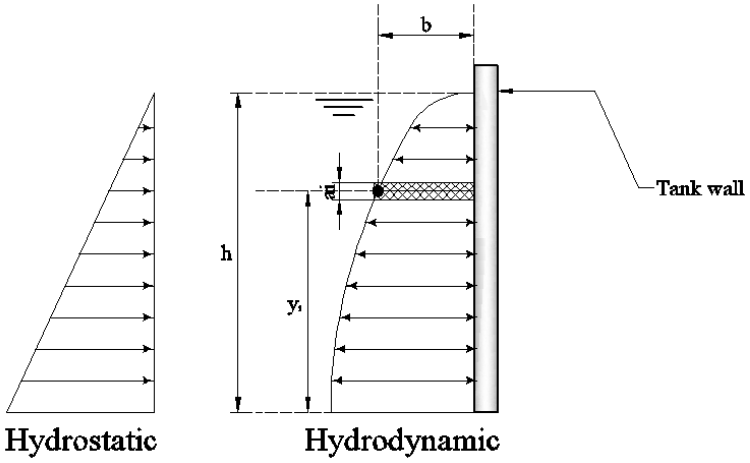

Figure 2.14. Westergaard Added Mass Concept (Gareane, A. I et al, 2011)

2.3.3.3 Simplified Westergaard approach

Algreane, et al. (2009; 2011) suggested a method of adding impulsive mass to the walls of water tanks alternative to Westergaard approach (Figure 2.15). Six models with alternative to Westergaard approach distributed masses were simulated to determine the fundamental period. This study showed that the effect of alternative mass distribution has a minor effect on the dynamic response of elevated tank (Figure 2.16). Additionally, it was concluded that the mass can be distributed by any pattern instead of using the Westergaard method.

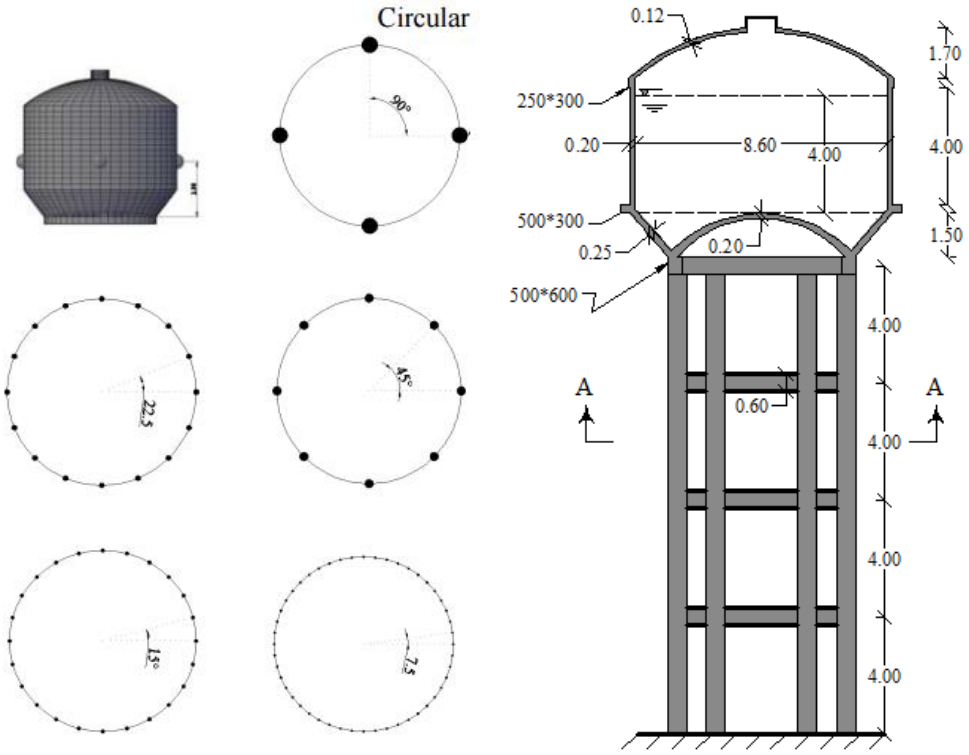

Figure 2.15. Alternative masses distribution in case of circular tanks (Algreane, et al., 2011)

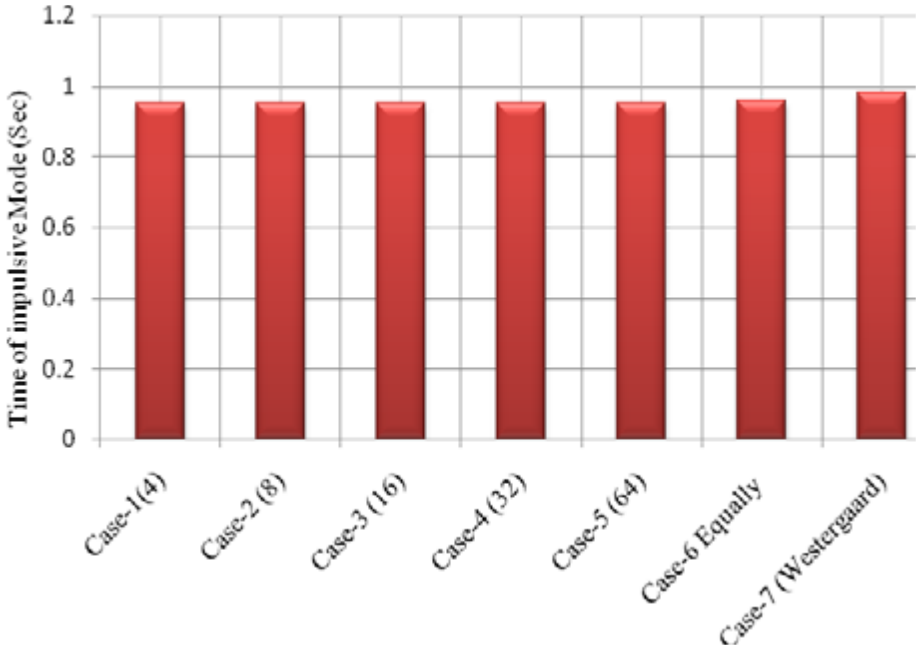

Figure 2.16. Values of impulsive mode for the circular tank (Algreane, et al., 2011)

2.3.3.4 The Eulerian approach

The Eulerian approach is widely used in fluid mechanics. This approach uses the fixed computational mesh and the fluid moves with respect to the grid. In the Eulerian approach a velocity potential function is assumed and the behaviour of the liquid is described through pressure or velocity variables at the element nodes. However, using this configuration it is difficult to describe the structure configuration. Since the structure configuration needs displacement variables (Meslouris, 2000; Donea and Huerta, 2003).

2.3.3.5 Lagrangian approach

In order to overcome the above complication, Lagrangian elements can be used and the fluid elements use displacement as fluid element variables. In the Lagrangian algorithms, each individual node of the computational mesh follows the associated material particle during motion. These formulations are frequently used in structural mechanics, in combination with both solid and structural (beam, plate, shell) elements. Also it allows easy tracking of free surfaces and interfaces between different materials (Meslouris, 2000; Donea and Huerta, 2003).

2.3.3.6 Eulerian-Lagrangian approach

Eulerian-Lagrangian algorithms are particularly useful in flow problems involving large distortions. The key idea in this formulation is the introduction of a computational mesh which can move with a velocity independent of the velocity of the material particles. It is the generalized description of the above two formulations (Donea and Huerta, 2003).

2.4 Slit shear walls

Teran (2001) defined that hysteric energy was a parameter which should be utilised with the earthquake resistant design purpose. Its benefits include consideration of the cumulative inelastic deformation demands that account for both earthquake magnitude and duration. Then inelastic deformation energy would be suitably considered as energy demand. The input energy from the earthquake could be dissipated through two mechanisms; hysteretic energy and damping energy. It was concluded that hysteretic energy was more meaningful in energy base design because it could represent the structure energy needs to deform through inelastic

deformation related to damage. RC structures dissipated energy due to concrete crack relative friction and rebar yielding.

Park and Paulay (1975) stated that the reason of failure of the shear walls was generally focused in the base plastic hinge region, where concrete damage leaded to reduction of cross-section area, loss of bearing capacity and stiffness, and decrease in the shear and anti-slip capacity. Study concluded that shear strength was mainly dependent on the reinforcement and to improve performance of shear walls some necessary measures should be done. In order to improve the ductility, the construction of boundary elements were considered in some relevant specifications however that could increase the amount of material used.

Muto (1973) proposed a reinforced concrete structural wall, with good properties of seismic energy dissipation, called slit wall. The first building constructed with slit wall technique was the Keio Plaza in Tokyo, 1968 (Aoyama, 2005). In the structure frameworks, vertical strips of concrete forming a slit panel were introduced. The contact between the strips were made with plaster, asbestos sheets, synthetic resin or metal plates. Seismic energy dissipation was achieved by destroying the connection between the reinforced concrete strips. The purpose of the slit wall invention was to create an ideal structure for high multi-storey buildings, which under reduced seismic actions behaves as a rigid structure and under the action of high intensity earthquakes turns into a flexible one.

Kwan, et al. (1999) improved a model of a slit wall. Reinforced concrete beams connected two parts of slit walls though out all height of a slit wall and connectors formed a dissipative zone (Figure 2.17(a)). The comparison between solid and slit walls were made and results showed the efficiency of the slit the wall: the displacements and story drift decreased by 20% as well as overall ductility of a structure was improved. It was concluded that, seismic performance depended on the yielding resistance of the connections. Therefore rational design of connectors was of great importance.

The use of rubber belts instead of reinforced concrete connectors was proposed by Lu and Wu (2000). To improve the seismic behaviour, the rubber belt were anchored into the slit in the slit wall at each level of the structure (Figure 2.18(b)). Results showed that the system had a very good ability to dissipate the seismic energy by the elastic rubber deformation, the yielding of the reinforcements from the connections and the friction between concrete and rubber straps.

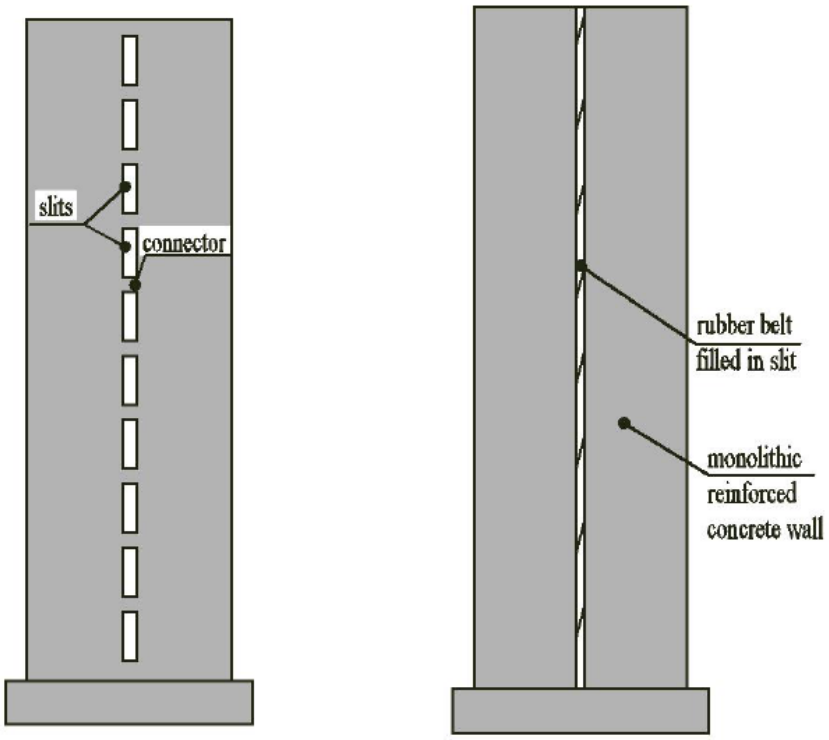

Figure 2.17. (a) Slit wall with connectors, (b) Slit wall with rubber belt filled in (Baetu, 2011)

Labafzadeh and Ziyaeifar (2008) studied the seismic behaviour of slit shear walls in 70 m height building. A series of linear and nonlinear dynamic analyses were conducted. The results showed that the centre of dissipated energy in the slit shear walls higher than in the solid wall. It was pointed out that the input energy of earthquake could be dissipated without any localisation at the specific part in slit walls. The other advantages included decreasing in the story displacements, interstory drifts, base shear and moment and increasing in ductility and damping ratio.

Labafzadeh and Ziyaeifar (2011) studied inelastic dynamic analysis on a variety of shear was with different arrangement of openings. Results showed that using rational arrangement of openings in the shear wall leaded to disperse the hysteric energy across the height of the wall and employed both flexural and shear ductility capacity of the system at the base and around the openings, respectively (Figure 2.18). In addition, the responses of the slit shear wall such as base shear, base moment, top story displacement, and average value of inter-story drift along the height were reduced compare to the solid wall.

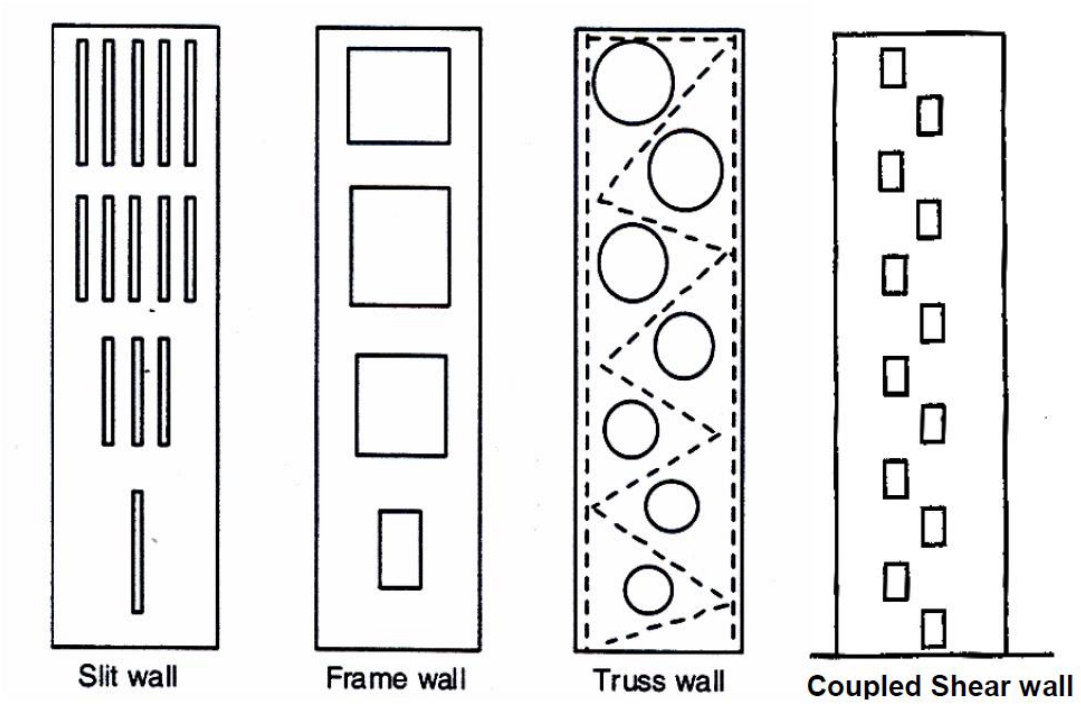

Fiigure 2.18. Sample layouts of dual ductility mode shear wall (Labafzadeh and Ziyaeifar, 2011)

Zhiyuan, et al. (2013) conducted the experimental cyclic loading test and FE analysis on a new type of adaptive slit shear walls which were introduced to improve the seismic performance of conventional shear wall structures. Studies showed that failure process of proposed slit shear walls was progressive and could be divided into two stages, i.e., the whole wall stage and the slit wall stage. It was concluded that ductile failure can be achieved for the design of adaptive slit shear walls and brittle shear failure can be avoided, which happens in ordinary shear walls.

Baetu, et al. (2012; 2013) carried out a nonlinear finite element analysis of the reinforced concrete slit wall. The nonlinear behaviour, cracking and crashing propagation patterns and hysteretic energy dissipation in solid and slit walls were compared. Results showed that the slit wall provided more ductility and energy dissipation in comparison to the solid wall (Figure 2.19). It also was shown that the slit wall had better crack pattern. In addition it was concluded that the slit wall dissipated seismic energy by cracks uniformly distributed on all the surface of the wall and by crushing of the shear connections, however the solid wall dissipated seismic energy only by cracks at the base of the wall.

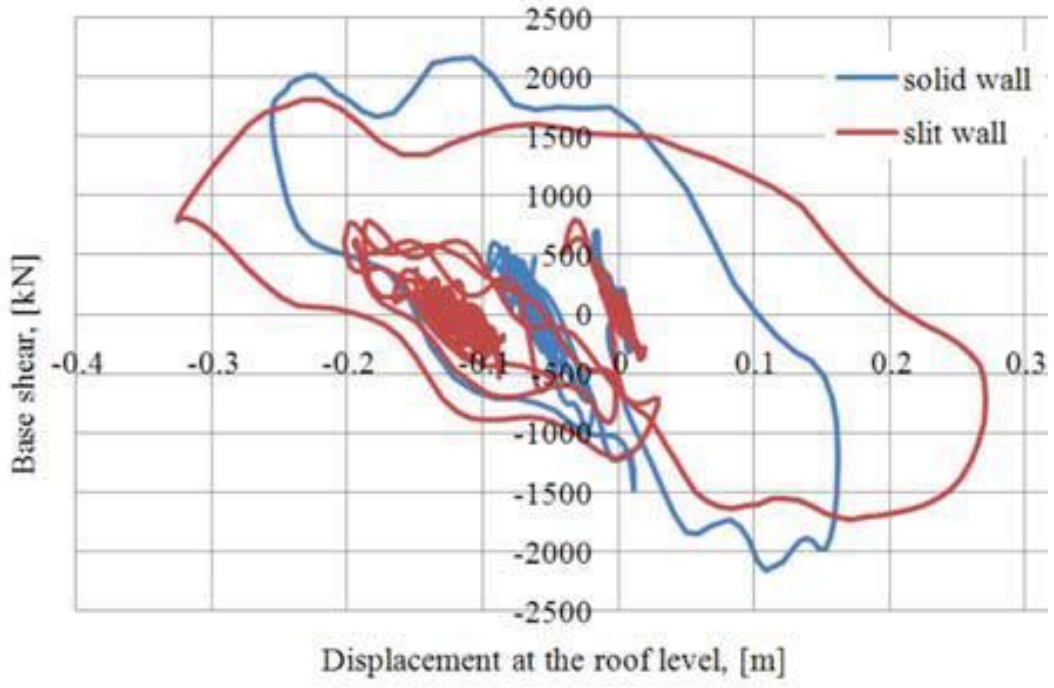

(a)

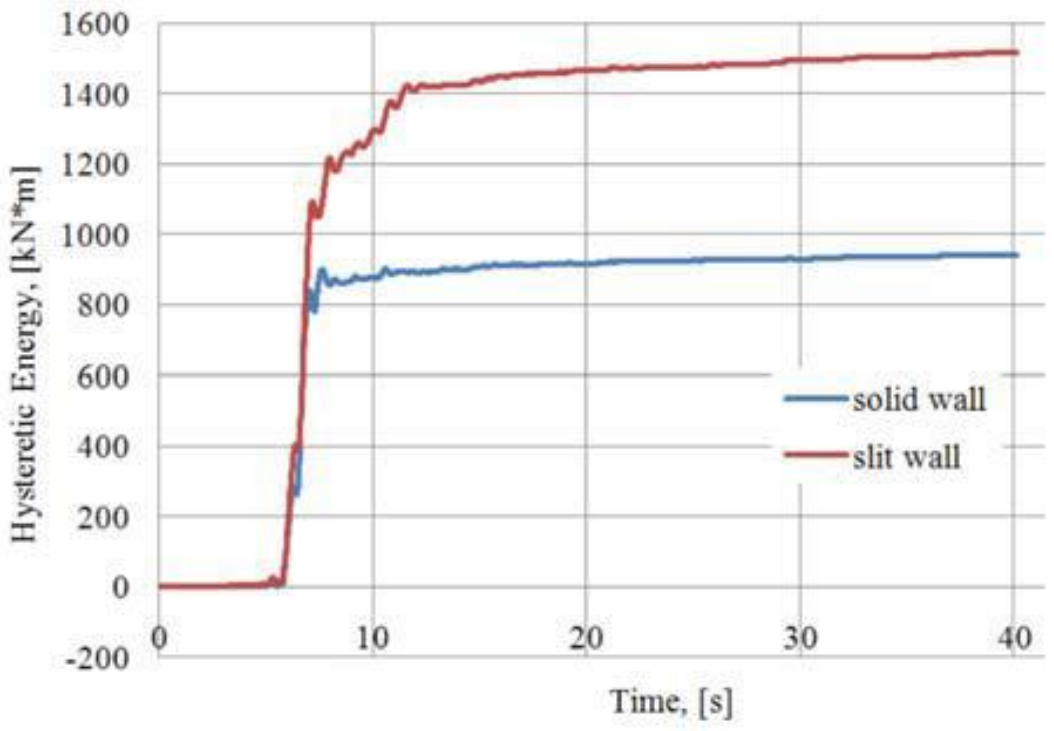

(b)

Fiigure 2.19. Sample layouts of dual ductility mode shear wall (a) Hysteretic behaviour of the walls at Vrancea 1977 N-S earthquake, PGA = 0.3 g. (b) Hysteretic energy dissipation of the walls at Vrancea 1977 N-S earthquake, PGA = 0.3 g. (Baetu, et al., 2013)

2.5 Design codes and standards

Eurocode-8 (2006) employed Veletsos and Yang's model (1977) for determining the seismic forces associated with the accelerated contained liquid in rigid circular tanks. Dynamic analysis of flexible circular tanks recommended to be performed using models developed by Veletsos (1984) and Haroun and Housner (1981B) together with the approach proposed by Malhotra et al (2000). Rigid rectangular tanks should be evaluating using Housner's method (1963) and there is no practical approach considered for flexible rectangular containers.

Most of north American standards including ACI 350.3-06, AWWA D100, AWWA D110, and API 650 have employed the Housner's mechanical model (Housner,1963) with some modifications for determining the dynamic behaviours of liquid in a container. In NZS 3106 (2010), the mechanical model proposed by Veletsos and Yang (1977) is used for seismic analysis of rigid tanks while the model developed by Haroun and Housner (1981B) is used for flexible liquid storage tanks.

In seismic design, the seismic response values corresponding to the impulsive and convective parts are combined using an appropriate combination method. All codes and standards except the Eurocode-8, recommend SRSS (Square Root of Sum of Squares) rule to be used for combining the impulsive and convective seismic effects. Eurocode-8 suggests absolute summation combination rule.

Different standards specify different damping values to be considered for impulsive component. However, all codes and standards use 0.5% for convective component. In Eurocode-8, a damping ratio of 5% is proposed for the impulsive component of concrete tanks while 2% damping is specified for steel tanks. ACI 350.3-06, ASCE 7-05, AWWA D100, AWWA D110, AWWA D115, and API 650 recommend a damping ratio of 5% for impulsive component for all tank types. In NZS 3106 (2010), the appropriate damping ratio for the impulsive component is determined based on the tank geometry, tank aspect ratio, tank material, and shear wave velocity in foundation soil.

According to Eurocode 8 when performing a modal response spectrum analysis the response of all modes of vibration contributing significantly to the global response shall be taken into account. That is done by either demonstrating that the sum of the effective modal masses for the modes taken into account amounts to at least 90% of

the total mass of the structure or by demonstrating that all modes with effective modal masses greater than 5% of the total mass are considered (Dubina, 2000).

Chapter 3

Methodology

3.1 Introduction

This chapter describes seismic analysis methods employed in this thesis for studying static and dynamic response behaviour of proposed reinforced concrete (RC) elevated water tanks. The analysis of proposed RC elevated water tanks was carried out in three steps and each step was performed using a specific analysis method. The purpose of each step is explained in this chapter as well as general equations and formulations for each analysis method are briefly reviewed. The finite element (FE) approach is used for performing the analyses.

The chapter starts with selecting methodology and description of advantages, disadvantages and considerations of proposed methodology. The methods of seismic analysis as well as sources of nonlinearity in the nonlinear seismic analysis applied in this study are discussed.

The next part of this chapter includes methodology for response spectrum design by Eurocode 8. Furthermore, a method of performing a nonlinear static analysis as a powerful method for evaluation of seismic response of elevated water tanks is addressed in this chapter. In addition, capacity spectrum analysis, which is combination of pushover analysis and response spectrums, is discussed.

This chapter continues with discussing the equations of time history dynamic analysis as the most accurate seismic analysis. Modal time history and direct integration nonlinear time history dynamic analyses were employed in this study. In this chapter the equations of motion of a nonlinear MDOF system are established. In addition, this chapter provides numerical solution methods for solving MDOF system along with nonlinear static equilibrium equations.

The final part of the chapter explains fluid-structure interaction using two mass idealisation. The impulsive and convective components are discussed separately. Finally, two degree of freedom water design according to Eurocode 8 is explained.

3.2 Methodology selection

Previously, laboratory tests were the only option for design rules and standards established. Laboratory experiments of small scale models were the only option for investigation of behaviour of structures subjected to earthquake and wind loads. Laboratory tests were also used to develop full-scale structures and structural elements. However, that tests were very time consuming and expensive, thus, full-scale models experiments were generally avoided.

However, during the last two decades computer aided engineering have changed this situation significantly in civil engineering industry. Computer aided engineering allowed to investigate structures and structural elements under lateral forces without time consuming and expensive laboratory experiments.

Finite element analysis (FEA) is the most significant and appropriate computer aided engineering method currently available in industry for realistic structural behaviour simulation without laboratory experiments. Structures, such as elevated water tanks, present excessive difficulties in experimental analysis because of both the required complexity and considerable costs involved with large scale experiments. To avoid this inconveniences FEA have become very popular among researches.

FEA combines areas such as mathematics, physics, engineering and computer science. In practice, a FEA usually consists of three principal steps (Chopra, 2007):

- Pre-processing: This step includes development of a model in which geometry is divided in a number of elements connected by nodes to each other. Material properties, constrains, loads and boundary conditions also should be applied in this stage.
- Analysis: In this step, the geometry, constraints, mechanical properties and loads are applied to generate matrix equations for each element, which are then assembled to generate a global matrix equation of the structure. The equation is then solved for displacements. Using the displacement values, strain, stress, and reactions are calculated.
- Post-processing: The post-processing stage deals with the representation of results. Typically, the deformed configuration, mode shapes, temperature, and stress distribution are computed and displayed at this stage.

Before any further step is taken towards the selection of a methodology that will be followed it is of crucial importance to clarify some important aspects that govern all analytical analysis (Chung, 2003). In general, mathematical FE models are mostly considered for the purposes (Pedgen, et al., 1995) of:

- Gaining a true insight to a systems operation
- Developing operating or resource policies to improve system performance
- Enable the extensive testing of new concepts before actual implementation
- Acquiring information without causing a disturbance to the actual system

From the above, the most important purposes for this particular study include enabling the extensive testing of new concepts before actual implementation as well as gaining a true insight to a systems operation. The FEA has a number of advantages as well as disadvantages which are discussed in next sections.

3.2.1 Advantages of final element analysis

A number of important advantages of FEA can be observed for engineering field. One of the main benefits of FEA is an availability of modelling full scale structures and simulate realistic behaviour under various load environments. Once a mathematical model is developed, FE software can analyse the model in detail under variety of loads without damaging a structure or structural elements. In addition, FEA can be performed on computer workstations or personal computers, together with professional assistance. Advantages of FEA can be summarised (Chopra, 2007):

- Can be used to compress a time frame, a simulation model run on a computer system can be used to investigate quickly the effects of a change in a real life situation that take place over several years.
- Can be used to study complex systems that would otherwise be difficult to investigate.
- Can be used in engineering and product design to investigate the effect of changes without producing a physical model.
- Can be used to investigate situation that would be dangerous in real life.

Furthermore, since computer simulation and modelling tools were developed it is now possible to carry out studies of models for a great variety of researchers that would otherwise require excessive complexity in order to be simulated.

Finally, nowadays most FE packages provide some form of result visualisation that allows to make observations, check for logical mistakes and intuitively evaluate results. The ability of analytical simulation, to provide full access to every step of model analysis can be a useful tool that allows to fix both the model and analytical procedure if any problems appear.

3.2.2 Disadvantages of finite element analysis

Despite the advantageous nature of FE simulation it is important to understand the disadvantages of this type of analysis as well. Those disadvantages are not only directly involved with the modelling and the employed analysis but also with the actual results expected by analysis. Some of these disadvantages were highlighted by Chung (2003):

- Simulation can be as accurate as its data input.
- A simulation's result complexity is directly relevant with the complexity of the simulation itself.
- Simulation cannot solve problems by itself.

It is vital to realise that a poorly constructed methodology can yield bad results and vice versa. The methodology used is of equal importance for both correct data input and collection. It is therefore important to utilise the selection of each different data input point to exclude any errors to the actual analytical system due to them.

A researcher should not feel overconfident and relies just on results from FE analysis. Since FE analysis usually includes complicated mathematic formulas and complex algorithms the verification of developed models and obtained results should always be included into a study.

On the other hand the system should be formulated in a way to have a clear sight of the objectives without trying to oversimplify the input data and output results of complex problems. Although a very complex model can have a significant influence on the amount of a time for analysis, oversimplifying a model and missing important elements of the analysis can have a detrimental effect on result accuracy. Thus necessary to be completely aware regarding the analytical model's capabilities and limitations.

3.2.3 Considerations in finite element analysis

In addition to the advantages and disadvantages to FE modelling and analysis, some considerations should be discussed. These considerations may influence on both the complexity of the model required and the research actual feasibility within a given time or resource frame. These include the following (Chung, 2003):

- Simulation model building might require specialized training.
- Simulation modelling and analysis can be costly.
- Simulation results involve many statistics.

Simulation modelling should be tackled with a proper training. Serious mistakes in an analytical simulation can be made without both a complete understanding of a model and model's behaviour during the FE model creation and ability to use the specific simulation program required for the analysis. It is of vital importance to be comprehensively informed of the program's capabilities and limitations to avoid mistakes in results.

Complex FE models can be very time consuming and/or require a variety of specialists for their creation. Simulation modelling can be a rather costly endeavour that can greatly benefit from some solid preparation. Nevertheless, even for seasoned researchers a complex model can require a great deal of work for its construction and although simplifications can and must be made in order to make it more manageable is necessary to realize that the important elements that can lead to inaccuracies of the end results cannot be avoided.

Finally, since the essential ability of the analytical simulation to be performed in a particular time period and usually requires a number of repetitions the results usually require some form of statistic interpretation and post processing. It is therefore important to have a good grasp of statistic knowledge to avoid getting lost in the details of each individual result.

3.2.4 Assumptions and limitations

This research is focused on the reinforced concrete shafts therefore it has been assumed that:

1) The foundation is assumed to be rigid and the shaft wall is fixed at the level of foundation. This is applied by constraining all degrees of freedom at the base nodes of RC shaft FE models.
2) Only the unidirectional horizontal component of seismic excitation was considered and the influence of the vertical component was neglected.
3) Study of the contained liquid in a water tank is based on the two spring theory.
4) Only the full tank condition was assumed for analyses
5) Liquid sloshing component was neglected in pushover and nonlinear time history analyses.

3.3 Methods of seismic analysis

Selection of analysis method for seismic design depends on many factors such as the structure type and configuration, design goals and performance, seismic design category, and importance of the structure. In general, analysis methods could be divided into two main categories of static and dynamic analysis. On the other hand, both static and dynamic analysis can be performed as linear or nonlinear.

Linear methods mentioned in Eurocode 8: Part 1 (2004) are as follows:

- Lateral force method of analysis may be applied to structures whose response is not significantly affected by contributions from modes of vibration higher than the fundamental mode in each principal direction.
- Modal response spectrum analysis which can be used for all structures whose response is/or can be significantly affected by contributions from modes of vibration higher than the fundamental mode in each principal direction.

Nonlinear methods mentioned in Eurocode 8: Part 1 (2004) are as follows:

- Non-linear static (pushover) analysis
- Nonlinear dynamic analysis (time history)

Figure 3.1 shows seismic analysis employed in this research. Capacity spectrum analysis is a static nonlinear method used for estimation of structures capacity during an earthquake. It combines MDOF pushover analysis with response spectrums of equivalent SDOF system. A plastic demanded spectrum is obtained from an elastic spectrum designed according to Eurocode 8. The other part of the capacity spectrum analysis is nonlinear static (pushover) analysis. A plastic behaviour of materials are included in the analysis. With pushover analysis characteristic nonlinear force-displacement relation for MDOF can be developed (usually base shear and top lateral displacement).

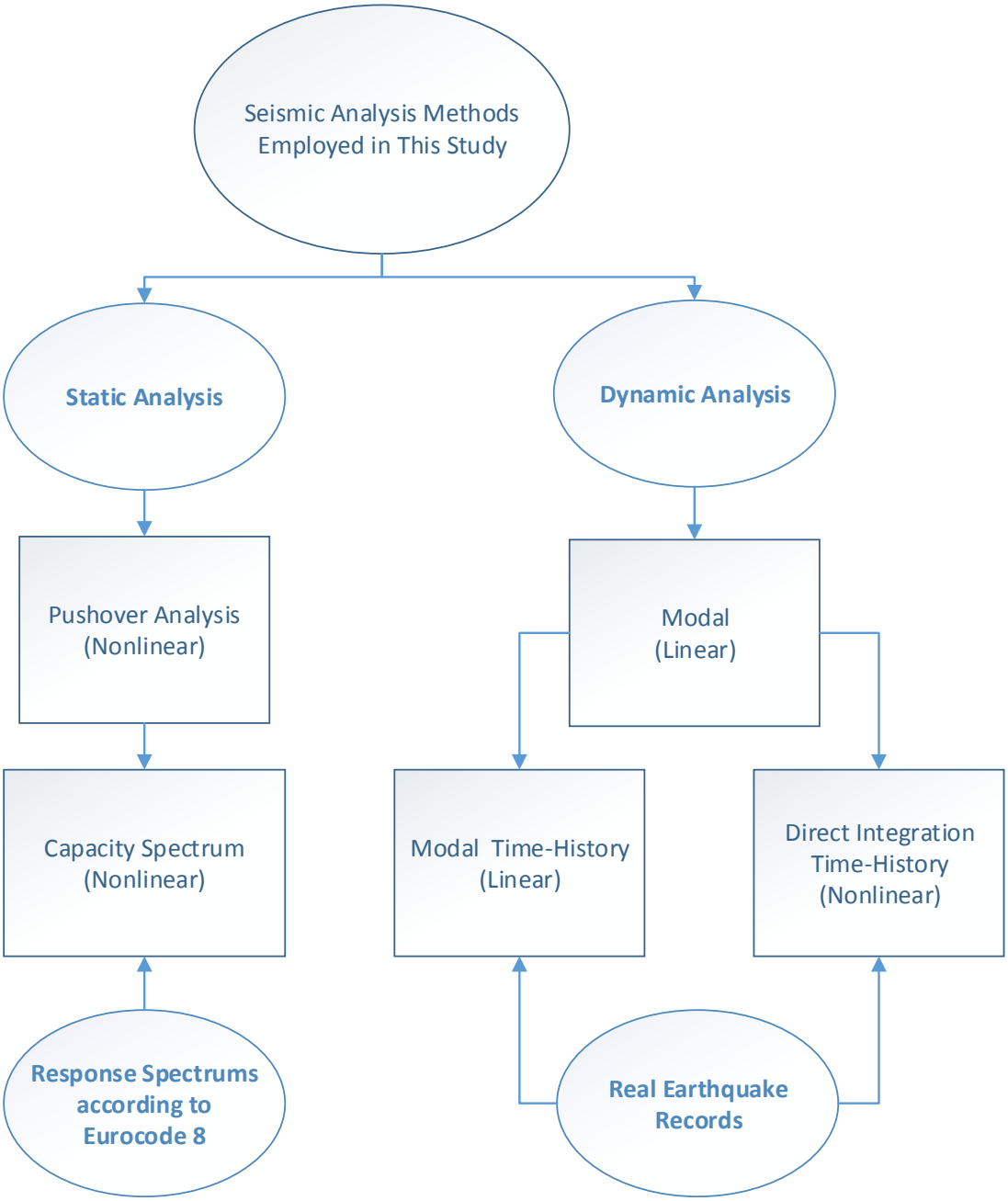

Figure 3.1. Seismic analysis methods employed in this study.

Modal analysis, or the mode-superposition method, is a linear dynamic response procedure which evaluates and superimposes free-vibration mode shapes to characterise displacement patterns of a particular structure. Mode shapes describe the configurations into which a structure will naturally behave. Typically, lateral displacement patterns are of primary concern. As orders increase, mode shapes contribute less, and are predicted less reliably.

Modal time history analysis is used for linear response of structures subjected to seismic excitations.

Finally, time history nonlinear direct integration dynamic analysis, also known as full time history analysis, is the most accurate method for finding the actual response of structures subjected to strong ground motions. This analysis technique is the most accurate and sophisticated method for validation and analysis of the actual nonlinear response of structures subjected to seismic loads.

3.4 Nonlinearities in reinforced concrete structure analysis

In general there two types of nonlinearities which can be observed in reinforced concrete structures that were considered for developing of FE models:

- geometric nonlinearity
- material nonlinearity

Geometric nonlinearity is the change in geometry where it significantly effects load deformation treatment in either the structure's elements (local) or the entire structure (global). Change in geometry could affect the analysis of the structure by changing the stiffness matrix hence change the equilibrium equation of the structure.

P-Δ effect is the most known geometric nonlinearity in structures. During severe earthquake loads elevated water tank experience large deformation at the top levels of concrete shaft combined with gravity load of the tank that resulted to global instability of the staging and failure of the entire structure could occur (Ghateh et al, 2015). Taller staging systems with large height to diameter ratio and larger tank capacities are more vulnerable to P-Δ effect (Figure 3.2(a)). Both P-Δ effect and large deformations were included in the FE nonlinear analyses.

On the other hand, material nonlinearity is associated with the inelastic behaviour of a component or system. Inelastic behaviour of materials was generated as a result of nonlinear stress-strain relationship and may be characterized by a force-deformation relationship. During a nonlinear static or dynamic analysis, stress level in shaft increases beyond the elastic limit of concrete and causes nonlinearity in stress-strain behaviour of materials as shown in Figure 3.2(b).

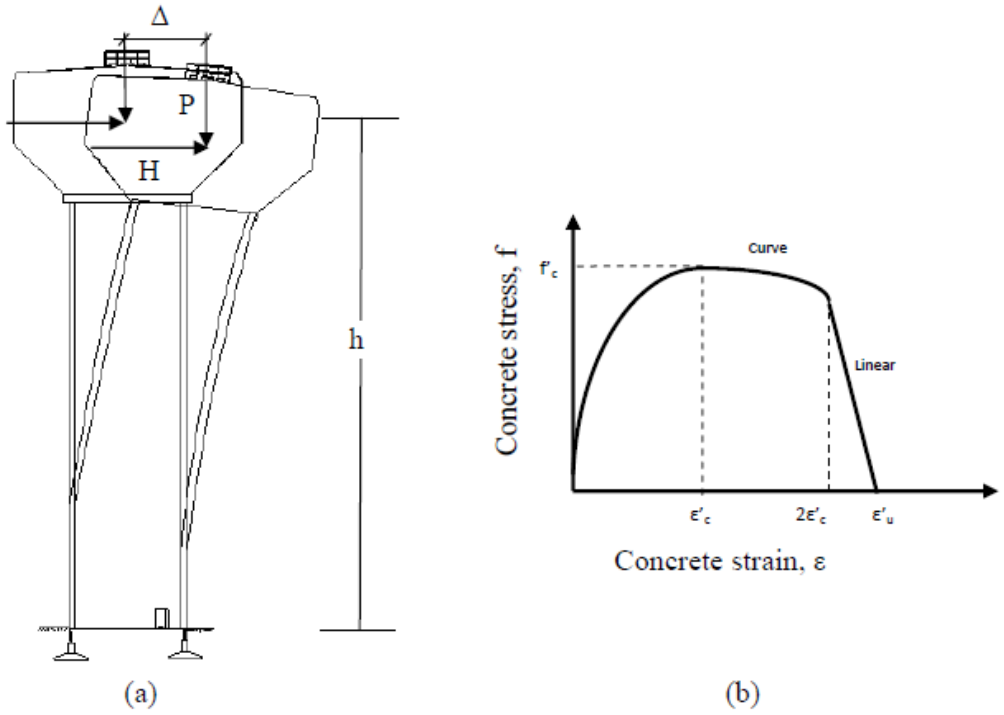

Figure 3.2. Type of nonlinearities; (a) geometric nonlinearity and (b) concrete nonlinearity (Ghateh, 2014)

3.5 Response spectrum design

Acceleration response spectrum of the structure defined in Eurocode 8 represents the horizontal design forces obtained from the maximum response acceleration of the structure, under the expected earthquake.

To develop an elastic response spectrum for an expected peak ground acceleration and soil type usually 5% damping for RC structures proposed by Eurocode 8 if not other damping is specified. Eurocode 8 suggests two different design spectrums, Type 1 (Figure 3.3) for the more seismically active regions of southern Europe, and Type 2 for the less seismic regions of central and northern Europe. Spectrum Type 1 refers to earthquake with magnitude higher than 5.5, while spectrum Type 2 is suitable

for earthquakes with magnitude less than 5.5. Furthermore, Eurocode 8 recommends different ground types to include soil structure interaction. The hardest ground, recommended by Eurocode 8, is soil type A, rock and the softest ground type is D, sand. Description of all ground types are provided in Table 3.1 and Figure 3.3 shows the difference between elastic response spectrums regarding a ground type.

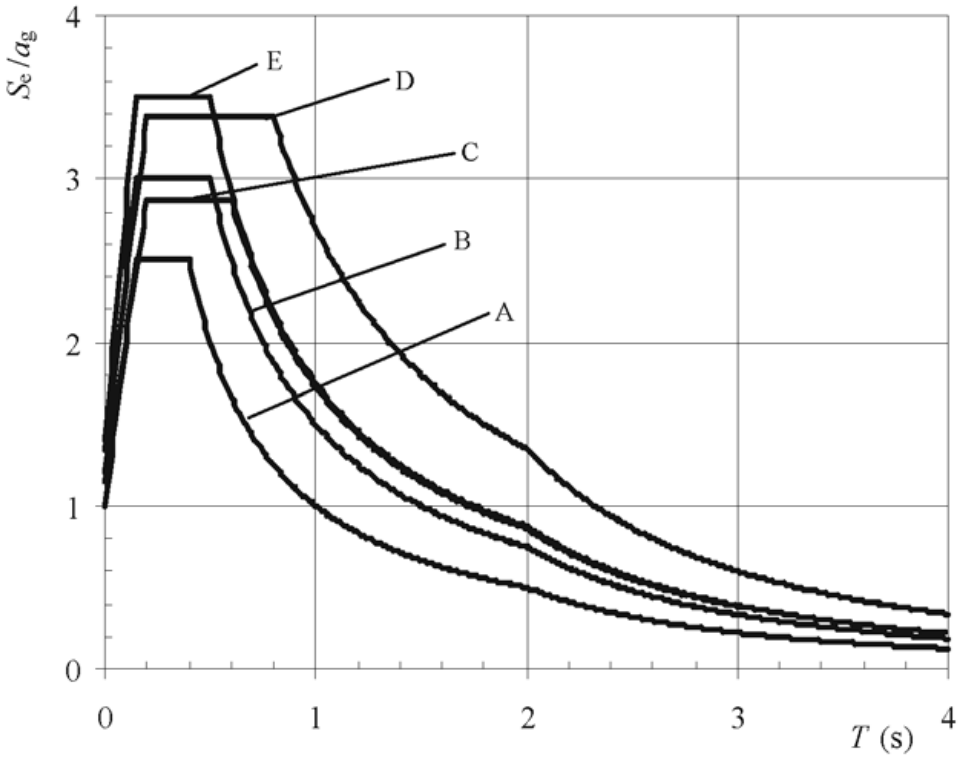

Figure 3.3. Recommended Type 1 elastic response spectra for ground types A to E for 5% damping (Eurocode 8: Part 1, 2004)

The elastic acceleration spectrum with a damping of 5% is graphically illustrated in Figure 3.4. It contains an area of constant spectral acceleration, between the periods T_B and T_C with a value 2.5 times the maximum soil acceleration $a_g S$. That period is followed by an area of constant spectral velocity between the periods T_C and T_D, where the spectral acceleration is proportional to 1/T. Finally, an area of constant spectral displacement beyond the period T_D, where the spectral acceleration is proportional to $1/T^2$.

Table 3.1 Ground Types (Eurocode 8: Part 1, 2004)

Ground type	Description of stratigraphic profile.
A	Rock or other rock-like geological formation, including at most 5 m of weaker material at the surface.
B	Deposits of very dense sand, gravel, or very stiff clay, at least several tens of metres in thickness, characterised by a gradual increase of mechanical properties with depth.
C	Deep deposits of dense or medium – dense sand, gravel or stiff clay with thickness from several tens to many hundreds of metres.
D	Deposits of loose-to-medium cohesionless soil (with or without some soft cohesive layers), or of predominantly soft-to-firm cohesive soil.
E	A soil profile consisting of a surface alluvium layer with vs values of type C or D and thickness varying between about 5 m and 20 m, underlain by stiffer material with vs > 800 m/s.

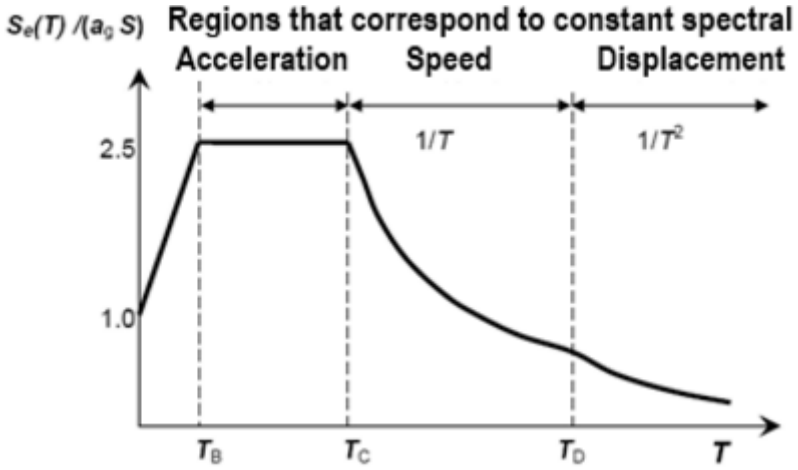

Figure 3.4. Elastic spectrum in the horizontal direction for a 5% damping (Fardis, 2009a)

Designing structures to remain elastic in large earthquakes it is uneconomic in most cases, as the force demands can be very large. A more economical design can be achieved by accepting some level of damage that making use of ductility a structure to reduce the force demands to acceptable levels (Williams, 2009).

Ductility is defined as the ability of a structure or a structural element to withstand large deformations beyond its yield point without failure. In earthquake engineering, ductility is expressed in terms of demand and supply. The ductility demand is the maximum ductility that a structure experiences during an earthquake, which is a function of both the structure and the earthquake. The ductility supply is the maximum ductility that a structure can sustain without failure.

The design response spectrum defined from the elastic response spectrum can be reduced according to factors that take into consideration the ability of the structure to absorb seismic energy through rigid deformations. In the areas of constant spectral acceleration, velocity and displacement the design spectrum originates can be obtained from an elastic response with a 5% damping divided by q, behaviour factor. Exceptionally, the increasing part for a vibration period from T up to $T \leq T_B$ comes from the linear interpolation between: (α) the maximum ground acceleration S_{ag}, divided by 1.5, that expresses overstrength compared with the design capacity and the fixed design acceleration, for $T = 0$ and (β) $2.5\ a_g/q$ for $T = T_B$. Moreover, there is a lower limit in the design spectral acceleration, equal to the 20% of the maximum acceleration on the rock, a_g (Fardis, 2009a).

The behaviour factor $\boldsymbol{q}$ in Equations 3.1 – 3.4 is an approximation of the ratio of the seismic forces that the structure would experience if its response was completely elastic with 5% viscous damping, to the seismic forces that may be used in the design, with a conventional elastic analysis model, still ensuring a satisfactory response of the structure (Borzi and Elnashai, 2000). It is assumed that an elevated water tank dissipates hysteretic energy during its response to an earthquake. The over strength, dissipation of energy by the tank-liquid system and the local plastic deformations which may occur are all considered with the use of a behaviour factor $q = 2.0$ for development of design response spectrums according to Eurocode 8: Part 4 (2006).

Using Equations 3.1 to 3.4 and the parameters of Table 3.2, design spectra for different seismicity conditions and subsoil classes can be created. The range between corner periods T_B and T_C constitutes the branch of constant spectral acceleration, whereas periods T_C and T_D are the limits of the constant spectral velocity branch. In addition, constant spectral displacement starts at control period T_D.

When $0 \leq T \leq T_B$: $$S_d(T) = a_g \cdot S \cdot \left[\frac{2}{3} + \frac{T}{T_B} \cdot \left(\frac{2.5}{q} - \frac{2}{3}\right)\right]$$ *Equation 3.1*

When $T_B \leq T \leq T_C$: $$S_d(T) = a_g \cdot S \cdot \frac{2.5}{q}$$ *Equation 3.2*

When $T_C \leq T < T_D$: $$S_d(T) = \begin{cases} a_g \cdot S \cdot \frac{2.5}{q} \cdot \left[\frac{T_C}{T}\right] \\ \leq \beta \cdot a_g \end{cases}$$ *Equation 3.3*

When $T_D < T$: $$S_d(T) = \begin{cases} a_g \cdot S \cdot \frac{2.5}{q} \cdot \left[\frac{T_C T_D}{T^2}\right] \\ \leq \beta \cdot a_g \end{cases}$$ *Equation 3.4*

Where:

$S_d(T)$	is the design response spectrum;
T	is the vibration period of a linear single-degree-of-freedom system;
a_g	is the design ground acceleration on type A ground ($a_g = \gamma_1 \times a_{gR}$);
T_B	is the lower limit of the period of the constant spectral acceleration branch;
T_C	is the upper limit of the period of the constant spectral acceleration branch
T_D	is the value defining the beginning of the constant displacement response range of the spectrum;
S	is the soil factor;
q	is the behaviour factor; for elevated tanks recommended value for q is 2.0
β	is the lower bound factor for the horizontal design spectrum. The recommended value for β is 0.2

Table 3.2. Values of the parameters describing the recommended Type 1 and Type 2 elastic response spectra (Eurocode 8: Part 1, 2004)

Soil Type	Soil factor S		Period T_B (s)		Period T_C (s)		Period T_D (s)	
	Type 1	Type 2	Type 1	Type 2	Type 1	Type 2	Type 1	Type 2
A	1.0	1.0	0.15	0.05	0.4	0.25	2.0	1.2
B	1.2	1.35	0.15	0.05	0.5	0.25	2.0	1.2
C	1.15	1.5	0.20	0.10	0.6	0.25	2.0	1.2
D	1.35	1.8	0.20	0.10	0.8	0.30	2.0	1.2
E	1.4	1.6	0.15	0.05	0.5	0.25	2.0	1.2

Data and figures for design spectrums developed by Eurocode 8 for soil types A, B, C and D are presented in Appendix C.1.

3.6 Static nonlinear (pushover) analysis

In case of structure deformation with yielding of structural elements, force-deformation relationship could not be determined using linear approaches, thus nonlinear analysis should be performed. One of the methods for obtaining inelastic relationship of a structure is the nonlinear static analysis, also known as a pushover analysis. Inelastic behaviour may be characterised by a force-deformation relationship, also known as a backbone curve, which measures strength against translational or rotational deformation (Chopra and Goel, 2002). The pushover analysis is a simple way for determining a force-deformation nonlinear response for a structure subject to incrementally increasing lateral forces or displacements (Figure 3.5). The general force-deformation relationship shown in Figure 3.6. Figure showed that once a structure achieves its yielding strength nonlinear response took place until the structure reaches ultimate strength and finally degradation of strength leads formation of a failure mechanism and therefore collapse of the structure.

Pushover analysis was introduced in the early 1980s (Saiidi and Sozen, 1981), however there were a number of modifications since that time. Originally, it was established as an analytical method for nonlinear analysis of structures for evaluating weak points and potential structural damages during seismic activity. Nowadays, pushover analysis is one of the most popular nonlinear analyses in seismic engineering suggested by many codes.

The nonlinear static analysis was documented as an acceptable method of analysis in Eurocode 8 (2004). The main advantage of the pushover analysis is avoiding the complexity of a time history analysis, however including important features of materials and geometry nonlinearities that are significant to seismic response (El-Tawil, et al., 2009).

The main purpose of conducting a pushover analysis in this thesis is to establish the base shear versus roof displacement curve that could provide valuable information regarding seismic response properties of structures. Maximum developed base shear, ductility of the structure and maximum deformation prior to collapse are among the most useful information that might be derived from pushover curve. Additionally, pushover curve is a capacity curve for capacity spectrum analysis which combined with response spectrums provides an information of structure performance subjected to particular earthquake.

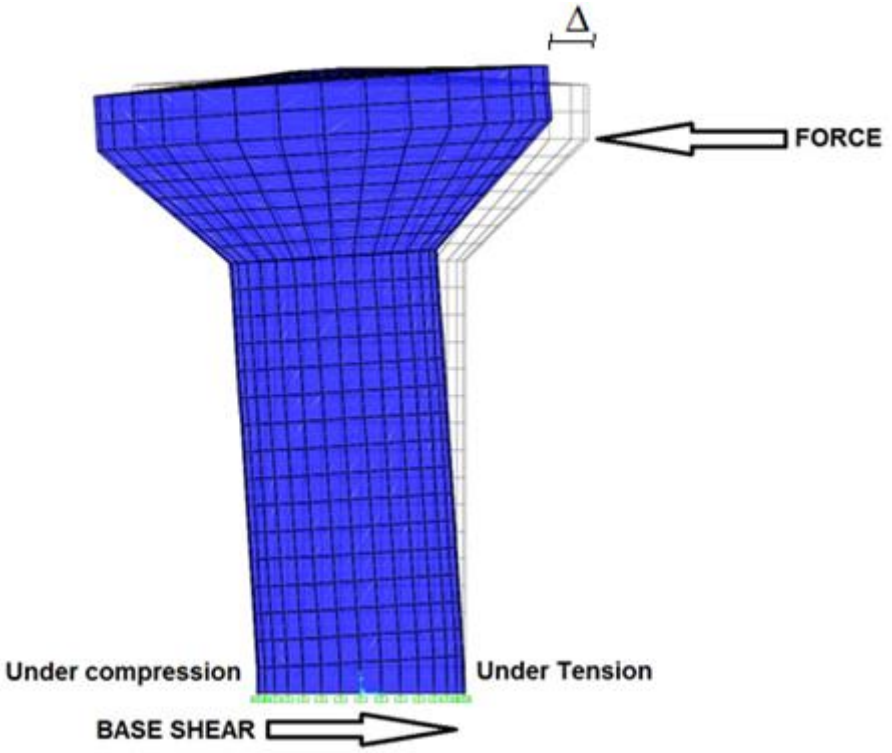

Figure 3.5. Typical RC elevated water tank subjected to pushover analysis

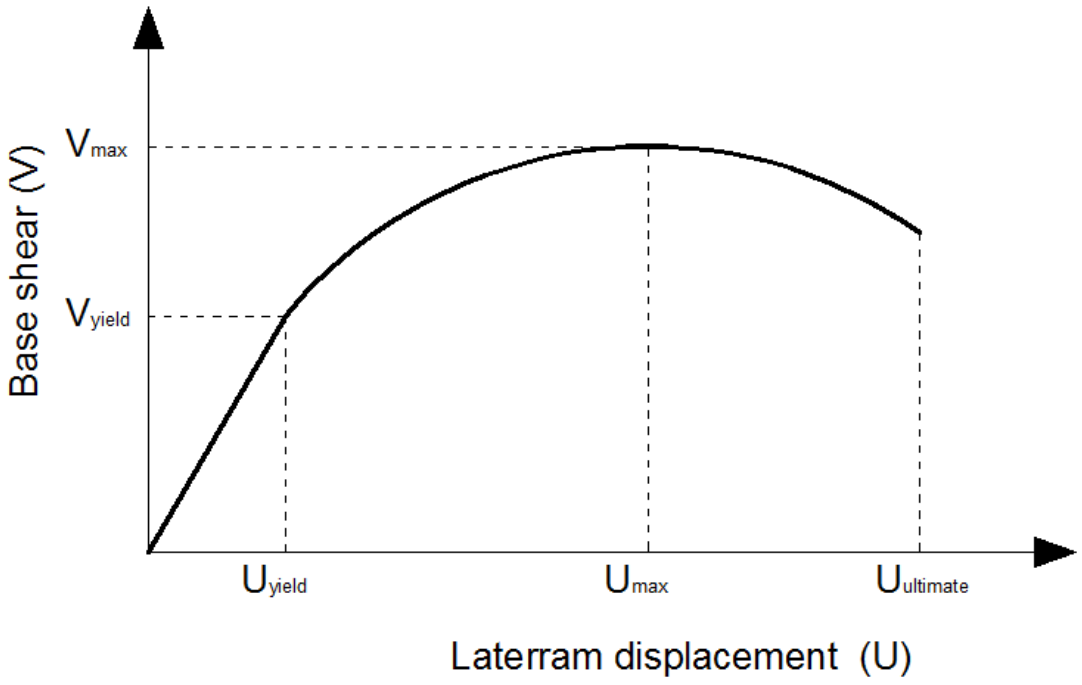

Figure 3.6. Typical pushover curve developed

3.6.1 Types of pushover analysis

In general there are two main types of pushover analysis known as conventional pushover analysis and adaptive pushover analysis (Elnashai, 2008). In conventional pushover analysis, which recommended by Eurocode 8 (2004) lateral load is applied to the structure with a specific load pattern. The analysis continues until the lateral displacement of control node reaches to a specific value which is called target displacement or the structure collapses. In these methods, only the effect of dominant mode is considered and distribution of force or displacement remains constant during the analysis. On the other hand, in adaptive pushover analysis which considering higher modes effects the force pattern can be changed in different steps of analysis.

Selection of the proper method of pushover analysis highly depends on the configuration of the structures. In an extensive investigation, Chopra and Goel (2002) concluded that adaptive analysis demonstrates better performance comparing to conventional analysis for irregular and high-raised structures. However, there was not any significant differences in obtained results for symmetrical and middle-raised structures whose behaviour was dominated by first mode response.

An elevated water tank is a symmetrical structure which acts as an inverse pendulum and often more than 80% of the weight concentrates in the tank. Thus, in these structures usually more than 90% of the total mass participates in the fundamental mode. Because of the domination of the first mode in the behaviour of elevated water tanks conventional pushover analysis is assumed to be suitable for this study.

3.6.2 Procedure of performing pushover analysis

In order to perform a pushover analysis, initially the gravity load is applied to the mathematical model of structure. Next according to the defined force pattern, the model is subjected to an incremental lateral force (Shinde, et al., 2014). To get reliable results, the applied force pattern should be similar to the force produced during seismic excitations.

Consequently, the lateral load is increased until either the displacement at controlling point reaches a target displacement or the structure collapses. At each increment level, the base shear along with the corresponding displacement at the controlling point is recorded. *Equation 3.5* shows the static equilibrium of the structure with small increments in linear region (Chopra and Goel, 2002):

$$\Delta F = K\Delta U \qquad \textit{Equation 3.5}$$

Where:

- ΔF is the incremental lateral load
- K is the stiffness
- ΔU is the incremental lateral displacement

Equation 3.5 can be rewritten by including the tangent stiffness matrix and accounting for nonlinear variation of both geometry and material in each load increment:

$$F = K_t\Delta U + R_t \qquad \textit{Equation 3.6}$$

Where:

- K_t is the target stiffness matrix
- R_t is the restoring forces at the beginning of each load increment as showed in *Equation 3.7*:

$$R_t = \sum_{i=1}^{j-1} K_{t,i}\Delta U_i \qquad \textit{Equation 3.7}$$

There are many numerical methods for solving the above equations from which the "Newton- Raphson" method was selected and employed in this research using FE software SAP2000. According to this method the load is divided into a number of load increments which can be applied during several load steps. In each step, after convergence of equations, the tangent stiffness matrix is revised and next load (or displacement) increment is applied. The increments continue until either the structure reaches to the target displacement or the integrations cease to converge (Chopra, 2007).

The equation of equilibrium of a nonlinear static system subjected to a loading denoted by vector {F} is:

$$\{F\} = [K]\{U\} \qquad \textit{Equation 3.8}$$

Where:

- $[K]$ is the stiffness matrix
- $\{U\}$ is the displacement vector

For one iteration, the equation of equilibrium can be written as:

$$\left[K_i^T\right]\{\Delta U_i\} = \{F^a\} - \{F_i^r\} \qquad \textit{Equation 3.9}$$

$$\{U_{i+1}\} = \{U_i\} + \{\Delta U_i\} \qquad \textit{Equation 3.10}$$

Where:

$\left[K_i^T\right]$ is the tangent or Jacobian matrix;
$\{F_i^r\}$ is the restoring load;
i is the index indicating the current iteration vector.

The following algorithm should be employed until the convergence is achieved:

1. Initial state: assume U_0 , at the beginning U_0 is usually $\{0\}$

2. Calculation for each iteration:

- Calculate Jacobian matrix $\left[K_i^T\right]$ and restoring vector $\{F_i^r\}$ for the current step
- Calculate ΔU_i
- Substitute ΔU_i in *Equation 3.10* and find ΔU_{i+1}

3. Repeat step 2 until the convergence is attained.

3.7 Capacity spectrum analysis

In this study elevated water tanks were analysed using capacity spectrum method suggested by N2 (Eurocode 8: Part 1, 2004) and ATC-40 (ATC, 2010). Capacity spectrum method is simple nonlinear method used for calculation of structures subjected to seismic loads. Capacity spectrum method can be considered as combination of pushover analysis and response spectrum analysis. Inelastic demanded spectrum is obtained from elastic spectrum. The accuracy of the method is satisfactory if the structure had dominant first mode of oscillation, such as elevated water tank (Zahenter, 2006).

The capacity spectrum method requires that both the capacity curve (pushover curve) and the demand curve (response spectrum) are represented in response spectral ordinates. It characterises the seismic demand initially using a 5% damped linear-elastic response spectrum and reduces the spectrum to reflect the effects of energy

dissipation to estimate the inelastic displacement demand. The point at which the capacity curve intersects the reduced demand curve represents the performance point at which capacity and demand are equal (Chopra and Goel, 2002). Evaluation of performance point shown in Figure 3.7. The location of this performance point relative to the performance levels defined by the capacity curve indicates whether or not the performance objective is met.

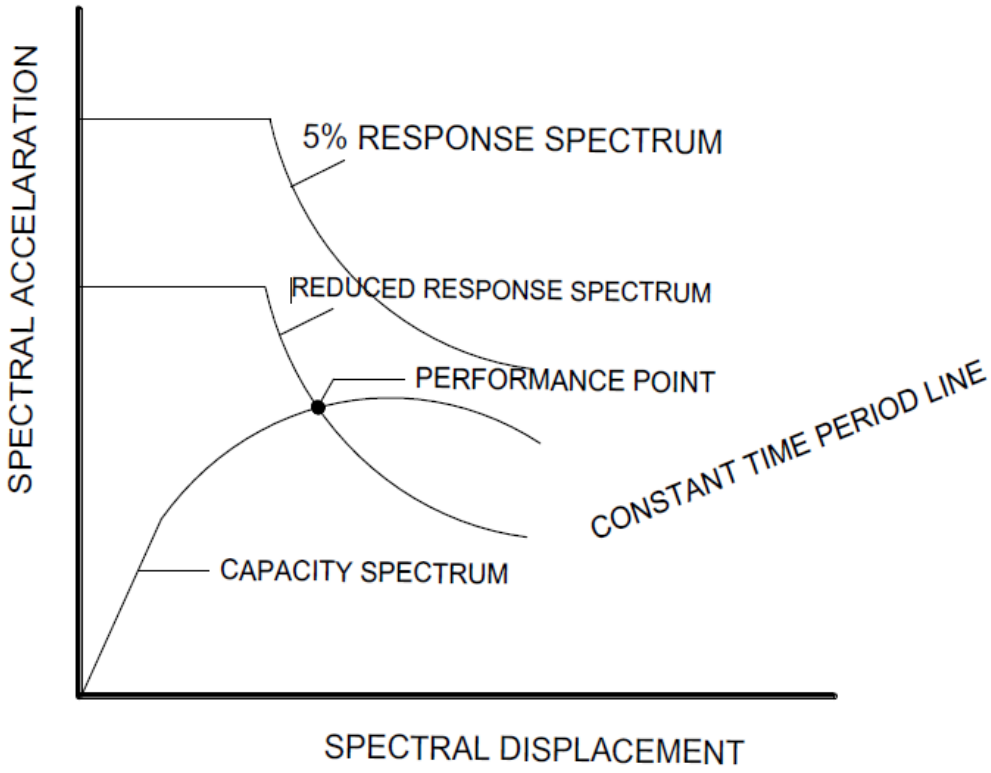

Figure 3.7. Evaluation of a performance point (Rajesh and Prasad, 2014)

The employment of the non-linear static procedure involves four distinct phases as described below and illustrated in Figure 3.8 (Bento et al, 2004):

- Define the mathematical model with the non-linear force deformation relationships for the various components/elements;
- Define a suitable lateral load pattern and use the same pattern to define the capacity of the structure;
- Define the seismic demand in the form of an elastic response spectrum;
- Evaluate the performance of the building.

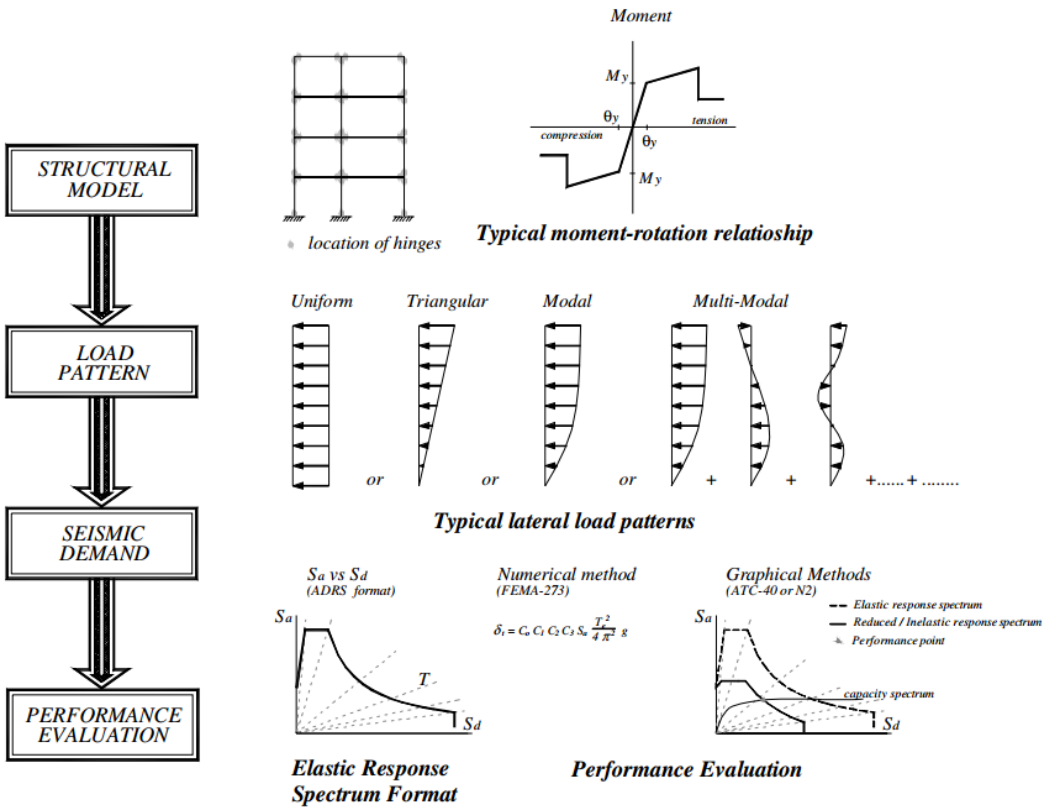

Figure 3.8. General flowchart for capacity spectrum analysis (Bento et al, 2004)

3.8 Nonlinear dynamic analysis

The most realistic behaviour of structures subjected to seismic loading can be observed conducting dynamic time history analysis, also known as transient analysis, with real ground motion records applied on the structure (Haselton, et al, 2012). The main difference between time history analyses from other analyses is that the inertial forces directly determined from the ground motions and the responses of the structure are calculated as a function of time, considering the dynamic properties of the building structure (Chopra, 2007). This makes transient analysis method different from all of the other approximate analysis methods.

Nonlinear dynamic time history analysis is the most accurate method for seismic analysis of structures since effects of damping, inertia forces of higher modes of vibration, hysteresis behaviour of material, material nonlinearity and velocity of masses could be considered in analysis, while static analysis cannot consider these parameters. Moreover, linear time history analysis cannot consider effects such as higher modes of vibration, damping of material and geometrical and material nonlinearity. In this research the dynamic time history nonlinear method is employed.

Although all advantages, a time history analysis is being highly demanding in terms of computational time. In next sections the computational theory of time history analysis is explained.

3.8.1 Equation of motion of a SDOF system subjected to force P(t)

Using D'Alembert principle, a state of dynamic equilibrium can be defined by assuming that a fictitious inertial force f_I acts on the mass during motion (Chopra, 2007). The D'Alembert principle is showed in Figure 3.9, which illustrates that the dynamic external force of a mass equal to sum of the internal, elastic and damping forces. Equation 3.11 represents that principle:

$$p(t) = f_I(t) + f_D(t) + f_S(t) \qquad \textit{Equation 3.11}$$

Where:

- $p(t)$ is the dynamic external force applied to the mass
- $f_I(t)$ is the inertial force, can be represented as product of mass and acceleration ($f_I = m\ddot{u}$)
- $f_D(t)$ is the viscous damping mechanism, may be also expressed as the product of velocity and damping constant ($f_D = c\dot{u}$).
- $f_S(t)$ is the stiffness force, can be rewrite as the product of structure stiffness and displacement ($f_S = ku$).

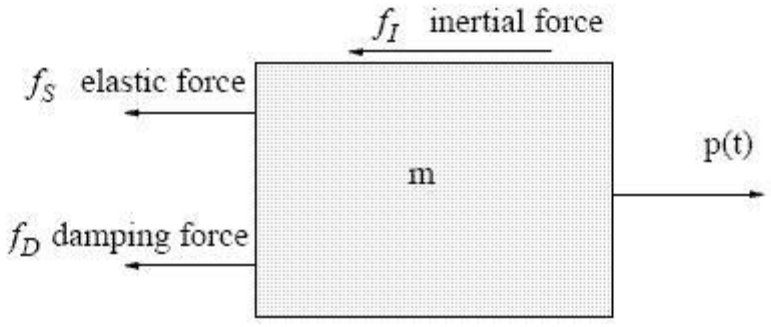

Figure 3.9. D'Alembert principle (Chopra, 2007)

By replacing the above terms in Equation 3.11 the equation of motion of a SDOF system subjected to a force $P(t)$ can be rewritten by Equation 3.12 and it is illustrated in Figure 3.10.

$$p(t) = m\ddot{u}_g(t) + c\dot{u}(t) + ku(t)$$ *Equation 3.12*

Where:

m	is the mass of a SDOF system
c	is the damping constant of a SDOF system
k	is the stiffness of a SDOF system
$\{u\}$	is the displacement
$\{\dot{u}\}$	is the velocity
$\{\ddot{u}\}$	is the acceleration

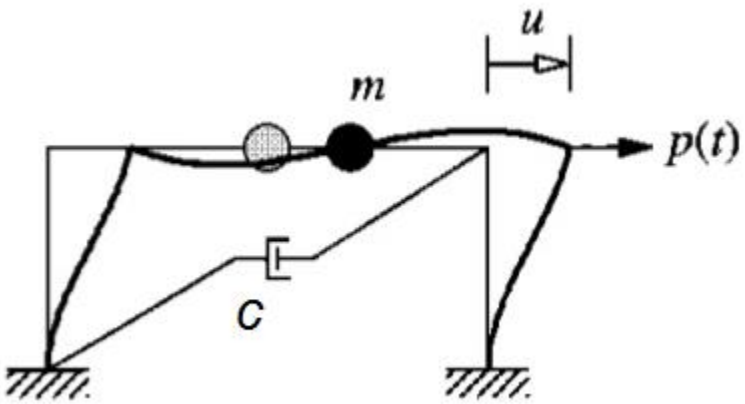

Figure 3.10. SDOF system (Chopra, 2007)

3.8.2 Equation of motion of a SDOF system subjected to seismic excitations

Equation of motion of a SDOF structure subjected to seismic excitations could be formulated in quite the same fashion as for external load. The seismic motion affects the structure by imposing horizontal ground motions at the support level. The equation of dynamic equilibrium of these forces using D'Alembert principle in Equation 3.11 could be expressed as:

$$f_I(t) + f_D(t) + f_S(t) = 0$$ *Equation 3.13*

Assume that $u^t(t)$ represents the total displacement of the system respecting to the original location of structure that gives:

$$u^t(t) = u(t) + u_g(t)$$ *Equation 3.14*

Subsequently by substituting Equation 3.14 in Equation 3.13 and performing the appropriate derivations combined with D'Alembert principle, Equation 3.6 can be expressed as:

$$m\ddot{u}(t) + m\ddot{u}_g(t) + c\dot{u}(t) + ku(t) = 0 \qquad \textit{Equation 3.15}$$

Finally rearranging Equation 3.15 by moving $M\ddot{u}_g(t)$ to the right side of the equation:

$$m\ddot{u}(t) + c\dot{u}(t) + ku(t) = -m\ddot{u}_g(t) = p(t) \qquad \textit{Equation 3.16}$$

Where:

$p(t) = -m\ddot{u}_g(t)$ is the effective force at the support

By comparison Equation 3.11 and 3.16 it can be observed that response of a SDOF system subjected to a ground motion $\ddot{u}_g(t)$ is the same as the one subjected to an external force $P(t)$.

3.8.3 Equation of motion of a multi-degree-of-freedom system

Usually analysing structures SDOF does not provide an adequate accuracy for modelling dynamic response. Despite most of the weight concentrated in the water tank, an elevated water tank may not give a realistic dynamic response using SDOF assumption because the other weights, such as a shaft and a tank slab should also be taken into account. In this case multi degree of freedom (MDOF) system should be used. The example of three mass approximation of an elevated water tank is shown in Figure 3.11.

The dynamic equations of motion for a MDOF employed the same principle as SDOF equation of motion. However, Instead of scalars used in the Equation 3.16, vectors and matrices were used (Chopra, 2007). The MDOF system shown in Figure 3.12 which can be summarised in Equation 3.17.

$$[M]\{\ddot{U}\} + [C]\{\dot{U}\} + [K]\{U\} = -[M]\{J\}\ddot{U}_g \qquad \textit{Equation 3.17}$$

Where:

$[M]$ is the mass matrix

$[C]$ is the damping matrix

$[K]$ is the stiffness matrix

$\{U\}$ is the displacement vector

$\{\dot{U}\}$ is the velocity vector

$\{\ddot{U}\}$ is the acceleration vector

N is the differential equations in which N represents the number of degrees of freedom.

$\{J\}$ is the influence vector which contains 1 and 0. Number 1 is assigned to horizontal degree of freedom and 0 is assigned to vertical and rotational degrees of freedom.

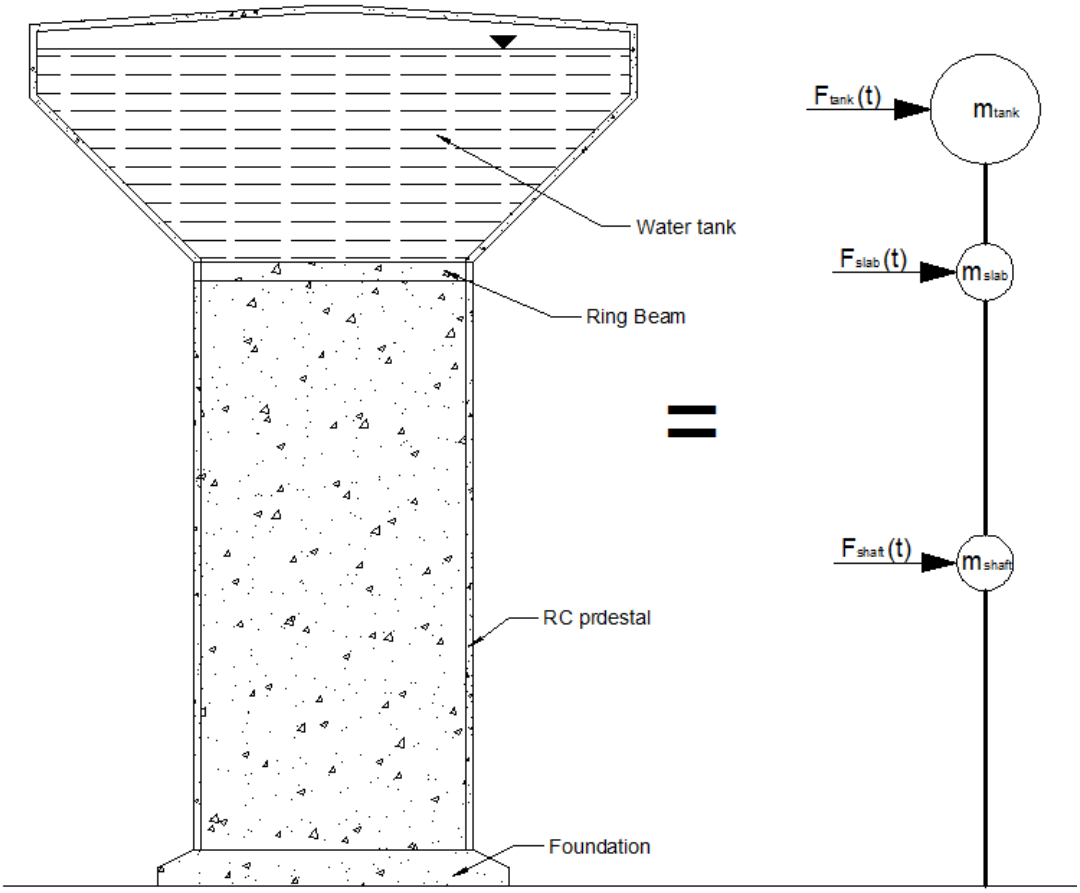

Figure 3.11. Idealised MDOF model of RC elevated water tank with only horizontal degrees of freedom

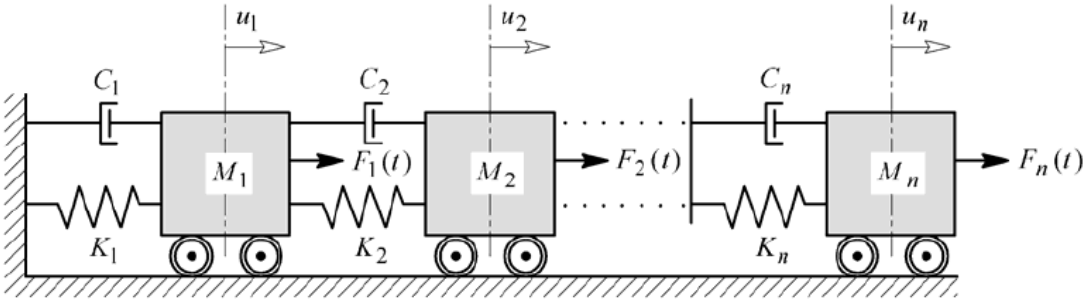

Figure 3.12 Classic MDOF system (Chopra, 2007)

3.8.4 Equation of motion of a nonlinear system

In previous sections, the equations of motion of a seismically excited system were developed assuming the linear response. The material nonlinearity and therefore variation of stiffness was not taken into account. However in reality during severe earthquakes structures excide linear strength and nonlinear response occur. The nonlinear equation of motion of MDOF system is described in this section.

In order to define the equation of motion of MDOF system for a nonlinear system, equation of motion of a MDOF elastic system (Equation 3.17) can be developed (Villaverde, 2009). In the Equation 3.17, matrices [C] and [K] are dependent variables of time. In order to consider effects of nonlinearity, matrices [C] and [K] should be represented in a vector form as $[C(t)] = \{F_D(t_i)\}$ and $[K(t)] = \{F_S(t_i)\}$ respectivelly. The equation of motion of such system at time t_i is:

$$[M]\{\ddot{U}(t_i)\} + \{F_D(t_i)\} + \{F_S(t_i)\} = -[M]\{J\}\ddot{U}_g(t_i) \qquad \textit{Equation 3.18}$$

Where:

$$t_i = \tau = i\Delta t$$

Where:

τ	is the small time variable between 0 and Δt.
Δt	is the small time increment
i	is the integer

Assume that time $t = t_i + \tau$, by rearranging Equation 3.18:

$$[M]\{\ddot{U}(t_i + \tau)\} + \{F_D(t_i + \tau)\} + \{F_S(t_i + \tau)\} = -[M]\{J\}\ddot{U}_g(t_i + \tau) \qquad \textit{Equation 3.19}$$

Also it can be accepted that properties of the MDOF system does not change with small time increment Δt, that gives:

$$\{F_S(t_i + \tau)\} = \{F_S(t_i)\} + [K]_i\{\Delta U(\tau)\} \qquad \textit{Equation 3.20}$$

$$\{F_D(t_i + \tau)\} = \{F_D(t_i)\} + [C]_i\{\Delta \dot{U}(\tau)\} \qquad \textit{Equation 3.21}$$

Accept that stiffness matrix $[K]_i$ and damping matrix $[C]_i$ in the Equations 3.20 and 3.18 are the properties of the MDOF system at the beginning of the interval, so equations can be rewritten and acceleration vector can be expressed by same method as displacement and velocity vectors:

$$\{\Delta U(\tau)\} = \{U(t_i + \tau)\} - \{U(t_i)\} \qquad \textit{Equation 3.22}$$

$$\{\Delta \dot{U}(\tau)\} = \{\dot{U}(t_i + \tau)\} - \{\dot{U}(t_i)\} \qquad \textit{Equation 3.23}$$

$$\{\Delta \ddot{U}(\tau)\} = \{\ddot{U}(t_i + \tau)\} - \{\ddot{U}(t_i)\} \qquad \textit{Equation 3.24}$$

As a result the Equation 3.26 might be rewritten using Equations 3.22, 3.23 and 3.24 that provide:

$$[M]\{\ddot{U}(t_i + \tau)\} + \{F_D(t_i)\} + [C]_i\{\Delta \dot{U}(\tau)\} + \{F_S(t_i)\} + [K]_i\{\Delta U(\tau)\} == -[M]\{J\}\ddot{U}_g(t_i) - [M]\{J\}\ddot{U}_g(\tau) \qquad \textit{Equation 3.25}$$

Finally by combination of Equation 3.19 and Equation 3.25, the equation of motion of MDOF nonlinear system can be expressed as:

$$[M]\{\ddot{U}(\tau)\} + [C]_i\{\Delta \dot{U}(\tau)\} + [K]_i\{\Delta U(\tau)\} = -[M]\{J\}\ddot{U}_g(\tau) \qquad \textit{Equation 3.26}$$

Where:

$\{\Delta U(\tau)\}$ is the differential equation with the incremental displacement factor

The value of the displacement vector at the end of the time interval $\{U(t_i + \tau)\}$ can be found by solving Equation 3.33.

The most effective way to include the effects of nonlinearity in dynamic analysis is a time domain solution, which is also known as response history analysis. This approach is based on step-by-step integration. In the step-by-step method the loading and the response history are divided into series of intervals (Yu, et al., 2012). The response during each time increments is calculated from initial condition. Furthermore, the structural properties are assumed to be constant and the equation of motion remains elastic in each time increment Δt.

In case of performing a nonlinear dynamic analysis the equations are adjusted for the effects of geometrical and material nonlinearity in time increments by modifying the tangent stiffness matrix. However, for linear dynamic analysis, these properties remain the same during all time intervals.

The step-by-step method could be conducted by employing either explicit or implicit approach (Vedge, 2004). In an explicit method, the new response values calculated in each time increment only depend on the response properties at the beginning of the step.

On the other hand, in the implicit method, the new response values for a time increment has one or more values related to the same step and as a result it requires a trial value and successive iterations are necessary.

In this study, implicit method is employed for the nonlinear response history analysis of elevated water tanks. Many numerical solution methods have been developed and can be found in the literature to solve nonlinear MDOF system. SAP2000 employs the Newmark method along with Newton-Raphson approach to solve MDOF equation of motion (Equation 3.17)

The matrices and vectors in Equation 3.17 were explained in previous sections. According to Newmark method (Chopra, 2007), velocity and displacement vectors at the time t_{n+1} can be calculated based on Equations 3.27 and 3.28 respectively:

$$\{\dot{U}_{n+1}\} = \{\dot{U}_n\} + [(1-\delta)\{\ddot{U}_n\} + \delta\{\ddot{U}_{n+1}\}]\Delta t \qquad \textit{Equation 3.27}$$

$$\{U_{n+1}\} = \{U_n\} + \{U_n\}\Delta t + \left[\left(\frac{1}{2} - \alpha\right)\{\ddot{U}_n\} + \alpha\{\ddot{U}_{n+1}\}\right]\Delta t^2 \qquad \textit{Equation 3.28}$$

Where:

α and δ	are the Newmark integration parameters
$\Delta t = t_{n+1} - t_n$	is the time increment

At time t_{n+1} Equation 3.17 can be written as:

$$[M]\{\ddot{U}_{n+1}\} + [C]\{\dot{U}_{n+1}\} + [K]\{U_{n+1}\} = -[M]\{J\}\ddot{U}_g \qquad \textit{Equation 3.29}$$

By rearranging Equations 3.27 and 3.28 and adjusting for Equation 3.29, acceleration and velocity at time t_{n+1} can be represented as:

$$\{\ddot{U}_{n+1}\} = a_0(\{U_{n+1}\} - \{U_n\}) - a_2\{\dot{U}_n\} - a_3\{\ddot{U}_n\} \quad \textit{Equation 3.30}$$

$$\{\dot{U}_{n+1}\} = \{\dot{U}_n\} - a_6\{\ddot{U}_n\} + \alpha_7\{\ddot{U}_{n+1}\} \quad \textit{Equation 3.31}$$

Substituting $\{\ddot{U}_{n+1}\}$ in Equation 3.31 and combining the results with Equation 3.29 results in an equation which can be solved for $\{U_{n+1}\}$. Finally, $\{U_{n+1}\}$ can be substituted in Equations 3.30 and 3.31 in order to update velocity and acceleration vectors. This solution method is stable if Equation 3.38 satisfied:

- $\alpha \geq \frac{1}{4}\left(\frac{1}{2} + \delta\right)^2$
- $\delta \geq \frac{1}{2}$
- $\frac{1}{2} + \delta + \alpha > 0$

Convergence of the structural system highly depends on the selection of time steps, meshing sizes and geometry of the structure.

3.9 Modal Analysis

Equation of motion of MDOF dynamic systems can be solved either in time domain or frequency domain (Chopra, 2007). The most widely used frequency domain is modal analysis. In modal analysis, MDOF equations of motion are represented by a number of SDOF systems. Each SDOF system is solved and the responses are combined using certain algebraic methods.

The responses over time of a structure subjected to an earthquake can be determined using the modal analysis, also known as free vibration analysis. A structure has many modes corresponding to different frequencies. Each eigenfrequencies triggers the building into movement in a curtain way. In modal analysis the responses from each mode up to a cut off frequency are combined to obtain the total response.

Eurocode 8 requires that the following rules should be met:

- The sum of the effective modal masses for the modes taken into account amounts must be at least 90% of the total mass of the structure.

- All modes with greater than 5% total mass participation must be taken into account.

A free vibration analysis is done on a multi-degree-of-freedom (MDOF) system without damping to find the fundamental frequencies. The arbitrary structure's equation of motion in free vibration formulated as equation 3.32 (Chopra, 2007):

$$[M]\{\ddot{U}\} + [K]\{U\} = 0 \qquad \textit{Equation 3.32}$$

Where:

$[M]$ is the mass matrix
$[K]$ is the stiffness matrix
$\{U\}$ is the displacement vector
$\{\ddot{U}\}$ is the acceleration vector

A harmonic solution of the displacement vector can be written in a form:

$$\{U\} = Acos(w_n t)\Phi \qquad \textit{Equation 3.33}$$

Where:

Φ is the mode shapes
A is the constant

Acceleration vector in respect to time t results in:

$$\{\ddot{U}\} = -\omega_n^2 Acos(w_n t)\Phi \qquad \textit{Equation 3.34}$$

By replacing displacement and acceleration vectors as well as angle frequency $\omega = 2\pi f$ into Equation 3.32, the homogeneous system can be rewritten as:

$$([K] - (2\pi f_n)^2[\mathrm{M}])\Phi = 0 \qquad \textit{Equation 3.35}$$

The fundamental frequencies in an eigenfrequencies problem can be found using Equation 3.35. The eigenfrequencies problem has a trivial solution for an equation system with a determinant equivalent to zero as shown in Equation 3.36.

$$det([K] - (2\pi f_n)^2[\mathrm{M}]) = 0 \qquad \textit{Equation 3.36}$$

The modes shapes equal to eigenfrequencies obtained from Equation 3.36. The response for each mode is found when the mode shapes and corresponding fundamental frequencies are known. Modal coordinates can be found by:

$$\{U\} = \sum_{i=1}^{N} \phi_i q_i(t) = [\Phi]q \qquad \textit{Equation 3.37}$$

Where:

$[\Phi]$ is the modal matrix containing the mode shapes of the system

q is the modal coordinates

Equation 3.17 of motion of a MDOF system can be rewritten using modal coordinates from Equation 3.37 and multiplied by Φ^T:

$$\sum_{i=1}^{N} \phi_n^T[M]\phi_n\ddot{q} + \sum_{i=1}^{N} \phi_n^T[C]\phi_n\dot{q} + \sum_{i=1}^{N} \phi_n^T[K]\phi_n q = -\phi_n^T[M]\{J\}\ddot{u}_g \qquad \textit{Equation 3.38}$$

This equation is solved for eigenvalues up to the cut of mode N. In order to determine the modes of vibration, the following mechanism should be employed:

1. Assembly of the element stiffness and mass matrices to form the global matrices.
2. Solve the eigenvalue problem to obtain frequency of vibration.

3.10 Rayleigh Damping

Rayleigh damping is the viscous damping that is proportional to a linear combination of mass and stiffness. Calculation of viscous damping is a very difficult procedure and only can be estimated from laboratory or field tests on the structure. In most cases, modal damping is used in the computer model to visualize the nonlinear energy dissipation of the structure (Chopra, 2007). Another approximation to assume that damping is proportional to mass and stiffness called Rayleigh damping method is a very common way to introduce damping in the analysis of the structures. This method reduces the difficulties of applying the damping matrix based on the physical properties of the structures (Adhikara, 2000). It should be noted that Rayleigh

damping varies with frequency; whereas, modal damping is constant for all frequencies.

Rayleigh damping is a classical method for constructing the damping matrix within the structure using the following equation:

$$[C] = \alpha[M] + \beta[K] \qquad \textit{Equation 3.49}$$

Where:

- $[M]$ is the mass matrix
- $[K]$ is the stiffness matrix
- α is the scale factor determined based on the fundamental frequency of the fundamental sloshing mode and accounts for the damping due to sloshing on the liquid free surface.
- β is the scale factor determined based on the fundamental frequency of the tank and simulates the damping due to the impulsive component.

The damping ratio for each mode i can thereafter be calculated from Equation 3.40:

$$\zeta = \frac{\alpha}{2\omega_i} + \frac{\beta\omega_i}{2} \qquad \textit{Equation 3.40}$$

Where:

- ζ is the ratio of actual damping to critical damping for a particular mode of vibration, i.
- ω_i is the natural circular frequency of mode i .

The fundamental frequencies corresponding to the fundamental convective and impulsive modes are obtained through finite element analysis and are used to determine the damping constants α and β.

Figure 3.13 shows the schematic variation of Rayleigh damping with respect to damping ratio ζ and natural circular frequency ω.

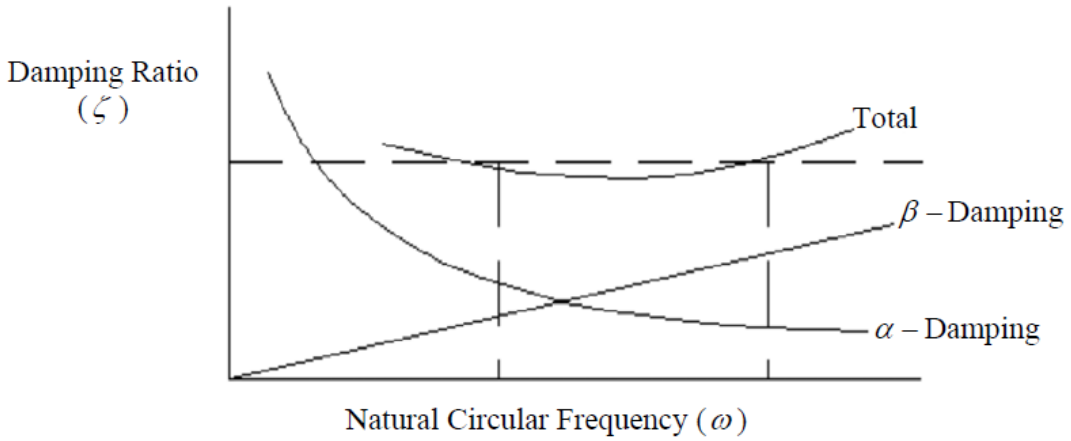

Figure 3.13. Rayleigh damping (Chopra, 2007)

As suggested by EC-8, the damping ratios of 0.5 and 5 percent are assigned for the convective and impulsive components, respectively. Furthermore, the stiffness proportional damping equivalent to 5 percent of critical damping is assumed as structural damping.

3.11 Water modelling

The main dynamic effect of liquid sloshing is a horizontal oscillation of the liquid waves in a tank. If a tank with liquid is subjected to horizontal ground acceleration, the forces employed on the tank wall can be divided into two components. The first component which rigidly moves together with a tank structure referees to impulsive force and the second component which corresponds to the liquid sloshing referees to convective force (Housner, 1963).

Impulsive and convective components can be equally well represented by an equivalent mechanical model as illustrated in Figure 3.14. The impulsive component is rigidly attached to the tank walls, however convective component is connected to the rigid walls by two springs. This model has been established by Housner (1963). The mechanical model shows that a horizontal motion of the tank causes the liquid to slosh. However, vertical oscillation of the tank does not have an influence on the liquid.

Figure 3.14(a) shows a slosh wave that has one peak and one valley. This is the fundamental antisymmetric wave, and it has the lowest fundamental frequency. Waves with two or more peaks or valleys with higher fundamental frequencies can also occur. The mechanical model shown in Figure 3.14(b) can represent these higher

order waves by incorporating an additional spring mass for each mode. The magnitudes of the spring mass for these modes are very small compared to the fundamental mode and, thus, higher order modes are usually of little concern and are neglected.

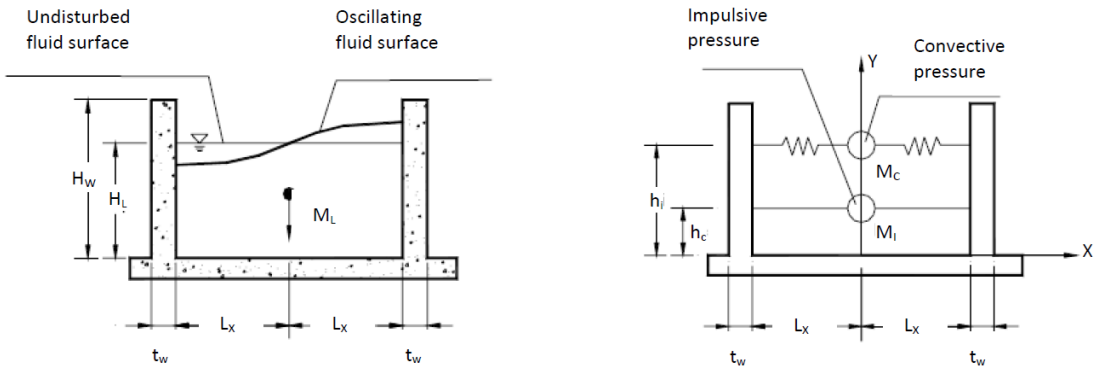

Figure 3.14. Mechanical model of dynamic behaviour of liquid (Housner, 1963)

Combination of impulsive and convective forces resulted in hydrodynamic pressure. The hydrodynamic pressure varies along the height of the tank wall and along the perimeter of the wall, with maximum pressure obtained in the direction of excitation while zero hydrodynamic pressure is obtained perpendicular to the direction of excitation (Chaduvula, et al., 2012). The inertia effect of the wall during horizontal motion is also considered and the computation of each component is discussed in the following sections with reference to Eurocode 8: Part 4 (2006).

3.11.1 Fundamental Period

The determination of the fundamental period, also known as fundamental period of a water-retaining structure subjected to earthquake excitation is of critical importance because the majority of tank failures under seismic loads resulted by a resonance effect (Nachtigall, 2003).

Determination of a fundamental period of a water tank is a significant problem in which a number of different aspects should be considered, such as the flexibility of tank walls, the influence of the contained liquid on the behaviour of the tank, the support system and soil conditions.

Housner (1963) concluded that the behaviour of the liquid in a water tank can be accurately represented with the use of two components known as the impulsive and convective component respectively. The impulsive component satisfies the boundary conditions in tank walls but does not include the effect of the liquid sloshing. Sloshing of the liquid results in a nonzero pressure at the original surface of the liquid and the convective component satisfies this condition without altering the boundaries of the impulsive component.

The fundamental periods of the impulsive and convective components differ significantly that results in a weak coupling of convective and impulsive components. Because combination of both components is insufficient, components should be evaluated separately.

It is mentioned in Eurocode 8: Part 4 (2006) that the fundamental mode shape of a water retaining structure is similar to the fundamental mode shape of a vertical cantilever beam. This assumption of Eurocode 8 is of great importance because cross-section wall remains in same shape during oscillation and no deformation of the cross-section is considered. This is a critical point, since the higher modes of vibration associated with deformation of the cross-section are neglected for the purpose of estimating a fundamental period.

For assessment of fluid-structure interaction the liquid in a water tank should be modelled by two SDOF systems represented impulsive and convective components. The impulsive component of the liquid is considered to move rigidly with the tank wall. In the case of rigid structures the motion of the tank-liquid system is the same as the ground motion. Impulsive fundamental period of elevated water tanks can be calculated according to Eurocode 8 using Equation 3.41.

$$T_i = 2\pi \sqrt{\frac{m}{K_s}} \qquad \textit{Equation 3.41}$$

Where:

- T_i is the fundamental impulsive period of the tank-liquid system
- m is the mass of impulsive component, mass of container and one-third mass of staging

K_S is the lateral stiffness of the staging,

$$K_s = \frac{3EI}{L^3} \qquad \textit{Equation 3.42}$$

Where:

L is the height to the centre of the tank

E is the modulus of elasticity of tank material

I is the second moment of inertia of the staging

On the other hand, the convective component represents the sloshing motion of the liquid and has a different fundamental period than the ground motion impulsive component of the tank. A large difference can be observed between convective and impulsive fundamental periods and the convective component is not influenced by the flexibility of the tank wall and staging. The convective component is therefore considered separately and can be calculated according to Equation 3.43:

$$T_c = \frac{2\pi}{\omega_0} \qquad \textit{Equation 3.43}$$

Where:

T_c is the fundamental convective period of the tank-liquid system

ω_0 is the natural circular frequency

$$\omega_0 = \sqrt{g\frac{\lambda_1}{R}\tanh(\lambda_1\gamma)} \qquad \textit{Equation 3.44}$$

Where:

g is the gravitational acceleration

λ_1 is the dimensionless parameter equal to 1.841

R is the radius of the tank

γ is the tank height-to-radius ratio

3.11.2 Impulsive Component

The impulsive component of the liquid is assumed to be rigidly attached to the tank walls during ground acceleration, regardless whether the structure is considered to

be rigid or flexible. The pressure applied on the tank wall by the impulsive component can be calculated using equation 3.45 (Eurocode 8: Part 4, 2006):

$$p_i(\xi, \varsigma, \theta, t) = C_i(\xi, \varsigma)\rho H cos\theta A_g(t) \qquad \textit{Equation 3.45}$$

Where:

$\xi = r/R$	is the considered equal to 1, since the pressure acting on the wall is being determined
$\varsigma = z/H$	is the height with z measures upwards from the base of the wall
ρ	is the density of the contained liquid
H	is the height from the base to the free surface of the liquid
θ	is the circumferential angle, taken as 0 degrees to obtain maximum pressure
$Ag(t) = ag$	is the peak ground acceleration

The distribution of the impulsive component over the height of the tank wall is illustrated in Figure 3.15 for different height-to-radius ratio (γ).

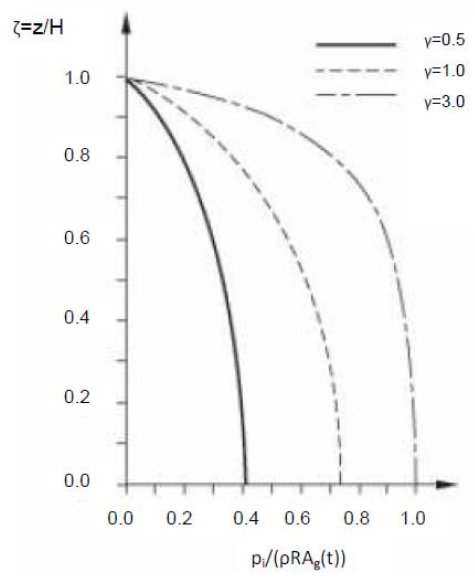

Figure 3.15. Distribution of impulsive pressure (Eurocode 8: Part 4, 2006)

The impulsive pressure is associated with impulsive mass of water inside a water tank. The impulsive mass is rigidly attached to the tank walls and may have a significant influence on the seismic response of elevated water tanks.

The impulsive mass may be expressed as a fraction of the total liquid mass that varies with the height-to-radius ratio of the tank. In broad tanks the impulsive mass is about half of the total liquid mass but an increase in height-to-radius ratio results in an increase in fraction of impulsive mass to total liquid mass. The influence of the impulsive component becomes more pronounced in taller tanks. The impulsive mass can be calculated using Equation 3.46 by Eurocode 8: Part 4 (2006):

$$m_i = m2\gamma \frac{I_1\left(\frac{v_1}{\gamma}\right)}{v_1^3 l_1'\left(\frac{v_1}{\gamma}\right)} \qquad \textit{Equation 3.46}$$

Where:

m is the total contained liquid mass

γ is the height/Radius ratio of tank

I_1 is the modified Bessel function of order 1

I_1' is the first derivation of the modified Bessel function of order 1

v_1 is the dimensionless parameter defined in Eurocode 8: Part 4 (2006)

An acceleration of the liquid mass during ground excitations produces shear forces and overturning moments in a structure about an axis perpendicular to the direction of excitation. The maximum values of shears force and overturning moments generally localised at the base of an elevated water tank. These values, which are calculated immediately above the foundation, are used for the seismic design of a supporting system.

The base shear force and overturning moment of impulsive mass resulted from the horizontal acceleration can be calculated according to Equation 3.47 and Equation 3.48 respectively.

$$Q_i(t) = m_i A_g(t) \qquad \textit{Equation 3.47}$$

$$M_i(t) = m_i h_i A_g(t) \qquad \textit{Equation 3.48}$$

Where:

m_i is the impulsive mass

h_i is the height of the impulsive mass

$A_g(t)$ is the peak ground acceleration

3.11.3 Convective Component

The convective component represents the sloshing motion of the liquid and has a different fundamental period than the ground motion impulsive component of the tank. The pressure exerted on a water tank wall by the convective component can be calculated by Eurocode 8: Part 4 (2006) method:

$$p_c(\xi, \varsigma, \theta, t) = \rho\psi_1 \cosh(\lambda_1 \gamma \varsigma) J_1(\lambda_1 \xi) \cos\theta \, A_{c1}(t) \qquad \textit{Equation 3.49}$$

Where:

ψ_1	is the dimensionless parameter determined from Eurocode 8
λ_1	is the dimensionless parameter equal to 1.841
ρ	is the density of the contained liquid
γ	is the height/radius ratio
$\varsigma = z/H$	is the height with z measured from base of tank
J_1	is the Bessel function of the first order
$\xi = r/R$	is equal to 1.0 since pressure acting on wall is measured
$A_{c1}(t)$	is the acceleration corresponding to the first mode of vibration

The distribution of the convective pressure, with consideration of the first and second mode of vibration, along the height of the tank wall is illustrated in Figure 3.16 (Eurocode 8: Part 4, 2006) for different height-to-radius ratio (γ).

The convective pressure is associated with convective mass of water inside a water tank. The convective mass moves independently of the tank wall at its fundamental frequency during seismic excitations and it is attached to the tank walls by springs with stiffness k. The convective mass may be significant for broad tanks but influence of convective mass become less pronounce with increase in height-to-radius ratio until the influence of the sloshing motion becomes negligible for tall tanks. The convective mass can be calculated according to Eurocode 8: Part 4 (2006) method by Equation 3.50.

$$m_{c1} = m\frac{2\tanh(\lambda_1\gamma)}{\gamma\lambda_1(\lambda_1^2-1)} \qquad \textit{Equation 3.50}$$

Where:

m is the total contained liquid mass

λ_1 is the dimensionless parameter equal 1.841

γ is the height/radius ratio of a tank

The base shear force and overturning moment resulted from the convective component can be calculated by Eurocode 8: Part 4 (2006):

$$Q_{c1}(t) = m_{c1}A_{c1}(t) \qquad \textit{Equation 3.51}$$

$$M_{c1}(t) = m_{c1}h_{c1}A_{c1}(t) \qquad \textit{Equation 3.52}$$

Where:

m_{c1} is the convective mass associated with first mode of vibration

$A_{c1}(t)$ is the pseudoacceleration of first mode of vibration

h_{c1} is the height of convective mass

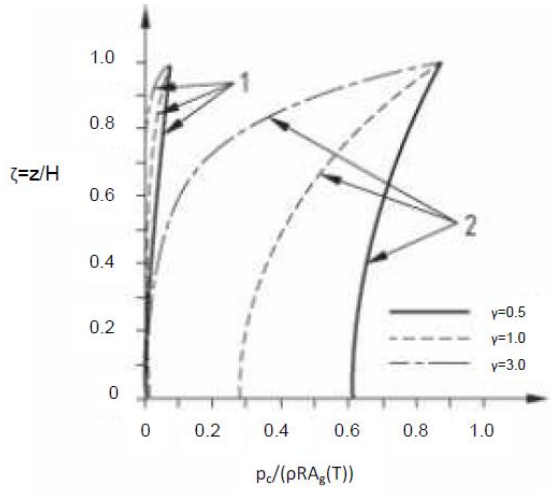

Figure 3.16. Distribution of convective pressure (Eurocode 8: Part 4, 2006)

3.11.4 Two degree of freedom design according to Eurocode 8

The magnitude and influence of the impulsive and convective components on a water tank behaviour is highly dependent on the height-to-radius ratio of the tank. Increase in height-to-radius ratio resulted in larger contribution of the impulsive component to the global response. On the other hand, the contribution of the convective component to the global response decreases with increase in height-to-radius ratio. According to Eurocode 8 (2006) the convective component has a significant influence on the hydrodynamic pressure in broad tanks, but is restricted to the liquid surface in the case of tall tanks with height-to-radius greater than 1.0. The sloshing frequency becomes independent of the height-to-radius ratio for tall tanks due to the superficial influence of the convective component as illustrated in Figure 3.17 with the first mode of vibration of the sloshing component indicated as 1 and the second mode of vibration indicated with 2.

Eurocode 8 (2006) provides a recommended values for impulsive $\boldsymbol{m_i}$ and convective $\boldsymbol{m_c}$ masses in Table 3.3 as fractions of the total liquid mass $\boldsymbol{m}$, along with the heights from the base of the point of application of the resultant of the impulsive and convective hydrodynamic wall pressure, $\boldsymbol{h_i}$ and $\boldsymbol{h_c}$.

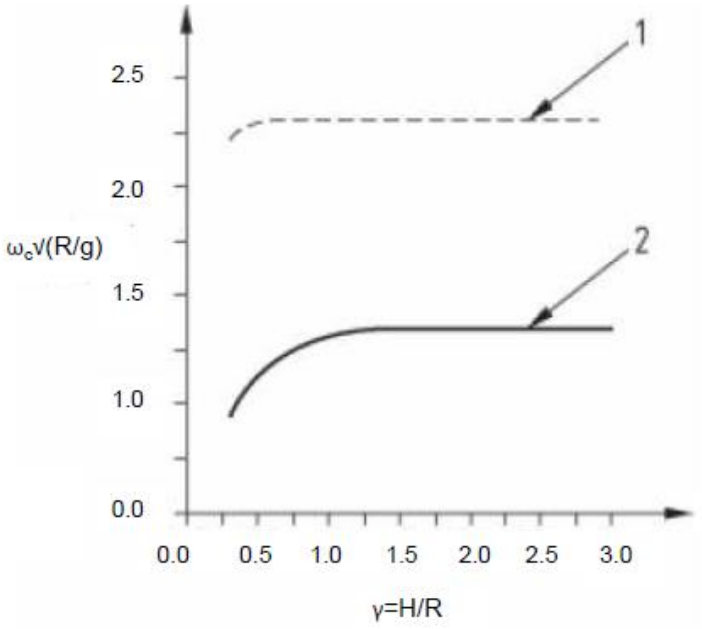

Figure 3.17. Variation of sloshing frequency with height-to-radius ratio (Eurocode 8: Part 4, 2006)

Table 3.3 Recommended design values for the first impulsive and convective modes of vibration as a function of the tank height-to-radius ratio (Eurocode 8: Part 4, 2006)

H/R	m_i/m	m_c/m	h_i/H	h_c/H
0.3	0.176	0.824	0.400	0.521
0.5	0.300	0.700	0.400	0.543
0.7	0.414	0.586	0.401	0.571
1.0	0.548	0.452	0.419	0.616
1.5	0.686	0.314	0.439	0.690
2.0	0.763	0.237	0.448	0.751
2.5	0.810	0.190	0.452	0.794
3.0	0.842	0.158	0.453	0.825

As recommended by Eurocode 8: Part 4 (2006) and Joshi (2000) a close approximation for impulsive and convective masses of axisymmetric tanks, other than cylindrical, may be obtained from an equivalent cylindrical tank having the same free surface diameter and an equivalent water depth that results in an equal volume of water for both the original and the equivalent tanks. The two degree of freedom water model by Eurocode 8:Part 4 (2006) showed in Figure 3.18.

The impulsive component of the liquid is considered to move rigidly with the tank wall. An impulsive mass $\boldsymbol{m_i}$ rigidly connected to the tank walls, located at a height $\boldsymbol{h_i}$ above the tank base.

The convective component of the liquid is considered to simulate sloshing effect on the water. A convective mass $\boldsymbol{m_c}$ connected by spring to the tank walls, located at a height $\boldsymbol{h_c}$ above the tank base. The stiffness of a spring can be calculated by Equation 3.53. The stiffness of every spring for convective mass is equal to $k_c/2$ for conical tanks as presented in Figure 3.18.

$$k_c = \omega_c^2 m_c \qquad \textit{Equation 3.53}$$

Where:

ω_c is the natural circular frequency

m_c is the convective mass

$$\omega_c = \sqrt{g\frac{\lambda_1}{R}\tanh(\lambda_1\gamma)}$$ *Equation 3.54*

Where:

- g is the gravitational acceleration
- λ_1 is the dimensionless parameter equal to 1.841
- R is the radius of the tank
- γ is the height-to-radius ratio of the tank

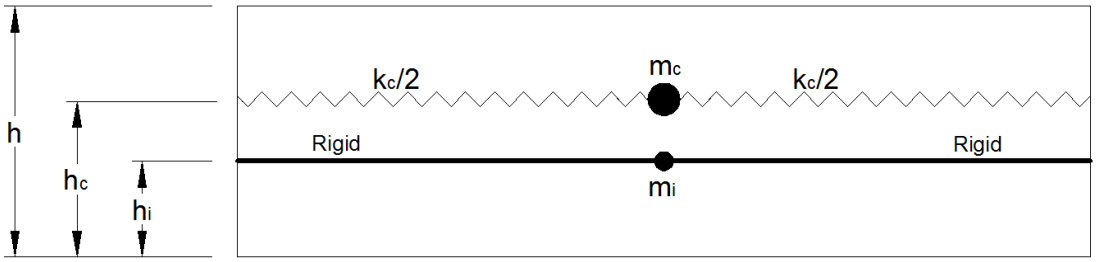

Figure 3.18. Two degree of freedom system by Eurocode 8: Part 4 (2006).

Chapter 4

Building and Corroborating the Finite Element Model

4.1 Introduction

Under a strong earthquake excitations, a structure usually subjected to forces beyond its elastic limit. Therefore, nonlinear relationship between the lateral shear force and lateral deformation of RC shaft should be considered. With the availability of fast computers, these relations where inelastic structural analysis is combined with seismic hazard assessment can be defined more easily.

The main objective of this chapter is to define and corroborate a finite element (FE) technique for modelling RC elevated water tanks in order to perform a proper and accurate seismic analysis. The general purpose FE modelling software SAP2000 is employed for this purpose.

The chapter begins with properties and finite element modelling of reinforced concrete. The most important in developing the reinforced concrete finite element model is to define each element's characteristics under different loading cases. Explanation of elastic and inelastic behaviour of concrete and steel took place in this chapter. Some mathematical approximations of stress-strain curve development of concrete and steel materials are proposed and briefly described in this chapter. Moreover, proposed hysteresis models for inelastic energy dissipation of concrete and steel materials are discussed.

The chapter continuous with model verification by comparing to previous studies available in literature.

In the last part of the chapter, the configuration, geometry and assumptions for FE models of proposed RC elevated water tanks are discussed. Finally, the FE models are designed based on the proposed methodology.

4.2 Multi-Layer Shell Element

A number of finite element (FE) programs have been developed during last years. Among these programs are general and specific purpose FE programs. The model was developed using the existing capabilities of the general purpose finite element

program SAP2000 which is popular software for both academic researches and commercial analyses. As an advanced analytical FE program, SAP2000 is capable of modelling a nonlinear reinforced concrete using multi-layer shell element. This element is able to model essential mechanical elastic and inelastic characteristics of concrete and steel materials.

The proposed multi-layer shell element is based on the principles of composite material mechanics and it can simulate the coupled in-plane/out-plane bending and the coupled in-plane bending-shear nonlinear behaviours of a RC shaft (Miao et al, 2006). Basic principles of multi-layer shell element are illustrated by Figure 4.1. The multi-layer shell element is a combination of a number of layers. Different material properties and thickness can be assigned to every layer separately. This means that the rebars and concrete can be assigned separately (Hafjan, et al., 2010). During the finite element analysis, the axial strain and curvature of the middle layer can be obtained in one element. After that, according to the assumption that plane remains plane, the strains and the curvatures of the other layers can be calculated. Finally, the corresponding stress can be calculated through the constitutive relations of the material assigned to the layer. From the above principles, it is seen that the structural performance of the RC shaft can be directly connected with the material constitutive law.

The constitutive model of the rebars is set as the perfect elasto-plastic model. The rebars in different directions are smeared into one layer, so if the ratios of the amounts of the distributing rebars to the concrete in the longitudinal direction and transverse direction are the same, the rebar layer can be set as isotropic. But if the ratios in the two directions are different, the rebar layer should be set as orthotropic with two principal axes as shown in Figure 4.2. Moreover, in different principal axis, the stiffness is set different according to the ratio of the amount of rebars to concrete to simulate longitudinal rebars and transverse rebars respectively (Jiang J.J., et al, 2005).The nonlinear RC properties are discussed in detail in the next sections.

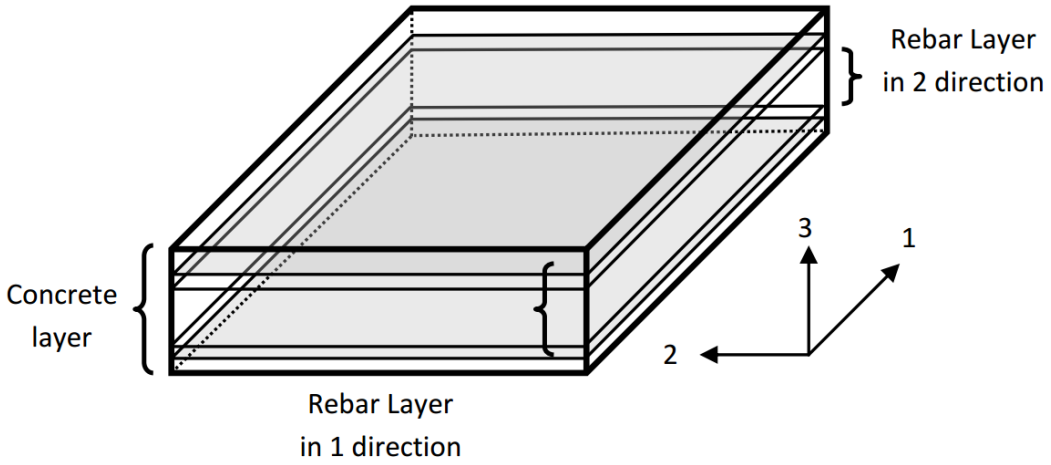

Figure 4.1 Multi-layer shell element (Miao, et al., 2006)

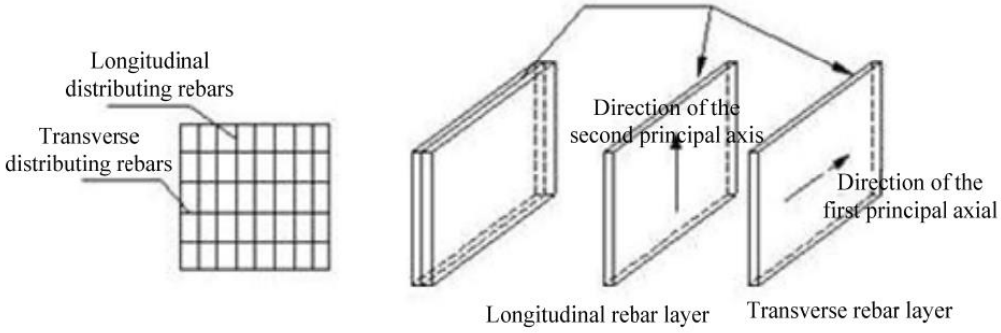

Figure 4.2 Settings of the rebar layers (Miao, et al., 2006)

4.3 The elastic mechanical properties of materials

The main principle of elastic mechanical properties of materials is linear relationships between the components of stress and strain. Also, elastic mechanical properties are valid only for stress states that do not produce yielding (Chopra, 2007). These assumptions are reasonable for many engineering materials and engineering design scenarios. Elastic material behaviour is therefore used extensively in structural analysis and engineering design, often with the aid of finite element analysis.

The elastic mechanical properties relate the behaviour of the stresses and strains within the material. The stresses are defined as forces per unit area acting on an elemental cube aligned with the material axes as shown in Figure 4.3. The stresses σ_{11}, σ_{22} and σ_{33} are called the direct stresses and tend to cause length change, while σ_{12}, σ_{13} and σ_{23} are called the shear stresses and tend to cause angle change (CSI, 2015).

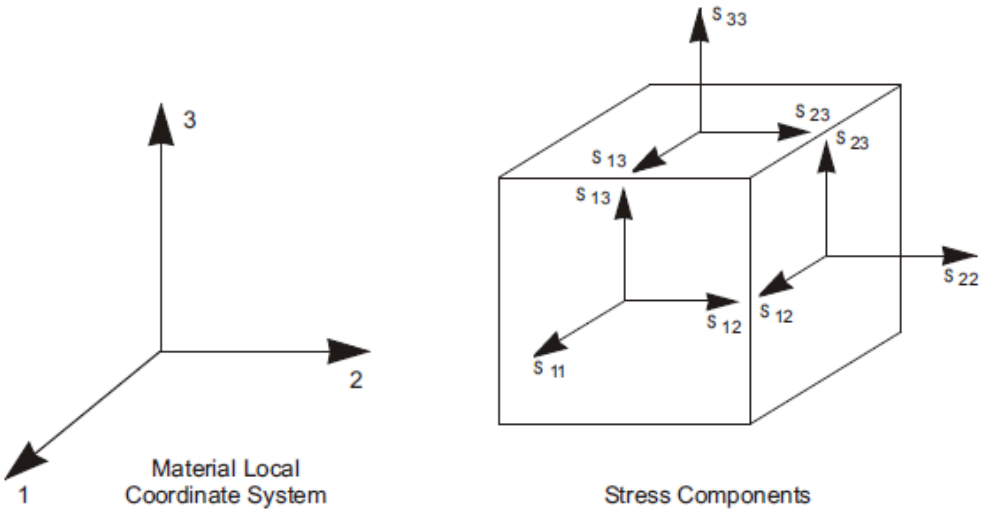

Figure 4.3 Definition of stress components in the material local coordinate system (CSI, 2015)

The direct strains measure the change in length along the material local 1, 2, and 3 axes, respectively, and are de fined as:

$$\varepsilon_{11} = \frac{du_1}{dx_1} \qquad \textit{Equation 4.1}$$

$$\varepsilon_{22} = \frac{du_2}{dx_2} \qquad \textit{Equation 4.2}$$

$$\varepsilon_{33} = \frac{du_3}{dx_3} \qquad \textit{Equation 4.3}$$

Where:

ε_{11}, ε_{22} and ε_{33}	are the direct strains
u_1, u_2 and u_3	are the displacements
x_1, x_2 and x_3	are the coordinates in the material 1, 2, and 3 directions, respectively.

The engineering shear strains γ_{12}, γ_{13}, and γ_{23}, measure the change in angle in the material local 1-2, 1-3, and 2-3 planes, respectively, and are de fined as:

$$\gamma_{12} = \frac{du_1}{dx_2} + \frac{du_2}{dx_1} \qquad \textit{Equation 4.4}$$

$$\gamma_{13} = \frac{du_1}{dx_3} + \frac{du_3}{dx_1} \qquad \textit{Equation 4.5}$$

$$\gamma_{23} = \frac{du_2}{dx_3} + \frac{du_3}{dx_2}$$ *Equation 4.6*

Where:

γ_{12}, γ_{13} and γ_{23} are the engineering shear strains

Normally, the reinforced concrete elements are linear elastic at the initial state of loading. By increasing the loads, the tension stresses may reach above maximum tension strength and that cause the reinforcement to yield, that results to nonlinear behaviour of rebar and concrete. For properly designed RC structures, yielding of rebars must occur prior to concrete compression stress reach maximum. The nonlinear behaviour on reinforced concrete is discussed in the next sections.

4.4 The inelastic mechanical properties of reinforced concrete

An inelastic finite element modelling of reinforced concrete structures requires defining an accurate stress-strain curve for both concrete and rebar. Nonlinear static and dynamic analyses, examine the response of the structures up to extreme deformations in which concrete and steel material reach failure point and the structures collapse. A number of mathematical models have been proposed and can be found in the literature for analysing nonlinear behaviour of reinforced concrete structures. Concrete and steel stress-strain curves should be developed separately since the behaviour of that materials are highly different .The mathematical models of concrete and steel are discussed in the following sections.

4.4.1 Stress-strain behaviour of concrete

The stress-strain behaviour of concrete is initially linear and elastic. However, with applied force increase results the generation of micro-cracks, thus the behaviour of a structure becomes nonlinear and inelastic. After a structure reaches the peak stress, the resisting stress decreases with increase in strain failure point is reached at ultimate strain (Chopra, 2007). It may be difficult to define the stress-strain relationship by one approach due to the fact that the shape of uniaxial stress-strain curve of concrete is influenced by many factors. Several mathematical models have been proposed and adopted in analytical models of reinforced concrete structures.

One of the first mathematical models for concrete was proposed by Hognestad (1951). The stress-strain concrete model was consisted of two parts. The first part was an increasing parabola and the second part a decreasing line. That model was valid for maximum strength up to 40 Mpa.

Nowadays, the stress-strain model proposed by Mander, et al. (1988) is widely used among researchers and commercially thus that model was selected for modelling concrete in this study. The model is displayed in Figure 4.4 for two conditions of confined and unconfined concrete. As shown in this figure, the unconfined model consists of two a curve and a linear regions. To develop unconfined concrete model three parameters should be defined:

f'_c is the maximum concrete strength for unconfined concrete
ε'_c is the concrete strain for unconfined concrete at f'_c
ε_u is the ultimate concrete strain capacity for unconfined concrete

For developing confined concrete model three other parameters should be defined:

f'_{cc} is the compressive strength of confined concrete
ε'_{cc} is the concrete strain at f'_{cc}
ε_{cu} is the ultimate concrete strain for confined concrete

f'_{cc}, ε'_{cc} and ε_{cu} are determined based on the type, size and spacing of confinement.

The equation of the curve part of the Mander,s stress-strain concrete model for unconfined concrete can be calculated by Equation 4.7:

$$f = \frac{f'_c x r}{r - 1 + x^r} \qquad \textit{Equation 4.7}$$

Where:

$$x = \frac{\varepsilon}{\varepsilon'} \qquad \textit{Equation 4.8}$$

$$r = \frac{E}{E - \left(\frac{f'_c}{\varepsilon'_c}\right)} \qquad \textit{Equation 4.9}$$

Where:

E is the modulus of elasticity

The equation for linear part of the Mander's stress-strain concrete model for unconfined concrete can be calculated by Equation 4.10:

$$f = \left(\frac{2f_c' r}{r - 1 + 2^r}\right)\left(\frac{\varepsilon_u - \varepsilon}{\varepsilon_u - 2\varepsilon_c'}\right) \qquad \textit{Equation 4.10}$$

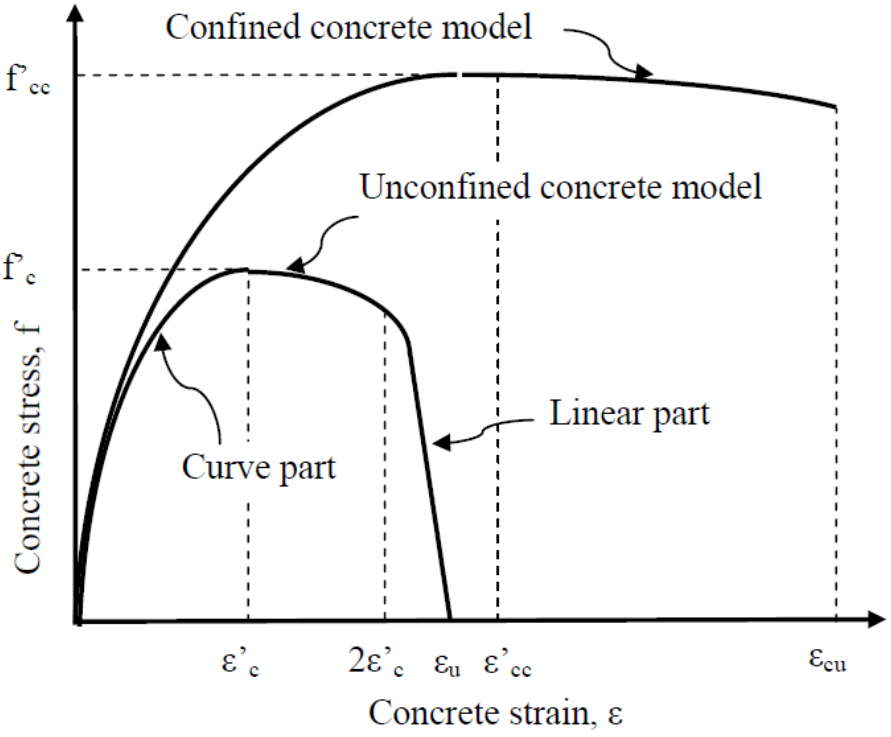

Figure 4.4. The Mander's stress-strain concrete model (Mander, et al., 1988)

In this study was used C20/25 concrete which was used for construction of RC elevated water tanks studied by Rai (2002; 2004). Table 4.1 shows C20/25 concrete mechanical properties used in the FE model for this study. This table shows only the linear properties of the material. When it comes to material nonlinearity, Figure 4.5 illustrates the nonlinear stress-strain curve for concrete. The stress-strain curve was developed using a reasonable number of plotted points. The coordination of each point of the graph was used as the input to the finite element software SAP2000. Data for the stress-strain curve for C20/25 concrete are presented in Appendix A.1.

Table 4.1. Mechanical properties of concrete C20/25

Density	$25\ kN/m3$
Young's Modulus	$30\ GPa$
Poisson's Ratio	0.2
Compressive strength, $f'c$	$20\ N/mm^2$
Shear Modulus	$12.5\ GPa$
Strain at compressive strength, ε'_c	$1.33 \times 10^{-3}\ mm/mm$
Ultimate strain, ε_u	$3.83 \times 10^{-3}\ mm/mm$

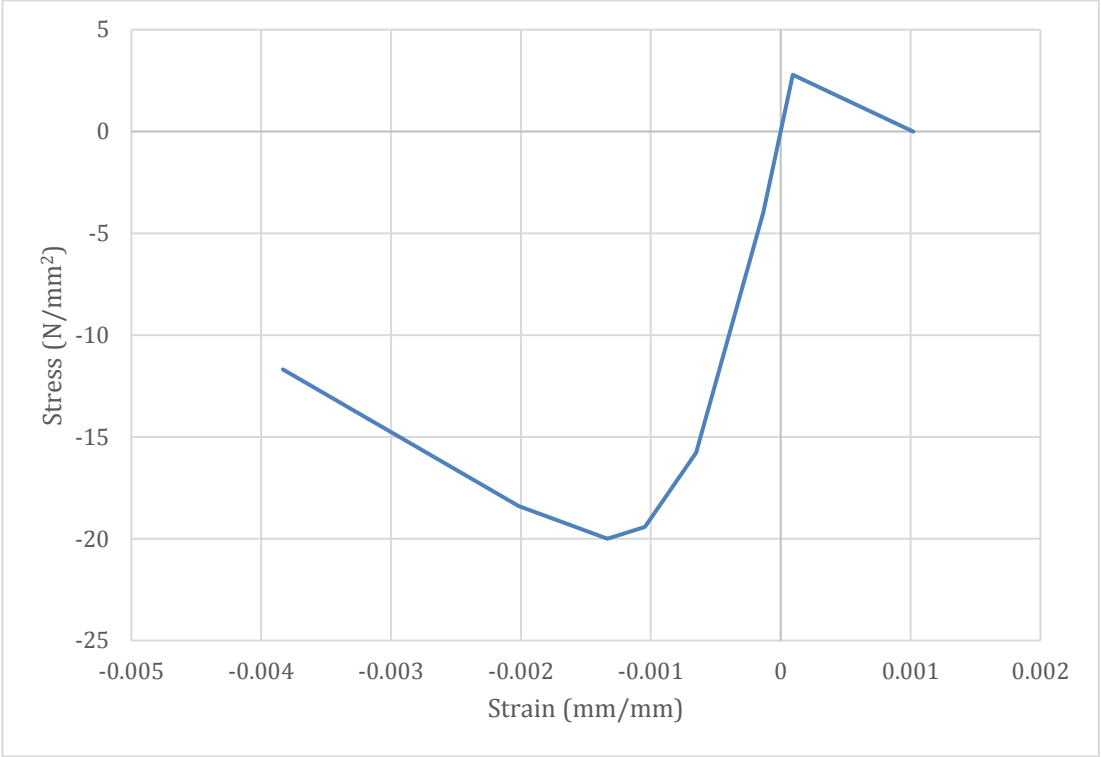

Figure 4.5. The stress-strain curve for C20/25 concrete (CSI,2015)

4.4.2 Stress-strain behaviour of rebar

The stress-strain curve of the steel rebar mainly depends on steel grade and rebar's size. Figure 4.6 shows the stress-strain curve for steel rebar proposed by Holzer (1975). This model consists of three regions:

- Elastic region
- Perfectly plastic region
- Ptrain hardening region.

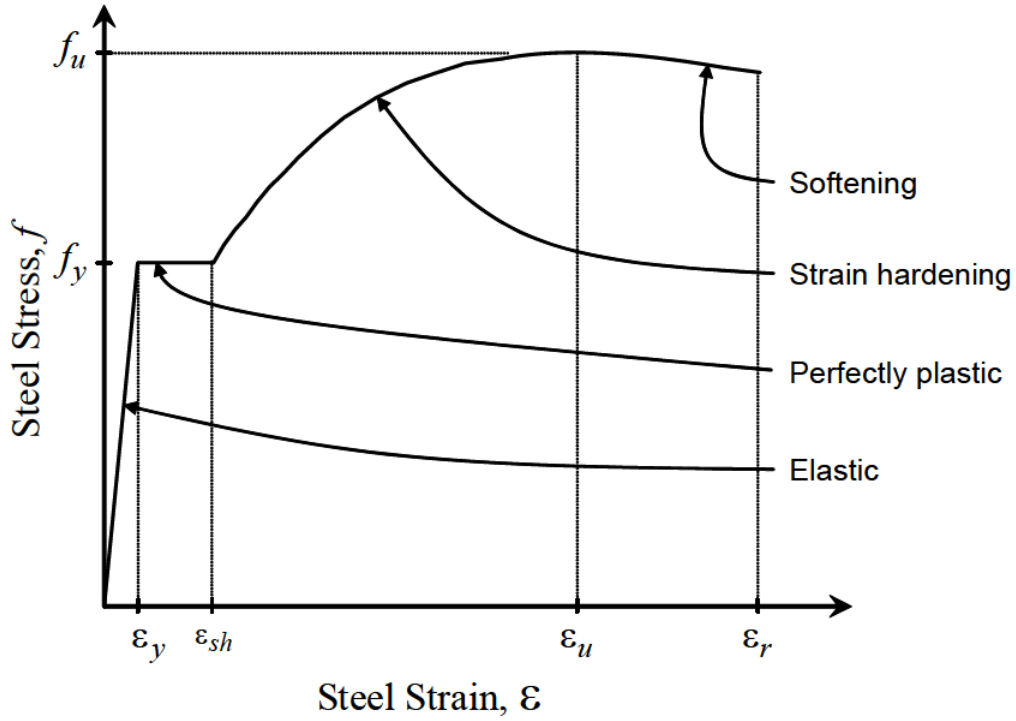

Figure 4.6. The stress-strain rebar model (Holzer, et al., 1975)

The equation for elastic region, when $0 \leq \varepsilon_s \leq \varepsilon_y$, is:

$$f_s = E_s \varepsilon_s \qquad \textit{Equation 4.11}$$

The equation for perfectly plastic region, when $\varepsilon_y \leq \varepsilon_s \leq \varepsilon_{sh}$, is

$$f_s = f_y \qquad \textit{Equation 4.12}$$

The equation for hardening and softening regions, when $\varepsilon_{sh} \leq \varepsilon_s \leq \varepsilon_r$, is:

$$f_s = f_y[1 + \left(\frac{\varepsilon_s - \varepsilon_{sh}}{\varepsilon_u - \varepsilon_{sh}}\right)\left(\frac{f_u}{f_y} - 1\right)\exp\left(1 - \frac{\varepsilon_s - \varepsilon_{sh}}{\varepsilon_u - \varepsilon_{sh}}\right) \qquad \textit{Equation 4.13}$$

Where:

f_s is the rebar stress
f_y is the rebar yield stress
f_u is the rebar ultimate stress capacity
ε_s is the rebar strain
ε_{sh} is the strain in rebar at the onset of strain hardening
ε_u is the rebar ultimate strain capacity
ε_r is the rebar strain fracture point
E_s is the rebar modulus of elasticity

In this study was used 0.25% reinforcement that was used for construction of RC elevated water tanks studied by Rai (2002; 2004). Table 4.2 shows steel rebar's mechanical properties used in the FE model of this study. This table shows only the linear properties of the rebar. When it comes to material nonlinearity, Figure 4.7 illustrates the stress-strain curve for rebar. Data for the stress-strain curve for steel rebar are presented in Appendix A.2.

Table 4.2. Mechanical properties of rebar

Density	$77\ kN/m^3$
Young's Modulus	$200\ GPa$
Yield Strength, f_y	$414\ N/mm^2$
Ultimate Strength, f_u	$620\ N/mm^2$
Yielding strain, ε_y	$2.07 \times 10^{-3}\ mm/mm$
Strain at onset of strain hardening, ε_{sh}	$1.00 \times 10^{-2}\ mm/mm$
Ultimate strain, ε_u	$9.00 \times 10^{-2}\ mm/mm$
Strain fracture point, ε_r	$1.08 \times 10^{-1}\ mm/mm$

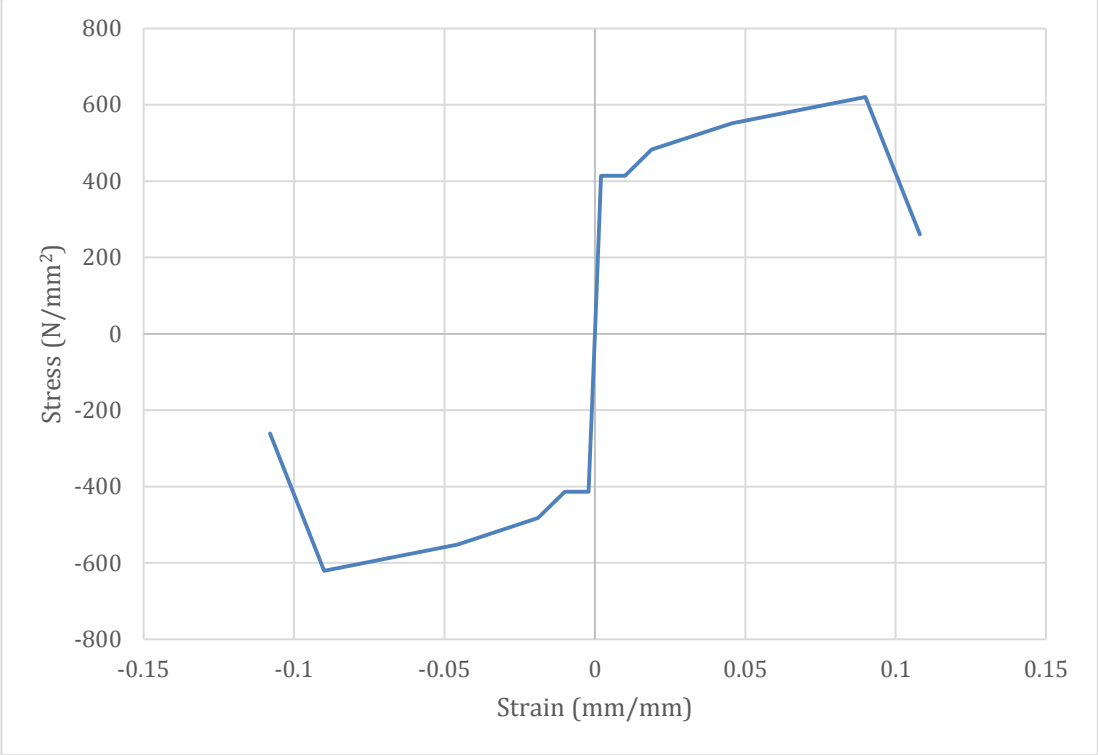

Figure 4.7. The stress-strain curve for rebar (CSI, 2015)

4.5 Hysteresis models

Hysteresis is the process of energy dissipation through deformation (displacement), as opposed to viscosity which is energy dissipation through deformation rate (velocity). Hysteretic behaviour may affect nonlinear static and nonlinear time-history load cases that exhibit load reversals and cyclic loading (CSI, 2015).

A number different hysteresis models are available to describe the behaviour of different types of materials. For the most part, these differ in the amount of energy they dissipate in a given cycle of deformation, and how the energy dissipation behaviour changes with an increasing amount of deformation.

Each hysteresis model may be used for the material stress-strain behaviour. SAP2000 includes several hysteresis models for dynamic nonlinear analyses. Typical hysteresis process can be described as:

- Initial loading in the positive or negative direction follows the back bone curve
- Upon reversal of deformation, unloading occurs along a different path, usually steeper than the loading path. This is often parallel or nearly parallel to the initial elastic slope.

- After the load level is reduced to zero, continued reversal of deformation causes re verse loading along a path that eventually joins the backbone curve on the opposite side, usually at a deformation equal to the maximum previous deformation in that direction or the opposite direction.

4.5.1 Concrete hysteresis model

Tension and compression behaviour are independent and behave differently. The stress-strain curve is used to determine the sign of compression, which can be positive or negative. The point having the largest absolute value of stress is considered to be in compression, so that the sign of compression can be either positive or negative (CSI, 2015). Figure 4.8 shows an example of hysteresis concrete model behaviour.

Compression behaviour is modelled as follows:

- Initial loading is along the back bone curve
- Unloading to zero occurs along a line nearly parallel to the compression elastic line. The line is actually directed to a pivot point on the extension of the compressive elastic line, located so that the unloading slope at maximum compressive force has half the stiff ness of the elastic loading line.
- At zero force, re verse loading to ward tension occurs at zero force.
- Sub sequent loading in compression occurs along the previous unloading line if the energy factor $f = 0.0$, and along the secant from the origin to the point of maximum previous compressive deformation if the energy factor is 1.0.

Tension behaviour, if non-zero, is modelled as follows:

- Initial loading is along the backbone curve
- Unloading occurs along a secant line to the origin.
- Subsequent loading occurs along the unloading secant from the origin to the point of maximum previous tensile deformation.

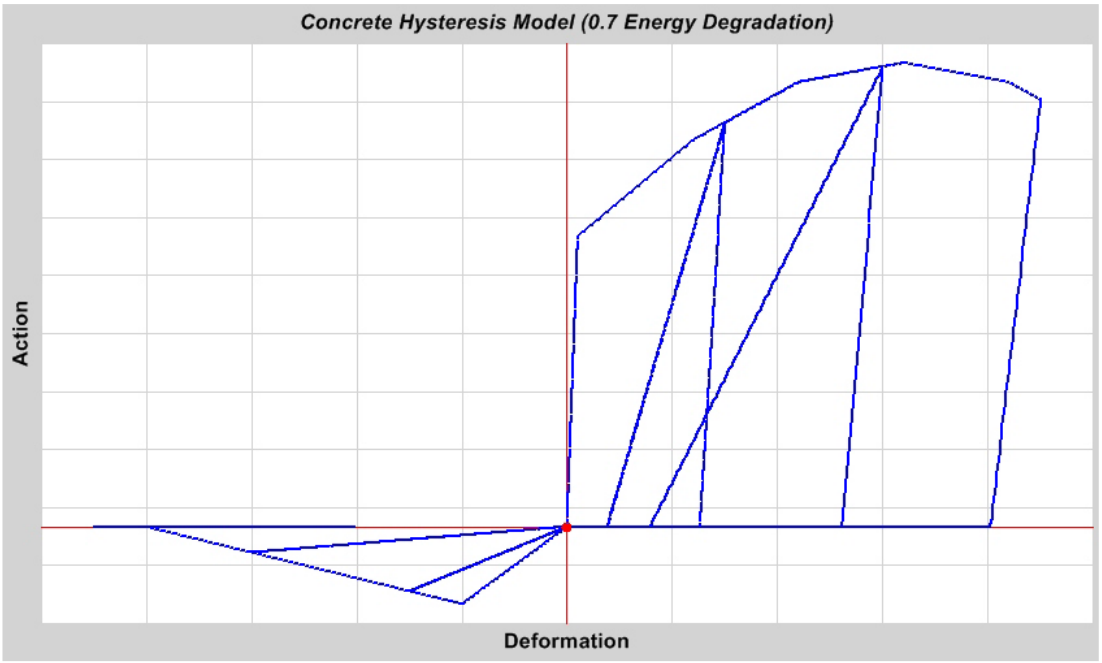

Figure 4.8. Concrete hysteresis model under Increasing cyclic load with compression as positive (CSI, 2015)

4.5.2 Rebar hysteresis model

The stress-strain curve of the steel rebar mainly depends on steel grade and rebar's sizes. This research uses the model which is based upon kinematic hardening behaviour that is commonly observed in metals, and it is the default hysteresis model for all metal materials in the SAP2000 (CSI, 2015). This model dissipates a significant amount of energy, and is appropriate for ductile materials.

Under the rules of kinematic hardening, plastic deformation in one direction "pulls" the curve for the other direction along with it. Matching pairs of points are linked.

Upon unloading and reverse loading, the curve follows a path made of segments parallel to and of the same length as the previously loaded segments and their opposite-direction counter parts until it re-joins the backbone curve when loading in the opposite direction. This behaviour is shown in Figure 4.9 for cycles of increasing deformation (CSI, 2015).

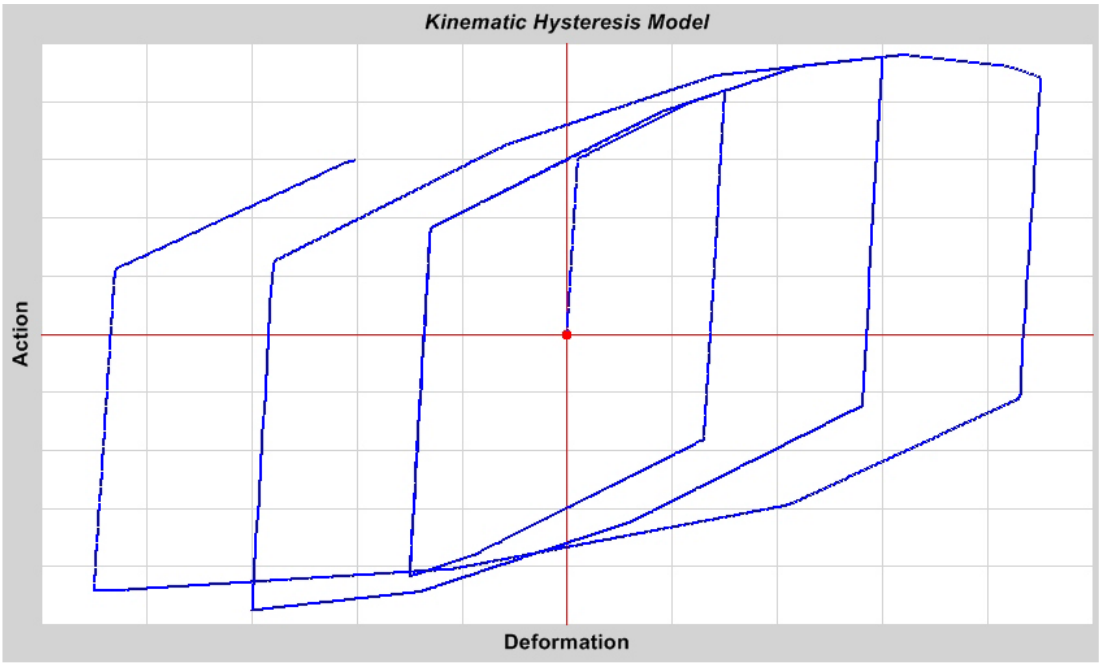

Figure 4.9. Kinematic hysteresis model under increasing cyclic load (CSI, 2015)

4.6 Gravity load

The gravity load (elevated water tank self-weight) can be created by defining a uniform acceleration which is the ground acceleration ($g = 9.807\ m/s^2$) in a fixed direction (-Z), where Z is the vertical direction. SAP2000 calculates the loading using the acceleration magnitude, the material density specified in the material definition, and the section thickness from section properties. Therefore, the gravity load is the combination weight of the RC tank and RC shaft. However, if non-structural mass included in the model in a given element, it will accordingly participate in any mass proportional distributed loads, such as gravity loading, defined on that element. The gravity force is included as concentrated loads at element nodes.

4.7 Nonlinear Time History Analysis using SAP2000

A variety of common methods are available for performing direct integration time-history analysis which are well documented in the literature, however Chopra (2007) and CSI (2015) suggest to use Hilbert-Hughes Taylor alpha method. Hilbert-Hughes Taylor is an implicit method that can handle numerical damping, without degrading the order of accuracy. This is useful because Rayleigh proportional damping in the

Newmark method mostly damps just the middle modes, and barely affects the higher and lower modes. To overcome these limitations, the algorithmic damping can be introduced in the Newmark method by assigning with a value γ larger than 0.5. The problem with doing that, is a reduction of accuracy.

Hilber-Hughes-Taylor method is more effective than Newmark to suppress high frequency noise, and decreasing the parameter α_H keeps appropriate level of accuracy while increasing the amount of numerical dissipation. In this study, Hilber-Hughes-Taylor was applied with $\alpha_H = 0$, practically making Hilbert-Hughes-Taylor equal to Newmarks average acceleration method. The reason for this choice is the lack of high frequency noise in the models, keeping the accuracy on a good level with the choice of $\alpha_H = 0$.

For the damping calculations, there are three options in SAP2000. These options are; 'direct specification', 'specifying modal damping by period' and 'specifying damping by frequency'. In the 'direct specification' option, the damping values are entered considering mass and stiffness proportional coefficients. In the 'specify modal damping by period' option, the damping values with the first and second periods are assigned. Using these values, the program calculates the mass proportional and stiffness proportional coefficients. 'Specify modal damping by period' option was used in the study for time history analysis (CSI, 2015).

4.7.1 Time history record El Centro

The ground motion used for the time history analysis is the horizontal component of 1940 El-Centro earthquake with peak ground acceleration (PGA) equal to 0.32 g as shown in Figure 4.10. An integration time step of 0.05 second was used for time history analysis of the elevated water tanks in performing the time history direct integration analysis. The data of the 1940 El-Centro earthquake were obtained from Pacific Earthquake Engineering Research Centre (PEER) ground motion database (PEER, 2015) and presented in Appendix D.1

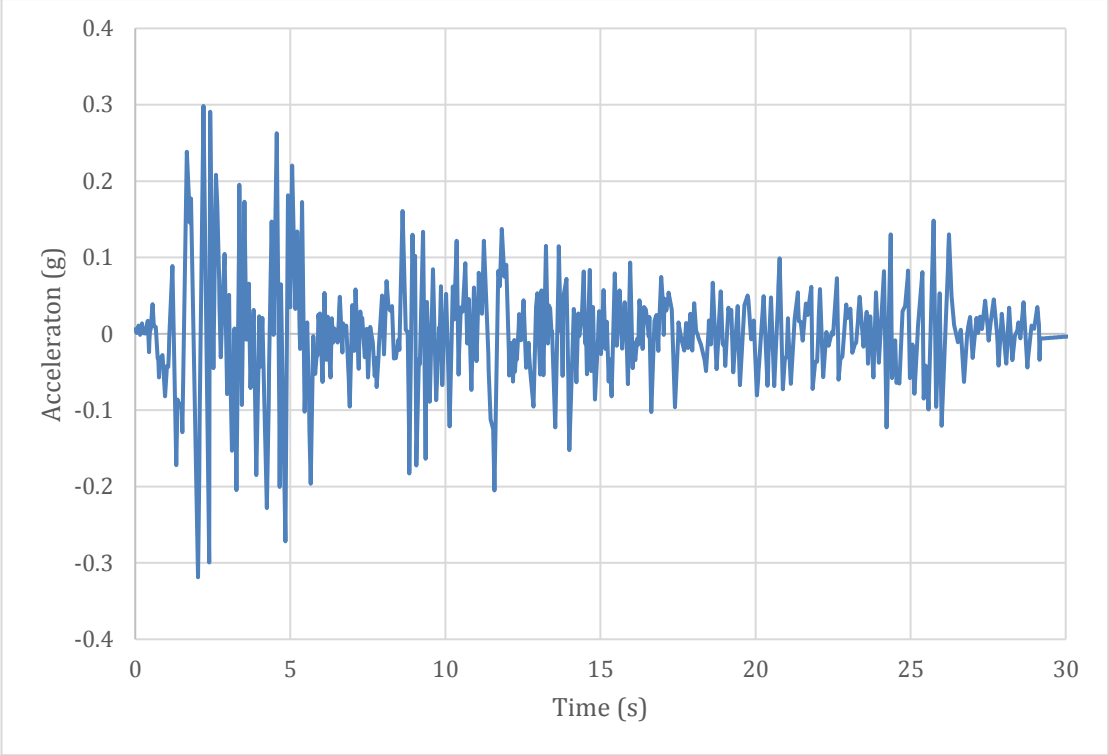

Figure 4.10. 1940 El-Centro ground motion, horizontal component (PGA=0.32g)

4.8 FE Model corroboration

The proposed finite element mathematical model requires corroboration by results of previous researches available in literature. Since the main objective of this study is to investigate nonlinear behaviour of elevated RC water tanks with proposed slit shaft two previous studies were chosen for model verification:

- Nonlinear Finite Element Analysis of Reinforced Concrete Slit Walls with ANSYS by Baetu and Ciongradi (2012)
- Seismic Design of Concrete Pedestal Supported tanks by Rai (2004)

4.8.1 FE model corroboration by pushover analysis

The geometry of the RC shaft of elevated water tank resembles a shear wall with circular plan thus makes the shear wall an excellent choice for corroborating the finite element model. The analytical nonlinear finite element analysis of the reinforced concrete slit wall performed by published and previewed data by Baetu and Ciongradi (2012) was selected for model corroboration by pushover analysis.

4.8.1.1 FE slit and shear walls modelling

All material and geometry properties for FE analysis of a slit wall were taken from Baetu and Ciongradi (2012) to simulate exactly the same model. The concrete used in the analysis for model verification was C32/40. The reinforcement bars were included in the finite element model through a smeared model. The structural walls were reinforced with vertical bars diameter 14 mm at spacing 150 mm and horizontal bars were used 10 mm diameter every 150 mm. The bilinear kinematic hardening model proposed by Kachlakev, et al., 2001 was used in this corroboration. The bilinear model required the yield stress ($f_y = 3.55 \times 10^8\ Pa$) and the hardening modulus of the steel ($E = 2.1 \times 10^9\ Pa$).

The slit wall proposed for verification had 60 m in height, 10 m in length, each level has a height of 3 m and the wall thickness was 40 cm. There were five connections on the wall height disposed at equal length of 12 m. The height of each connection was of 0.40 m and the thickness of the slit was 5 cm. The solid wall with same dimensions and material properties was also simulated. The slit wall is shown in Figure 4.11. The slit and solid walls were fully restrained at the base. The gravity loads of 47.3 kN/m included walls weight and loads from floor connected to the wall every floor level which is 3 meters.

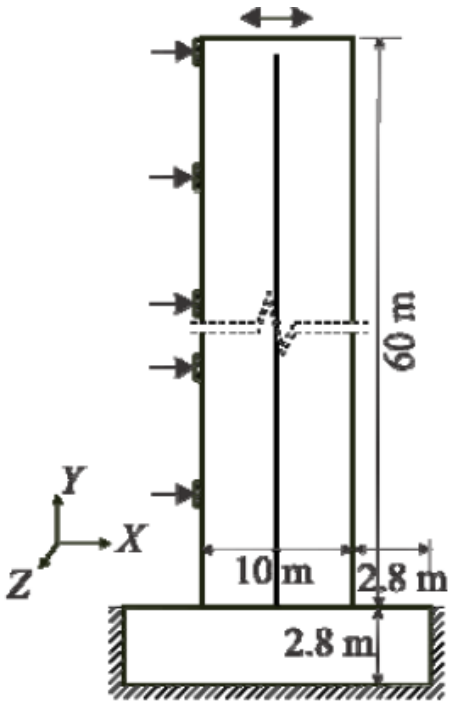

Figure 4.11. Loading and boundary conditions of the slit wall (Baetu, 2012)

4.8.1.2 Pushover analysis results comparison

The comparison between the current study and published study by Baetu and Ciongradi (2012) results are shown in Figure 4.12 and 4.13. The graphs demonstrates excellent agreement between the pushover patterns of solid and slit walls. Developed FE model is perfectly capable of estimating maximum lateral strength of the shear walls. The difference between the Baetu and Ciongradi (2012) result and current FE estimation is limited to less than 5% for both solid and slit walls that indicates that the FE models in this study are able to produce reliable results.

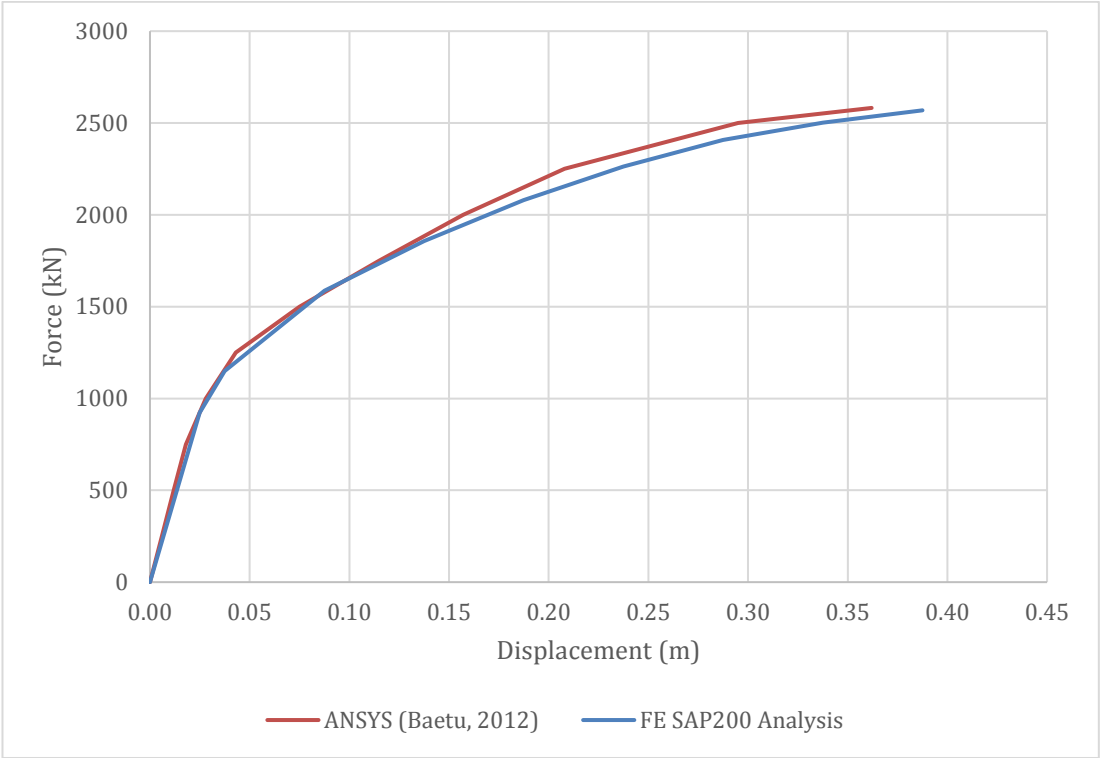

Figure 4.12. Comparison between the FE results of solid walls

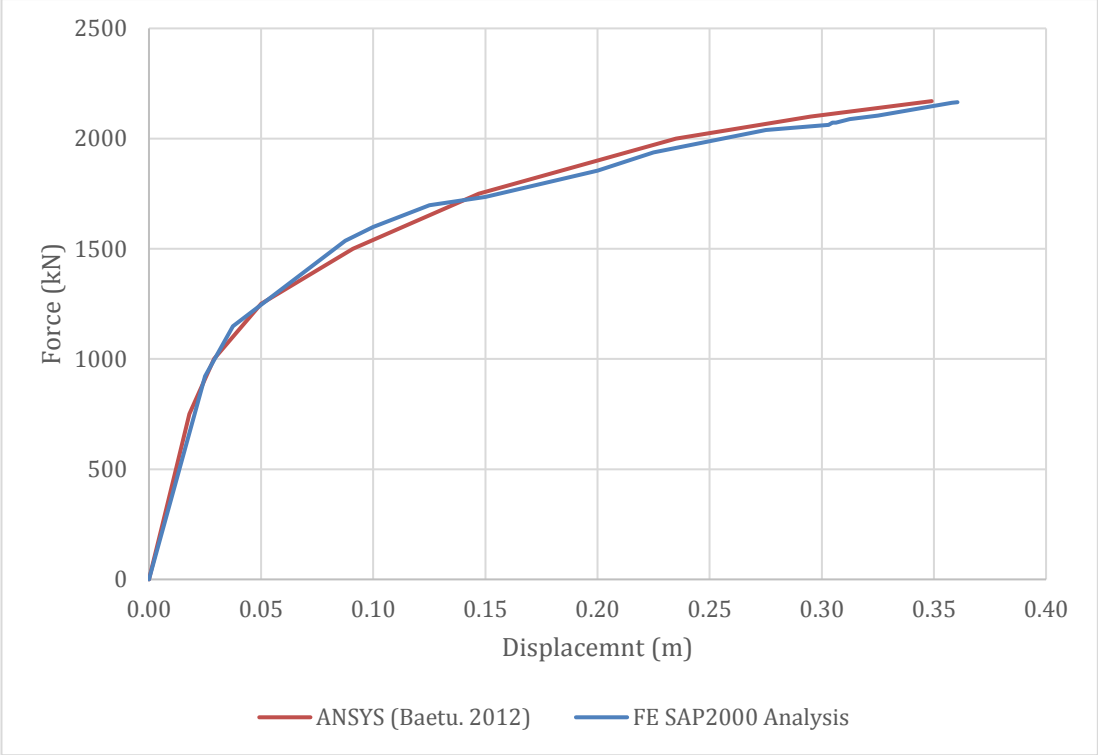

Figure 4.13. Comparison between the FE results of slit walls

4.8.2 FE model Corroboration by analytical results

Rai (2002; 2004) conducted an extensive theoretical study on reinforced concrete elevated water tanks with a variety of height-to-radius ratios damaged due to the 2001 Bhuj earthquake. A set of eight tanks affected in Bhuj earthquake, covering a wide range of possible geometry for RC shafts, was analysed in that study.

The collapsed 265 kL water tank in Chobari village about 20km from the epicentre was modelled using finite element software SAP2000. Analyses of both empty and full conditions of the elevated water tank were performed. Obtained results of fundamental period, critical shear force and critical bending moment were compared with analytical results obtained by Rai (2004).

Figure 4.14 shows (a) the collapsed elevated water tank and (b) equivalent FE model. Main characteristics of the elevated water tank analysed by Rai (2004) included:

- Water tank capacity – 265 kL
- Shaft diameter – 4.5 m
- Shaft wall thickness – 160 mm
- Shaft height – 10.5 m
- Water tank diameter – 9.0 m
- Water tank height – 5.5 m

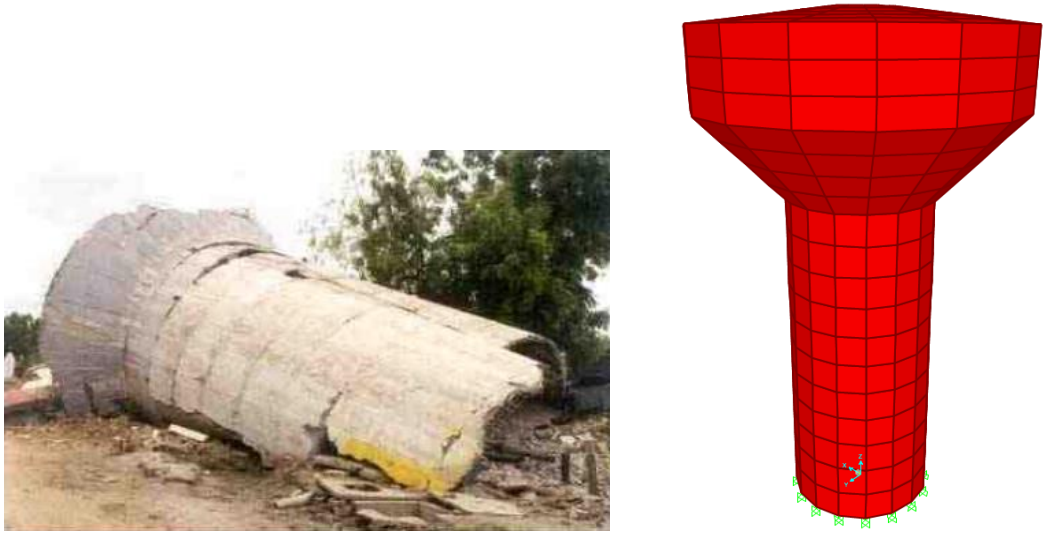

(a) (b)

Figure 4.14 (a) Collapsed 265 kL water tank in Chobari village about 20 km from the epicentre (b) FE model of the collapsed elevated water tank in Chobari village

Table 4.3 shows the fundamental periods of the FE model results and the analytical results obtained by Rai (2004) which were based on the single-degree-of-freedom model of the elevated water tank ignoring the convective vibration modes of water and assumed the shaft to act as a cantilever beam with a concentrated mass in tank container. It can be observed from the table that there is an excellent agreement between the results of this study and those reported by Rai (2004). The difference between the results in fundamental period was limited to 3%.

Table 4.3. Verification with codes.

	Fundamental period (s)		Difference
	Analytical Analysis (D. Rai)	FE SAP2000 Analysis	
Empty	0.166	0.171	3 %
Full	0.314	0.317	1 %

In addition, for comparison of critical moment (M_{cr}) and critical shear force (V_{cr}) the FE model was modelled ignoring the reinforcement. Figure 4.15 shows the obtained base moment and base shear results for the empty and full FE model respectively. Table 4.4 compares the critical moment and critical shear force for empty and full conditions for analytical results by Rai (2004) and FE analysis results obtained in this study. The difference between results is limited to 6% for critical moment and 8% for critical shear force for full condition model and 2% for both critical shear and critical moment for empty condition. The difference in results could be explained by difference in idealisation of the centre of mass inside the tank in FE model and analytical analysis conducted by Rai (2004). The two mass approach was used in FE model but SDF approach was used in analytical analysis carried out by Rai (2004).

Table 4.4. Comparison between analytical and FE results (Rai, 2004) of the base shear and base moment of the Chobari water tank in empty and full conditions

	Tank Empty		Tank Full	
	M_{cr} (kNm)	V_{cr} (kN)	M_{cr} (kNm)	V_{cr} (kN)
Analytical Analysis (Rai, 2004)	8490	798	11120	1035
FE SAP2000 Analysis	8574	818	11826	959

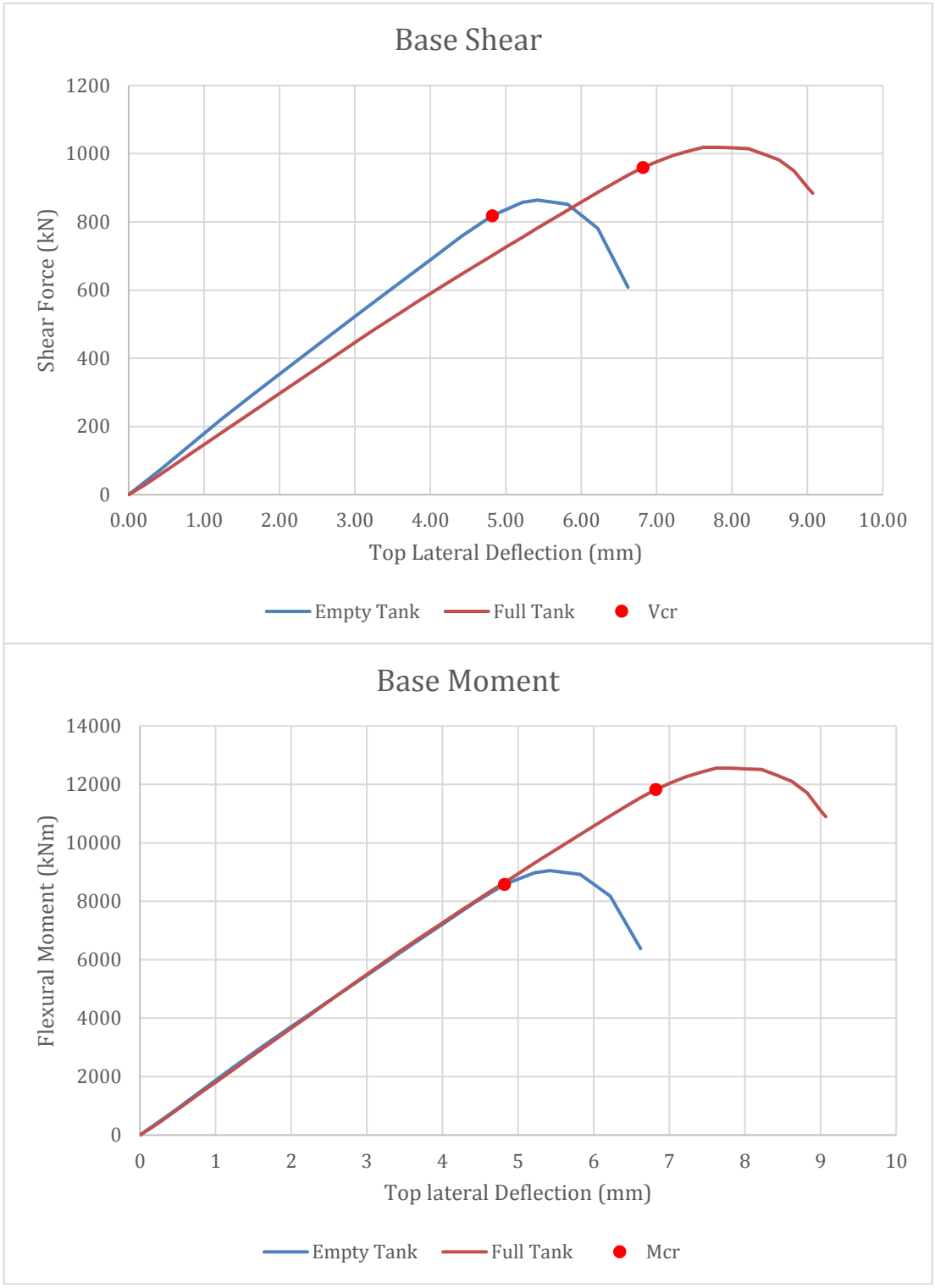

Figure 4.15. FE results of the base shear and base moment of the Chobari water tank in empty and full conditions

4.9 Design of the elevated water tank FE models

Elevated water tanks are built in different heights and sizes depending on the demand in the water system network. Many factors can affect shaft height and tank size among which the site location, pumping facility capacity, seismicity and water pressure demand are the most significant to mention.

In conventional structures such as buildings, the dead and live load values do not differ significantly from each other with the height. However, in case of elevated water tanks, the main mass is concentrated inside a water tank and the gravity load may drastically changes with water tank size and amount of water.

In order to address abovementioned issue, several elevated water tank models with variable tank capacity and shaft dimensions were developed in this research. Selection of the models was made based on Rai (2004) research that studied eight damaged elevated water tanks in Bhuj earthquake (Table 4.5).

Table 4.5. Characteristics water tanks used in the study conducted by Rai (2004).

Name and Location	capacity (kL)	Geometry of Shaft Support				Time Period (impulsive mode) sec			
						Tank Empty		Tank Full	
		Dia. d (m)	Thick. t (mm)	Height H (m)	Slenderness H/d	Fixed Base	With SSI	Fixed Base	With SSI
Gandhidham (T-1)	1000	8.00	250	14.60	1.85	0.164	0.25	0.313	0.449
Anjar (T-2)	1000	7.60	225	16.00	2.11	0.187	0.315	0.421	0.622
Chobari (T-3)	265	4.50	160	10.50	2.35	0.166	0.248	0.314	0.424
Morbi (T-4)	500	6.60	200	16.00	2.42	0.209	0.286	0.366	0.475
Bhachau (T-5)	200	4.00	150	11.00	2.75	0.195	0.274	0.348	0.533
Sapeda (T-6)	100	3.00	150	12.50	4.15	0.285	0.393	0.468	0.593
Samakhiali (T-7)	80	2.75	175	11.50	4.18	0.248	0.362	0.427	0.55
Gala (T-8)	300	3.66	125	20.00	5.45	0.698	0.736	1.171	1.221

Generally, the RC elevated tank structures could be divided into three substructures including a tank, shaft and foundation. This study is focused on the nonlinear response of the RC shaft and therefore a number of simplifications were made for modelling of the other two substructures. Figure 4.16 shows the simplified configuration of an RC elevated water tank.

The tank itself consists of the vessel and the liquid inside. The FE analysis of a water-retaining structure can be very complex with consideration of the interaction between the fluid and structure at the fluid-structure boundary. However, in the engineering practice complicated FE models are rarely used and simplified models which provide

accurate results are preferred. For the purposes of this study simplified two mass model of water was adopted from Eurocode 8. The Eurocode 8 suggests the uniform distribution of the impulsive mass among the nodes in a model, with the lumped masses attached directly to the wall element nodes and convective mass attached to the wall element nodes by springs.

The foundation was assumed to be rigid and shaft was fixed at the level of foundation. Boundary conditions were applied by constraining all degrees of freedom at the base level of the RC shaft.

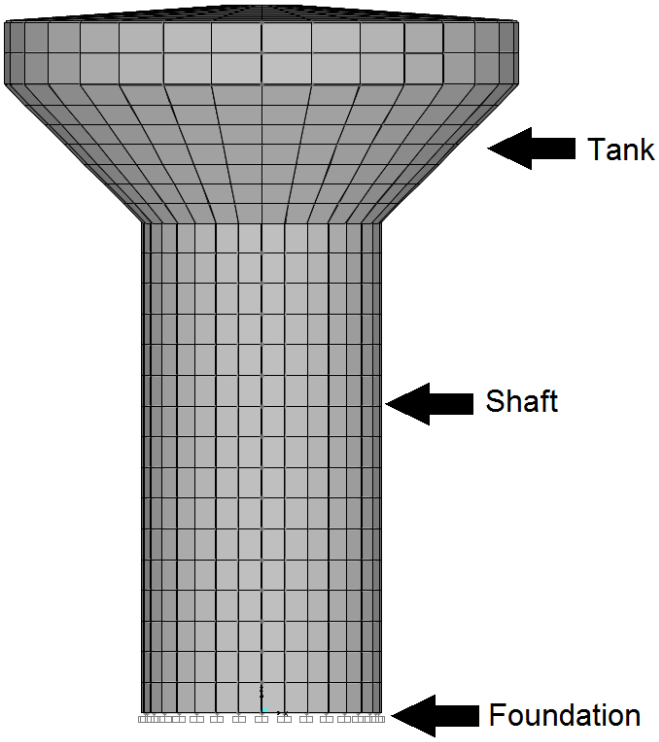

Figure 4.16. Simplified configuration of RC elevated water tank

4.9.1 Selection criteria for constructing the FE models

Selecting the number and configuration of the FE models in the study is a multi-objective task. The selection criteria should be able to address all design features of elevated water tanks. In addition, any other parameter that may affect the seismic response of the structure should be considered. The main selection criteria employed in this study included RC shaft height, RC shaft diameter and tank capacity.

Generally, the effect of structural plan configuration must also be considered as a criteria, however in case of elevated water tanks this is not required as the plan of a structure is a circular RC shaft and no specific irregularity exists.

In addition, structures with different structural plans demonstrate different seismic response when subjected to seismic loads in different directions. That criteria was also eliminated for the analysis of the elevated water tanks since the symmetrical plan of these structures provided.

In practice both hinged and fixed base foundation are used for elevated tanks. In this study, the tanks are assumed to have the fixed boundary condition at the base of the shaft.

Among the number of elevated water tanks affected in the Bhuj earthquake, a set of three tanks was selected to cover a wide range of possible geometry. A shaft wall thickness, height and radius of a shaft and a tank capacity were taken into account as a selection criteria. The characteristics of the tanks selected for this study presented in Table 4.6. Thickness of the tank wall varied from 160 mm to 225 mm, height of the shaft was taken 10.5 m and 16 m and the diameter of staging was taken between 4.5 m to 7.6 m that depended on the capacity of the water tanks which varied from 265 kL to 1000 kL.

Table 4.6. Characteristics of selected elevated water tanks for the study

		Geometry of shaft support			Geometry of water tank		
Name and Location	Capacity (kL)	Diameter, d (m)	Wall thickness, t (mm)	Height, H (m)	Diameter, d (m)	Wall thickness, t (mm)	Height, H (m)
Anjar	1000	7.6	225	16	16.6	25	6.50
Morbi	500	6.6	200	16	14.0	20	5.00
Chobari	265	4.5	160	10.5	10.4	20	5.25

Each FE model was assigned a finite element model identification number (FE model ID) as presented in Table 4.7. The first term represents the elevated water tank group and the second term stands for the slit width in mm. Therefore the FE model ID M1-50 represents an elevated water tank located in Anjar zone with 50 mm slits. Each model has been designed in accordance with the current practice.

Table 4.7. FE model ID of selected water tanks for the study

Name of Location	Anjar	Morbi	Chobari
	FE Model ID		
Solid shaft	M1-Soild	M2	M3
Slit width 50 mm	M1-50	M2-50	M3-50
Slit width 100 mm	M1-100		
Slit width 200 mm	M1-200		
Slit width 300 mm	M1-300		
Slit width 500 mm	M1-500	M2-500	M3-500
Slit width 1000 mm	M1-1000	M2-1000	M3-1000
Slit width 1500 mm	M1-1500		
Slit width 2000 mm	M1-2000		

4.9.2 Finite element model of RC shafts in elevated water tanks

The entire FE models were simulated using four-node quadrilateral shell elements (Figure 4.17). The wall thickness of the RC shaft in elevated water tanks is significantly smaller than the shaft height and diameter, therefore, shell elements can considered appropriate to be used in modelling the tank walls. In this study, the thickness was defined through the section property definition (Miao, et al., 2006). Connection beams in slit shaft models were simulated using frame beam element (Figure 4.18).

The primary assumptions and theories for developing finite element models of the RC elevated water tanks were illustrated in previous sections of this chapter. At this stage, the FE model of each elevated water tank was constructed in accordance with those assumptions. The FE models and simplified geometry of the proposed elevated water tanks showed in Figure 4.19. It was assumed to develop models with slits in the RC shafts from 50 mm to 2000 mm as well as a solid shaft model. However, 2000 mm

slits are not practical for theoretical understanding of slit shaft behaviour the full range between 50 mm and 2000 mm were investigated.

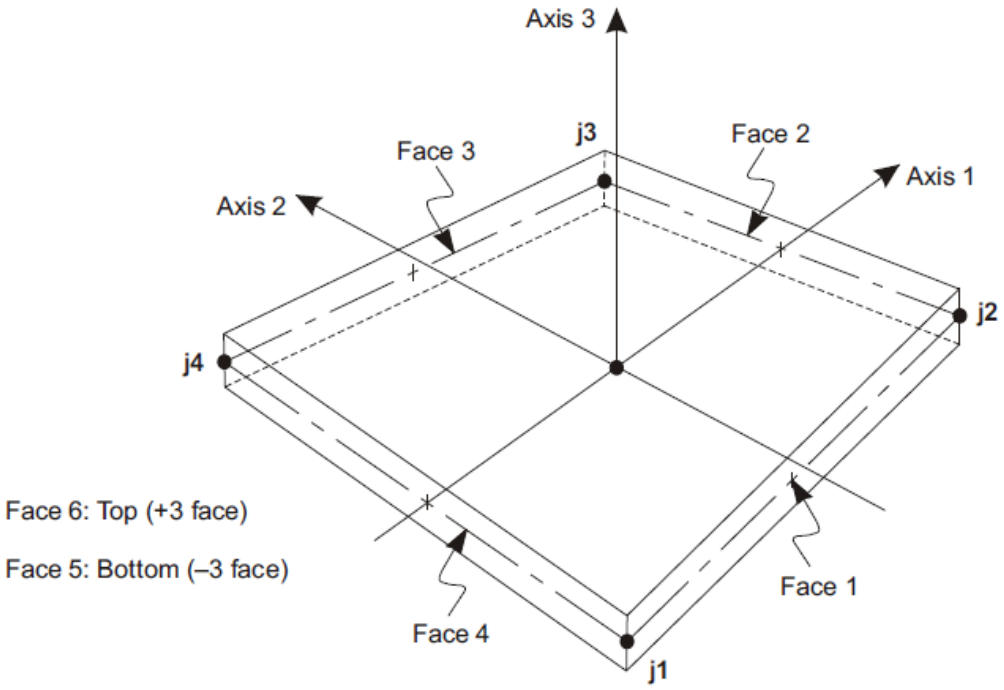

Figure 4.17. Four-node Quadrilateral Shell Element (CSI, 2015)

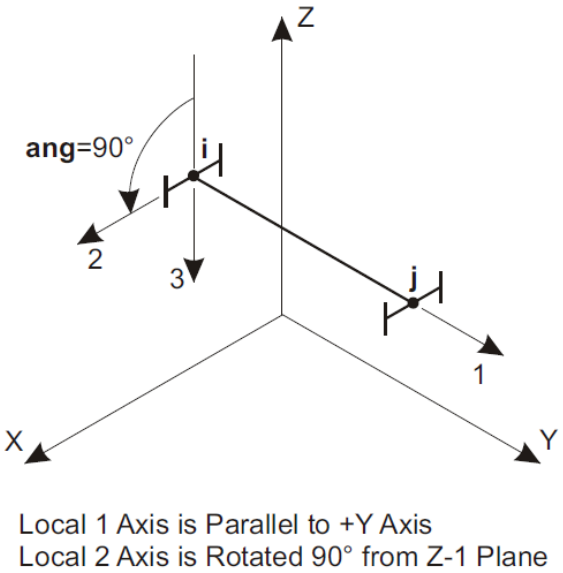

Figure 4.18. Frame beam element (CSI, 2015)

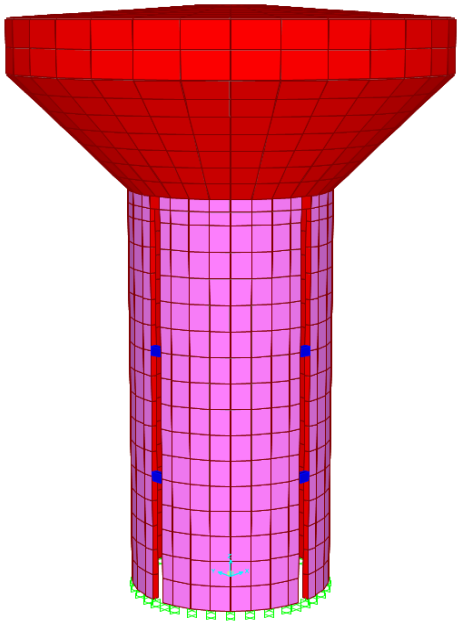

FE model M1-500

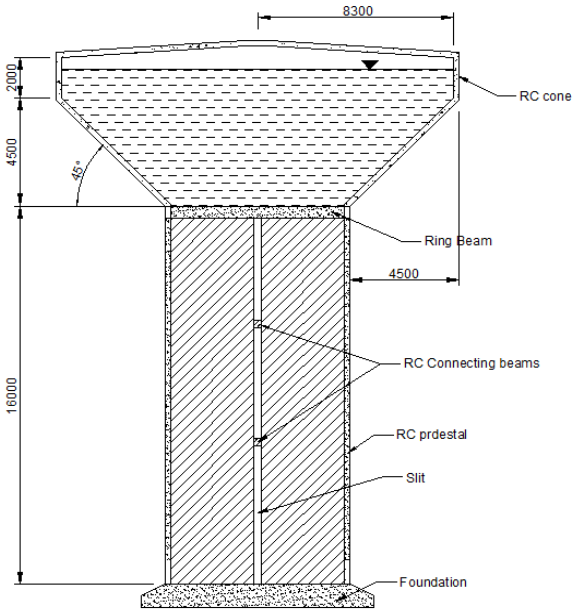

Elevated tank M1-500 - geometry

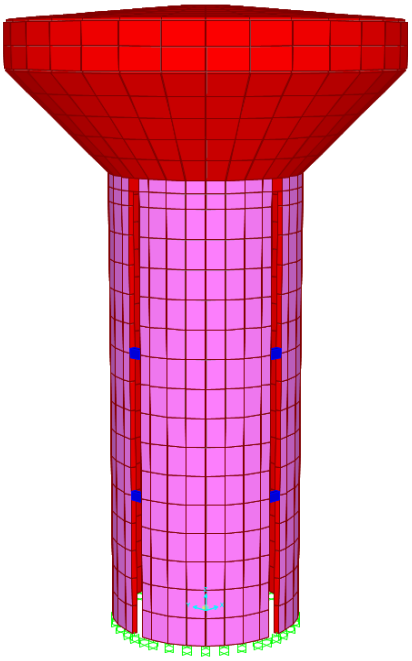

FE model M2-500

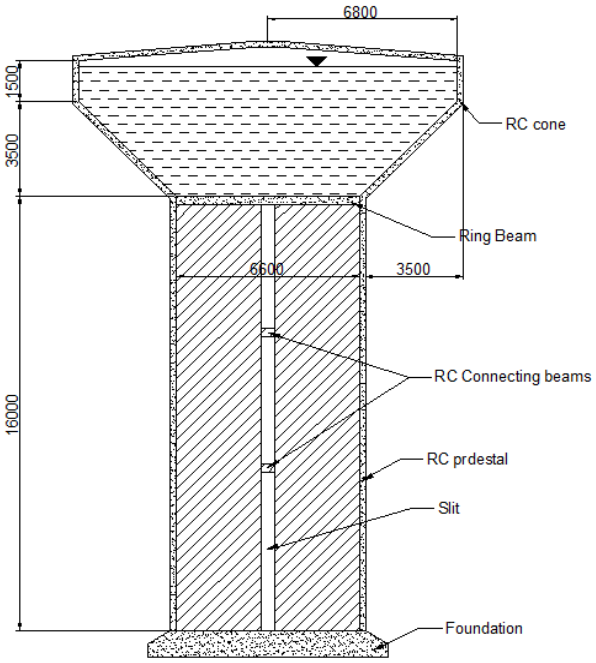

Elevated tank M2-500 geometry

Figure 4.19. FE models and geometry of selected water tanks for analysis

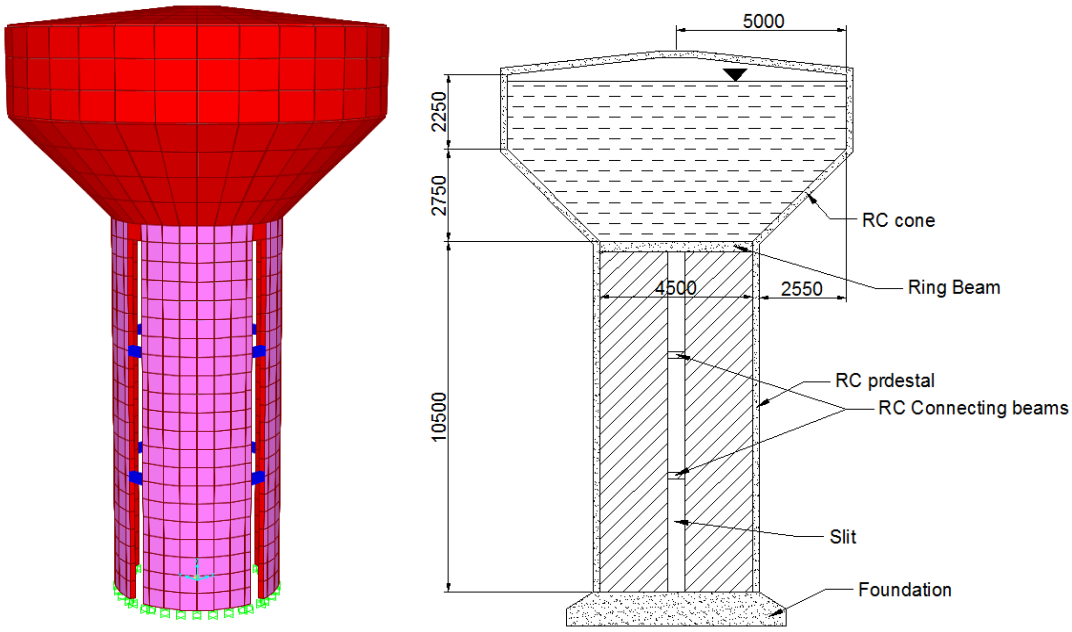

FE model M3-500 Elevated tank M3-500 geometry

Figure 4.19. FE models and geometry of selected water tanks for the study (continue)

4.9.3 Water model inside M1 group water tank

In this study, a two degree of freedom (2DOF) spring-system of fluid-structure interaction (FSI) was adopted from Eurocode 8.

The water tank capacity of M1 water tank is 1000 m^3. The assumption was made that, $1\,m^3 = 1{,}000\,l = 1{,}000\,kg$ and total mass inside the M1 water tank was assumed to be 1,000,000 kg. An approximation of water height for calculation impulsive and convective masses of the axisymmetric tank obtained from an equivalent cylindrical tank having the same free surface diameter and an equivalent water depth was made according to Eurocode 8 showed in Figure 4.20.

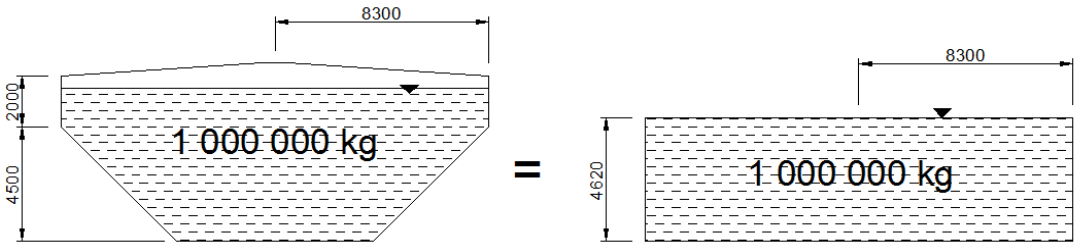

Figure 4.20. Cylindrical approximation of the conical water tank

The impulsive and convective masses $\boldsymbol{m_i}$ and $\boldsymbol{m_c}$ were found using Table 3.3 as fractions of the total liquid mass $\boldsymbol{m}$, along with the heights from the base of the point of application of the resultant of the impulsive and convective hydrodynamic wall pressure, $\boldsymbol{h_i}$ and $\boldsymbol{h_c}$.

The impulsive component of the liquid was considered to move rigidly with the tank wall. An impulsive mass $\boldsymbol{m_i}$ rigidly connected to the tank walls, located at a height $\boldsymbol{h_i}$ above the tank base. For M1 water tank $\boldsymbol{m_i = 331{,}000\ kg}$ and $\boldsymbol{h_i = 1.848\ m}$.

The second component of the liquid was considered to simulate sloshing effect of the water. A convective mass $\boldsymbol{m_c}$ connected by springs to the tank walls, located at a height $\boldsymbol{h_c}$ above the tank base. For M1 water tank $\boldsymbol{m_c = 669{,}000\ kg}$ and $\boldsymbol{h_c = 2.546\ m}$.

For the proposed water tank the first mode of vibration of the sloshing component was found using Equation 3.54:

$$\omega_{c1} = \sqrt{g\frac{\lambda_1}{R}\tanh(\lambda_1\gamma)} = \sqrt{9.807\frac{1.841}{8.3}\tanh(1.841 \times 0.554)}$$

$$\omega_{c1} = 1.294\ rad/s$$

Where:

ω_{c1}	is the first mode of vibration of sloshing component
$g = 9.81\ m/s^2$	is the gravitational acceleration
$\lambda_1 = 1.841$	is the dimensionless parameter equal to 1.841
$R = 8.3\ m$	is the radius of the tank
$\gamma = \frac{H}{R} = 0.554$	is the height/radius ratio

Using Equation 3.53 the stiffness of springs which connect mass $\boldsymbol{m_c}$ to the walls of water tank was calculated:

$$k_c = \omega_{c1}^2 m_c = 1.29^2 \times 669000 = 1.11 \times 10^6\ N/m$$

Where:

ω_{c1}	is the first mode of vibration of the sloshing component
m_c	is the convective mass

The impulsive mass $\boldsymbol{m_i}$ was uniform distributed among the nodes in tank model, with the lumped masses attached directly to the wall element nodes at height $\boldsymbol{h_i}$. On the other hand, the convective mass $\boldsymbol{m_c}$ was attached to the water tank with the use of non-structural mass element by four springs to interior walls of the tank at height $\boldsymbol{h_c}$. The stiffness of every spring for convective mass was equal to $k_c/2$. The two mass system defined for model M1 schematically illustrated in Figure 4.21.

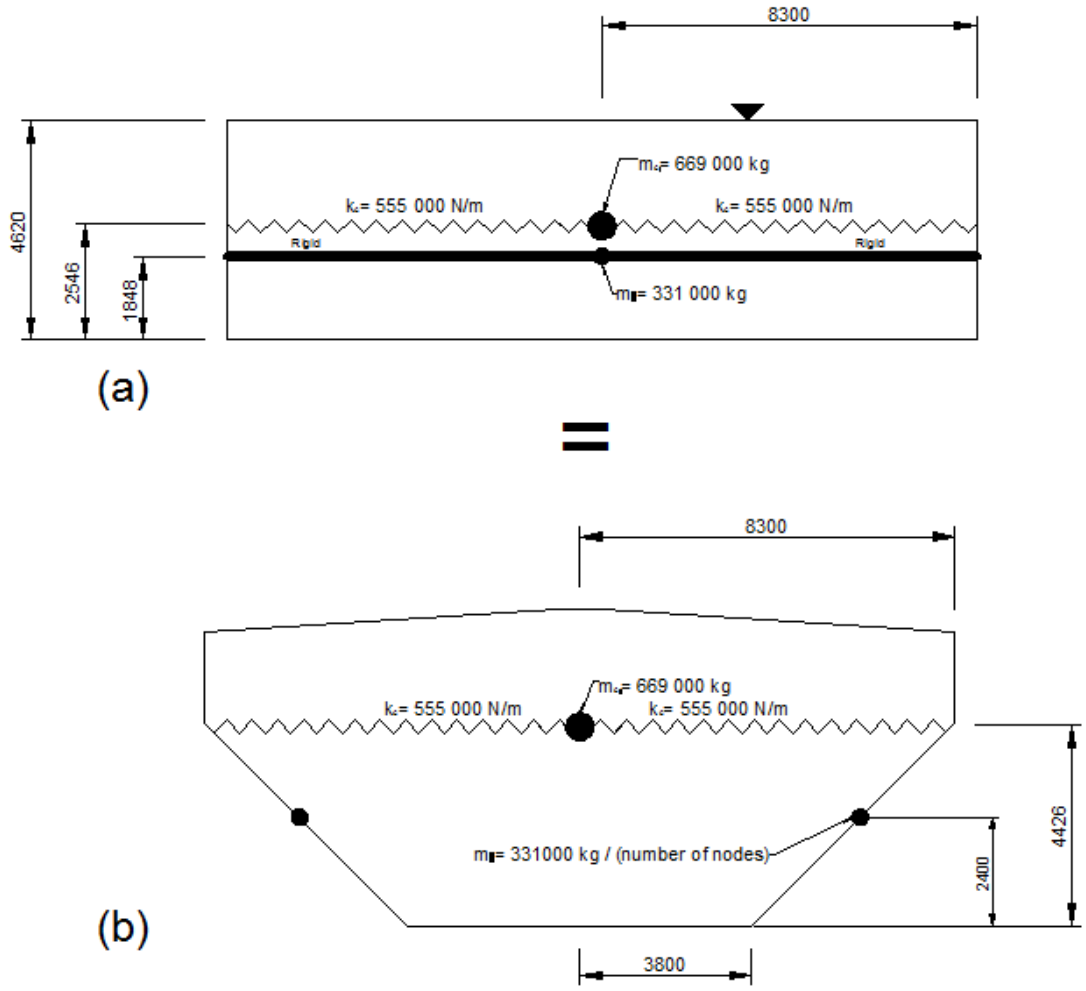

Figure 4.21. (a) Equivalent cylindrical two mass model and (b) Two mass model for M1 water tank model M1

4.9.4 Comparison between full and empty water tanks

Basically, there are three conditions that are generally considered while analyse the elevated water tank: Empty condition, partially filled condition and full condition.

Time history analysis was performed to compare seismic responses of M1 elevated water tank in empty and full conditions. The ground motion used for analysis was the horizontal component of 1940 El-Centro earthquake showed in Figure 4.10 and scaled to the peak ground acceleration of 0.4g. An integration time step of 0.05 second was used for time history analysis of the tanks.

Time history analysis was performed on FE model M1 under two loading conditions, full and empty tank. The results of base shear and base moment showed in Figure 4.22. Since the water inside the tank consider a major amount of the overall gravity load of the elevated water tank structure, there was a significant difference between the seismic base shear forces and top lateral displacement induced in empty and full tank states.

In this study the case of full tank condition was investigated because maximum base shear and top lateral displacement in RC shaft elevated water tanks occurred in full condition.

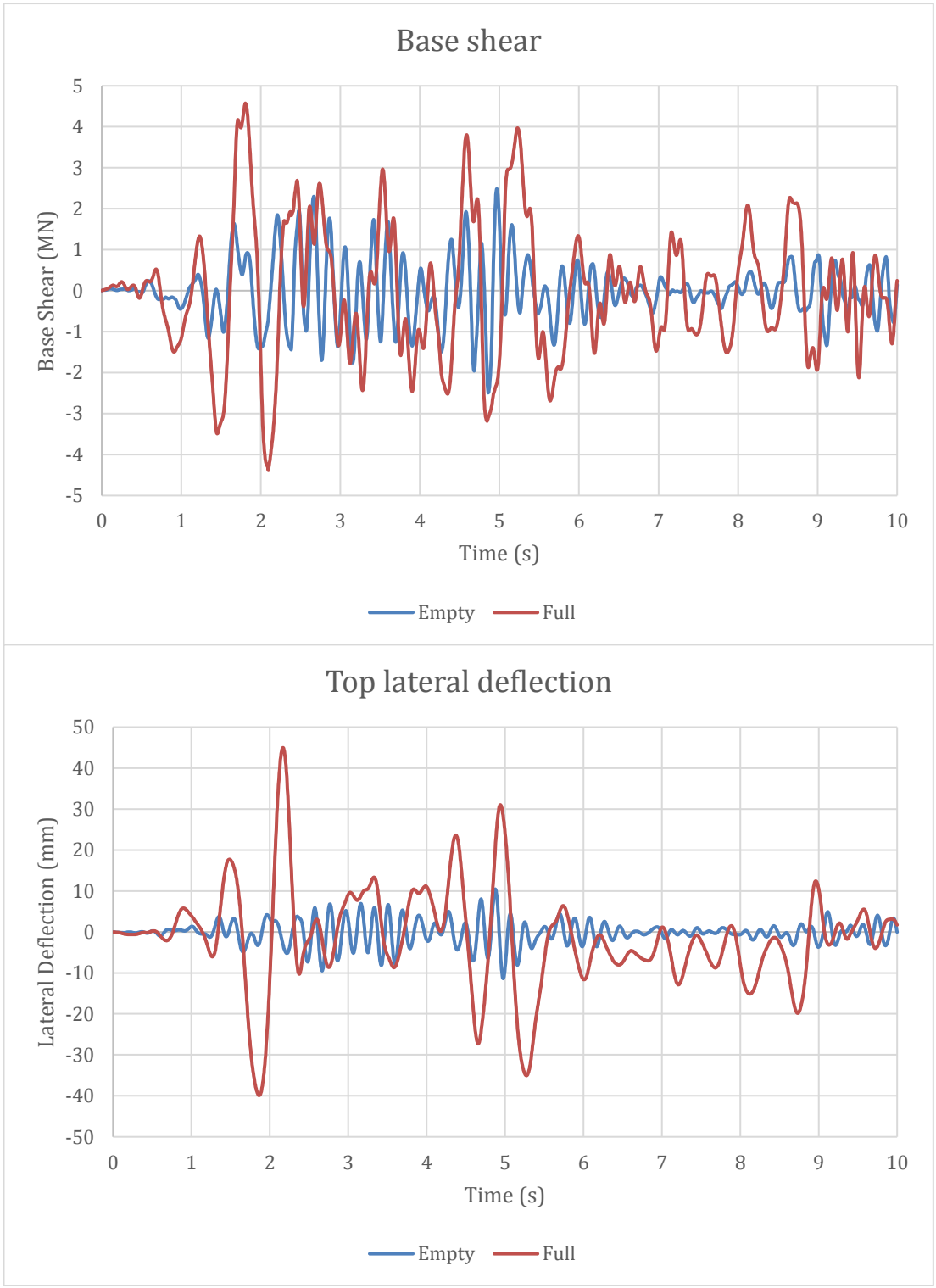

Figure 4.22. Time history base shear and top lateral displacement responses of M1-Solid model in empty and full cases subjected to El-Centro horizontal excitation scaled to PGA=0.4g

Chapter 5

Results and Discussion – Modal Analysis

5.1 Introduction

In this chapter, the dynamic behaviour of the proposed FE elevated tank models were studied in a three dimensional space and the modal analysis of the constructed models were conducted. Such an analysis can be compared with the approximations and serve to troubleshoot the model. Additionally, such analyses may verify some of the assumptions or limitations used in the design process. SAP2000 software was used to conduct the modal analysis of the FE model.

A study of the dynamic behaviour of slit RC shafts with four bands of vertical slits located at 90 degrees intervals was carried out using modal analysis. Slits ranging from 50 mm to 2000 mm are examined in this study. The slit shaft model has the same overall dimensions and material properties as the solid shaft. In order to investigate the effects of seismic load on the performance of slit shafts, the slit width was taken as the parameter to be studied. A total of three slit models were analysed. For comparison, a solid shaft model was also included in the study. The geometry and other considerations were taken into account in modelling of the tanks are described in the methodology chapter.

The primary objective of this chapter was to perform modal analyses on the studied elevated water tanks. Using the proposed FE technique, impulsive and convective response components were obtained separately. The values for the first convective and impulsive responses were obtained and compared against the current practice values. According to Eurocode 8 the total mass participation ratio should not be less than 90% of the total mass, therefore the convective and first two impulsive masses were found in this analysis.

The main focus of the second section was to investigate energy dissipation in FE models. To do so, the modal time history analysis was performed on the proposed elevated water tank models.

However, presenting and analysing the results of the modal analysis for all models in the thesis is not practical, therefore the modal analysis will only be further explained

for the “M1 group”. The rest of the results are presented in the Appendix A. The definition of the M1 group was based on a number of selection criteria. The M1 group should be able to precisely represent the majority of the possible response features of all the designed model. Four models were included in M1 group, namely M1-Solid, M1-50, M1-500 and M1-1000.

5.2 Convective and impulsive components

In this study, the modal analyses were carried out on the three-dimensional M1 group FE models. The results of the modal analysis are summarized in Table 5.1 and Figure 5.1. Data and graphs for modal analysis results for the all models included in the research within M1 group are presented in Appendix B.1.

The fundamental convective and impulsive modes were identified as those with the largest participation factors in the horizontal X direction. Given in the table is the mass participation ratio (Ri) of the effective modal mass in X direction to the total mass of the system. As can be observed from the table, the effective mass corresponding to the fundamental modes, were much greater than those of other modes. This indicates that the response of the system was dominated by the fundamental modes under horizontal excitations.

Table 5.1. Modal analysis results for the M1 group models

FE model ID	Convective mode		Fundamental mode		2nd Impulsive mode		Total (Ri)
	Period (s)	(Ri)	Period (s)	(Ri)	Period (s)	(Ri)	
M1-Solid	4.91	0.54	0.42	0.3	0.13	0.1	0.94
M1-50	4.92	0.55	0.48	0.33	0.16	0.03	0.90
M1-500	4.93	0.59	0.55	0.32	0.18	0.02	0.94
M1-1000	4.93	0.61	0.61	0.31	0.19	0.02	0.94

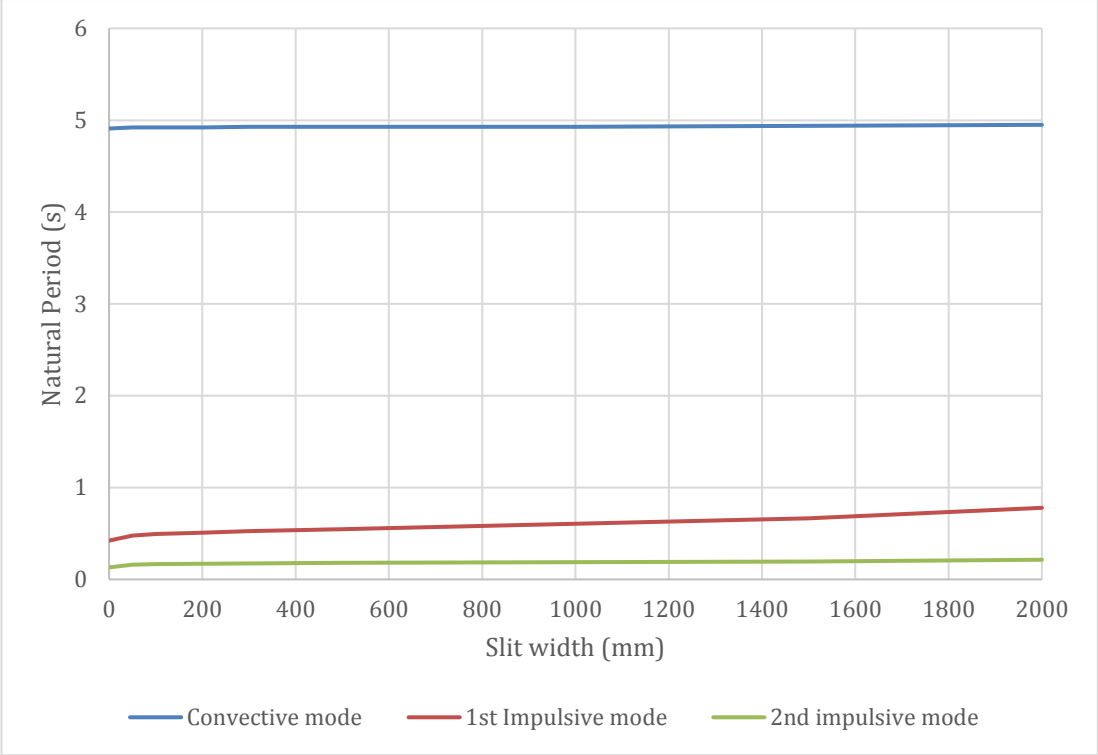

Figure 5.1. Modal analysis results for the M1 group models

By reviewing the table, it can be observed that the calculated FE results corresponded with those given by the Eurocode 8 method for convective mode and Rai (2004) for the impulsive fundamental mode.

For comparison of fundamental periods, obtained through Eurocode 8 method (Eurocode 8: Part 4, 2006) assumed the vessels to be rigid according Equation 3.44:

$$\omega_{c1} = \sqrt{g \frac{\lambda_1}{R} \tanh(\lambda_1 \gamma)}$$

Where:

ω_{c1}	is the natural circular frequency
$g = 9.81\ m/s^2$	is the gravitational acceleration
$\lambda_1 = 1.841$	is the dimensionless parameter equal to 1.841
$R = 8.3\ m$	is the radius of the tank
$\gamma = \frac{H}{R} = 0.554$	is the height/radius ratio

The relation between fundamental period, T, and natural circular frequency, ω_{c1}, is given by Equation 3.43:

$$T = \frac{2\pi}{\omega_{c1}}$$

The fundamental sloshing periods obtained through FE modal analysis for the solid model M1-Solid corresponds with the Eurocode 8 method assuming vessels to be rigid, was equal to 4.91 seconds. The difference in the convective mass values was less than 1 percent between Eurocode 8 calculations and FE results for all M1 group models.

This difference was even smaller for the impulsive periods between FE results and Rai (2004) theoretical calculations (less than 1 percent). The fundamental period of the comparable elevated water tank obtained by Rai (2004) was 0.421 second compared to 0.42 seconds for fundamental mode obtained from FE results.

Joshi (2000) recommended that maximum errors for the impulsive and convective masses should be less than 5 percent for the impulsive and convective masses for tanks with the equivalent depth to radius ratios between 0.5 and 1.0 (which is the case here). The equivalent depth to radius ratio for the model considered in this study was 0.554.

The modes given in Table 5.1 were greater than 90 percent of the total mass of the system. This sum of the effective mass ratio was more than the minimum criterion recommended by Eurocode 8.

Modes with exactly similar fundamental periods represented the same mode in two perpendicular directions (X and Y). Each of these modes was deviated from X or Y-axis by a small angle (Figure 5.2(b) and Figure 5.2(c)). The effective masses were given as their projections on the X-axis. As a result, the mode shapes and other modal properties remained the same for the first two convective and the first two impulsive modes.

The fundamental impulsive mode presented in the Table 5.1 was a translational mode. According to Moslemi (2011) this mode was classified as the cosθ type mode during which the tank's cross-section remains circular. During the fundamental impulsive mode, the entire tank behaved like a vertical beam.

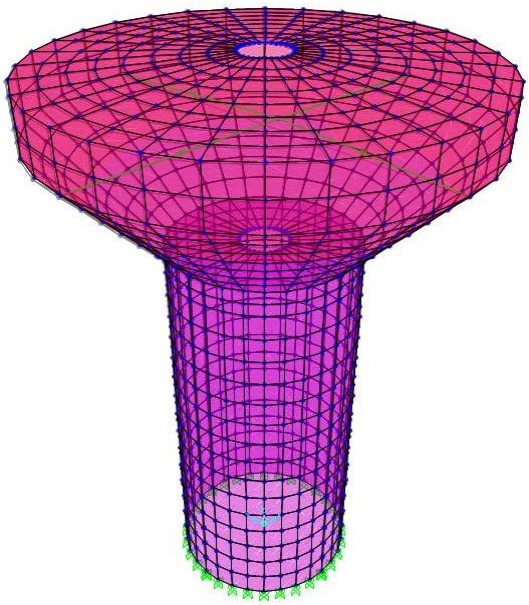

(a) Convective Mode

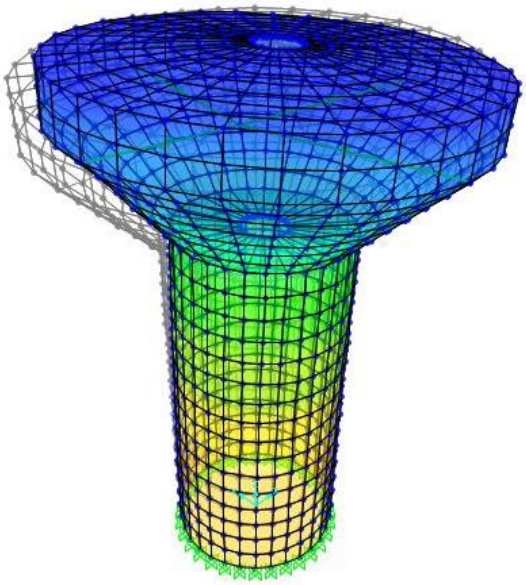

(b) 1st Impulsive Mode – X Direction

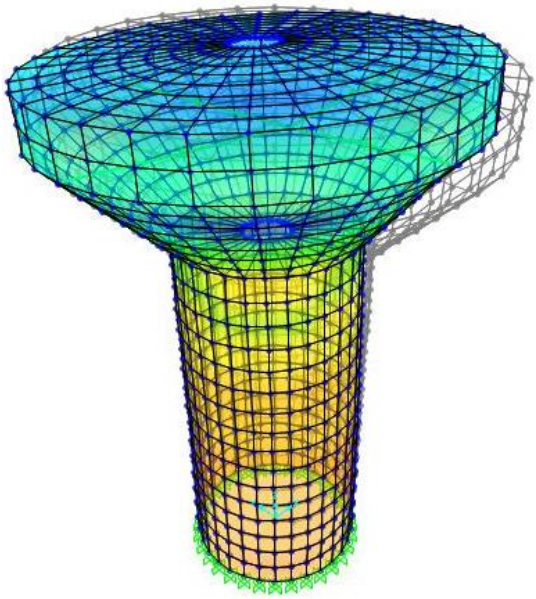

(c) 1st Impulsive Mode – Y Direction

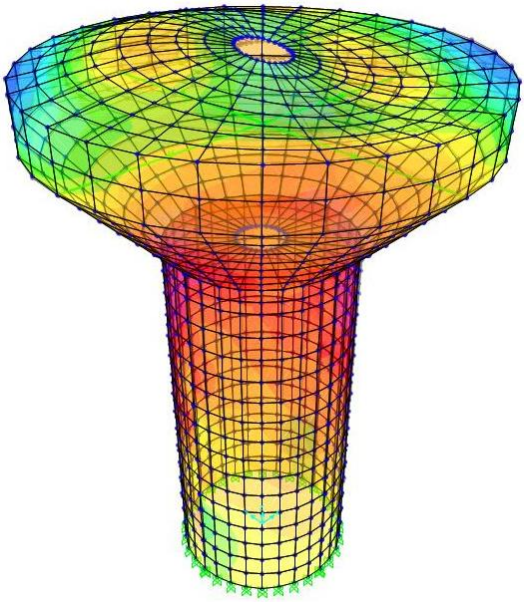

(d) 2nd Impulsive mode

Figure 5.2. M1-Solid model mode shapes

For higher impulsive modes (modes 2 to 3), the top part of the vessel experiences more pronounced deformation compared to the rest of the tank. Moslemi (2011) explained this phenomena by the higher stiffness attributes associated with the conical part, compared to the cylindrical part. Figure 5.2 (c) represents this effect.

Bozorgmehrnia, et al. (2013) conducted a research on seismic behaviour on concrete elevated water tanks. Results showed that the difference in the impulsive and convective periods was primarily due to the different stiffness and damping of the structure and water. It was assumed 5 percent damping for structures and 0.5 percent for the liquid inside the structures.

Comparing the mass ratios obtained for different models, it was observed that by increasing the slit width from 0 to 1000 millimetres, the convective and fundamental mass ratio increased by 12% and 13% whilst an inverse trend was observed for the 2nd impulsive mode mass ratio, which decreased by 80%.

5.3 Fundamental Period

One parameter that represents both geometry and dynamic response properties of the structures is the fundamental period. The determination of the fundamental period of a water-retaining structure subjected to horizontal seismic excitation is of critical importance since the majority of tank failures under seismic conditions occur due to resonance effects (Nachtigall, 2003). Determining the fundamental period of a structure is complex and a number of different aspects need to be considered. These aspects include:

- the flexibility of the tank wall
- the influence of the contained liquid on the behaviour of the tank,
- the fixity of the shaft to the base and soil conditions.

The fundamental periods elongated as the slit became wider (Figure 5.1). This was expected since the slit width increase resulted in a more flexible structure. The period of elongation was increased by 14%, 31% and 45% for models M1-50, M1-500 and M1-1000 in respect to model M1-Solid.

As indicated by the mass participation ratio (Table 5.1), the models were dominated by first convective and two impulsive modes, which were adequate to capture 90% of the structural response in all cases. This modes of vibration for model M1-Solid are

illustrated in Figure 5.2. The illustration of those modes are suitable for all models in this study.

Lopes and Oliveira (2012), performed analyses on a large set of RC elevated water tanks (44 tanks). It was found that in all elevated water tanks the dominant was the 1st impulsive mode. It was also concluded that fundamental period elongated when water shaft height increased and diameter of a shaft decreased.

Shakib, et al. (2010) carried out investigation on the seismic nonlinear response of concrete elevated water by using FE analysis. Three RC elevated water tanks were subjected to horizontal seismic excitations. The results showed that the reduction of stiffness of the reinforced concrete staging resulted in fundamental period increase.

Moreover, Rai, (2002; 2004), investigated eight elevated RC water tanks with different geometrical properties of shafts and water tank sizes. It was observed from the results that an increase of the stiffness of a shaft resulted in shorter fundamental period.

On the other hand, Livaoglu and Dogangun (2006) showed that the flexibility of the shaft does not have a significant impact on the convective mode in the elevated water tanks.

5.4 Modal damping

Damping is useful for simulating energy dissipation that is not clearly modelled within a structural system. Nonlinear behaviour such as friction is an example of such a mechanism. The plastic-hinge formulation can be account for energy dissipation, within the hinge region, which is caused by yielding during dynamic analysis.

In structural engineering, viscous velocity-dependent damping is very difficult to visualize for most real structural systems. Only a small number of structures have a finite number of damping elements where real viscous dynamic properties can be measured. In most cases modal damping ratios are used in the computer model to approximate the unknown nonlinear energy dissipation within the structure (Wilson and Penzien, 1972).

To find modal damping energy dissipation in proposed models the modal time history analysis was performed. The ground motion used for the modal time history analysis was the horizontal component of the 1940 El-Centro earthquake scaled to the peak ground acceleration (PGA) of 0.4g as shown in Figure 5.3. An integration time step of 0.005 seconds was used for the time history analysis of the tanks.

The comparative dissipated modal damping energies of the slit and solid models that were obtained by performing their modal time-history analysis are shown in Figure 5.4. It is found that the slit shaft has better energy dissipation capacity that can prevent severe damage of the shaft base. The energy dissipation mechanism is different for slit and solid shaft. The solid shaft dissipates seismic energy mainly at the base while models with slits has different modes resulting in to greater energy dissipation. Figure 5.4 shows the modal damping energy dissipation of four models proposed in this analysis. From this figure we can observe that the slit shafts dissipate above 1.5 times more hysteretic energy than the solid wall. Graphs for modal damping energy dissipation results for the all models included in the research within M1 group are presented in Appendix B.2.

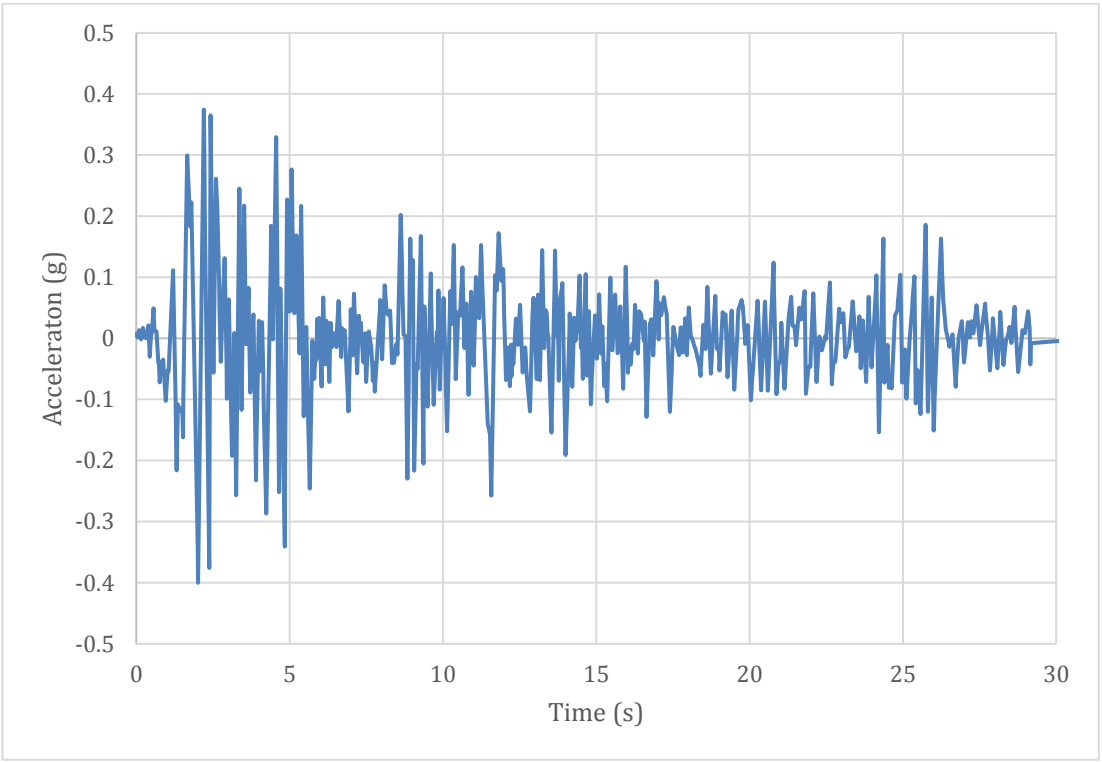

Figure 5.3 El-Centro ground motion horizontal component scaled to PGA=0.4g

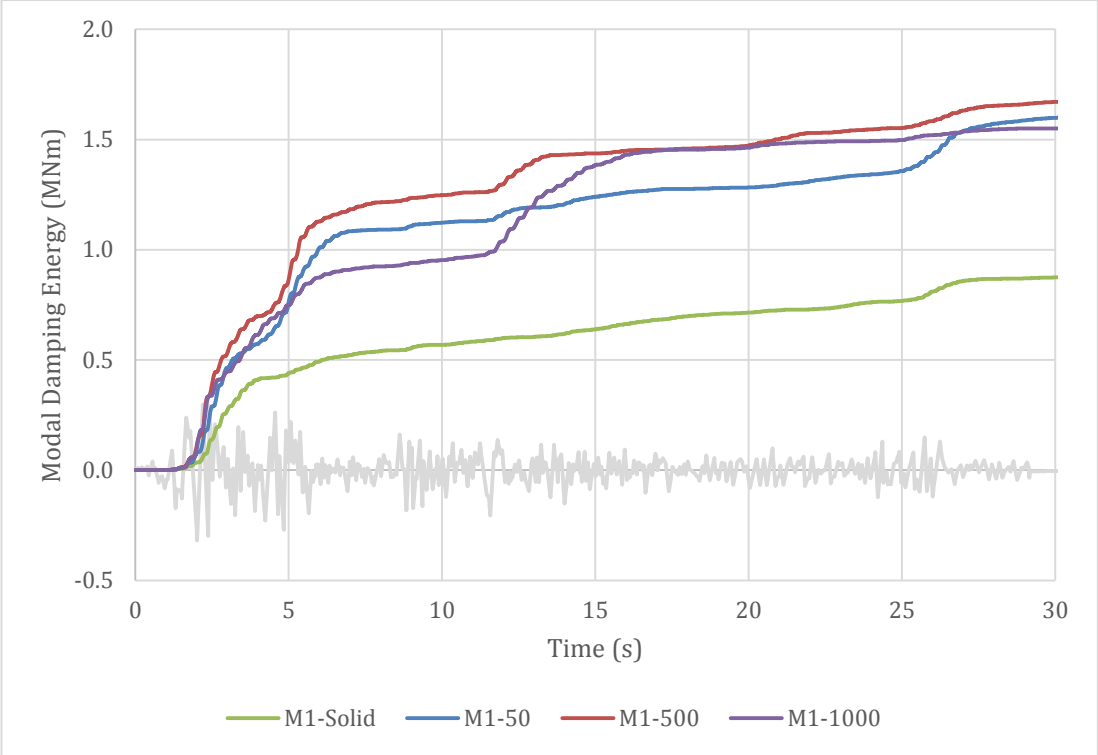

Figure 5.4. Modal damping energy dissipation of M1 group models subjected to El-Centro earthquake scaled to PGA=0.4g

As shown in Figure 5.4, first 1.5 seconds there was not any hysteric energy dissipation. That phenomenon is due to the elastic behaviour of models. Figure 5.3 provides the earthquake spectrum, which shows that severe ground acceleration starts at approximately 1 second. In addition to that time the fundamental period should be added as a reaction time of a structure to the seismic excitations.

It can be observed that there is a significant difference in the modal damping energy escalations between the different models. This is as a result of the significant influence of slit width variation on the relative stiffness distribution of structural components, which results in introducing new types of modes with different dynamic characteristics to the tank-shaft system.

Several researchers have recognized the energy, absorbed by a structural system during a seismic event that was strong enough to induce a certain amount of nonlinearity to the system, as a potentially useful seismic performance indicator (Park, et al., 1987; Bojorquez, et al., 2011).

The increase of energy dissipation was shown by Baetu, et al (2013), in the study of slit walls (Figure 2.19). It has also stated that the damping increases in the case of the slit wall after the failure of the short connections and the spectral acceleration is reduced, the seismic forces being thus also reduced, allowing this fact an economical design.

Kazantzi and Vamvatsikos (2012) studied the correlation between energy dissipation and seismic performance. It was concluded that better energy dissipation resulted in a higher damping and therefore in a better performance of a structure

5.5 Summary

During this study, modal analysis was carried out to investigate the dynamic properties of proposed slit RC shaft elevated water tanks.

The results of the study compared very well with both analytical results, indicating the validity of the proposed FE method in studying the fluid-structure interaction effects in elevated water tanks. Modal FE analyses resulted in fundamental periods and effective water mass ratios very close to those obtained from Rai (2004) formulations with differences for the fundamental period being smaller than 1% for the solid shaft model. Furthermore, the convective mode results show a great agreement with Eurocode 8 methodology. The sloshing response of the elevated water tanks considered was mainly dominated with the fundamental sloshing mode.

From the results, can be concluded that both impulsive and sloshing behaviours of the considered models were practically dominated by their fundamental modes. The sloshing response of the elevated water tanks considered was mainly dominated by the fundamental sloshing mode. However, the results showed that the fundamental response of the tank models having narrow slit width or solid tanks could not be accurately predicted by only considering the fundamental impulsive mode. As a result, more impulsive modes other than the fundamental impulsive mode are needed in studying the dynamic behaviour of such models. The information of first and second impulsive modes will be used in Chapter 7, time history analysis.

It is important to note that the effects of the slit width variations on the fundamental periods of the impulsive modes were considerably pronounced from 0.42 to 0.61 seconds for M1-Solid and M1-1000 models respectively. This was because of the significant influence of slit width variation on the relative stiffness and ductility in the RC shafts in elevated water tanks. It can be concluded that slit width can be a regulator of the stiffness and ductility in RC shafts.

Modal time history analysis of the elevated water tanks in the second part of the study shows that energy dissipation through modal damping is approximately 1.5 times higher in slit shaft models compare to the solid model. Slit shaft has better energy dissipation capacity that can prevent serious damage of the shaft base. Models with slits in the shaft obtain new higher modes that benefit to energy dissipation. It can be concluded that dynamic response of slit shaft elevated water tanks should be better in comparison to the solid tan

Chapter 6

Results and Discussion – Static Nonlinear Analysis

6.1 Introduction

This chapter investigates the seismic performance of RC elevated water tanks by conducting capacity spectrum analysis. The focus is on evaluating the pushover curves that are obtained from the nonlinear static (pushover) analysis of models.

The pushover analyses conducted in this study were intended to verify the performance of the proposed models, and estimate their ultimate capacities for eventual comparison with earthquake demands of Eurocode 8 and results presented in Chapter 7. Pushover curves present valuable information regarding the seismic response behaviour of structures.

The M1 group of four RC shafts that was introduced in Chapter 5 was employed for conducting the analysis. The chapter starts with conducting a pushover analysis on study group elevated water tanks. By extracting the load-deformation results of the pushover analysis, the pushover curves were generated. The pushover curves of the study group were then presented and compared to each other. There were some general patterns exhibited by pushover curves, which were discussed. The effect of various factors in the pushover curves were addressed as well.

Performance point for all models to withstand earthquake with peak ground acceleration (PGA) equal to 0.4g for soil type A, B, C and D of Eurocode 8 was found according to capacity spectrum methodology explained in Chapter 3.

The tension and compression stress propagation patterns that was observed in the process of pushover analysis was analysed. According to the stress patterns, the crack propagation in shafts was explained. These patterns were compared and categorised based on the slit width of the elevated water tanks.

Finally, the vulnerable zones of all types of studied water tanks were examined and compared to the monolithic elevated water tank. The most efficient slit width was determined for all soil types.

6.2 Pushover analysis

The procedure of performing a pushover analysis in this study was adapted from Eurocode 8. First, the gravity loads including weights of tank, shaft and stored water was applied to the FE model. Next a gradually increasing lateral load was applied to the model until the structure collapses. The lateral load must match the effects of actual seismic loads as much as possible.

In case of elevated water tanks, the lateral load was applied with a load pattern similar to the fundamental mode shape. This is due to the fact that that most of the weight was concentrated in the tank and the modal mass participation factor of the fundamental mode was approximately 90%. Therefore the effect of other mode in the load pattern was negligible. It was assumed that entire tank behaved like a vertical beam.

In these analyses and under load control, the structure was subjected to gradually increasing lateral loads. The analysis was terminated when the structure achieved its performance criteria (reaches peak base shear) or fails (defined as a negative value in the stiffness matrix).

The results of pushover analysis for the study group are shown in Figure 6.1. The graph demonstrates the pushover curves for models, which were designed to have four slits at 90 degrees intervals along the full height of the shaft and connected with two beams at 5 and 10 meters heights from the ground. For comparison purpose the solid model (M1-Solid) was also presented. Data and graphs for pushover analysis results for the all models included in the research within the full M1 group are presented in Appendix C.2.

There are many definitions of ultimate displacement of a structure subjected to pushover analysis. Some studies recommend to define the ultimate displacement at a certain level of structure failure (Park, 1988). Other institutes, such as Federal Emergency Management Agency (FEMA), recommend to define the ultimate displacement at the point where the base shear falls to 80% of the peak of the base shear. However, the above recommendations are suitable for structures with high levels of ductility.

On the other hand, RC shafts have a very low level of ductility. Reduction in the stiffness due to plastic hinges at the shaft base could lead to extreme failure modes

such as collapse of an elevated water tank. The more conservative and realistic definition of maximum displacement for elevated water tanks was suggested by Ghateh (2006). The maximum displacement was defined at peak of base shear as this point represents the beginning of stiffness reduction.

The peak point of base shear was defined as failure criteria for FE models and it was denoted in the Figure 6.1 as 'Peak base shear'. Moreover, when compression concrete stresses reached ultimate compressive concrete strength $f_c' = 20\ N/mm^2$, concrete began to crash and reduce in strength, which resulted in failure of the elevated water tank. The Figure 6.1 presents the point at which the base concrete begins to crash at the opposite side of the applied load, was denoted as 'base crash'.

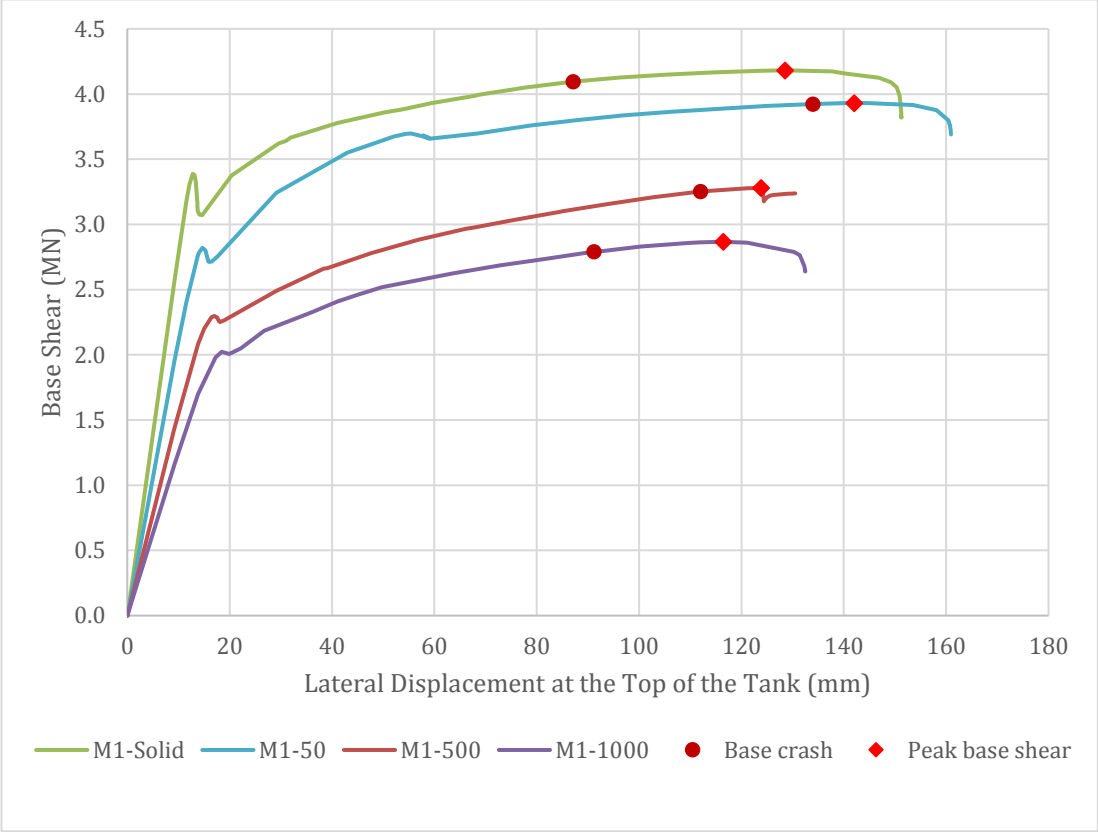

Figure 6.1. Results of pushover analysis for M1 group models

Table 6.1 summarises the results of the pushover analysis for the M1 group. This table presents results including the peak base shear (V_{max}), top lateral displacement at peak base shear ($\Delta_{V_{max}}$), base shear at the point of base crash (V_{Crash}) and top lateral displacement at the point of base crash ($\Delta_{V_{crash}}$).

As described in Chapter 5, since the main variable in this study was slit width, the structural behaviour of the system was expected to be different for stiffer or more flexible shafts.

Table 6.1. Results of pushover analysis for the M1 group models

FE model ID	Peak Base Shear		Base Crash	
	$V_{max}\ (MN)$	$\Delta_{V_{max}}\ (mm)$	$V_{Crash}\ (MN)$	$\Delta_{V_{crash}}\ (mm)$
M1-Solid	4.18	129	4.10	87
M1-50	3.93	142	3.92	134
M1-500	3.28	124	2.07	82
M1-1000	2.87	116	2.79	91

6.3 Discussion of results of pushover analysis

The first observation was that models with narrower slit width in RC shafts demonstrate higher maximum base shear compared to models with wider slits. Also, models with wide slit width were not able to tolerate as much lateral displacement capacity as shafts with narrow width do.

In all of the pushover analysis results, models with slits were presenting less maximum base shear than the solid model. This effect was more considerable for models with wider slits. The comparison of base shear indicated that base shear decreased by 6%, 27% and 46% for models M1-50, M1-500 and M1-1000 compared to model M1-Solid.

In addition, slit width did not appear to have a considerable effect on the maximum top lateral displacement (Δ_{max}) of the models with slits between 500 and 1000 millimetres. However the maximum top lateral displacement decreased by 19% between models M1-50 and M1-500.

It can be clearly seen that the base crash in FE models with slits 50 mm and 500 mm in the RC shafts appeared just prior to a point of maximum base shear. That phenomenon can be explained as the shear forces were distributed along the whole shaft and concentrated around slit connections. After the connections failed, all shear forces concentrated at the base that resulted to failure of a structure.

On the other hand, the solid model base crash started noticeable earlier the maximum base shear had been reached. The only compressive zone was in the base corner of a shaft opposite to the application of load and shear force increased gradually until reached the ultimate value. The concrete crash of a large area in that zone resulted the failure of the structure.

The model with 1000 mm slits in the RC shaft also showed a noticeable distance between base crash and peak base shear points. The increase in slit width resulted in coupling force reduction between shaft piers and increase of shear force concentration at the shaft base which increase gradually. In the other words, a large distance between base crash and peak base shear points means a poor distribution of shear force.

Ghateh (2006) conducted a number of pushover analysis for elevated water tanks. Results showed that the most realistic zone of failure for the elevated water tanks with RC shaft was the base of a shaft due to the extended cracks and crash of the concrete.

Livaoglu and Dogangun (2005) conducted research regarding the response of the supporting staging system of elevated water tanks. They were considered frame and shell supporting systems. Conclusions from the analysis results showed that the supporting system could considerably change the seismic behaviour of the elevated water tanks.

Tehrani (2014), compared pushover analysis of elevated water tanks supported on concrete shafts with nonlinear time-history analysis. The results demonstrated the acceptable accuracy of the proposed pushover analysis for elevated water tanks.

6.4 Capacity spectrum analysis

The method that was used to determine the performance point in this study was the capacity spectrum method, also known as the acceleration – displacement response spectra method. The capacity spectrum method is a graphical and approximate method used to compare the building capacity and an earthquake demand. Figure 6.2 represents a capacity spectrum for the determination of a performance point of M1-50 model capacity spectrum and demand spectrum of $PGA = 0.4g$ spectral acceleration for soil type C of Eurocode 8 using SAP2000. It considered the seismic demand initially using a 5% damped linear-elastic response spectrum and reduces the spectrum to reflect the effects of energy dissipation to estimate the inelastic

displacement demand. The point at which the capacity curve (green) intersects the reduced demand curve (orange) represents the performance point at which capacity and demand are equal (Naeim, 2003).

Figure 6.2. Capacity spectrum method to find performance point between M1-50 capacity curve and Eurocode 8 ground type C demand spectrum

This study considers four soil types defined in Eurocode 8, namely Soil-A, Soil-B, Soil-C and Soil-D. Seismic analyses of elevated water tanks for $PGA = 0.4g$ were done and performance points according to capacity spectrum method were found. The obtained performance points for the elevated tanks were comparatively illustrated in Figure 6.3 and Table 6.2 according to the soil types. The numbers in bold shows an increase (positive) or decrease (negative) percentage over the corresponding solid shaft model. These comparisons clearly showed that the ground types played a significant role in increasing top lateral displacement and stability of all models. As can be seen from Figure 6.3, the most dangerous was ground Type D, deposits of loose-to-medium cohesionless soil and most favourable was ground type A, rock. Eurocode 8 ground types provided 450% and 460% increase in top lateral displacement between the A and D ground types for model A-0 and A-50 respectively. Other models collapsed before could reach the performance point for ground type D. Data and figures for performance point determination by capacity spectrum method for the all models included in the research within M1 group are presented in Appendix C.3.

Table 6.2. Results of capacity spectrum analysis for M1 group models for different soil types located in a seismic zone with PGA = 0.4g by Eurocode 8

	$Soil - A$	$Soil - B$	$Soil - C$	$Soil - D$
FE model ID	Base Shear (MN)			
M1-Solid	3.64	3.89	3.99	3.99
M1-50	3.30 ***-10.33%***	3.66 ***-6.07%***	3.72 ***-7.01%***	3.72 ***-6.17%***
M1-500	2.66 ***-36.67%***	2.98 ***-30.46%***	3.10 ***-28.58%***	N/A
M1-1000	2.41 ***-51.20%***	2.70 ***-44.01%***	2.80 ***-42.50%***	N/A
	Top Lateral Displacement at the Top of the Tank (mm)			
M1-Solid	31	54	68	140
M1-50	33 ***+6.06%***	59 ***+8.47%***	73 ***+6.85%***	152 ***+7.78%***
M1-500	39 ***+20.51%***	68 ***+20.59%***	85 ***+28.58%***	N/A
M1-1000	41 ***+24.39%***	75 ***+28.00%***	93 ***+42.50%***	N/A

For all soil types, an increase in the slit width has a significant influence on the base shear and top lateral displacement. For example, comparison of base shear at soil type C indicated that base shear decreased by 7%, 29% and 43% for models M1-50, M1-500 and M1-1000 respectively, compared to model M1-Solid. On the other hand, top lateral displacement at soil type C increased by 7%, 29% and 43% for models M1-50, M1-500 and M1-1000 respectively, compared to model M1-Solid. The highest reduction in base shear and smallest increase in the top lateral displacement was noticed in soil type A.

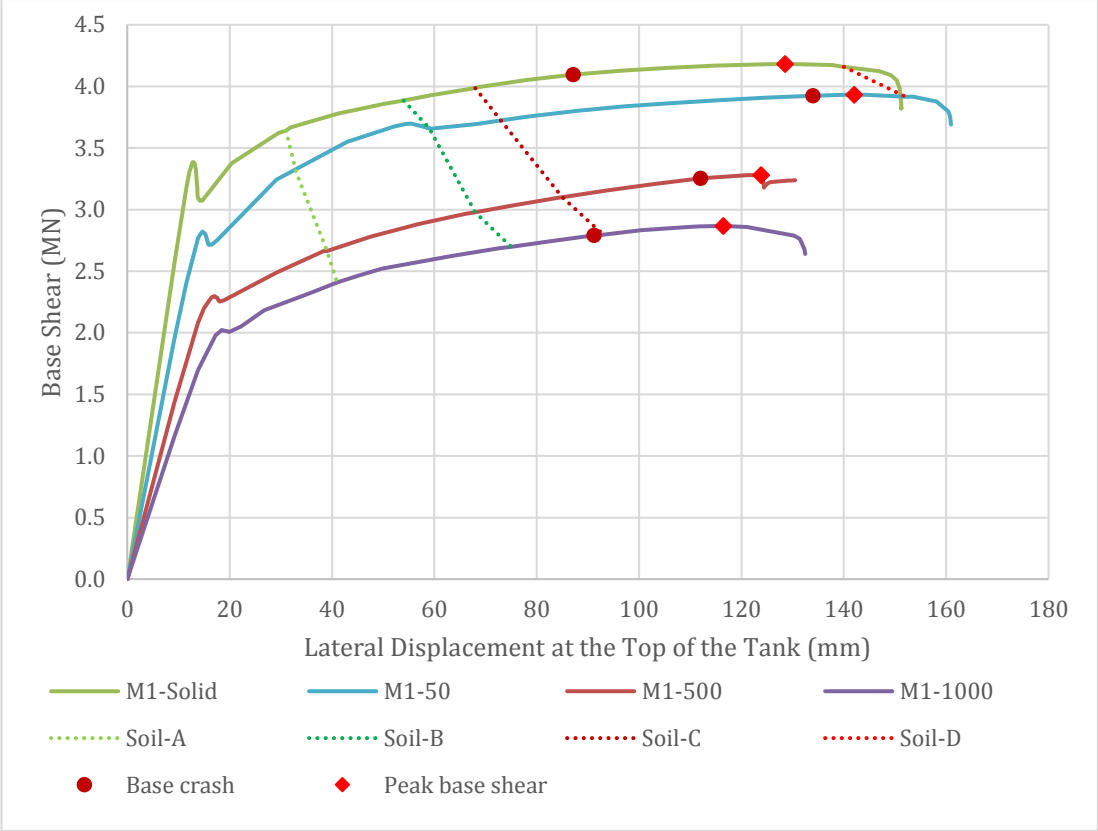

Figure 6.3. Results of capacity spectrum analysis for M1 group models for different soil types located in a seismic zone with PGA = 0.4g by Eurocode 8

The results corresponded with study of Livaoglu and Dogangun (2006), who demonstrated that subsoil classes largely affect the magnitude of the lateral displacement and shear forces which were very important for elevated water tanks subjected to strong earthquakes. It was concluded by researches that displacement for frame and shaft water tank models was estimated for ground type A increased more than two times for ground type C. So, subsoil parameters must be carefully determined for an earthquake resistant design of the elevated tanks, in accordance, to the classical design of elevated tanks.

Hirde and Hedaoo (2011) presented the study of seismic performance of the elevated water tank for various seismic zones of India for various heights and capacity of elevated water tanks for different soil conditions. The author concluded that seismic forces were higher in soft soil than medium soil, and greater in medium soil than hard soil. An earthquake force for soft soil was approximately 40 to 41 percent greater than that of hard soil for all earthquake zones and at tank full and tank empty conditions.

It was noticed that all proposed models had an adequate seismic capacity to withstand an earthquake with $PGA = 0.4g$ situated in A, B and C ground types. However, the increase of the slit width in RC shafts of elevated water tanks decreased the ability to withstand an earthquake of the elevated water tanks in softer soil. This was because of slit increase resulted to ductility increase and stiffness reduction of the RC shafts. Stiffer shafts were more appropriate for soft soils. As an example Figure 6.4 illustrates the effect of an increased slit width to 2000 mm. Figure 6.4 shows that the peak base shear point of model M1-2000 is located formerly than Soil-C and almost at the same location with Soil-B. It could be concluded that model M1-2000 could not withstand an earthquake with $PGA = 0.4g$ located in Soil-C and was dangerous to be located in Soil-B.

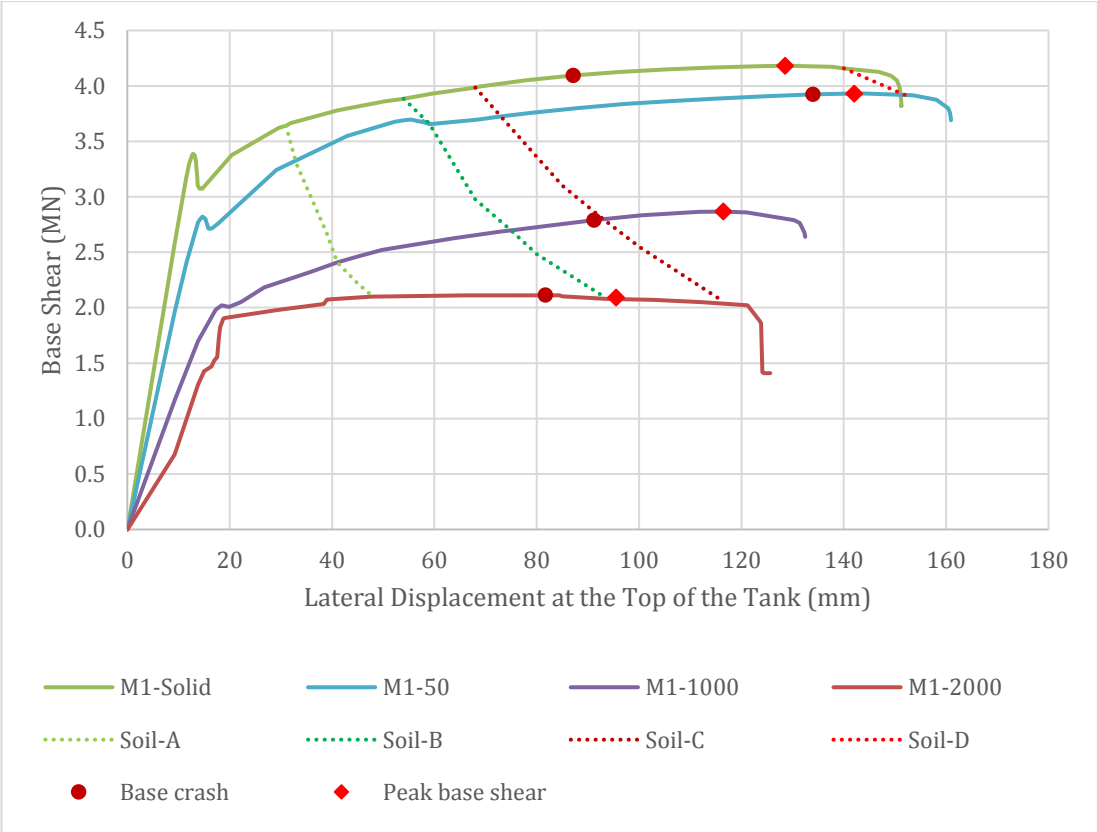

Figure 6.4. Results of capacity spectrum analysis for M1 group models including M1-2000 model for different soil types located in a seismic zone with PGA = 0.4g by Eurocode 8

6.5 Stress distribution in the RC shafts

The principles of the finite element model of the reinforced concrete structures including nonlinear behaviour were explained in the methodology chapter of the thesis. Studying the locations of compression and tension stress concentration provides a better understanding of the structure's weak points and response behaviour under seismic loads.

Cracking was found to occur across the tension regions where concrete reached the ultimate tension strength of $f_t' = 2.785\ N/mm^2$ thereafter rebars carried all tension load, and displacement started to be more pronounced in the area of cracking. Once this region began to crack, concrete stresses within that area relieved and distributed within the rest of the area, which had not cracks.

On the other hand, the opposite corner of tension was in compression. During concrete cracking loading was distributed along the un-cracked sections that were under compression. When compression stresses reached ultimate compressive concrete strength of $f_c' = -20\ N/mm^2$, concrete began to crash and reduced in strength, which resulted in failure of the elevated water tank.

Figure 6.5 demonstrates the distribution of tension and compression stresses in M1 group of elevated water tank models at the stage when shear force reached the maximum value (failure point). At this stage the cracks were propagated all over the RC shaft and the structure had experienced extensive deformation. Figures for distribution of ultimate tension and compression stresses as well as top lateral displacement for the all models included in the research within the full M1 group are presented in Appendix C.4.

As expected, this behaviour was the result of stress localisation in distinct locations. Reinforced concrete did not lose strength uniformly, and the entire shaft did not simultaneously crumble under tension. Instead, steel carried the entire load across the concrete stresses reaches the ultimate value. However when concrete stresses did not reaches the ultimate values, concrete shared the load with steel reinforcement. The stress patterns shown in Figure 6.5 are stable with above explanation.

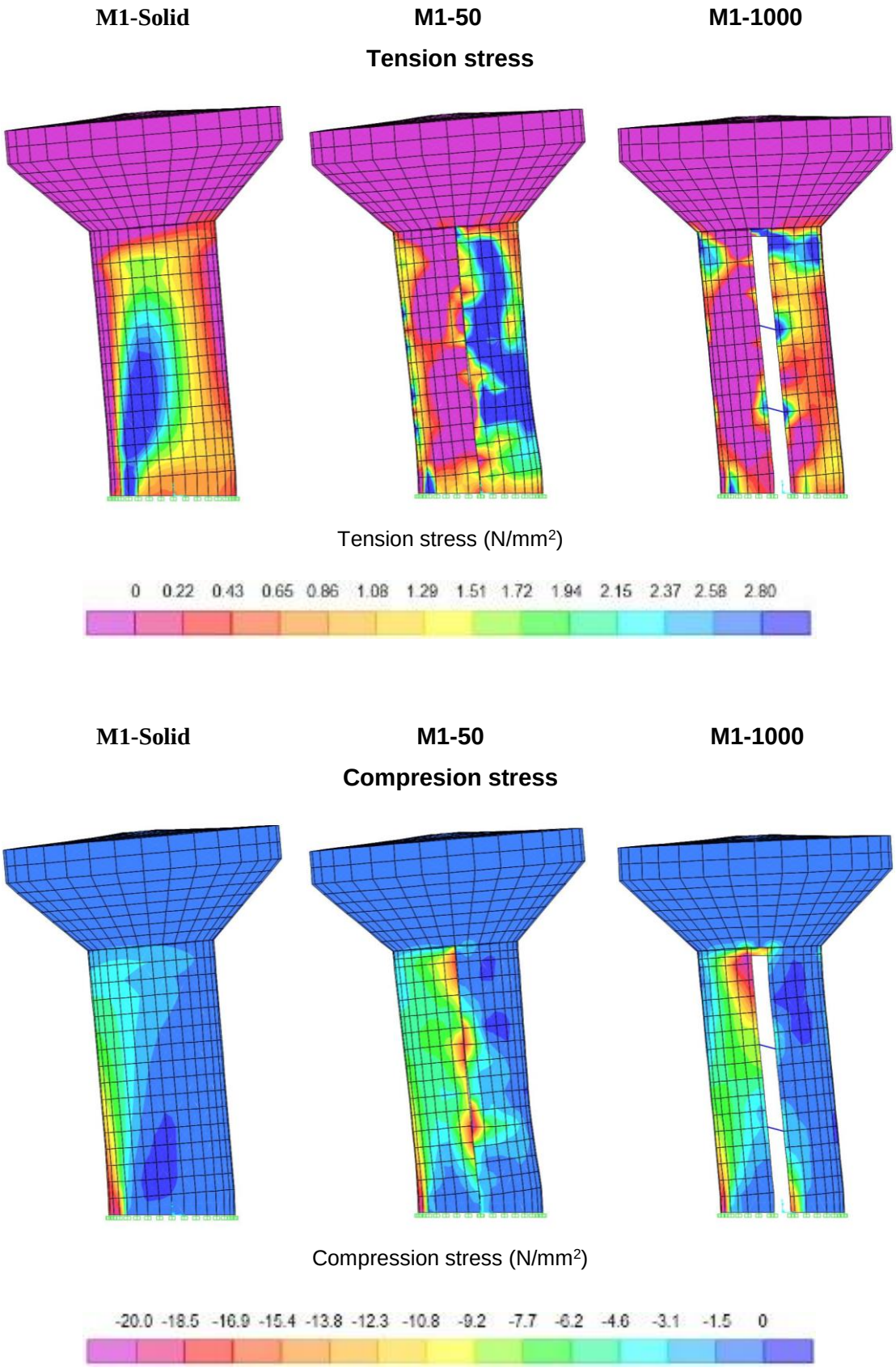

Figure 6.5. Contours of tension and compression stresses in RC shafts at peak base shear points of pushover analysis

The observations of stress patterns indicate three categories of cracking patterns in the RC shafts. These three categories were classified with respect to the slit width. This concept was best explained by studying the graphs of stress distribution presented in Figure 6.5. The distribution of tension and compression stresses varied for the solid and slit models. In solid model (M1-Solid), the ultimate compressive stress occurs in the base of the shaft.

On the other hand, slit shaft resulted in two different shapes of crack pattern development. The observed stress patterns showed that models with narrow slit width (M1-50) differed from the model with wide slit width (M1-1000). Unlike the solid model in those models ultimate compression stresses occurred in a few zones.

Many authors concluded the same results for the slit wall. Shinde, (2012) stated that with providing slit wall solution the degradation in the base of the shear wall was greatly reduced. The potential plastic zone was positioned along the height of the wall and energy dissipation was achieved by the crushing of the reinforced concrete shear connections.

As the shaft became more flexible (slit become wider), the area around coupled beams did not crack and the areas around the top ring connection began to crack at a lower base shear. As a result of the wider slits, the overall slit shaft capacity falls and the shaft piers crashed at a lower base shear.

As the coupling area become more flexible, the properties of the RC slit shaft change resulted in:

a) a decrease in the degree of coupling
b) a decrease in structural stiffness
c) an increase in the fundamental period of vibration
d) an increase in the damping properties of the structure resulting from increased concrete damage.

The difference in stress concentration patterns which is discussed in next section will explain the cracking patterns and the different failure of models.

6.6 Cracking propagation pattern in the RC shafts

Figure 6.7 demonstrates six stages of the progressive pushover analysis of FE models M1-Solid, M1-50, M-500 and M1-1000, which were investigated for crack propagation patterns. Table 6.3 and Figure 6.6 shows the stages of progression pushover analysis. The stages can be classified as:

- V1 = D1 – appearance of first local cracks
- V2 = D2 – the RC shaft reach the yielding (nonlinear) point
- V3 = D3 – performance point at Soil-A
- V4 = D4 – performance point at Soil-B
- V5 = D5 – performance point at Soil-C
- V6 = D6 – peak base shear

Table 6.3. Points of base shear and top lateral displacement for stress investigation under progressive loading of pushover analysis

FE model ID	Base Shear (MN)					
	$V1$	$V2$	$V3$	$V4$	$V5$	$V6$
M1-Solid	2.58	3.39	3.64	3.89	3.99	4.18
M1-50	1.96	2.82	3.30	3.66	3.72	3.93
M1-500	1.44	2.30	2.66	2.98	3.10	3.28
M1-1000	1.16	2.02	2.41	2.70	2.80	2.87
	Top Lateral Displacement (mm)					
	$D1$	$D2$	$D3$	$D4$	$D5$	$D6$
M1-Solid	9.24	12.84	31.00	54.00	68.00	128.50
M1-50	9.24	14.70	33.00	59.00	73.00	144.33
M1-500	9.24	17.00	39.00	68.00	85.00	123.81
M1-1000	9.24	18.44	41.00	75.00	93.00	116.48

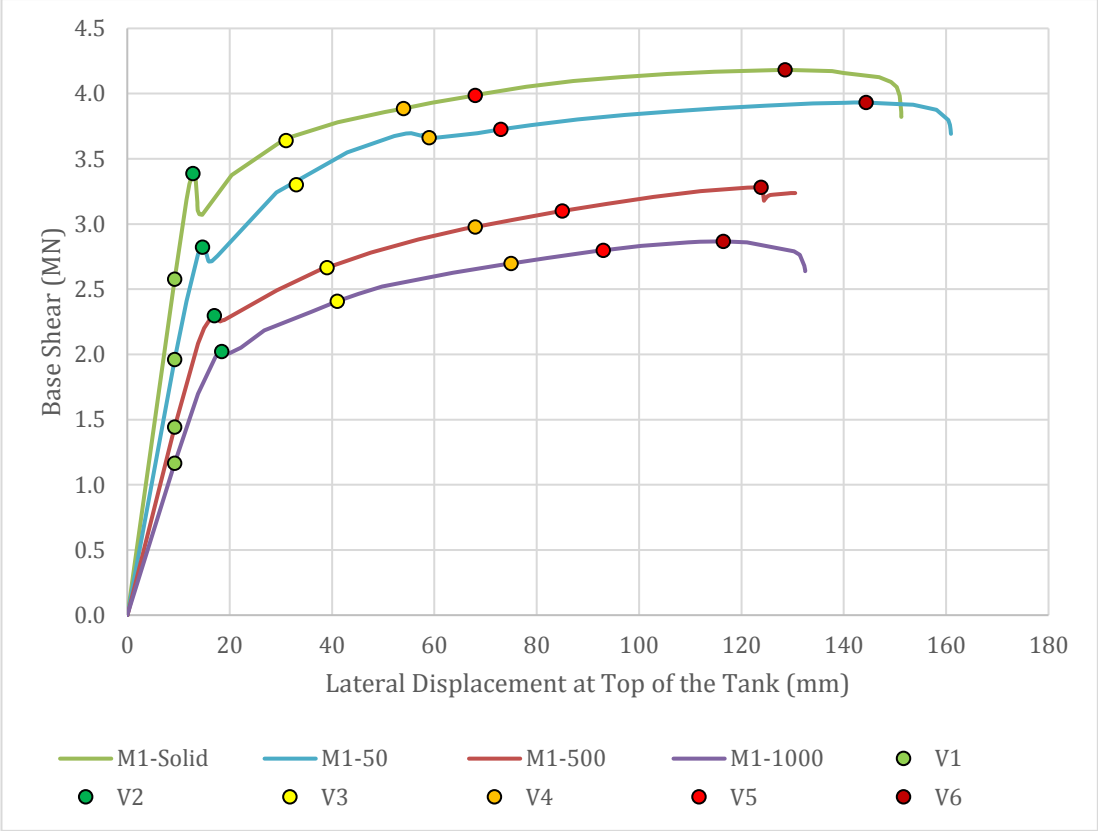

Figure 6.6. Points for stress investigation under progressive loading of pushover analysis

In case of model M1-Solid, as shown in further details in Figures 6.7 for tension stresses and Figure 6.11 for compression stresses, at stage one which is denoted by base shear of V1 the cracking development began with flexural tension cracks at the base of the shaft. These cracks were located at the base of shaft side perpendicular to the direction of lateral loading. By further increasing the lateral loads, cracks developed around the initial flexural cracks toward the sides of the shaft and parallel to the lateral load direction. The elevated water tank M1-Solid reached a yielding point at stage V2. At stage V3 the top lateral displacement considerably increased compared to the load applied. A number of cracks propagate along the structure. These were base-shear cracks that were the result of combined effects of flexure and shear at the base of the shaft. The base shear V4 and V5 represents the fourth and fifth stages of loading in which the cracks were considerably propagated across the shaft and structure has experienced substantial top lateral displacement. Finally, the base shear V6 shows the RC shaft at the sixth stage at which the structure was just prior to failure. At this stage the cracks were propagated all over the structure and shaft has undergone extensive deformation. For model M1-Solid, the ultimate tension stress was concentrated in the base of the shaft.

The observed stress pattern for FE model M1-50 differs from model M1-Solid. In this model, initial stresses were distributed as displayed in Figure 6.8 for tension stresses and Figure 6.12 for compression stresses. At stage V1 the slit shaft began to crack. Cracks occurred next to the connections. Once the region around the coupling beams began to crack, the coupling action started to degrade and the lateral forces once resisted by coupling frame action were distributed to the shaft piers (V2 and V3). The cracks located around the connections can be classified as web-shear cracks. Unlike the base-shear cracks that initiate simultaneously at the base corner of the shaft, web-shear cracks developed first only around connections on the sides parallel to the lateral load direction. At stage two, which represents base shear V2, slit shafts reached to the level when cracking of base part of shaft had begun and more shear cracks arise around the connections. In the solid shaft the cracks from the base of the wall extended rapidly parallel to the shear force. The wall still had a high stiffness. The base shear V3 represents the third stage of loading which represents seismic load for Type A soil according to Figure 6.3. The concrete near the connections started to crash. In this stage the cracks were considerably propagated across the shaft and the structure had experienced substantial top lateral displacement. Once the area around all the coupling beams crashed, the structure was no longer a coupled system but a collection of linked by ring beam wall piers. From V4 to V5, the structure was transitioning from being a coupled system to being a linked system and eventually the shaft reached the failure point (V6) and collapses.

As can be seen in Figure 6.8 and Figure 6.12, the progression of cracks around coupling beams initiated near the upper connections of the shaft and progresses both upwards and downwards. Typically the ring beam is remain elastic the longest. In this analysis, cracks around the lower beam were also delayed. This is a result of the very stiff restraining effect resulting from this beam being located so close to the fixed bases of the shaft. The similar observation of coupled wall were shown by Harries and McNeice, (2006).

The observed stress pattern for FE models M1-500 and M1-1000 differs from previous models. In this model, initial stresses were appeared as displayed in Figure 6.9 and Figure 6.10 for tension stresses and Figure 6.13 and Figure 6.14 for compression stresses. These stresses produced cracks located next to connection between shaft and top of shaft and classified as top-shear cracks (V1). Top-shear cracks developed first only around top connection on the sides parallel to the lateral load direction. By increasing the lateral load base-shear cracks appear at the base corner (V2) and later

cracks appeared around connections (V3). Later cracks distributed throughout the shaft under the top ring parallel to the applied load (V4 and V5) and eventually the water tank separated from the part of the shaft and the shaft collapsed (V6).

The model M1-500 and M1-1000 in Figure 6.9 and 6.10 represents the shaft crack process defined between connections of shaft to water tank. In comparison between the top-shear cracks and web-shear cracks, one can see the difference between a system with narrow slits designed to work together as a coupled shaft and a system with wider slits worked as system of cantilever pier of shafts designed to work separately and connected at the top by the ring beam.

The system with wider slits would have less capacity and stiffness, and hinge beginning formed immediately at the base in the middle and side of a shaft when the shaft achieved the appropriate base shear. Furthermore, it can be seen that connection stiffness decreased as the slit width increased.

The stress pattern in RC shafts were directly related to the slit width in the shaft. Basically web-shear stresses were more likely to occur in the narrow slit shaft and top-shear cracking was possibly observed in wide slit shafts. The definition of wide and narrow is relative and needs to be normalized.

The results correspond with Baetu (2012) who analysed the behaviour of solid and slit shear walls and concluded that slit shear walls gave more ductility, energy dissipation and an improved crack pattern. The slit wall dissipated seismic energy by cracks extended across all the surface of the wall and by crushing of the shear connections and the solid wall dissipated seismic energy only by cracks at the base of the wall.

Labafzadeh and Ziyaeifar (2011), studied new types of slit shear wall under pushover analysis. The results showed that the concentration of the considered cracks and subsequently, the significant damages occurred at the lower part of the solid wall. This indicated that most parts of the wall did not contribute in the energy dissipation procedure during lateral loading. Whilst in slit walls, the cracks propagated in link beams along the height of the wall. Therefore, the damages induced by the lateral loads spread across the height of the slit without any localization at any particular region and consequently, the local ductility demand was decreased. This improvement was very similar to model M1-50, which shows the stress propagation along the whole height of the shaft (Figure 6.8 and Figure 6.12).

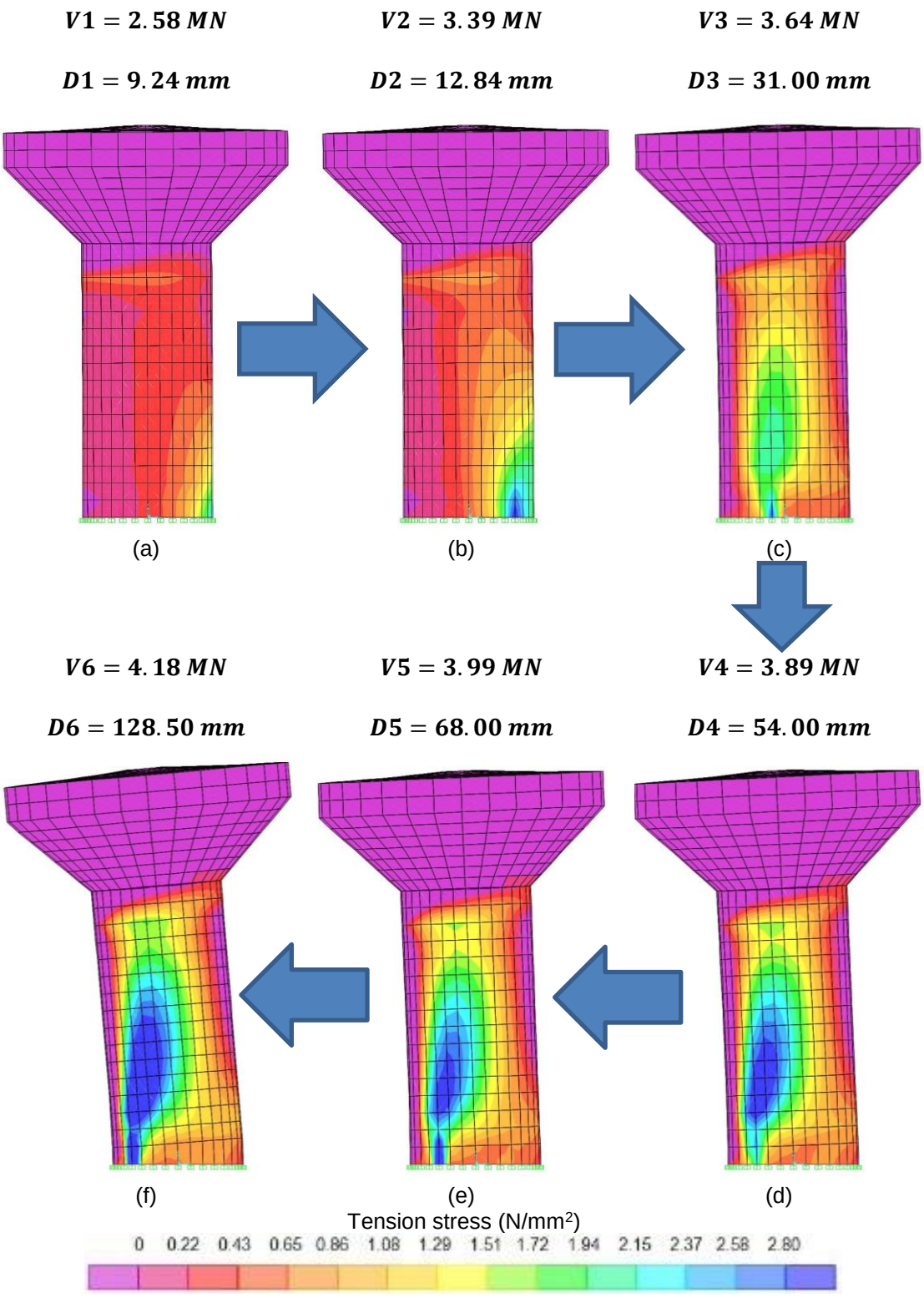

Figure 6.7. Contours of tension stress distribution in RC shafts under progressive loading of pushover analysis for model M1-Solid

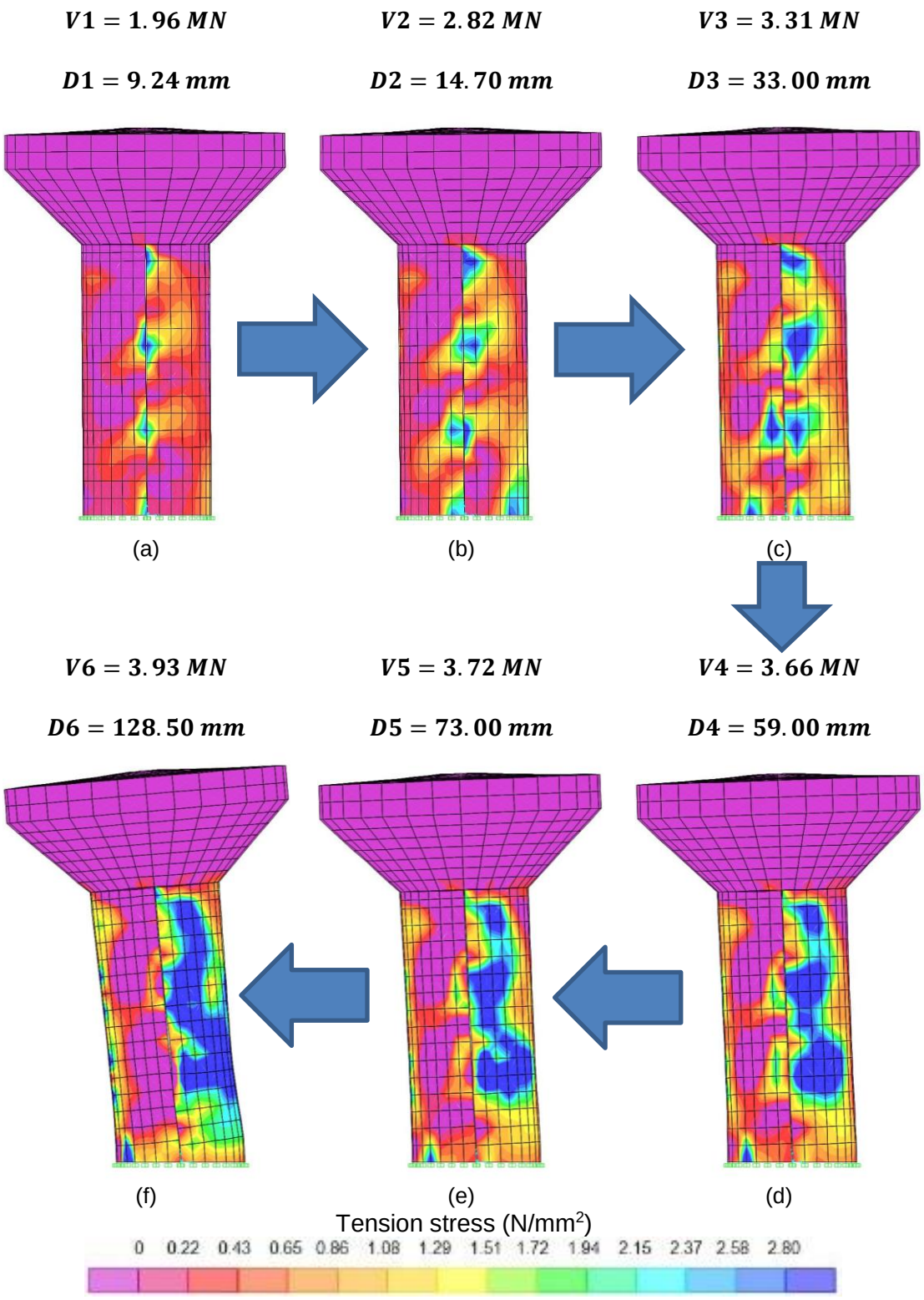

Figure 6.8. Contours of tension stress distribution in RC shafts under progressive loading of pushover analysis for model M1-50

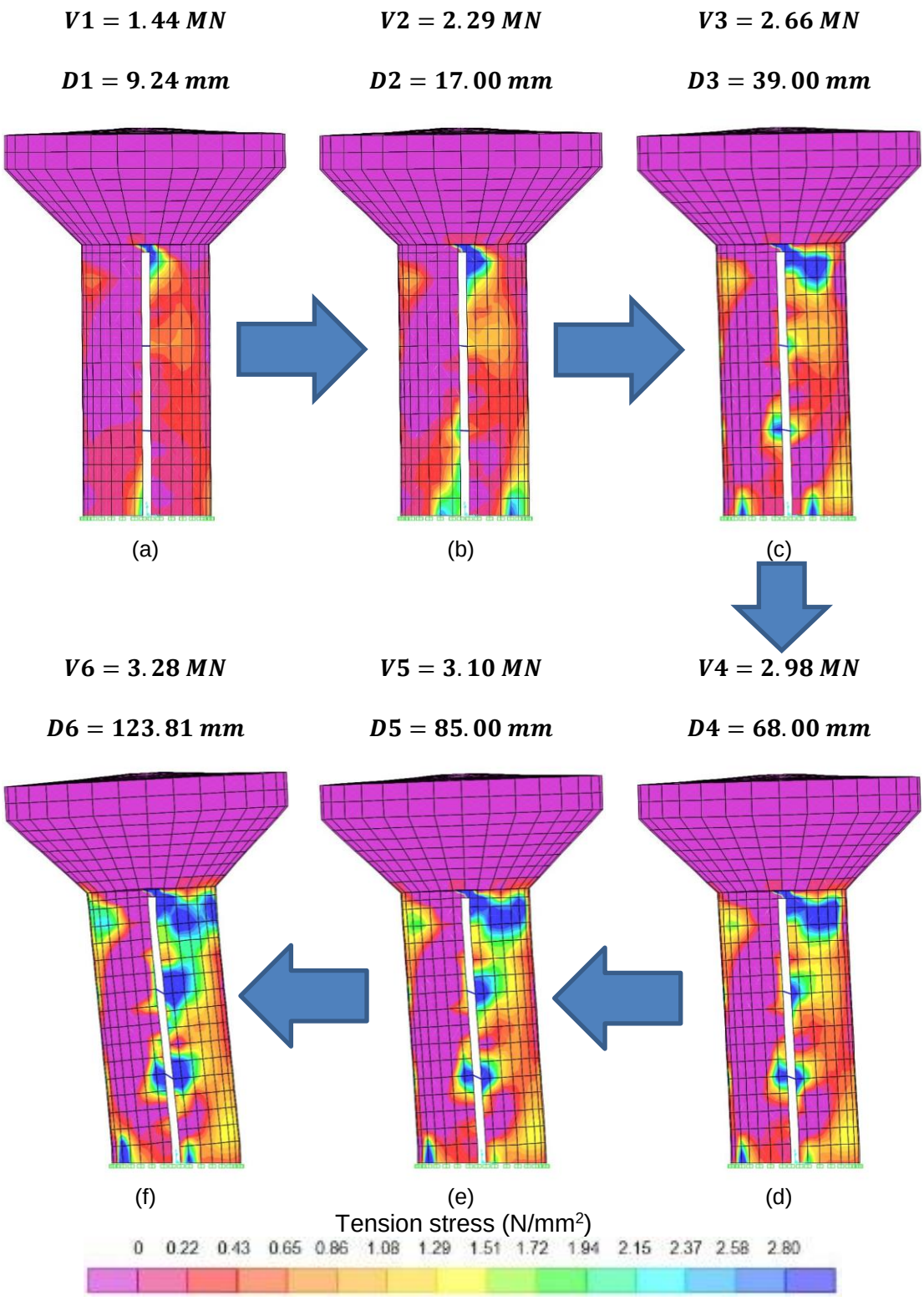

Figure 6.9. Contours of tension stress distribution in RC shafts under progressive loading of pushover analysis for model M1-500

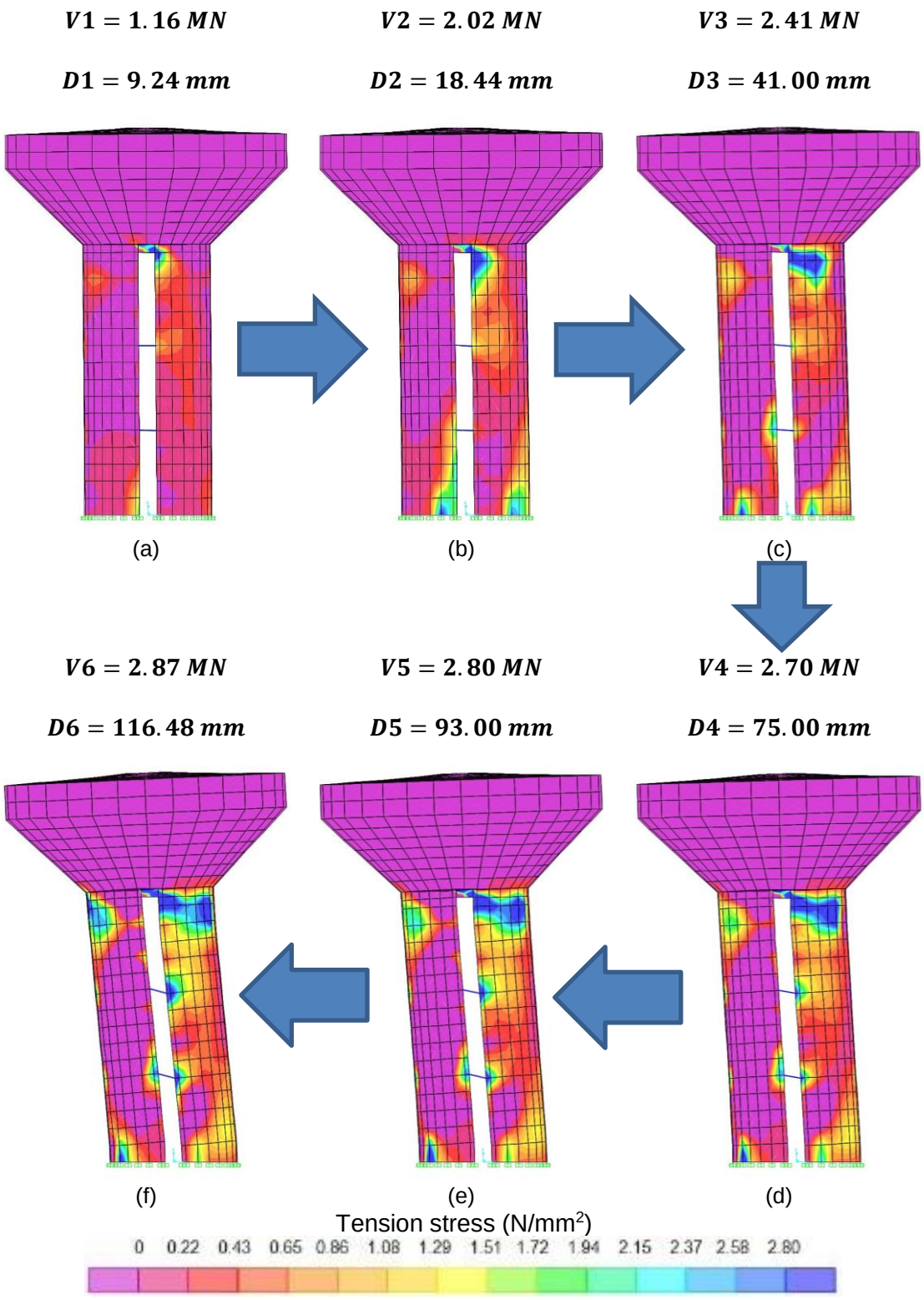

Figure 6.10. Contours of tension stress distribution in RC shafts under progressive loading of pushover analysis for model M1-1000

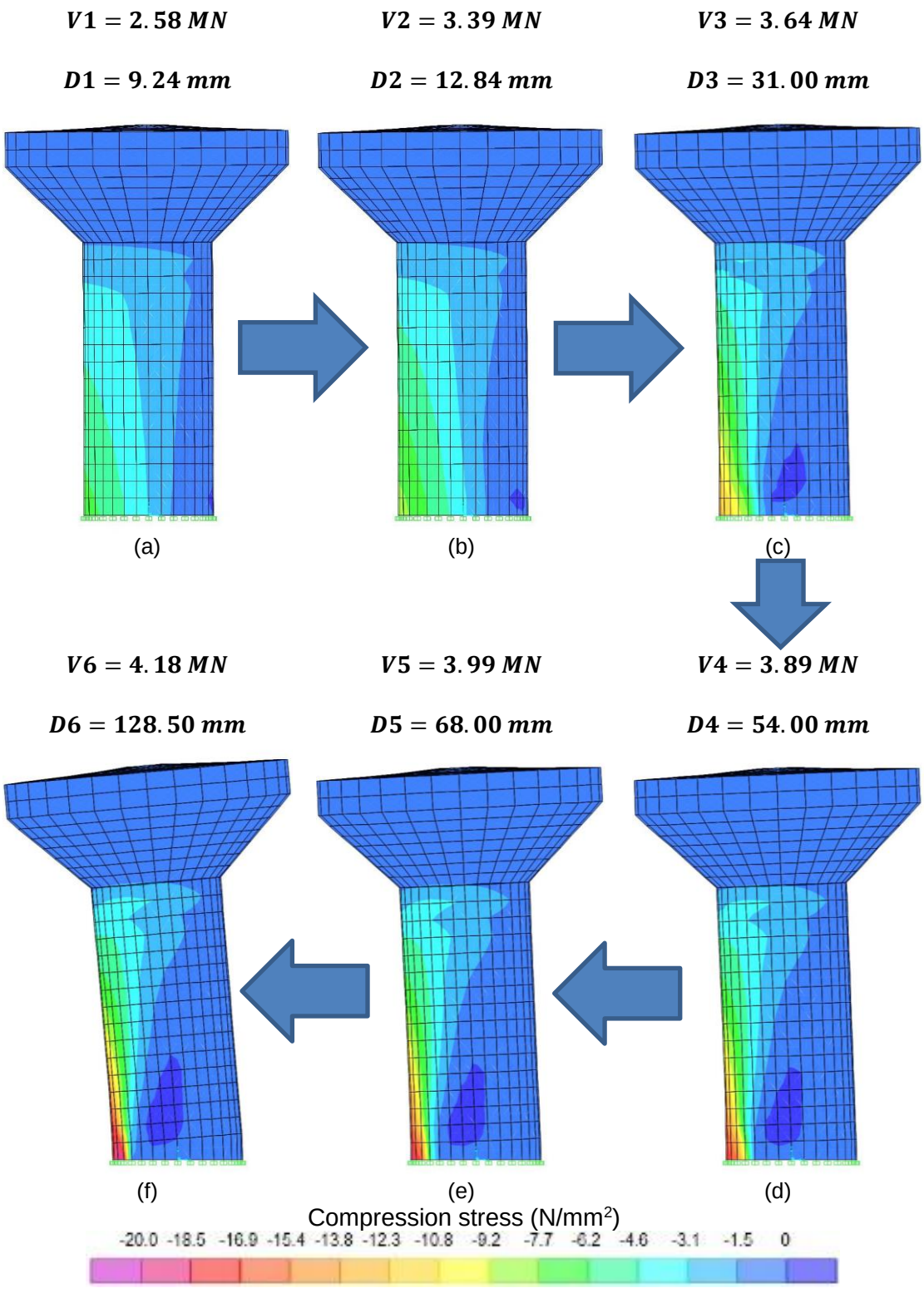

Figure 6.11. Contours of compression stress distribution in RC shafts under progressive loading of pushover analysis for model M1-Solid

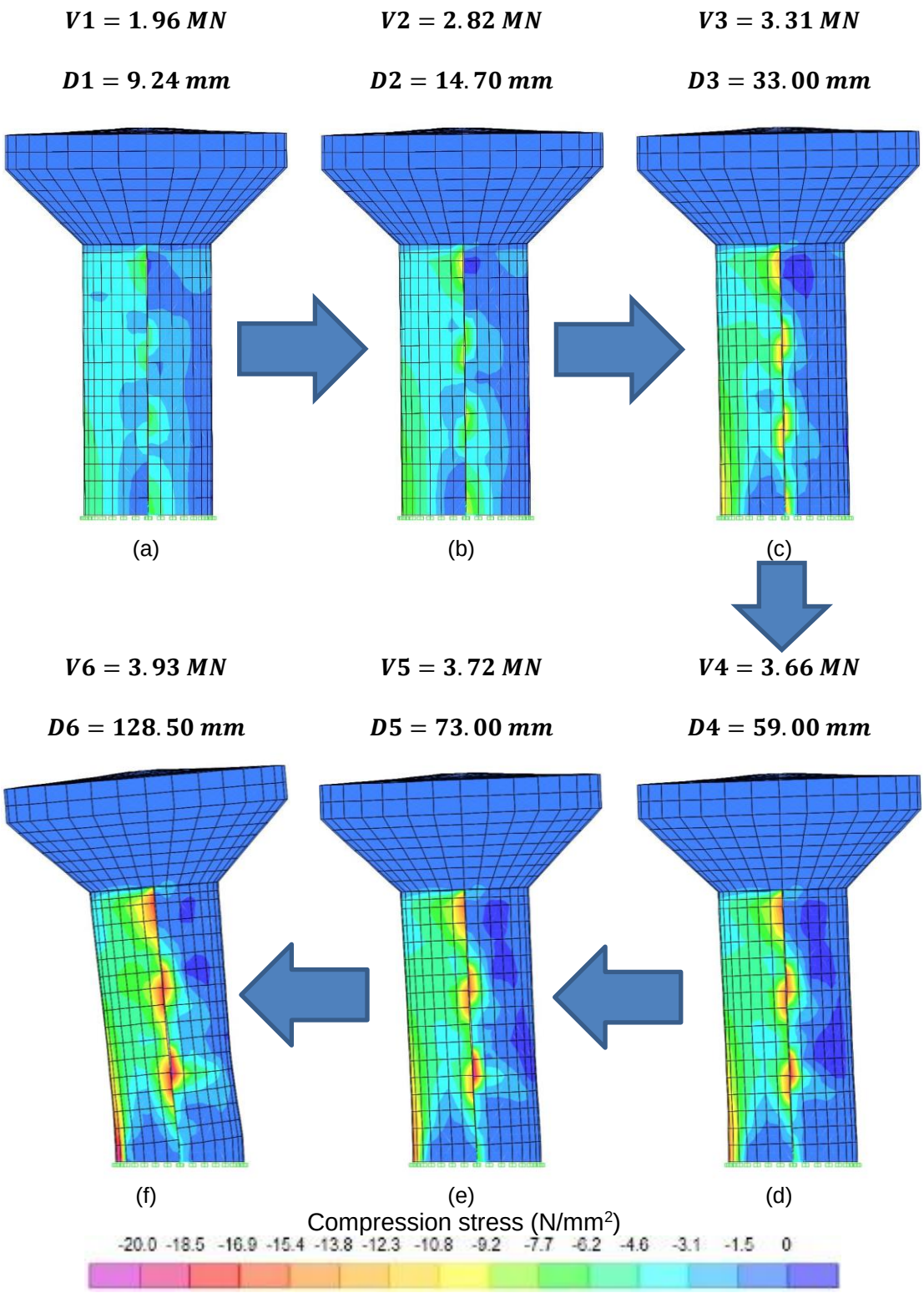

Figure 6.12. Contours of compression stress distribution in RC shafts under progressive loading of pushover analysis for model M1-50

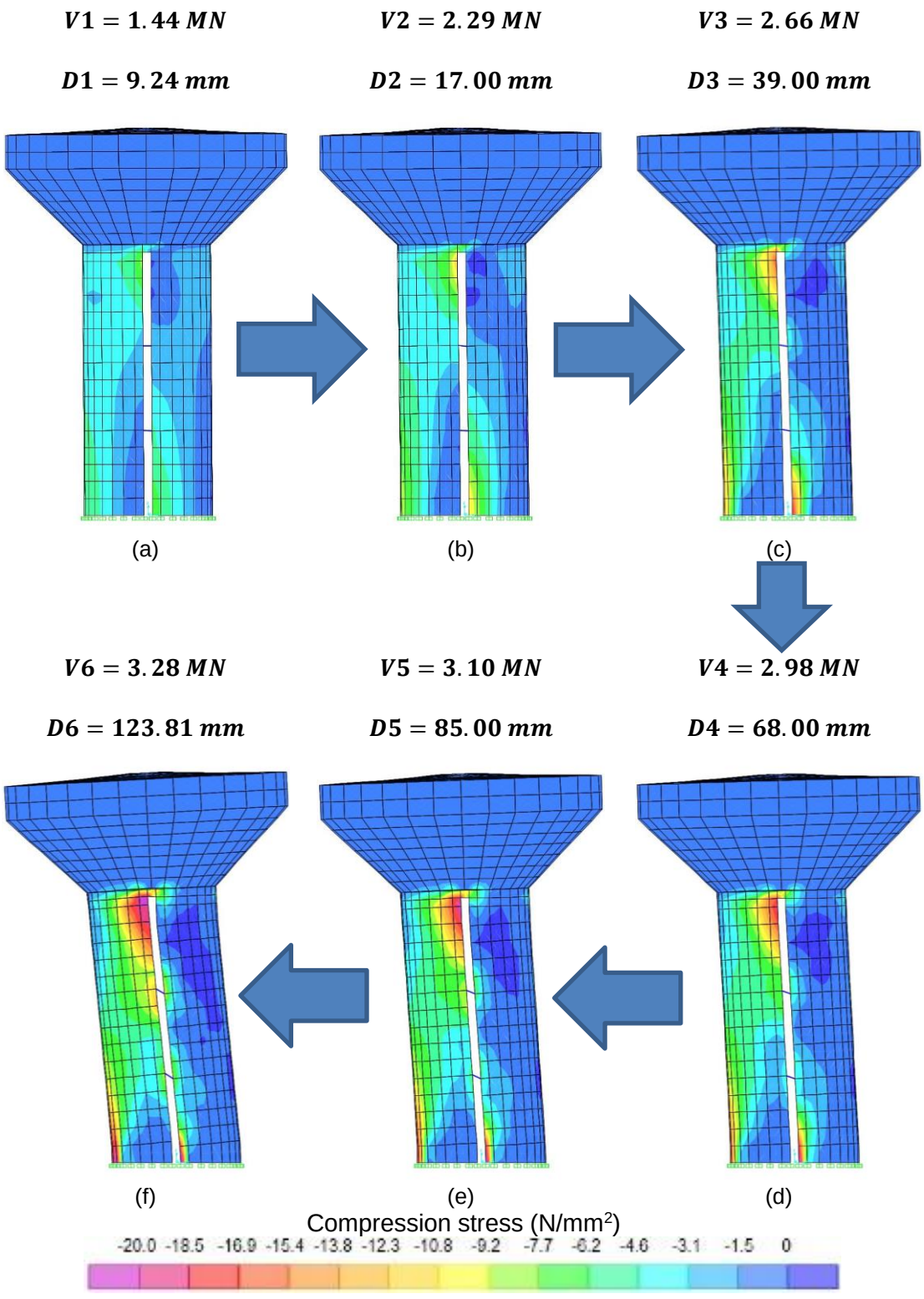

Figure 6.13. Contours of compression stress distribution in RC shafts under progressive loading of pushover analysis for model M1-500

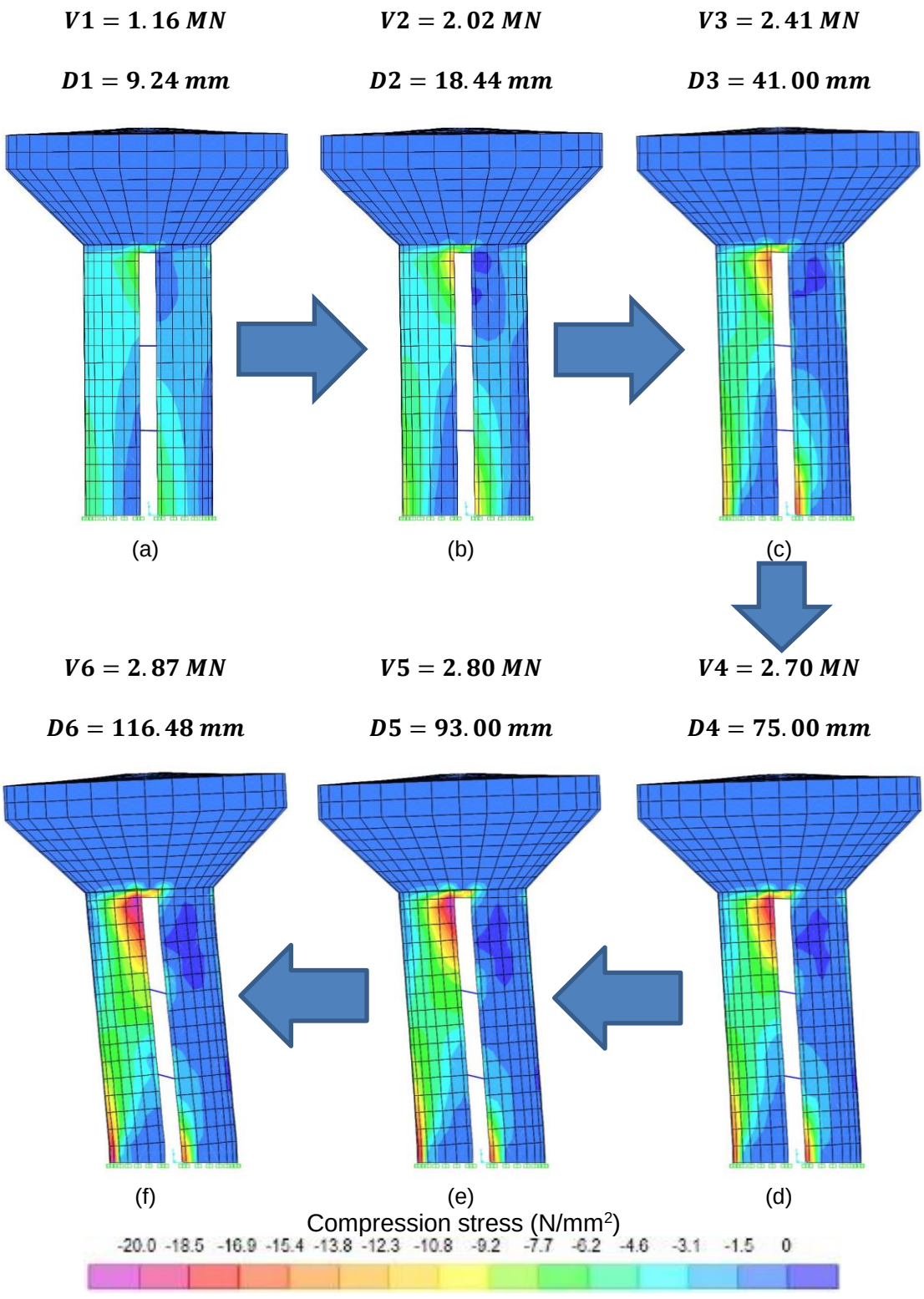

Figure 6.14. Contours of compression stress distribution in RC shafts under progressive loading of pushover analysis for model M1-1000

Another researcher, Musmar (2013) studied opening in shear walls. It was concluded that the walls in a case when openings were large enough, the load capacity was reduced and walls behaved as connected shear walls maintaining frame action behaviour and the initial cracking occurred at the joint between the upper lintel of the opening and the sidewalls. The similar description can be used for models with slits wider than 500 mm. It can be assumed that the shaft behaves as four piers of a shaft connected to each other by beams. That phenomenon explains the high amount of stresses at the base shear between pierces of the shafts (Figure 6.14).

In order to investigate the sensitivity of the proposed slit shafts elevated tank response to pushover analysis, the effects of various vulnerable zones such as the base corner opposite to the applied force, base centre and connections will be investigated and discussed in the next section of this chapter.

6.7 Concrete crash zones in the RC shafts

The effect of vulnerable concrete crash zones of slit shafts on seismic response of elevated water tanks was considered in this section. The vulnerable zones of the FE model M1-500 model are shown in Figure 6.15. The vulnerable zones included in this study:

- Zone I – around the base corner opposite to the applied force
- Zone II – around the base centre parallel to the applied force
- Zone III – around the lower connection beam parallel to the applied force
- Zone IV – around the upper connection beam parallel to the applied force
- Zone V – around the top connection to the ring beam parallel to the applied force

This observation provided some useful information regarding the compression stress distribution along the slit shafts in the elevated tanks that could help in obtaining an optimum slit width in the RC shaft.

To study the effect of slit width (shaft stiffness) on the distribution of compression stress, nine elevated tank models having different slit widths, from 50 mm to 2000 mm were considered and their pushover curves were found using the proposed methodology.

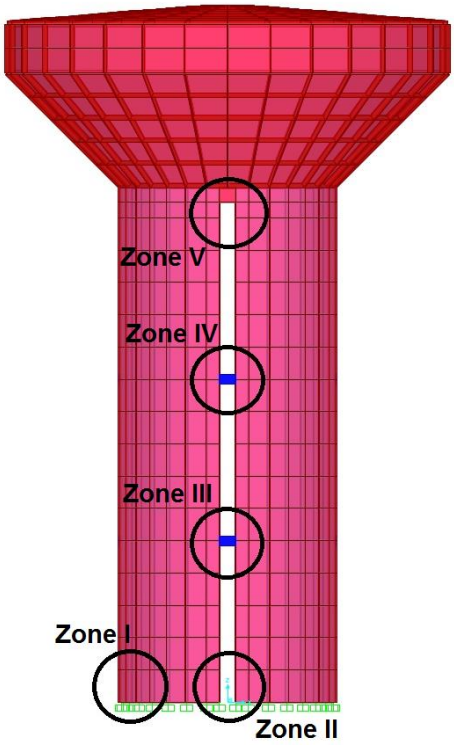

Figure 6.15. Vulnerable concrete crash zones in RC elevated water tanks

According to Figure 6.5 a failure of the water elevated water tanks occurred after the concrete started to crash in the compression base zone. Moreover after investigating Figures 6.11 to 6.14, it was concluded that the concrete crash in one of the vulnerable zones, demonstrated in Figure 6.15 led to an increased load in the vulnerable Zone I and resulted in the failure of the water tank.

Table 6.4 shows the compression stresses at the vulnerable zones for models considered under pushover analysis at the performance point of Eurocode 8 spectral acceleration designed for soil A, soil B and soil C.

It can be seen from the Table 6.4 that compression concrete stress in all zones was in elastic stage for models with slit widths less than 500 mm. Models with slits wider than 500 mm showed the increase of the concentration of compressive stress in zones I, II and V. Observing soil type A, compressive stress in zone V reached ultimate value for models wider than 2000 mm. That can be explained by sliding effect between water tank and top of the shaft, which could take place in shafts with reduced stiffness by the wide slits. All models with slits wider than 1000 m in shafts attained compressive stresses greater than $19\ N/mm^2$, also showed the dangerous behaviour. All other models were safe.

Table 6.4. Compression stress at vulnerable zones

FE model ID	Compression stress (N/mm^2)				
	Zone I	Zone II	Zone III	Zone IV	Zone V
	Soil Type A				
M1-Solid	13.50	0.34	1.02	2.38	3.89
M1-50	11.34	6.25	12.24	12.64	10.83
M1-100	11.43	9.68	9.49	11.08	12.47
M1-200	12.20	11.59	6.88	9.35	13.92
M1-300	12.19	12.97	5.86	7.24	14.31
M1-500	12.58	14.62	4.73	6.05	14.68
M1-1000	15.35	18.06	4.05	5.50	19.76
M1-1500	15.79	17.63	3.64	4.95	19.72
M1-2000	18.04	18.18	6.32	6.81	20.00
	Soil Type B				
M1-Solid	18.20	0.32	0.30	1.89	4.12
M1-50	15.62	2.57	16.21	17.5	13.08
M1-100	15.73	5.23	15.74	16.82	15.82
M1-200	16.00	7.95	10.9	14.22	17.55
M1-300	16.04	10.99	7.75	10.67	18.29
M1-500	16.36	15.73	5.64	9.04	18.48
M1-1000	18.4	19.33	4.35	7.95	20.00
M1-1500	19.85	19.4	2.93	8.86	20.00
M1-2000	20.00	18.57	4.36	8.92	20.00
	Soil Type C				
M1-Solid	19.39	0.34	0.21	1.86	4.16
M1-50	16.28	3.21	13.82	17.4	13.19
M1-100	17.07	3.82	19.21	19.05	17.46
M1-200	17.28	6.91	13.70	16.31	19.11
M1-300	17.5	8.93	9.73	12.99	19.69
M1-500	18.12	13.49	6.62	10.95	19.58
M1-1000	20.00	19.47	4.89	9.67	20.00
M1-1500	20.00	19.28	3.10	9.54	20.00
M1-2000	20.00	20.00	5.09	11.17	20.00

There was a similar compression stress distribution for soil type B, however all values increased and more models reached the ultimate stress value in Zone I and Zone V. It could be noticed that models M1-50 and M-100 showed a compression stress distribution more uniform along the shaft height than other models in all zones apart of Zone II.

When models reached soil type C the compression stress concentration in Zone V reached the ultimate value in all models with slit widths wider than 500 mm. Also the ultimate stress reaches $20\ N/mm^2$ in Zone I in models M1-1000, M1-1500 and M1-2000 as well as model M1-Solid reached stresses greater than $19\ N/mm^2$. On the other hand models M1-50 and M-100 showed a good distribution of compression stresses along the shaft height.

Baetu (2011) stated that the shear connections prevented a collapse of the structure under extreme seismic excitations by dissipating energy through shear yielding. For optimum performance, the shear connections should maintain their load carrying and energy dissipation capacities until the whole structure failure. Therefore, for best performance all connections should have similar stresses before the structure collapses. Also the crash in Zone III and IV should start before or together with crashing of other zones.

According to Table 6.4 slit shafts with widths up to 100 mm have similar stresses in connections and Zone I. It was concluded that the most effective wall types for stress distribution along the whole height of the shaft were slit shafts with slits not more than 100 mm. It also could be noticed from the table that an increase in slit width reduces the stiffness of the connections in Zone III and Zone IV.

6.8 Summary

This chapter aimed to evaluate the nonlinear seismic response of elevated water tanks by conducting capacity spectrum analysis. A finite element method was employed for this purpose, which was previously verified in the methodology.

In order to perform a comprehensive investigation on the nonlinear seismic response of the elevated water tanks, the M1 group of elevated water tanks with various slit shaft widths were generated. The slit shaft width in the study group varied between 50 mm to 2000 mm. Each elevated water tank was then designed according to the provisions of the related codes and standards.

A pushover analysis was performed on each finite element model. The finite element models of the elevated water tanks were subjected to a gradually increasing lateral load. The lateral load was increased until failure in the structure occurred. The results of each pushover analysis were recorded as a base shear – top lateral displacement graph.

The pushover curves indicated a number of certain patterns existing in the nonlinear seismic response of elevated tanks. The models which were designed with wide slit shafts presented a lower maximum base shear in comparison to the identical model designed with a narrow slit shaft. This is due to an increase in ductility and decrease in stiffness in RC shafts. However the response of the slit width did not have a considerable effect on the maximum top lateral displacement capacity.

The capacity spectrum analysis was applied to evaluate seismic resistance of models for seismicity zone with PGA=0.4g. Each model was evaluated for soil type A, B, C and D from Eurocode 8.

RC slit shaft elevated water tanks were very sensible to soil types because the slit width could significantly influenced the stiffness and ductility of the structure. The stiffer structures were more appropriate for softer soils then more ductile structures.

Three types of cracking propagation were observed. It was concluded that elevated solid water tanks shows base-shear cracks, models with slit widths less than 500 mm demonstrated web-connection shear cracking pattern. However, if the slit width was above 500 mm, then the cracking propagation was in the category of top-shear cracking.

Finally, vulnerable zones of possible concrete crash in slit elevated water tanks were detected and illustrated. All zones were investigated and the most efficient slit width was identified. According to the study, the best stress distribution height of the water tank shaft could be noticed in shafts with slits up to 100 mm. Models with slits wider than 100 mm showed the concentration of stresses at the base and top of the shafts that is not favourable.

The nonlinear dynamic analysis was performed in Chapter 7 and results was compared to nonlinear static analysis.

Chapter 7

Results and Discussion – Dynamic Nonlinear Analysis

7.1 Introduction

When structures are subjected to significant dynamic loads such as seismic excitation, their nonlinear response must be assessed. This is required in particular for structures that are designed to dissipate inelastic energy such as elevated water tanks. Reinforced concrete shafts, due to their stiffness, are usually the principal lateral force resisting a system in a structure. As discussed previously, the efficacy of slit RC shafts is based on their stiffness characteristics. Therefore, to be efficient, the response of slit RC shafts to earthquake excitation is expected to extend into the nonlinear range.

Nonlinear time history analysis is considered by design codes to be the most comprehensive level of analysis, where the effect of the transient and cyclic nature of the ground motion can be simulated. The influence of the ground motion characteristics, including the frequency content, magnitude, and its ability to trigger higher modes may be significant, requiring a suite of ground motions to be considered.

Structural characteristics beyond simple mass and stiffness and their distribution must also be considered. Stiffness and/or strength degradation are particularly important as this impacts the change in dynamic properties with accumulated energy dissipation (damage).

The pushover analyses described in Chapter 6 demonstrated that the models with slit shaft model behaved in an acceptable manner, in which reasonable base shear and roof displacement levels were achieved. This chapter describes the extension of these analyses to nonlinear time history analysis. The primary objective of this chapter is to evaluate the effect of a slit shaft on the dynamic behaviour of the entire elevated water tank. Selecting a number of models that are best representing most properties and seismic response characteristics of the initially designed model group would solve this problem. The M1 group of four RC shafts that was introduced in Chapter 5 was employed for conducting the analysis.

The selected elevated tank models were subjected to a unidirectional horizontal seismic excitation and the corresponding transient base shear and base moment

response values at the base of the shaft structure were determined. Furthermore, a lateral displacement at the top of the tank was determined. A comparison between the finite element results of elevated water tanks with slit and solid shafts was made.

The chapter continues with an observation of stress patterns and compares them to the pushover results from Chapter 6. The vulnerable zones were observed and most effective slit sizes were identified.

An earthquake intensity analysis was performed and an influence of the earthquake intensity on the vulnerable concrete crash zones opposite to the applied load were compared between slit and solid shaft models.

The ground motion used for the time history analysis was the horizontal component of 1940 El-Centro earthquake scaled to the peak ground acceleration of 0.4g as shown in Figure 7.1. The highest response occurred in the first 5 seconds of the record, thus was shoed just first 5 seconds of the record. An integration time step of 0.005 seconds was used for the time history analysis of the tanks. In performing the direct integration time history analysis, the proportional stiffness damping was assigned according to the first and second impulsive mode from Chapter 6.

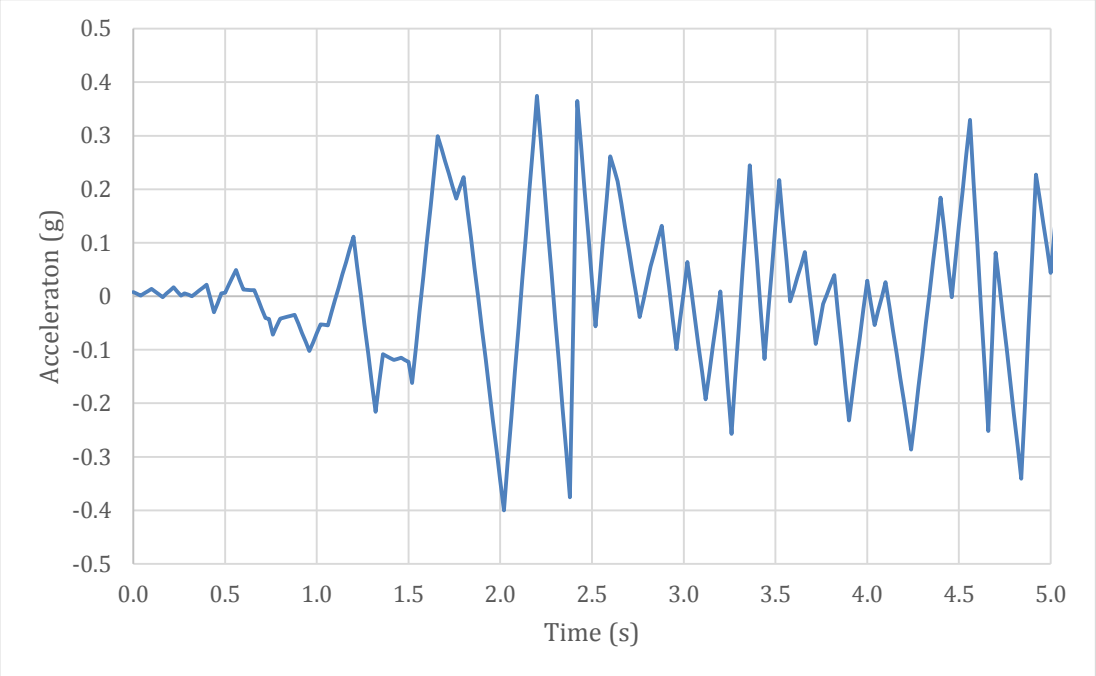

Figure 7.1. First 5 second of the 1940 El-Centro ground motion, horizontal component record scaled to PGA=0.4g

7.2 Results of nonlinear time-history analysis

The main focus of this section is based on the effect of slit width on the dynamic seismic response of the RC shafts in the elevated water tanks. Finite element (FE) technique was used to investigate such an effect. This FE technique was explained in detail in previous chapters in this thesis. Using this technique, the seismic behaviour of elevated water tanks having different slit widths under random excitation was investigated. The selected elevated tank models were subjected to a unidirectional horizontal seismic excitation and the corresponding transient shear force and flexural moment response values at the base of the shaft structure were determined. Furthermore, the lateral displacement at the top of the models also was determined.

The results of time history analysis for the M1 group water tank group FE models M1-Solid, M1-50, M1-500 and M1-1000 are shown in Figure 7.2 to 7.4. Each graph demonstrates the time history curve for base shear (V), flexural moment (M) and lateral displacement at the top of the tank (D) for four models included in the M1 group.

The comparisons among the response variations calculated for the solid and slit shaft models clearly showed the stiffness reduction effect in the time-history response of the slit shaft models. Moreover, was observed from that the base shear and base moment were significantly reduced due to slit shaft in all models. This verifies the effectiveness of slit shafts in elevated water tanks.

Examining the obtained results, it can be observed that in general more reduction was achieved by the wider slit shafts as compared to the narrower slit shaft. This is due to the additional horizontal flexibility in wide slit shaft models that a more ductile compared to the case of narrower slit shaft models, which are stiffer.

There was a pronounce reduction in base shear and base moment with an increased width of slits. The comparison of the maximum base shear Figure 7.2 indicated that the base shear decreased by 7%, 24% and 33% for models M1-50, M1-500 and M1-1000 respectively in comparison to model M1-Solid.

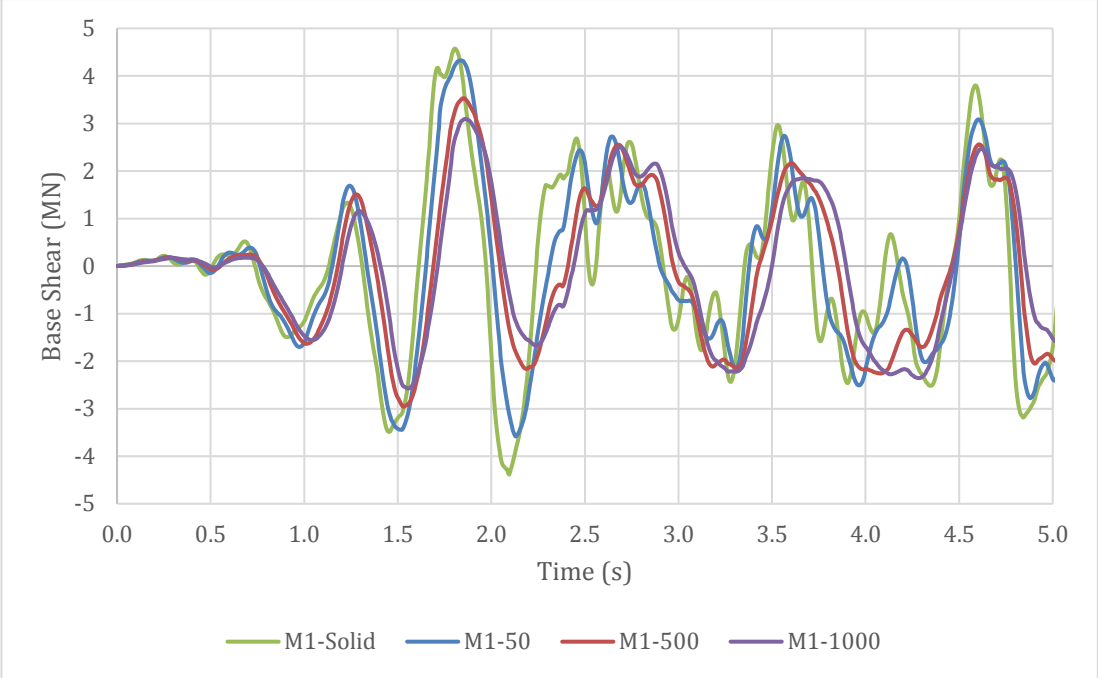

Figure 7.2. Time history base shear response of M1 group models subjected to El-Centro horizontal excitation scaled to PGA=0.4g

Comparison of the base moment presented in Figure 7.3 showed that the maximum base moment decreased by 11%, 25% and 33% for models M1-50, M1-500 and M1-1000 compared to model M1-Solid.

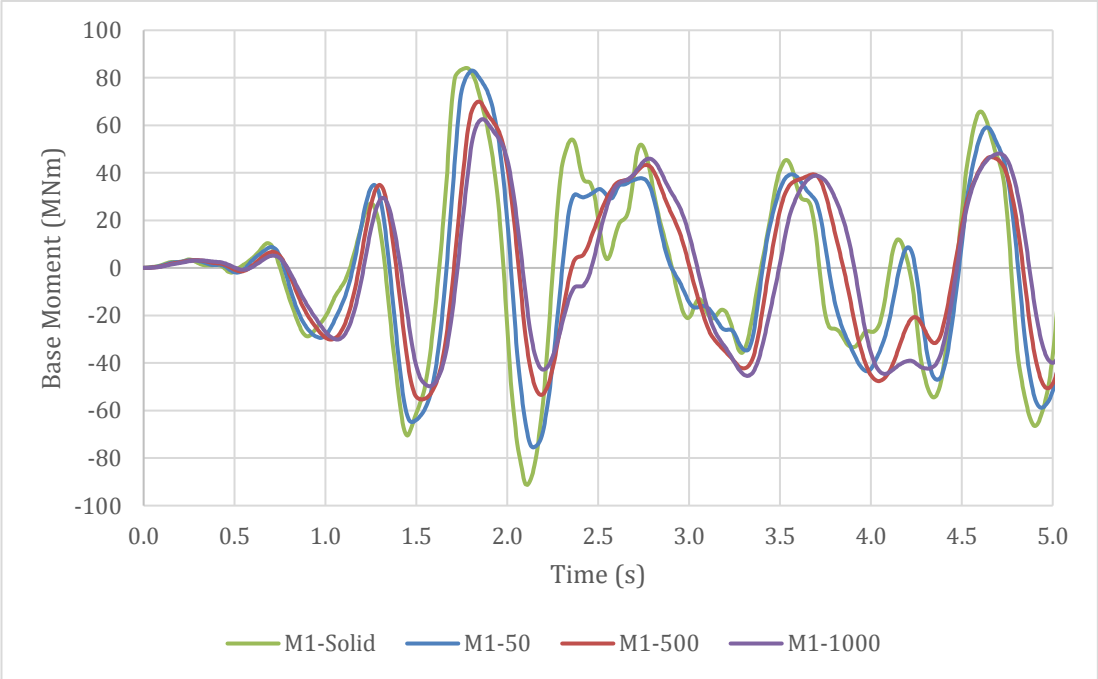

Figure 7.3. Time history base moment response of M1 group models subjected to El-Centro horizontal excitation scaled to PGA=0.4g

However, as indicated in Figure 7.4, a different trend was observed in terms of the lateral displacement response at the top of the tank level. The comparison of the top lateral displacement indicated that displacement increased by 31%, 51% and 57% for models M1-50, M1-500 and M1-1000 compared to model M1-Solid. As shown in this figure, the absolute maximum value of top lateral displacement was increased from 44.74 mm in the solid shaft case to 70.34 mm in 1000 mm slit shaft case. This can be the main disadvantage of slit shaft over solid shaft strategy, which arises from the excessive deformations usually experienced in more ductile structures. This issue is especially of great importance in elevated water tanks because of the piping system failure that may be experienced as a result of excessive lateral displacements.

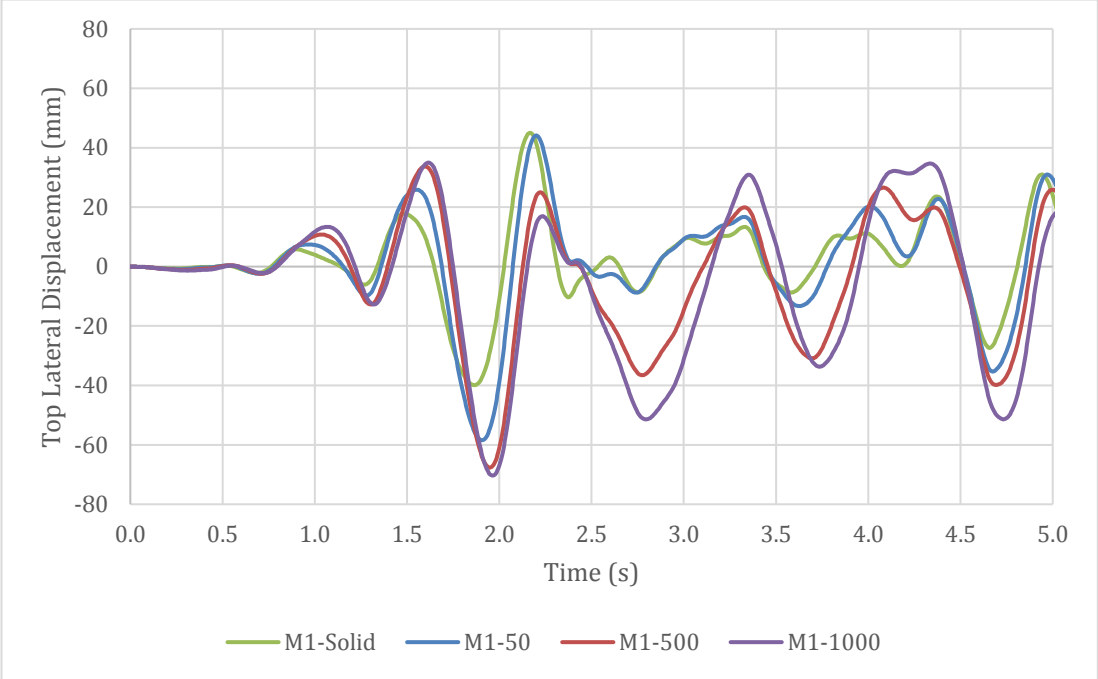

Figure 7.4. Time history top lateral displacement response of M1 group models subjected to El-Centro horizontal excitation scaled to PGA=0.4g

7.3 Discussion of results of nonlinear time-history analysis

From results of nonlinear time-history analysis it can be concluded that as soon as deformation limits is not of concern, wider slits is usually a better option leading to a more effective solution to the problem. On the other hand, if existing tank design cannot accommodate additional structural movements, narrower slit shafts are preferred over wider slit shafts.

The absolute maximum time history response values corresponding to the solid and slit shaft tank models were summarized in Table 7.1. The numbers in bold shows an

increase (positive) or decrease (negative) percentage over the corresponding solid shaft model. The table presents the results including the base shear (V), flexural moment (M) and top lateral displacement (D). Data of time history response values for the all models included in the research within the full M1 group are presented in Appendix D.2.

Table 7.1. Time history response values of M1 group subjected to El-Centro horizontal excitation scaled to PGA=0.4g

FE Model ID	Base Shear (MN)		Base Moment (MNm)		Top Lateral Displacement (mm)	
M1-Solid	4.64		93.08		44.74	
M1-50	4.33	***-6.76%***	83.06	***-10.76%***	58.46	***+30.67%***
M1-500	3.53	***-23.89%***	69.96	***-24.84%***	67.66	***+51.23%***
M1-1000	3.10	***-33.33%***	62.60	***-32.75%***	70.34	***+57.22%***

Reviewing the obtained results for all four models listed in Table 7.1 revealed that slit variations could have a significant effect on the dynamic response of the system. For comparison purposes, the maximum response values corresponding to different slit shafts considered were normalized with respect to those of the solid shaft model, as shown in Figure 7.5.

Comparing the normalized base shear and base moment ratios, it was further concluded that as expected model M1-Solid with total base shear and base moment of 4.64 MN and 93.08 MNm respectively had the highest reaction forces compared to other models.

On the other hand, model M1-1000 with base shear and base moment of 3.10 MN and 62.60 MNm respectively had the lowest base response values. The base shear and base moment of model M1-1000 were only 0.67 of those of model M1-Solid.

However, design considerations allowing for the probably large top lateral displacement of the response should be accounted for. The maximum top lateral displacement of model M1-1000 was 1.57 times higher of that of model M1-Solid, respectively.

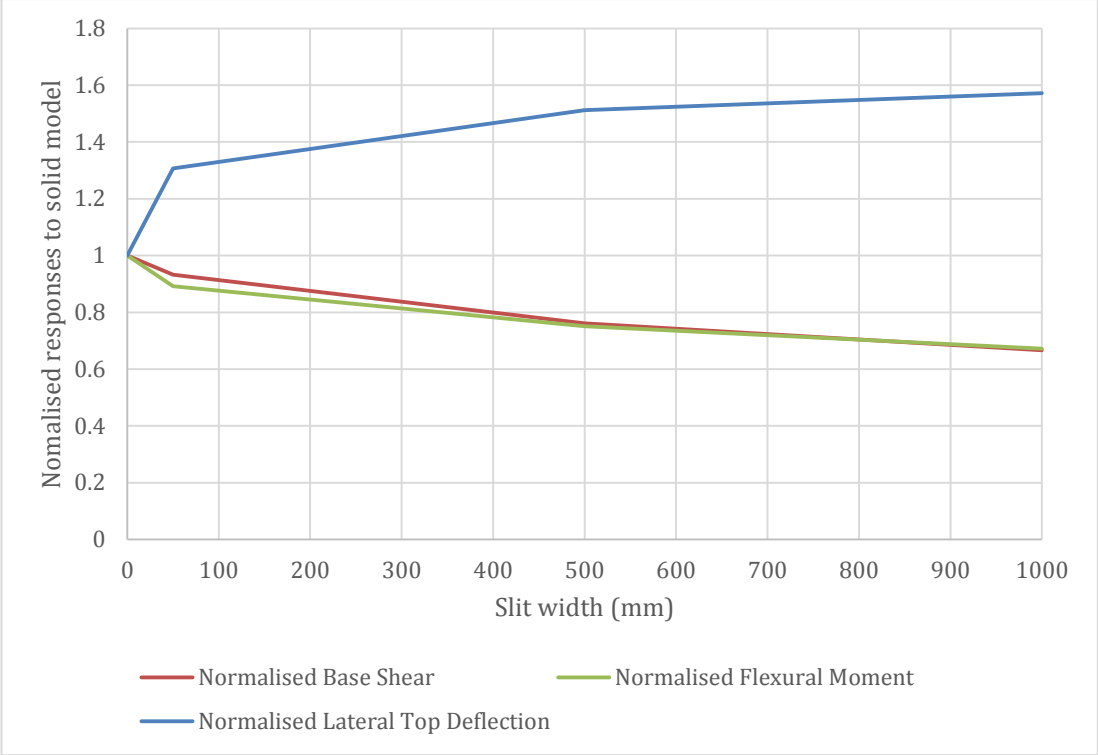

Figure 7.5. Normalised peak time history response values to M1-Solid model.

The maximum absolute top lateral displacement calculated of slit shaft models were significantly higher than the displacement of the solid shaft model. This indicated that the top lateral displacement increased in FE models respectively to an increase of the slit width since the stiffness of models decrease and ductility increased.

The slit width is the most important parameter and it should be utilised, as an elevated water tank has an inelastic behaviour over the height of the shaft. It is seen from the results that the base shear and base moment decreased in slit elevated water tanks, compared to the solid elevated water tanks. The same tendency were noticed by Labafzadeh and Ziyyaeifar (2008), who performed a dynamic analysis of a variety of shear walls and the results indicated that the rational arrangement of openings could improve the dynamic characteristics of shear walls such as ductility and damping ratio. This occurred by utilising the whole potential of dispersion of inelastic behaviour over the height of the shear wall.

Decreasing in the base shear one of the main advantages of slit shafts. This is obvious from Figure 7.6, which illustrates the base shear – top lateral displacement hysteretic loops during the considered earthquake motion corresponding to FE models M1-Solid, M1-50, M1-500 and M1-1000. That hysteretic loops were stable, so all models were stable during the proposed earthquake. The figure showed the elongation of the

hysteretic loops of slit models compared to the solid model. It is noticeable that the hysteric loops of elevated water tanks with slits in the shafts were more stable, which shows an improved inelastic response. According to the designed hysteretic loops in the current study, it was evident that the total amount of energy absorbed during the earthquake increases between solid and slit models. Figures of base shear – top lateral displacement hysteretic loops for the M1 group are presented in Appendix D.3.

It was discussed previously in the thesis that slit structural wall can be compared to the slit shaft. Some researchers in the literature concluded the similar behaviour of slit walls. Shinde, et al. (2012) compared nonlinear dynamic behaviour of slit and solid structural walls. The results showed that slits provided remarkable improvements of the structural walls, which included a very good seismic behaviour, stable hysteretic curves with high kinetic energy dissipation.

Several researchers recognized the hysteretic energy, absorbed by a structural system during a seismic event that was strong enough to induce a certain amount of nonlinearity to the system, as a potentially useful seismic performance indicator (Park, et al. 1987; Bojorquez, et al. 2011). In general, stable hysteretic loops with large energy dissipation capacity secure a better deformation performance of the system, implying that there is a good correlation between the dissipated hysteretic energy and the inelastic deformation demands. This conception was often founded between two systems with similar strength, tested under the same applied cyclic loading, the system with the higher energy absorption, i.e., “fuller” hysteresis loops, showed better performance. Thus, dissipated energy was a term that has become synonymous to the performance and it was universal part of modern seismic codes.

Baetu, et al. (2013), performed a comparative study of slit and solid walls and concluded that that the slit wall was dissipating approximately 1.5 times more hysteretic energy than the solid wall. This occurred due to the slit wall had a better hysteretic energy dissipation capacity and dissipates seismic energy by cracks extended on the entire surface of the wall and by crushing of the shear connections, while the solid wall dissipates seismic energy only by large cracks at the base of the wall (Figure 2.16).

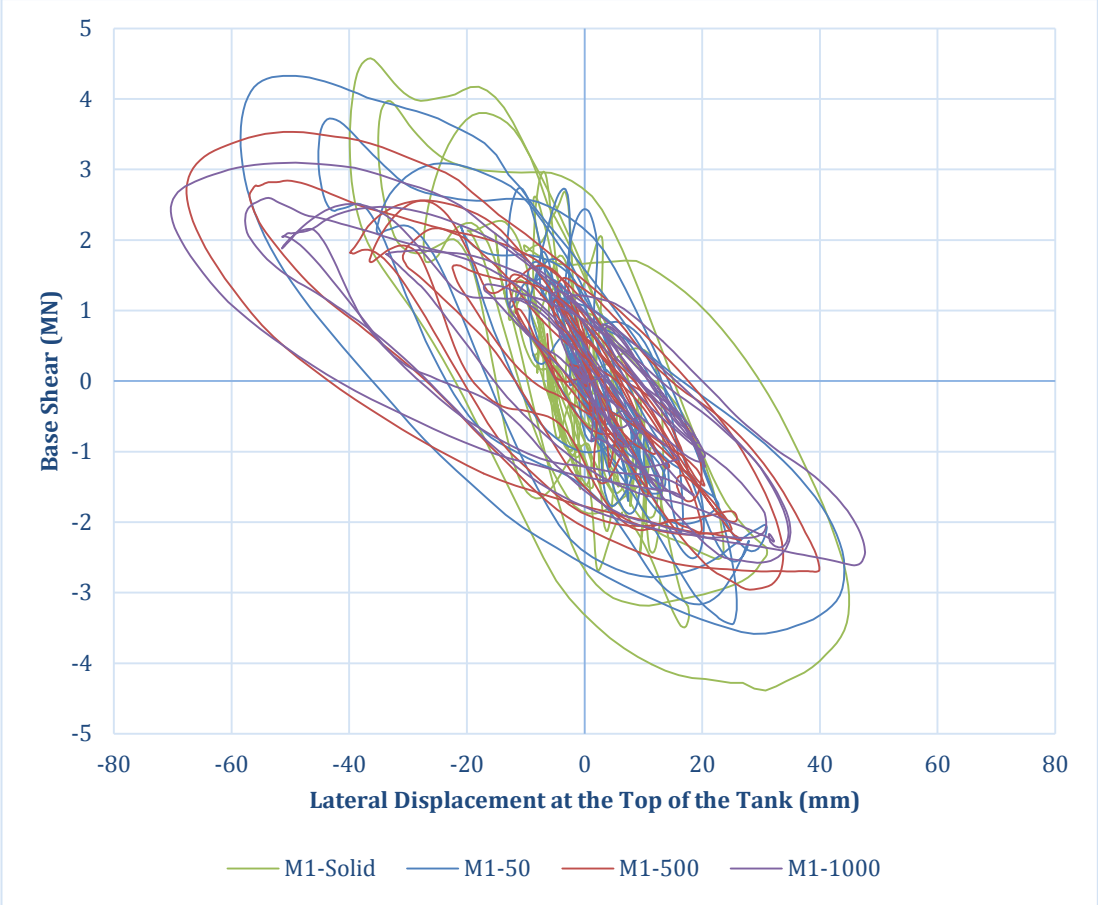

Figure 7.6. Hysteresis loops (Top Lateral Displacement – Base Shear) of M1 group models subjected to El-Centro horizontal excitation scaled to PGA=0.4g

7.5 Stress distribution in the RC shafts

The cracking propagation patterns of the RC shafts were discussed in Chapter 6. It was shown that the RC shafts could be categorised into three classes depending on the slit width and related cracking propagation pattern. The same behaviour was observed by investigating the results of the nonlinear dynamic analysis. The maximum stress was assumed to be at the moment of maximum top lateral displacement.

It was found that models achieved maximum top lateral displacement at a different time. However all slit shaft models reached the maximum top lateral displacement at first drift between 1.905 and 1.965 seconds. On the other hand, the maximum top lateral displacement in the solid model took place at 2.165 seconds. This could be

explained by significantly different fundamental periods between the solid model and slit models.

Three different patterns of tension and compression stress distribution at the level of maximum lateral displacement were observed. The locations of maximum tension and compression stress locations are demonstrated in Figure 7.7 and Figure 7.8. According to this patterns, the maximum tension stress distributed just in the lover one-third part of the shaft and rest of the shaft rest unexploited. Furthermore, the maximum compression stress occurred at the base corners of the shaft side perpendicular to the direction of the earthquake and also did not distribute along the shaft.

On the other hand, model M1-50, had maximum tension and compression stresses in shaft wall sides parallel to the direction of the ground motion as a result of excessive web-shear cracking. Those types of cracks were the most desirable because stresses were not concentrated in one place but uniformly distributed along the whole shaft that supported to energy dissipation along whole shaft.

Finally, models M1-500 and M1-1000 demonstrated to have maximum tension and compression stress concentration at the top of the shaft parallel to the direction of the ground motion and resulted to top-shear cracking. It could be concluded that a possible mode of failure for this category of RC shafts would be the tank-sliding failure, which was not desirable because this could lead to losing vertical load resistance in the RC shaft.

(a) Model: M1-Solid

(b) Model: M1-50

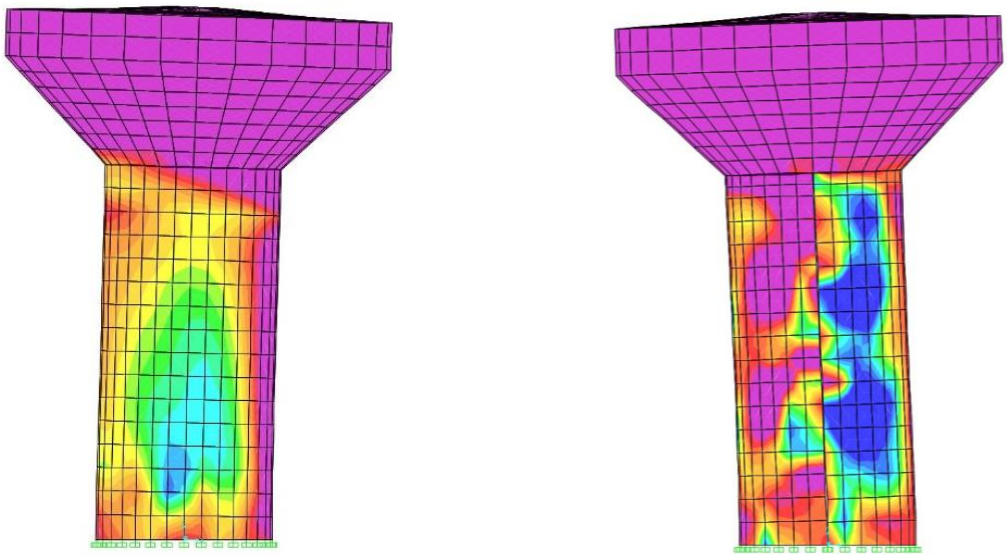

(c) Model: M1-500

(d) Model: M1-1000

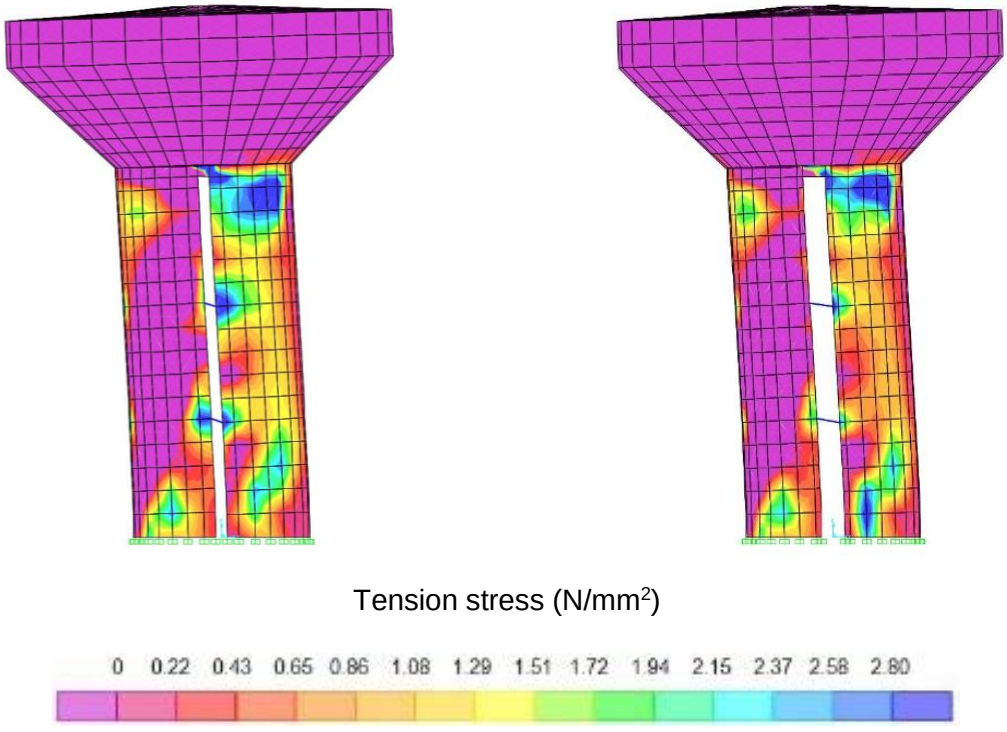

Figure 7.7. Contours of concrete tension stress distribution in RC shafts of M1 group models at peak top lateral deformation subjected to El Centro earthquake scaled to PGA = 0.4g

(a) Model: A-0

(b) Model: A-50

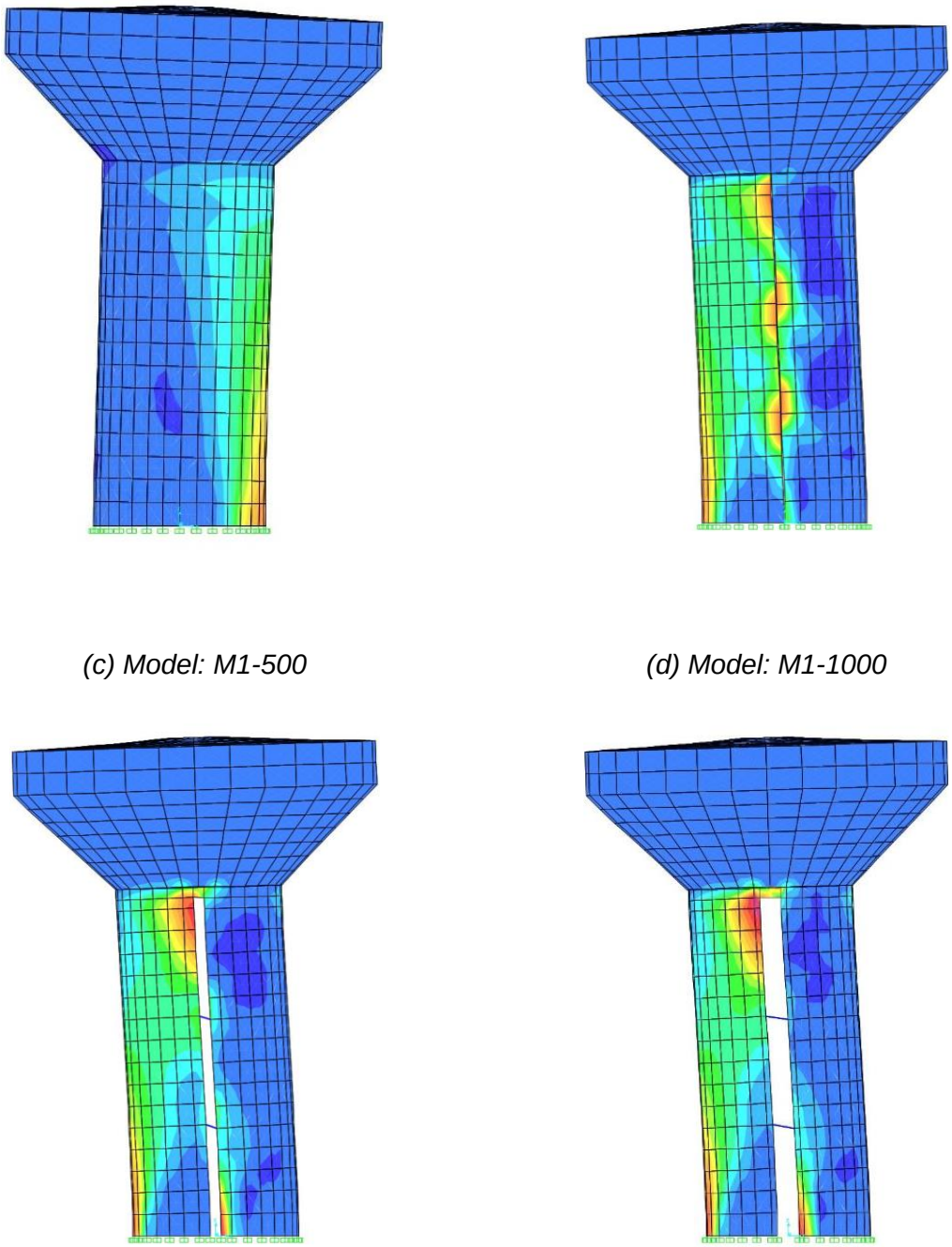

(c) Model: M1-500

(d) Model: M1-1000

Figure 7.8. Contours of concrete compression stress distribution in RC shafts of M1 group models at peak top lateral deformation subjected to El-Centro earthquake scaled to PGA = 0.4g

7.6 Concrete crash zones in the RC shafts under dynamic nonlinear analysis

The effect of vulnerable concrete crash zones of slit shafts on dynamic seismic response of elevated water tanks was considered in this section. The elevated tank models considered in this section were the same as used in Chapter 6. The vulnerable zones of the FE model M1-500 model are shown in Figure 6.15.

Table 7.2 shows the compression stresses at vulnerable zones for models considered in this study subjected to El-Centro earthquake horizontal component normalized to $PGA = 0.4g$. It can be seen from the Table 7.2 that the ultimate compression stress at Zone I was almost reached in models M1-1500 and M1-2000. This indicated that the concrete started to crash and the models almost reached a failure point.

Secondly, Models with slits wider than 1000 mm reached a compression stress of $19N/mm^2$ at Zone V and became vulnerable for concrete crush at the top of the shaft, this was not desirable.

Moreover, models with slits wider than 100 mm did not effectively distribute stresses along all the connections. The stress concentration could be seen in Zone I, II and V and almost negligible in Zone III and IV, which was not desirable too.

Table 7.2. Peak concrete compression stress values in vulnerable zones of all M1 group models subjected to El-Centro earthquake horizontal record scaled to PGA = 0.4g

FE model ID	Compression stress (N/mm^2)				
	Zone I	Zone II	Zone III	Zone IV	Zone V
M1-Solid	15.96	0.55	0.62	1.91	3.92
M1-50	16.19	4.95	18.59	19.36	14.46
M1-100	16.32	7.52	16.77	19.28	16.79
M1-200	16.41	10.72	10.53	12.84	18.29
M1-300	16.43	13.26	8.14	10.02	18.82
M1-500	16.77	16.03	6.69	8.86	19.02
M1-1000	18.42	18.75	5.63	6.92	20.00
M1-1500	19.54	18.97	3.87	6.40	20.00
M1-2000	19.84	18.16	5.04	7.58	20.00

Finally, the most effective stress distribution was in model M1-50 and M1-100, where compression stresses reached maximum values around connections and reasonable stress values in all other zones.

As a result, the RC shafts with slits equal to or less than 100 mm probably demonstrated a flexure mode of failure that was more ductile. The damages were expected to appear first around the connections parallel to the load applied and later at the shaft base perpendicular to the load applied.

For better understanding of the influence of the earthquake intensity on the stress distribution in slit shaft elevated water tanks, the El-Centro earthquake was scaled to 0.5g and 0.6g for models M1-Solid, M1-50 and M1-500. The results were provided in Table 7.3 and Table 7.4 for scaled earthquake to 0.5g and 0.6g respectively. The result showed that an increase in intensity had a higher influence on the solid model compared to the slit models. Zone I was the most vulnerable zone for the solid model. The increase in intensity drastically increased the compression stresses in Zone I for model M1-Solid. However model M1-50 was less effective to the earthquake intensity. The analysis of influence of earthquake sensitivity on the ultimate compression stress in Zone 1 was provided in the next section on this chapter.

It was stated by many researchers that crashing of concrete in connecting beams and around connections should appear first for better energy dissipation and distribution of cracks along the whole structure (Baetu, 2012).

Table 7.3 Peak concrete compression stress values in vulnerable zones of M1 group models subjected to El-Centro earthquake horizontal record scaled to PGA = 0.5g

FE model ID	Compression stress (N/mm^2)				
	Zone I	Zone II	Zone III	Zone IV	Zone V
M1-Solid	18.00				
M1-50	17.58	3.02	18.80	20.00	14.74
M1-500	18.34	12.79	7.07	9.83	19.03

Table 7.4 Peak concrete compression stress values in vulnerable zones of M1 group models subjected to El-Centro earthquake horizontal record scaled to PGA = 0.6g

FE model ID	Compression stress (N/mm^2)				
	Zone I	Zone II	Zone III	Zone IV	Zone V
M1-Solid	19.86				
M1-50	19.19	1.98	17.48	20.00	14.48
M1-500	19.63	11.77	6.94	9.82	19.80

7.7 Influence of earthquake intensity on the compression stress in the shaft base

In order to investigate the effect of earthquake intensity on the compression stress distribution on in the shaft base, four elevated tank models, namely M1-Solid, M1-50, M1-500 and M1-1000 were subjected to the El-Centro ground motion horizontal component scaled in such a way that its peak ground acceleration reaches 0.4g, 0,5g and 0.6g.

Figure 7.9 shows that the distribution of the compression stress at the base dramatically increased with an increase of the earthquake intensity. This was due to the fact that a higher value of PGA leads to higher amplitudes of the earthquake and it caused a higher shear forces. It was clear that a change in PGA could make a significant changes in the damage patterns of the shafts.

According to previous sections of this study the most dangerous case was when the concrete reached the ultimate compressive strength and started to crash. The area of crash concrete was located at the base (ground) level of the RC shafts perpendicular to the applied load. The area of the crashed concrete played a significant role on the stability of the elevated water tank. For all FE models, the compressive stress did not reach $17\ N/mm^2$ so it was below the crashing point when the El-Centro earthquake was scaled to $PGA = 0.4g$. However in this part of study it was assumed that dangerous zone for concrete crashing stated to develop when compressive concrete stress reached $f_c' = -15.8\ N/mm^2$ and concrete started to behave in inelastic way. Furthermore, when the earthquake was scaled to $PGA = 0.5g$, the stress at the sides of the openings in Model M1-1000 reached crashing point, moreover dangerous zones increased in all other models. It could be seen in Figure 7.9 that the dangerous zone in the model M1-Solid became two times wider than the dangerous zones in models M1-50 and M1-500.

Finally, under the earthquake scaled to $PGA = 0.6g$ all models reach the compressive ultimate strength. The zone when the compressive concrete stress reached $f_c' = -18\ N/mm^2$of concrete in models M1-Solid and M1-1000 were about 3 m width and 1 m height. However, this zone in model M1-50 was just approximately 1.5 meter wide and 0.5 meter height. It can be concluded that the compression stress was better distributed along the whole shaft in models with narrow slit shafts and more concentrated at the base in wide slit shafts and solid shafts.

(a) Model: M1-Solid

PGA=0.4g **PGA=0.5g** **PGA=0.6g**

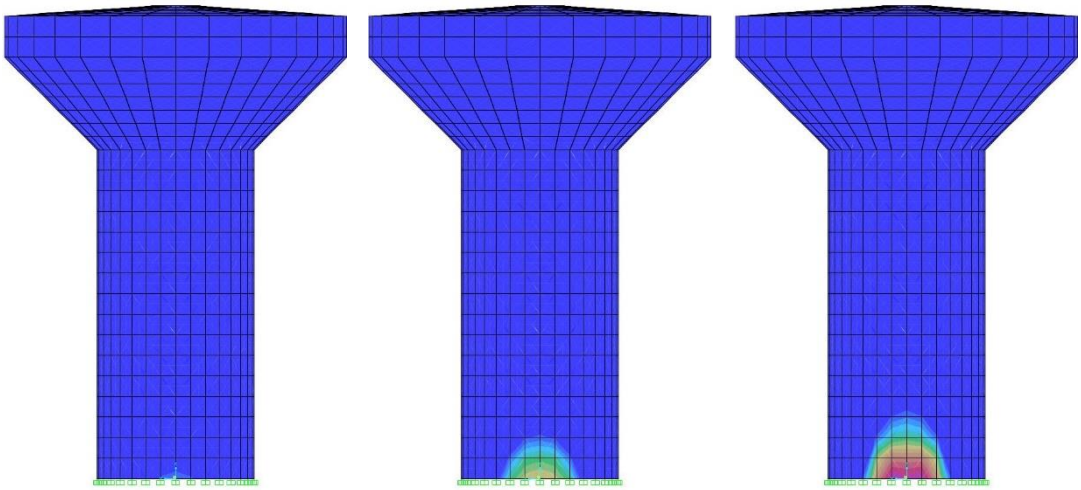

(b) Model: M1-50

PGA=0.4g **PGA=0.5g** **PGA=0.6g**

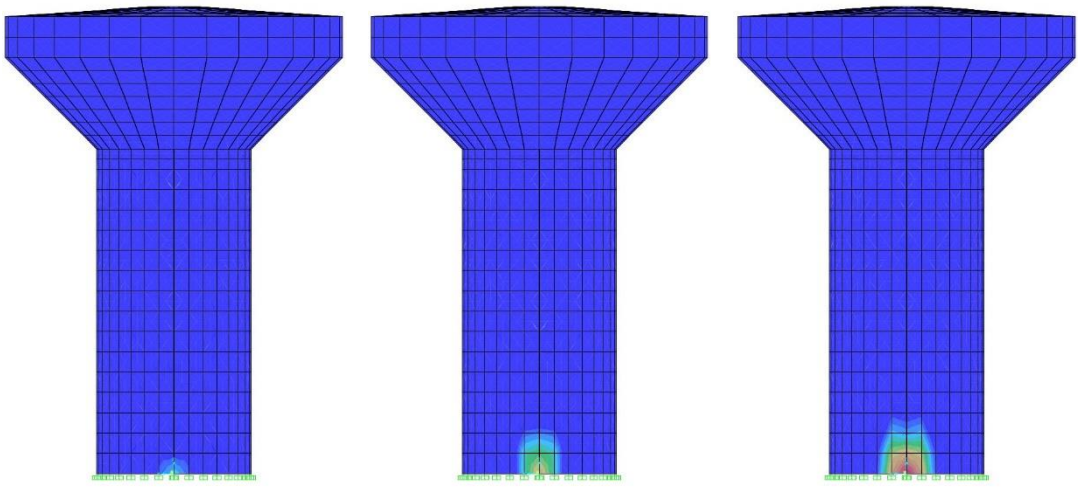

Compressive stress (N/mm^2)

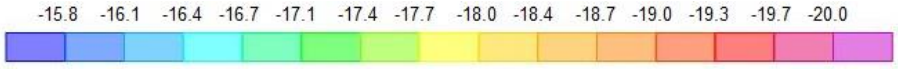

Figure 7.9 (a) Contours of concrete compressive stress distribution in M1 group models subjected to El-Centro horizontal component scaled to 0.4g, 0.5g and 0.6g.

(a) Model: M1-500

PGA=0.4g **PGA=0.5g** **PGA=0.6g**

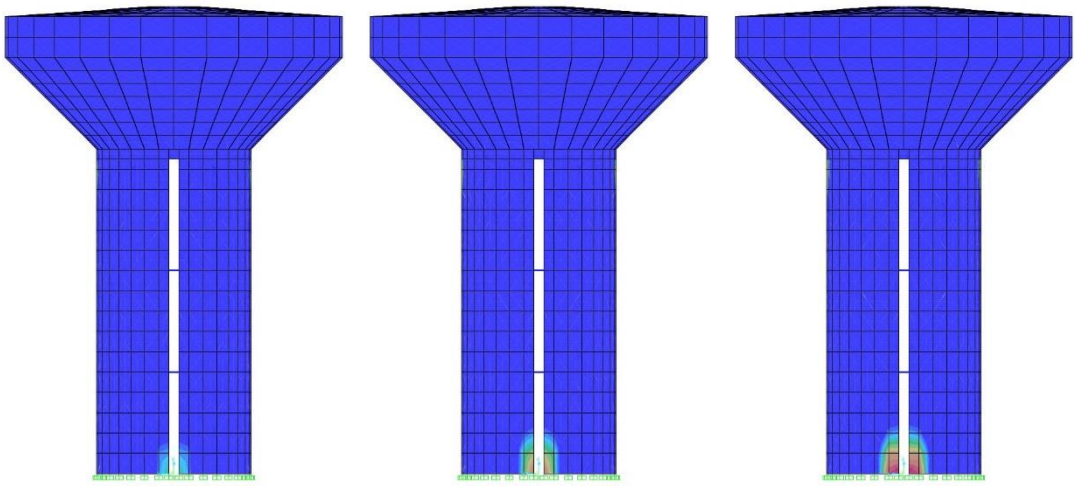

(b) Model: M1-1000

PGA=0.4g **PGA=0.5g** **PGA=0.6g**

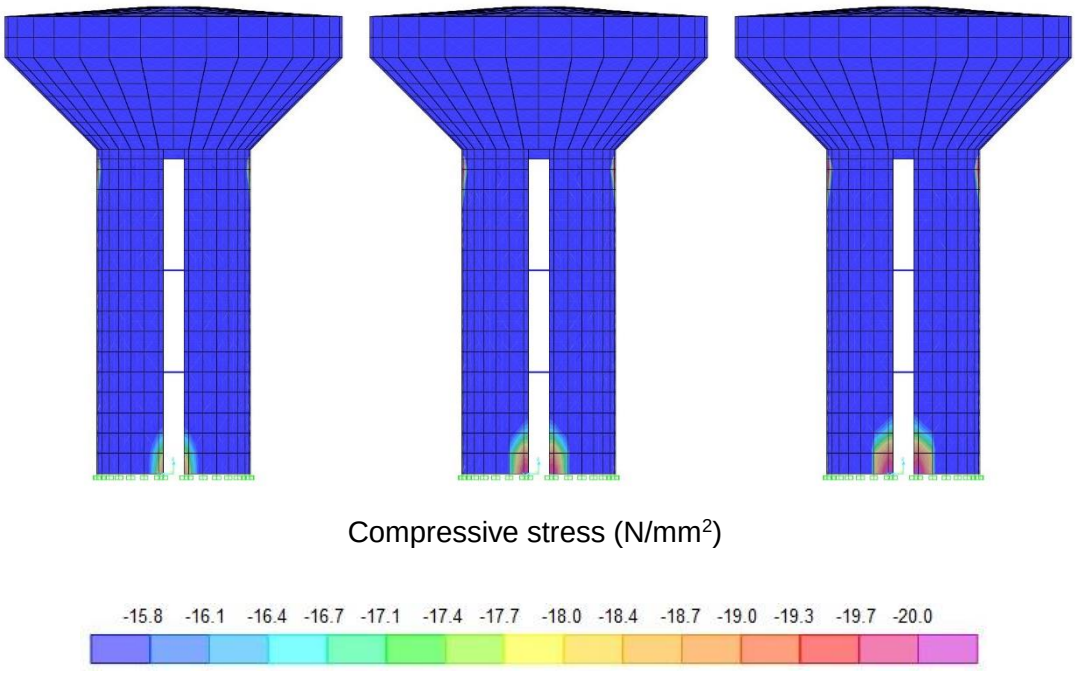

Figure 7.9 (b) Contours of concrete compressive stress distribution in M1 group models subjected to El-Centro horizontal component scaled to 0.4g, 0.5g and 0.6g.

7.8 Effect of shaft dimensions and tank capacity on dynamic response

The main focus of this section is the effect of water tank capacity and support shaft dimensions on the seismically induced response of the supporting structure for the proposed RC elevated tanks. Nonlinear direct integration dynamic analysis was used to investigate such effect. This FE technique was explained in detail in the previous sections of this this chapter. Using this technique, the seismic behaviour of elevated water tanks having different water tank capacities and shaft geometries under random excitation was investigated.

This study considered three groups of elevated water tanks, namely M1 group, M2 group and M3 group. Each group consisted of four FE models that consisted of the solid model and three models with slits (50 mm, 500 mm and 1000 mm). All models used in this study are shown in Figure 7.10.

The elevated tank models considered in this study were assumed to have fixed condition at the base. The original models M1, M2 and M3 were real elevated water tanks damaged in Bhuj earthquake studied by Rai (2002; 2004). All dimensions of models were described in Chapter 4 of this thesis.

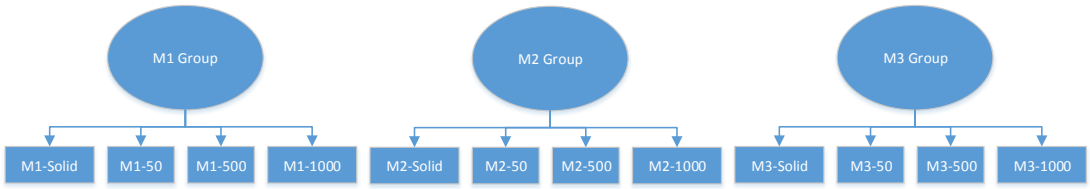

Figure 7.10 FE models selected for parametric study

The ground motion used for the time history analysis was the horizontal component of 1940 El-Centro earthquake scaled to the peak ground acceleration of 0.4g as shown in Figure 7.1. An integration time step of 0.005 seconds was used for time history analysis of the tanks. Better illustration was taken within the first 5 seconds of the record due to the highest response occurring in that range.

Table 7.5 lists the peak time history response values of the proposed slit shaft elevated tank models against the corresponding solid model. The numbers in bold show an increase (positive) or decrease (negative) percentage over the corresponding solid model.

The first observation of the table shows a decreased mass in the water tank resulted in a decrease for the seismic response. The same trend can be observed in a decrease in the shaft diameter. The reduction of base shear and base moment was more apparent than a reduction of the top lateral displacement. Top lateral displacement was less sensitive to water tank capacity and more sensitive to shaft dimensions.

There was a pronounce reduction in base shear and base moment with an increase of width of slits in all three groups of elevated water tanks. A comparison of the base shear indicated that the base shear decreased by 7%, 24% and 33% for models M1-50, M1-500 and M1-1000 respectively, in comparison to model M1-Solid in the M1 group (Figure 7.11). The similar trend was observed in the M2 group (Figure 7.12) and M3 group (Figure 7.13). The reduction of the shear force was between 8% and 32% and between 9% and 29% for the M2 group and M3 group respectively. It was obvious that the reduction of the shear force was higher in the M3 group compare to the other groups for models with narrow slits. However, an increase of the slit width in the M3 group resulted in the minor shear force reduction compare to other groups.

Comparison of the base moment indicated that the base moment decreased by 11%, 25% and 33% for models M1-50, M1-500 and M1-1000 compare to model M1-Solid in the M1 group (Figure 7.14). The similar trend can be observed in the M2 group (Figure 7.15) and M3 group (Figure 7.22). The reduction of shear force was between 14% and 33% and between 5% and 30% for the M2 group and M3 group respectively. In the case of the base moment the reduction was higher in the M2 group compared to other groups for models with narrower slits. However, an increase of the slit width resulted in similar reduction of the base moment in all groups.

On the other hand, top lateral displacement increased by 31%, 51% and 57% for models M1-50, M1-500 and M1-1000 compared to model M1-Solid in study group M1 (Figure 7.17). A greater difference in top lateral displacement increase were observed in the M2 group (Figure 7.18) and the M3 group (Figure 7.19). Top lateral displacement increased by 30%, 69% and 75% for models M2-50, M2-500 and M3-1000 compared to model M2-Solid in the M2 group. Finally, Top lateral displacement increased by 27%, 68% and 97% for models M3-50, M3-500 and M3-1000 compared to model M3-Solid in the M3 group.

It can be concluded that top lateral displacement was the most sensitive parameter to the capacity of an elevated water tank and shaft dimensions. The narrow slit shafts were less sensitive compared to wider slit shafts. Shaft with slits 50 mm showed similar responses for all model groups, however wider slit shafts (500 mm and 1000 mm) showed a radical increase in top lateral displacement. Slits in shafts with smaller diameters contribute in bigger openings that produce a higher reduction of stiffness and bigger improvement in ductility. However, it can be dangerous that an elevated water tank loose stiffness and stability.

Table 7.5. Peak response values of M1, M2 and M3 group models subjected to El-Centro horizontal excitation scaled to PGA=0.4g

FE Model ID	Base Shear (MN)		Base Moment (MNm)		Top Lateral Displacement (mm)	
M1 Group						
M1-Solid	*4.64*		*93.08*		*44.74*	
M1-50	*4.33*	**-6.76%**	*83.06*	**-10.76%**	*58.46*	**+30.67%**
M1-500	*3.53*	**-23.89%**	*69.96*	**-24.84%**	*67.66*	**+51.23%**
M1-1000	*3.10*	**-33.33%**	*62.60*	**-32.75%**	*70.34*	**+57.22%**
M2 Group						
M2-Solid	2.91		53.45		38.98	
M2-50	2.67	**-8.32%**	46.19	**-13.58%**	50.55	**+29.68%**
M2-500	2.24	**-22.89%**	39.56	**-25.99%**	65.80	**+68.80%**
M2-1000	1.98	**-32.13%**	35.55	**-33.49%**	68.32	**+75.27%**
M3 Group						
M3-Solid	1.39		18.15		32.81	
M3-50	1.26	**-9.03%**	17.26	**-4.90%**	41.68	**+27.03%**
M3-500	1.11	**-19.71%**	14.22	**-21.65%**	55.28	**+68.49%**
M3-1000	0.98	**-29.24%**	12.69	**-30.08%**	64.55	**+96.74%**

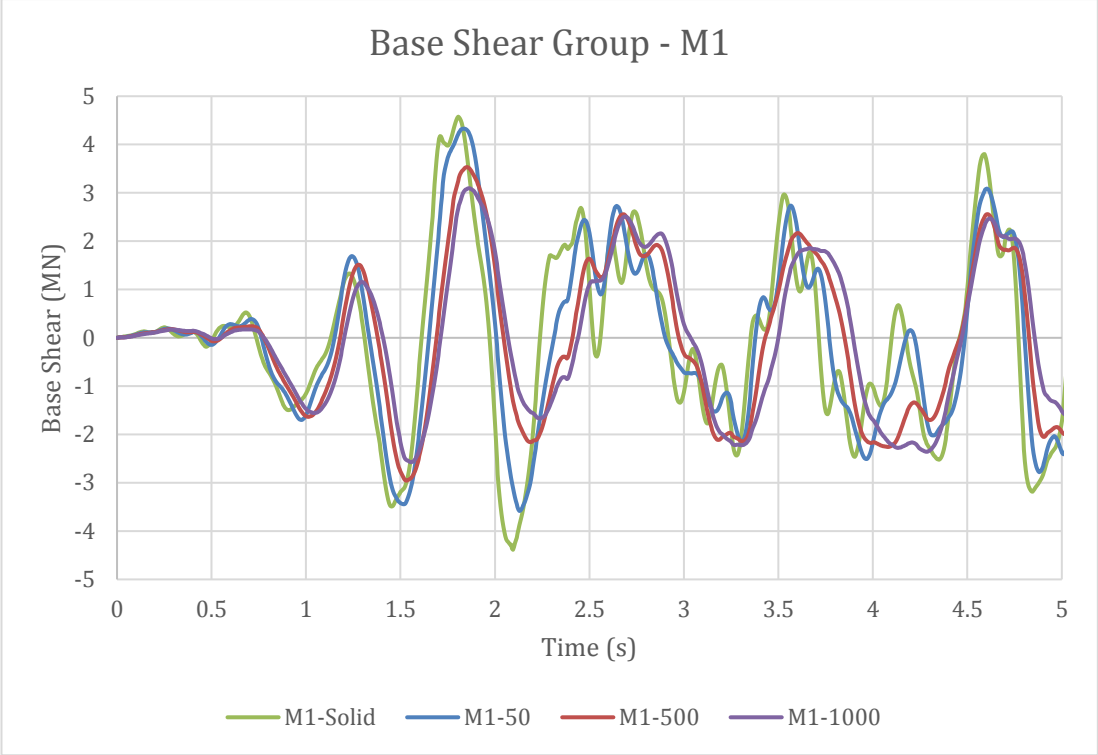

Figure 7.11.Time history base shear response of M1 group models subjected to El-Centro horizontal excitation scaled to PGA=0.4g

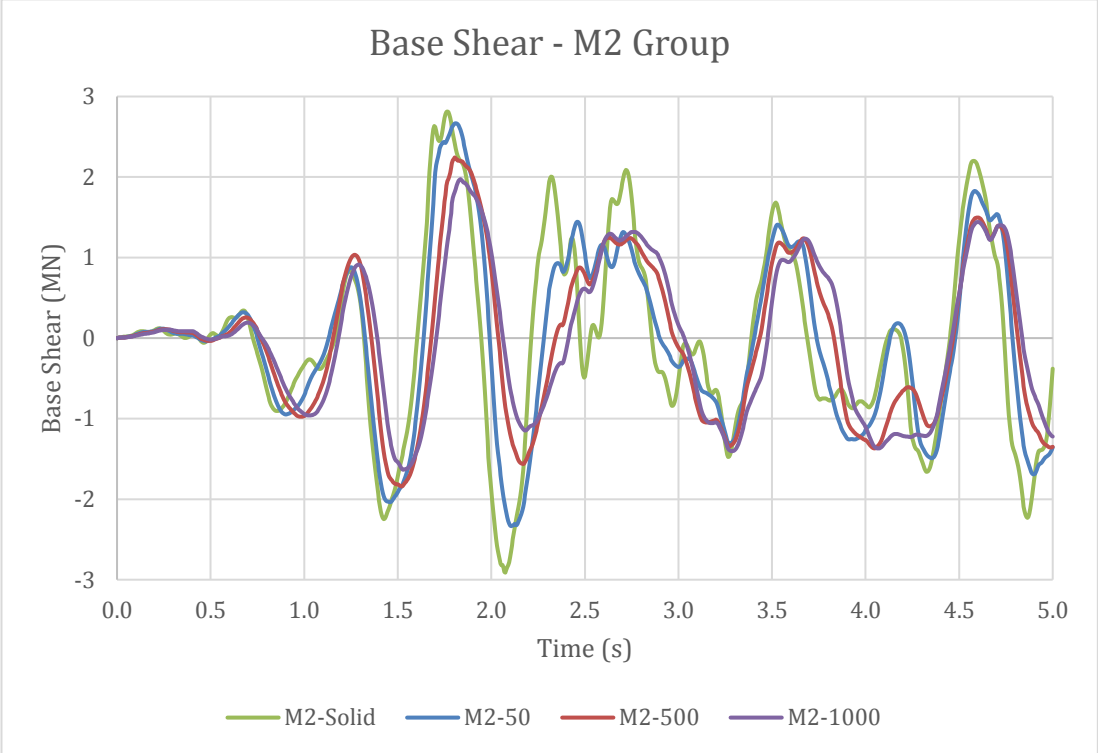

Figure 7.12.Time history base shear response of M2 group models subjected to El-Centro horizontal excitation scaled to PGA=0.4g

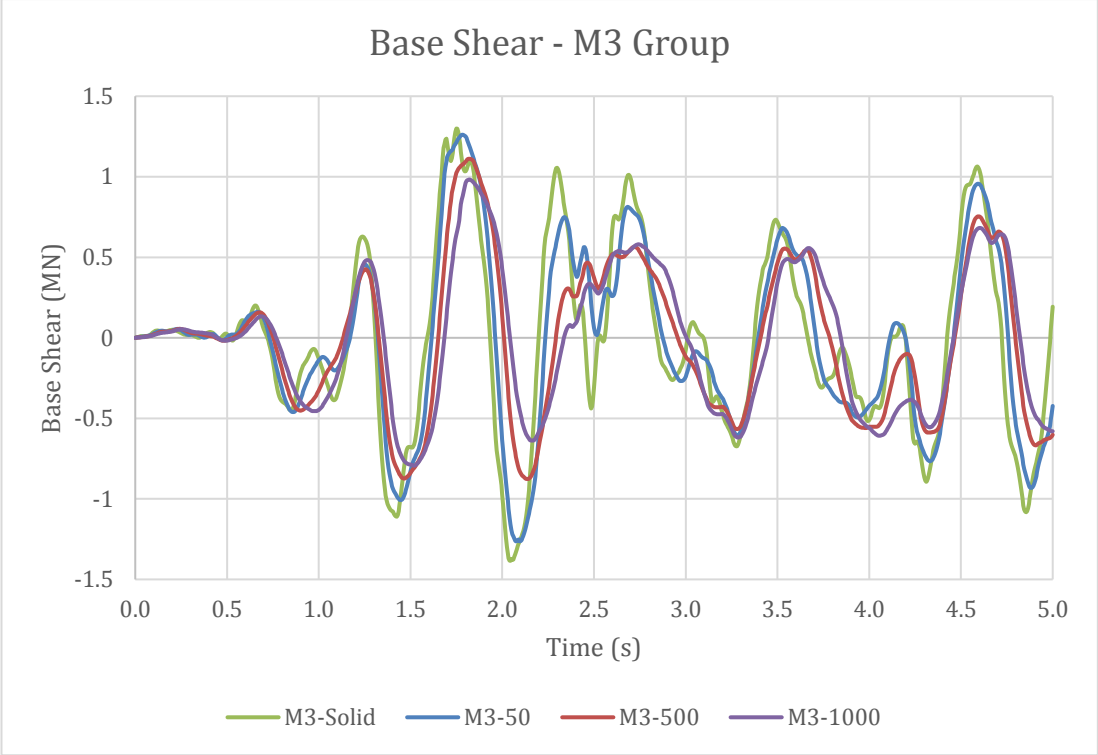

Figure 7.13.Time history base shear response of M3 group models subjected to El-Centro horizontal excitation scaled to PGA=0.4g

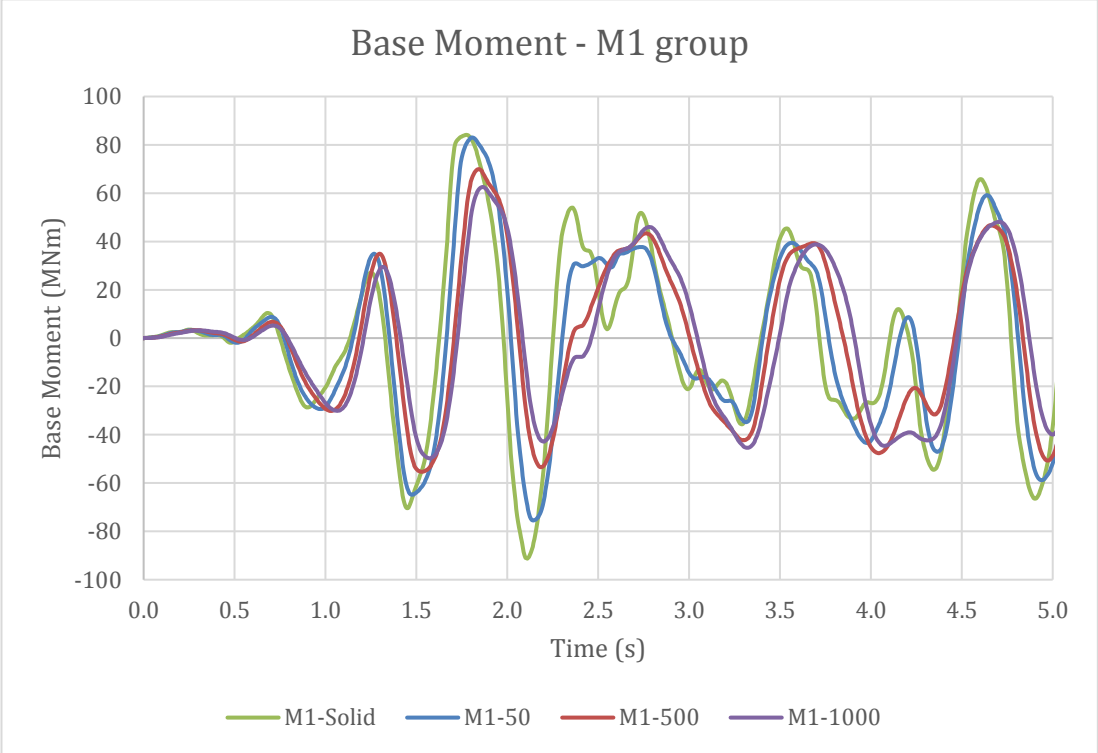

Figure 7.14.Time history base moment response of M1 group models subjected to El-Centro horizontal excitation scaled to PGA=0.4g

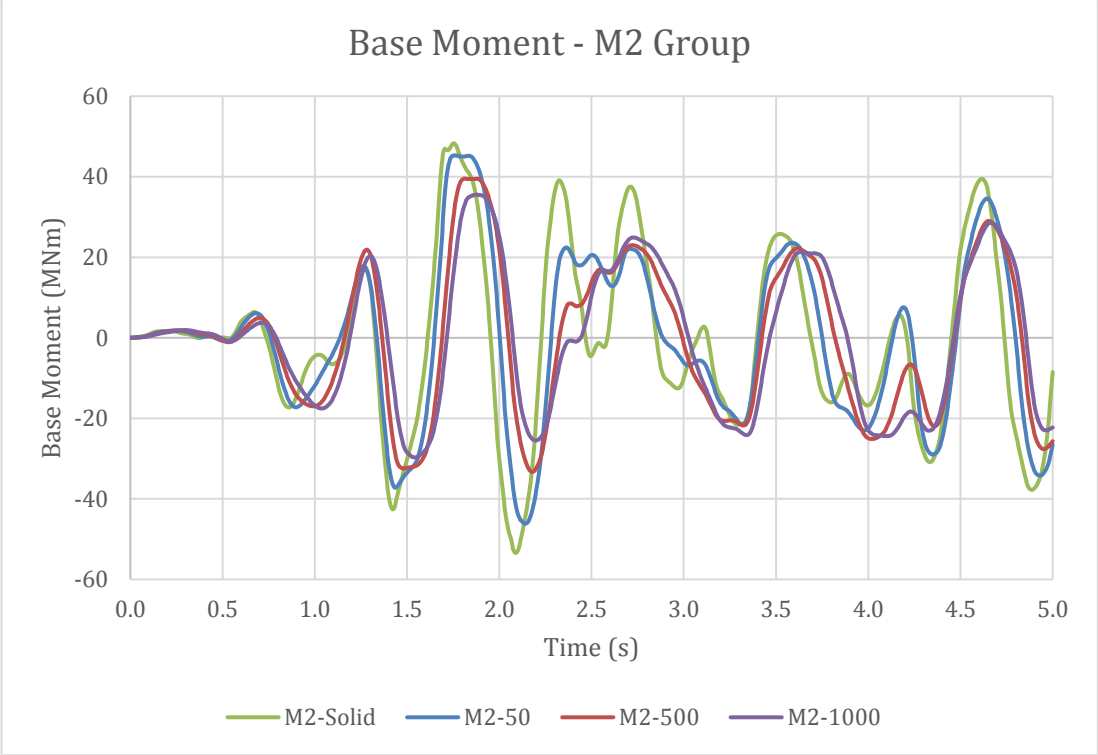

Figure 7.15.Time history base moment response of M2 group models subjected to El-Centro horizontal excitation scaled to PGA=0.4g

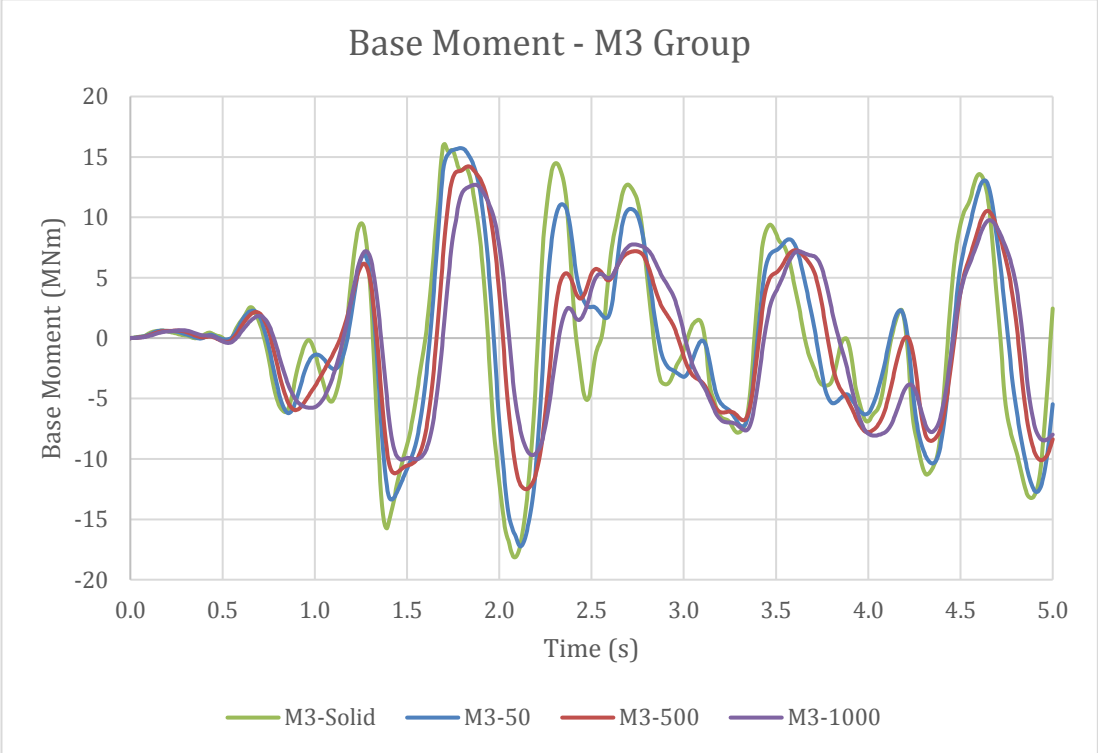

Figure 7.16.Time history base moment response of M3 group models subjected to El-Centro horizontal excitation scaled to PGA=0.4g

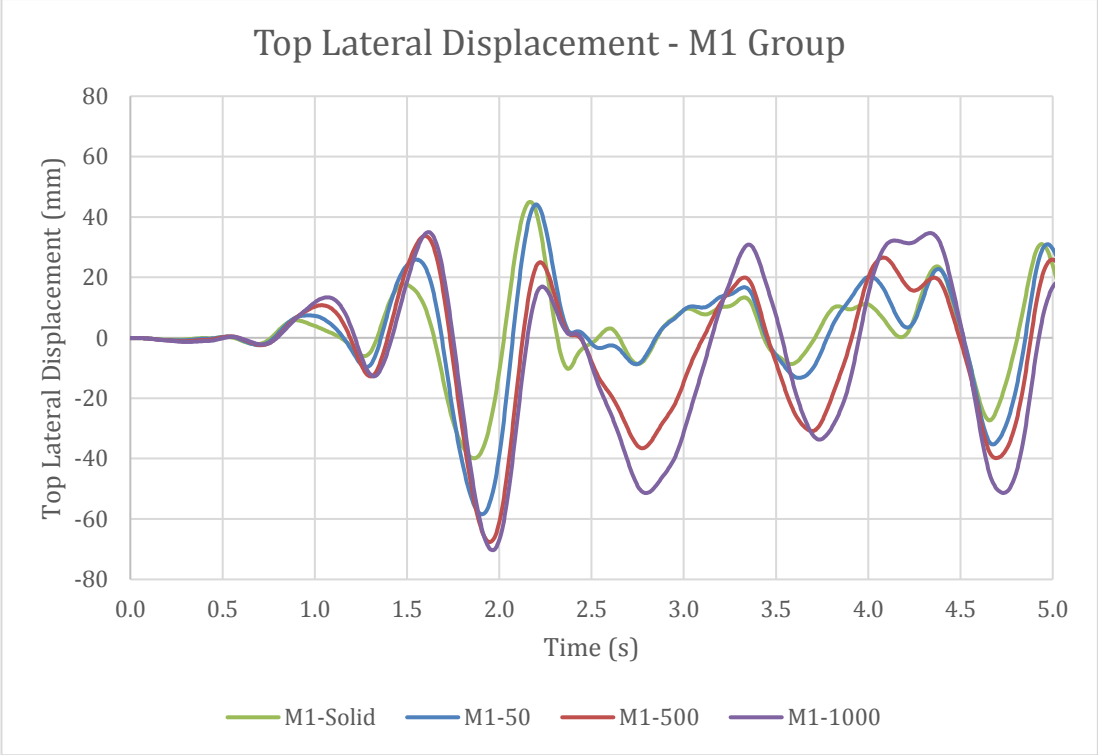

Figure 7.17.Time history top lateral displacement of M1 group models subjected to El-Centro horizontal excitation scaled to PGA=0.4g

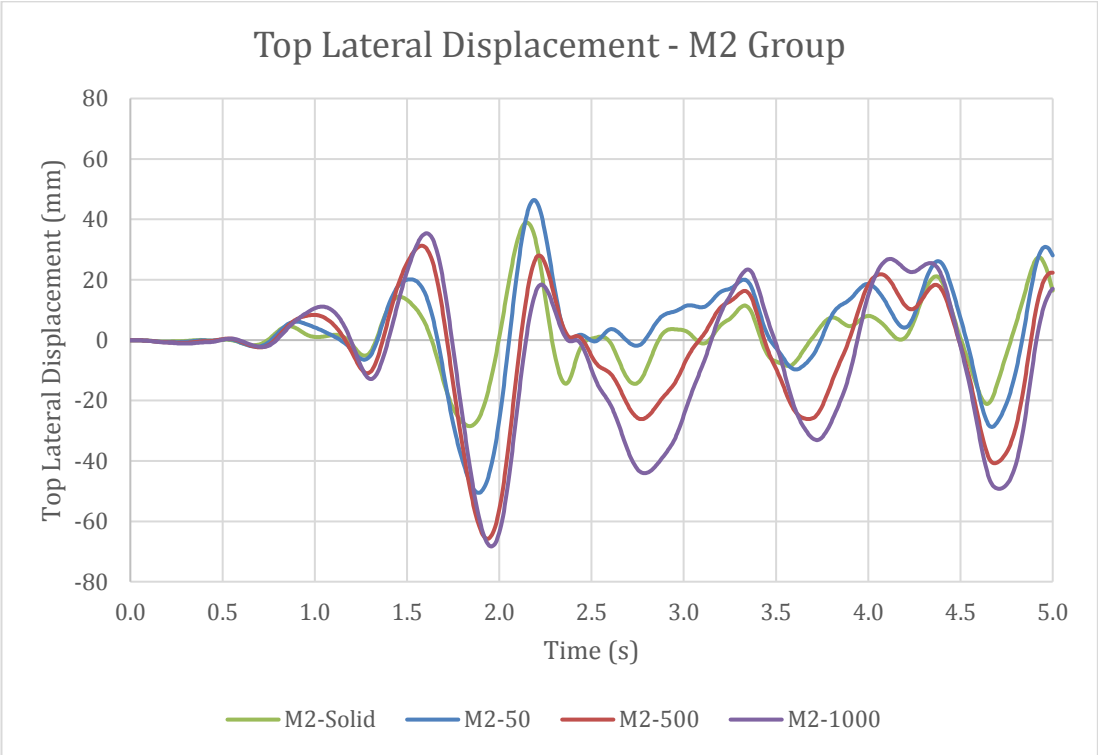

Figure 7.18.Time history top lateral displacement of M2 group models subjected to El-Centro horizontal excitation scaled to PGA=0.4g

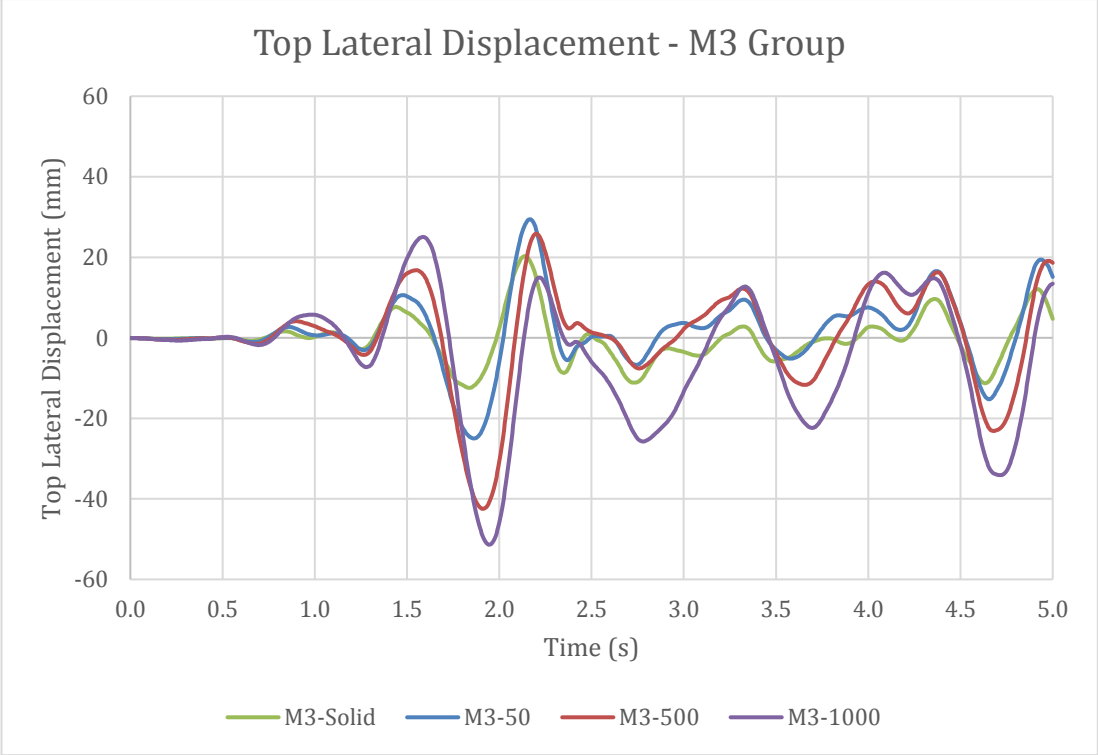

Figure 7.19.Time history top lateral displacement of M3 group models subjected to El-Centro horizontal excitation scaled to PGA=0.4g

7.9 Summary

During this study, transient analysis using the direct integration method was carried out to investigate the influence of width in shafts on the dynamic nonlinear response of elevated water tanks. Studied responses were for shear and overturning moment at the base of the shaft structure as well as lateral displacement at the top of the tank.

All models were subjected to time-history nonlinear direct integration analysis of El-Centro 1940 earthquake horizontal record scaled to PGA = 0.4g to obtain dynamic nonlinear properties of proposed elevated water tanks. The results of the nonlinear dynamic analysis of the RC shafts were demonstrated and discussed. It was concluded that an increase in slit width resulted in a reduction of the base shear by 7%, 24% and 33% for models with 50 mm, 500 mm and 1000 mm slits respectively compared to the solid model. A similar reduction could be observed for the base moment. On the other hand, top lateral displacement increased by 31%, 51% and 57% for models with 50 mm, 500 mm and 1000 mm slits respectively compared to the solid model.

Corresponding observations between the capacity spectrum analysis and FE time history results for the proposed elevated tank models were identified. This verified the validity of the capacity spectrum analysis in estimating the seismic response of the liquid filled elevated water tanks. However, results obtained from the dynamic nonlinear analysis showed significantly higher response values compare to the results obtained from the static nonlinear analysis for a seismic zone with PGA = 0.4g and rock soil. More pronounce difference was noticed for top lateral displacement, which reached 30%.

It was identified that the slit shaft has a better hysteresis energy dissipation capacity that can prevent severe damage of the shaft base. The energy dissipation mechanism is different for slit shaft and solid shaft. The slit shaft dissipates hysteresis energy via cracks extended on the entire surface of the shaft and by crushing of the connection beams. The solid shaft dissipates seismic energy only by cracks at the base of the shaft. The hysteretic loops for the proposed models displayed the total amount of energy absorbed during the earthquake resulted in noticeable increases in models with slits compared to the solid model.

In order to study stresses, tension and compression stress patterns at peak El-Centro earthquake response were examined and compared to the stresses from a pushover analysis, studied in Chapter 6. It was concluded that the pattern of stress distribution along the shaft was similar for dynamic and static nonlinear analysis. A comparison of stresses in the vulnerable zones detected in Chapter 6 was performed and analysed. Stresses in dynamic analysis show a higher value compared to the static analysis.

The study of the influence of the earthquake intensity showed that increase of PGA significantly influence the stress distribution in RC shafts. Increase of PGA from 0.4g to 0.6g showed that crash of the shaft base opposite to applied load occurred in solid shaft model however, models with narrow slit had not reached crash level. The slit shaft elevated water tanks were more effective to distribute seismic loads during strong earthquakes.

The study of the influence of the earthquake intensity on the compression stress at the shaft base opposite to the applied load demonstrated that the distribution area of the compression stress increased in a higher degree in the solid shaft in comparison to the slit shafts with an increase of the earthquake intensity. Increase of PGA from 0.4g to 0.6g showed that area of dangerous compression stress in the solid shaft

became 3 times as area of dangerous compression stress in the narrow slit shaft. However the increase in slit width increased a dangerous zone also.

Transient analysis using the direct integration method was carried out on three different groups of models to investigate the influence of water tank capacity and RC shaft dimensions on the dynamic behaviour of slit shaft elevated water tanks. It was concluded that the water tank capacity and diameter of the RC shaft did not significantly influence the base shear and base moment, however a significant increase in the top lateral displacement was observed in shafts with wide slits. On the other hand, narrow slit shafts were less sensitive to a difference in shaft diameter and water tank capacity. Top lateral displacement is the most sensitive response value to the slit width. Decrease in shaft dimensions with wide slits can drastically increase top lateral displacement, however does not provide efficient reduction of base shear and base moment.

Chapter 8

Recommendations

1. No experimental test on the RC shafts were conducted for enhanced understanding of the actual response of RC slit shafts. Shaking table test should be conducted for evaluation of theoretical results.

2. The results in this study should be used only in a case with a full water tank. The sloshing component of water was not taken into account.

3. The different cross sections and amount of reinforcement can influence the stability of the slit elevated water tanks.

4. Time history results are valid in the case of hard soil. The base of the shaft was assumed to be rigid and soil-structure interaction (SSI) effect were not investigated.

5. The only unidirectional horizontal record was studied. Vertical ground acceleration was neglected. The application of seismic records from both sides together can affect the reactions of the elevated water tanks.

6. Just hollow shafts without floors with different applications were investigated. The introduction of the applications can affect the stress distribution.

7. The number of connection beams were limited to two for every slit. The different number of connecting beams can be used but it can affect the stiffness of the slit shaft.

Chapter 9

Conclusions and suggested further research

The observations of the nonlinear static and dynamic analyses would appear to justify the slit shaft system approach proposed in this work: using the slits in reinforced concrete shaft design, reduces the stress concentration at the shaft base and distributes the stresses uniformly along the shaft height.

For conventional RC elevated water tanks, the failure mode of the solid RC shaft is difficult to control and the shear failure can easily occur. Even though the desired flexural failure mode could be obtained, damage and energy dissipation are generally concentrated in the plastic hinge regions at the base of the shaft. Therefore, loss of vertical bearing capacity and shear capacity occurs quickly and easily under the impact of a strong earthquake.

For the slit RC shaft elevated water tanks, the damage process can be better controlled. Most importantly, ductile failure can be achieved for the design of slit shaft and brittle shear failure can be avoided.

This study revealed that cracking and crushing of the concrete around the connection beams could significantly reduce the seismic response at the shaft base of the elevated RC water tank. The seismic performance can be controlled by the slit width, to satisfy the different design criteria under different earthquake levels.

In order to obtain the optimal control effect, the selection of the slit width should optimise the stiffness and ductility of the RC shaft. The solution proposed in this research alters the behaviour of the solid RC shaft and enhances the ductility, energy dissipation and crack pattern.

The following conclusions were drawn based on the results of this study in each part:

9.1. Modal Analysis

Modal analysis was implemented to evaluate the dynamic behaviour of the slit and solid models of the elevated water tanks as well as find first modes of models and investigate the elongation of the fundamental period resulted by the increase of slit width. Further conclusions were made:

1. The convective mode and first two impulsive modes dominated in the dynamic response of all the studied models because the sum of the effective modal masses exceeded 90% of the total mass.

2. The slit width did not have a significant influence on the convective period. The difference was less than 1% for all the slit models compared to the solid model. Water sloshing inside a water tank was primarily dependent on the dimensions of the water tank, such as diameter and height. Therefore the influence of the support system could be neglected.

3. The effect of the slit width variations was considerably pronounced on the fundamental period elongation. The fundamental period was increased by 14%, 31% and 45% for models with slits of 50, 500 and 1000 millimetres in the RC shafts respectively in comparison to the solid model.

4. The main reason for the fundamental period elongation was for the reduction of stiffness and an increase of the ductility in the RC shaft. The slit width regulates the elongation of a fundamental period of an elevated water tank and as a result this controls the RC shaft stiffness and ductility.

5. The modal energy dissipation increased by approximately 150% for all the models of the elevated water tanks with slits, in comparison to the solid model for El-Centro 1940 earthquake horizontal record scaled to PGA = 0.4g. An improved energy dissipation capacity proposes that a better deformation performance of the system can prevent serious damages of the shaft base, thus the dynamic properties of the slit shaft elevated water tanks, were improved in comparison to the solid elevated water tank.

9.2. Static nonlinear analysis

Pushover analysis was conducted on the slit and solid models of the elevated water tanks in order to construct the pushover curves and establish the top lateral displacement and observe the stress and crack propagation in the shafts. Further conclusions were made:

1. The peak point of the base shear – top lateral displacement curve was defined as the failure criteria for elevated water tanks because RC shafts have very low ductility and redundancy capacity.

2. The reduction of the peak base shear by 6%, 27% and 46% for models with slits of 50, 500 and 1000 millimetres in the RC shafts respectively was observed in comparison to the solid model. However, the maximum top lateral displacement was inconsequentially sensitive to an increase in the slit width, in comparison to the base shear.

3. Soil types A, B and C identified in Eurocode 8 were appropriate for the construction of the studied elevated water tanks with slits is equal to or less than 1000 mm. However, soil type D was not acceptable for the construction of any type of studied models.

4. The most favourable for elevated water tank construction was soil type A (rock), and the least favourable – soil type C. The difference in top lateral displacement between soil type A and C was more than two times for all models.

5. Reduction in the base shear was proportional to an increase of the top lateral displacement for all soil types and models. For soil type A, the reduction of the base shear by 10%, 37% and 51% in addition to an increase in the top lateral displacement by 6%, 21% and 24% for models with slits of 50, 500 and 1000 millimetres in the RC shafts respectively were observed in comparison to the solid model. For other soil types a similar trend was observed.

6. Three types of crack propagation were observed. The solid elevated water tank demonstrated a base-shear cracking pattern. However, the elevated water tanks with narrow slit shafts, where the slits are equal to or less than 100 millimetres, demonstrated a web-shear crack pattern and elevated water tanks with wide slit shafts, slits wider than 100 millimetres, displayed a top-shear cracking pattern. Web-shear crack propagation was the most favourable because stress distribution was uniform along the height of the shaft. Other crack propagation patterns showed a crack concentration in the base and top of the shaft for base-shear and top-shear crack patterns respectively.

7. The most effective stress distribution inside the RC shaft were defined to be in shafts with slit width equal to or less than 100 millimetres for all soil types. However, RC shafts with slits wider than 100 millimetres can be used on hard soil and in low seismicity regions.

9.3. Dynamic nonlinear analysis

Time history analysis was implemented to evaluate the dynamic seismic performance of the slit and solid models of the elevated water tanks in order to verify the static nonlinear analysis. The horizontal component of the El-Centro earthquake scaled to PGA=0.4g was applied to the models. Further conclusions were made:

1. The response values obtained from the time-history analysis of El-Centro earthquake scaled to PGA=0.4g, showed a reduction of the base shear by 7%, 24% and 33% and base moment by 11%, 25% and 33% for models with slits of 50, 500 and 1000 millimetres in the RC shafts respectively in comparison to the solid model.

2. Lateral displacement at the top of the tank increased by 31%, 51% and 57% for models with slits of 50, 500 and 1000 millimetres in the RC shafts respectively in comparison to the solid model.

3. The response values obtained from the time-history analysis of El-Centro earthquake scaled to PGA=0.4g showed significantly higher response values compared to the results obtained from the static nonlinear analysis for a seismic zone with PGA = 0.4g and rock soil. The difference between the results reached 33% and 77% for the base shear and top lateral displacement respectively.

4. The hysteretic loops displayed that the total amount of hysteresis energy absorbed during the El-Centro earthquake scaled to PGA=0.4g had noticeably increased in the models with slits, in comparison to the solid model that had a better deformation performance of the slit shaft elevated water tanks.

5. The pattern of tension and compression stresses distribution along the shaft was similar for the dynamic and static nonlinear analyses. The elevated water tank models with slits in the RC shaft, which are equal to or less than 100

millimetres were the most effective for stress distributions along the shaft height in comparison to other models.

6. The most effective stress distribution inside the RC shaft was defined to be in shafts with slit widths equal to or less than 100 millimetres due to the stresses reached the ultimate values firstly next to the connection beams and further distributed along the shaft height.

7. The concrete crash area of the shaft base opposite to the applied load in the solid shaft model was significantly more functional in the solid shaft model compared to the slit shaft models. This demonstrated a better performance of the slit shaft elevated water tanks in strong earthquakes.

8. Elevated water tanks with narrow slits were less sensitive to the variation of the shaft dimensions and water tank capacity. However, the top lateral displacement was the most sensitive response value in the tanks with wide slits RC shaft.

9.4. Suggested Further research

With regards to this research study, some suggestions for further research on nonlinear behaviour of elevated water tanks with slit shafts can be made as follows:

1. An experimental test such as shaking table test can be very beneficial for enhanced understanding of the actual response of RC slit shafts.

2. More case studies with varying tank capacity and shaft geometries can be carried out through a careful selection of a variety of elevated water tanks in order to verify the effects of these parameters on the nonlinear response of such structures.

3. Different liquid depths and empty condition can be a parameter for further studies. Moreover, the sloshing component of water was not taken into account in the nonlinear dynamic analysis of the FE models. This effect can be included by modelling the water inside the tank in future studies.

4. Therefore, further studies can investigate connection stiffness by a variety of dimensions and the amount of reinforcement in the connection beams.

5. Since the base of the shaft was assumed to be rigid, other restraining conditions at the base level could be investigated as well. The effect of deformable foundation on the behaviour of elevated water tanks can be investigated by simulating the soil-structure interaction (SSI) effect in a rigorous numerical model.

6. Effects of lateral and vertical stiffness shaft properties can be further investigated by varying the concrete grade and percentage of reinforcement.

7. The dynamic response of elevated tanks under vertical ground accelerations can be investigated using the proposed numerical procedure as well as investigation of both horizontal and vertical records together.

8. In some RC shafts, floors with different applications are constructed. This effect was not studied in this research and may be further investigated.

9. The application of seismic isolators or energy dissipaters can be investigated in controlling the seismic response of RC shafts.

References

Algreane, G. A.I., Osman, S.A., Karim, O. A. and Kasa, A., 2008. Investigate the Seismic Response of Elevated Concrete Water Tank. Engineering Postgraduate Conference (EPC)

Algreane, G. A.I., Osman, S.A., Karim, O. A. and Kasa, A., 2009. Dynamic Behaviour of Elevated Concrete Water Tank with Alternate Impulsive Mass Configurations. WSEAS, ISSN: 1790-2769.

Algreane, G. A.I., Osman, S.A., Karim, O. A. and Kasa, A., 2011. Behavior of Elevated Concrete Water Tank Subjected to Artificial Ground Motion. EJGE, Vol. 16, pp. 387-406

Algreane, G. A.I., Osman, S.A., Karim, O. A. and Kasa, A., 2011. Study The Fluid Structure Interaction Due to Dynamic Response of Elevated Concrete Water Tank. Australian Journal of Basic and Applied Sciences, 5(9): 1084-1087.

Arya, A. S., Thakkar, S. K., and Goyal, A. C., 1971, “Vibration analysis of thin cylindrical containers”, Journal of the Engineering Mechanics Division, ASCE, Vol. 97, pp. 317-331.

Ayazhussain M. Jabar and H. S. Patel, 2012. Seismic behaviour of RC elevated water tank under different staging pattern and earthquake characteristics. IJAERS/Vol. I/ Issue III/April-June, 2012/293-296.

Băetu S.A., Ciongradi I.P. and Barbat, A.H., 2013. Seismic Damage Evaluation of an RC Dissipative Wall. Bul. Inst. Politehnic, Iaşi, LVII (LXI), 1, s. Constr., Archit., 31-45.

Băetu S.A., Ciongradi I.P., 2011. Nonlinear Finite Element Analysis of Reinforced Concrete Slit Walls with ANSYS (I). Bul. Inst. Politehnic, Iaşi, LVII (LXI), 1, s. Constr., Archit., 31-45.

Băetu S.A., Ciongradi I.P., 2012. Nonlinear Finite Element Analysis of Reinforced Concrete Slit Walls with ANSYS (II). Bul. Inst. Politehnic, Iaşi, LVII (LXI), 1, s. Constr., Archit., 31-45.

References

Băetu S.A., Ciongradi I.P., Văsieş G., 2010. Static Nonlinear Analysis of Structural Reinforced Concrete Walls Energy Dissipators with Shear Connections.Internat. Symp. “Computational Civil Engineering 2010”, Iaşi, Romania, May 28, 2010, 87-98.

Balendra, T., 1979, “Earthquake finite element analysis of an annular cylindrical liquid storage tank”, In: Proc. 3rd Int. Conference on Finite Element Methods, Australia.

Barton, D.C., Parker, J.V., 1987. Finite element analysis of the seismic response of anchored and unanchored liquid storage tanks. Earthquake Engineering and Structural Dynamics 15, 299–322.

Bauer, H.F., 1964. Fluid oscillations in the containers of a space vehicle and their ınfluence upon stability. NASA TR R 187.

Bento, R., Falcao, S. and Rodrigues, F., 2004. Non-linear static procedures in performing based seismic design. 13th World Conference on Earthquake Engineering, Canada, paper 2522.

Burns, NH., Siess, CP., 1962, Load–deformation characteristics of beam-column connections in reinforced concrete. Civil Engineering Studies, SRS no. 234, University of Illinois, Urbana.

Chandrasekaran, A.R., Krishna, J., 1954. Water towers in seismic zones. In: Proceedings of the Third World Conference on Earthquake Engineering, New Zealand, vol. IV, pp. 161–171.

Chaduvula, U., Patel, D. and Gopalakrishnan, N., 2012. Fluid-Structure-Soil Interaction Effects on Seismic Behaviour of Elevated Water Tanks. Procedia Engineering (ELSEVIER), 2012, Vol. 51, pp. 84-91.

Chen, C.P., Barber, R.B., 1976. Seismic design of liquid storage tanks to earthquakes. International Symposium on Earthquake Structural Engineering, St. Louis, MO, vol. II, pp. 1231–1247.

Chen, J.Z., and Kianoush, M.R., 2005, Seismic response of concrete rectangular tanks for liquid containing structures, Canadian Journal of Civil Engineering, 32, 739-752.

References

Cheng-Tzu, T.H., Saeed Mirza,M., Sunny,C.S., 1981, Nonlinear Analysis of Reinforced Concrete Frames, Computer and Structures, Vol 13, pp. 223-227.

Chopra, A.K. and Goel, R.K., 2002. A modal pushover analysis procedures for estimating seismic demands for buildings. Earthquake Engineering and Structural Dynamics, 31, pp. 561-582.

Chopra, A. K., 2007. Dynamics of Structures: Theory and Application to Earthquake Engineering, University of California at Berkeley, Third Edition.

Claudio E. Todeschini, Albert C. Bianchini, and Clyde E. Kesler, "Behavior of Concrete Columns Reinforced with High Strength Steels," ACI Journal, Proceedings, Vol. 61, No. 6, June 1964,pp. 701–716.

Clough, D. P., 1977, Experimental evaluation of seismic design methods for broad cylindrical tanks, Report No. UCB/EERC-77/10, Earthquake Engineering Research Center, University of California, Berkeley.

Clough, R. W., Niwa, A., and Clough, D. P., 1979, Experimental Seismic Study of Cylindrical Tanks, Journal of the Structural Division, ASCE, Vol. 105, No. 12, pp. 2565-2590.

Clough, R. W., Niwa, A., and Clough, D. P., 1979, Experimental Seismic Study of Cylindrical Tanks, Journal of the Structural Division, ASCE, Vol. 105, No. 12, pp. 2565-2590.

Clough, R., Penzien, J., 1993, Dynamics of structures. 2nd Edition, New York: McGraw-Hill, Inc.

Clough, R.W., and Clough, D.P., 1977, Seismic response of flexible cylindrical tanks, Paper K 5/1 Trans. 4t h International Conference on Structural Mechanics in Reactor Technology, San Francisco, CA.

CSI, 2015. CSI Analysis Reference Manual. Computers & Structures, Inc.

Dahmani, A. Khennane, B., Kacia, S., 2010, Crack Identification in Reinforced Concrete Beams Using ANSYS Software, Strength of Materials, Vol. 42, No. 2.

References

Der Kiureghian, A. (1981). A Response Spectrum Method for Random Vibration Analysis of MDOF Systems, Earthquake Engineering & Structural Dynamics, Vol. 9, No. 5, p. 419-435.

Dogangun, A., Durmus, A., Ayvaz, Y., 1996a. Finite element analysis of seismic response of rectangular tanks using added mass and Lagrangian approach. Proceedings of the Second International Conference on Civil Engineering Computer Applications Research and Practice, Bahrain, April 6–8, vol. I, pp. 371–379.

Dogangun, A., Durmus, A., Ayvaz, Y., 1996b. Static and dynamic analysis of rectangular tanks by using the Lagrangian fluid finite element. Computers & Structures 59, 547–552.

Dogangun, A., Durmus, A., Ayvaz, Y., 1997. Earthquake analysis of flexible rectangular tanks using the Lagrangian fluid finite element. European Journal of Mechanics-A/Solids 16, 165–182.

Dogangun, A., Livaoglu, R., 2004. Hydrodynamic pressures acting on the walls of rectangular fluid containers, Structural Engineering and Mechanics 17, 203–214

Donea J. and Huerta, A., 2003. Finite Element Methods for Flow Problems, John Wiley & Sons Ltd, Chichester.

Donea, J., Gıuliani, S., Halleux, J.P., 1982. An arbitrary Lagrangian–Eulerian Finite Element method for transient dynamic fluidstructure interaction. Computer Methods in Applied Mechanics and Engineering 33, 689–723.

Duta, S. C., Jain, S. K. and Murty, C. V. R., 2000. Assessing the seismic torsional vulnerability of elevated tanks with RC frame-type staging. Soil Dynamics and Earthquake Engineering (ELSEVIER), 2000, Vol. 19, pp. 183-197.

Dutta, S., Mandal, A., Dutta, S.C, 2004, Soil-structure interaction in dynamic behavior of elevated tanks with alternate frame staging configurations. Journal of Sound and Vibration, 227: 4-5, 825-853.

Dutta, S.C., Dutta, S., Roy, R., 2009, Dynamic behavior of R/C elevated tanks with soil–structure interaction. Engineering Structures, Volume: 31 Issue: 11 Pages: 2617-2629.

References

Ekbote, P. S. and Kori J. G., 2013. Seismic Behavior of RC Elevated Water Tank under Different Types of Staging Pattern. CADmantra Technologies Pvt. Ltd.

El Damatty A.A, Saafan MS, Sweedan AMI, 2005. Experimental study conducted on a liquid-filled combined conical tank model. J Thin Walled Struct 2005;43: 1398–417.

El Damatty A.A., Korol RM, Mirza F.A., 1997, Stability of elevated liquid-filled conical tanks under seismic loading, part I—theory. Earthq Eng Struct Dyn, 26: 1191–208.

El Damatty, A.A, Korol RM, Mirza F.A., 1997, Stability of elevated liquid-filled conical tanks under seismic loading, part II—applications. Earthq Eng Struct Dyn, 26:1209–29.

Elnashai, A. S. & Di Sarno, L., 2008. Fundamentals of earthquake engineering. John Wiley & Sons. United Kingdom

Elnashai, A.S. and Mwafy, A.M., 2002. Overstrength and force reduction factors of multistorey reinforced-concrete buildings, The Structural Design of Tall Buildings, 11(5), 329 – 351.

Epstein, H.I., 1976. Seismic design of liquid storage tanks. Journal of the Structural Division, ASCE, 102(9): 1659-1673.

Eurocode 8, 2006. Design of structures for earthquake resistance. Part 1. 1:General rules – Seismic action and general requirements for structures. European Committee for Standardization.

Eurocode 8, 2006. Design of structures for earthquake resistance. Part 4: Silos, tanks and pipelines. European Committee for Standardization.

Fajfar P, Gaspersic P. The N2 method for the seismic damage analysis of RC buildings. Earthquake Engineering and Structural Dynamics 1996;25:31–46.

Ghaemmaghami, A.R., Moslemi, M., and Kianoush, M.R., 2010, "Dynamic behavior of concrete liquid tanks under horizontal and vertical ground motions using finite element method", 9th US National and 10th Canadian Conf. on Earthquake Eng., Toronto, Canada.

References

Ghateh, R., Kianoush, M.R. and Pogorzelski, W., 2015. Seismic response factors of reinforced concrete pedestal in elevated water tanks. Engineering structures, vol. 87, pp. 32-46.

Ghateh, R., 2014. Nonlinear seismic response of reinforced concrete pedestals in elevated water tanks. Ph. D. Ryerson University.Gollwitzer, S., and Rackwitz, R. (1990). “On the reliability of Daniels systems.” Struct. Safety, 7, 229–243.Gurkalo, F. and Poutos, K., 2012. Dynamic Properties of Watertowers Assembled from Interlocked Panels under Different Loading Conditions. International Journal of Engineering and Technology, Vol. 4, No. 5, pp. 649 – 652.

Gurkalo, F. and Poutos, K., 2012. Dynamic Response of a Water Tower Composed of Interlocked Panels. International Journal of Civil and Environmental Engineering, Vol. 6, pp. 224 – 230.

Haroun, M. A., and Housner, G. W., 1981. Seismic design of liquid-storage tanks. Journal of Technical Councils, ASCE, New York, Vol. 107, No. 1, pp. 191–207

Haroun, M.A., 1984, Stress analysis of rectangular walls under seismically induced hydrodynamic loads, Bulletin of the Seismological Society of America, 74(3), 1031-1041.

Haroun, M.A., and Tayel, M.A., 1985, Response of tanks to vertical seismic excitations, Earthquake Engng. And Struct. Dyn., 13, 583-595.

Haroun, M.A., Ellaithy, M.H., 1985. Seismically induced fluid forces on elevated tanks. Journal of Technical Topics in Civil Engineering 111, 1–15.

Haroun, M.A., Termaz, M.K., 1992. Effects of soil-structure interaction effects on seismic response of elevated tanks, Soil Dynamics Earthquake Engineering, 11: 2, 37-86.

He Liu, Daniel H. Schubert, Zhaohui Yang, Robert Lang, 2004. Comparative Study of Linear-Elastic and Nonlinear inelastic Seismic Responses of Fluid-Tank Systems

Hirde, S. et al, 2011, Seismic performance of elevated water tanks. International Journal of Advanced Engineering Research and Studies IJAERS/Vol. I /Issue I / 2011/ 78-87

References

Hognestad, E. A Study of Combined Bending and Axial Load in Reinforced Concrete Members, Bulletin 399, University of Illinois Engineering Experiment Station, Urbana, Ill., November 1951, 128 pp.

Holzer et al. 1975. SINDER. A Computer Code for General Analysis of Two-Dimensional Reinforced Concrete Structures. Report. AFWL-TR-74-228 Vol. 1. Air Force Weapons Laboratory, Kirt-land, AFB, New Mexico.

Hosseini, M., Vosoughifar, H. and Farshadmanesh, P., 2013. Simplified Dynamic Analysis of Sloshing in Rectangular Tanks with Multiple Vertical Baffles.

Hou G., Wang J., Layton A. (2012). Numerical Methods for Fluid-Structure Interaction - A Review. Communications in Computational Physics. Vol. 12. No. 2. pp. 337-377.

Housner G.W., Haroun M. A., 1979. Vibration tests of full-scaled liquid storage tanks. Proceedings of US National Conference on Earthquake Engineering. Stanford University, pp. 137-145.

Housner, G.W., 1963. The dynamic behavior of water tanks. Bulletin of the Seismological Society of America 53(2), 381-389.

Housner, G.W., 1963. The dynamic pressures on Fluid Containers. Technical Information Document (TID) 7024, Chapter 6 Appendix F, U.S Atomic Energy Commission.

Hunt, B., and Priestley, N., 1978. Seismic water waves in a storage tank. Bulletin of the Seismological Society of America, 68(2), 487-499.

Husain, M. 2011. Analysis of Shear Wall with Openings Using Brick Element, European Journal of Scientific Research, 50 (3): 359-371.

Husain, M., and Tsopelas, P. 2004. Measures of structural redundancy in R/C buildings. I: Redundancy indices. J. Struct. Eng. 130(11), 1651–1658.

Hwang, H. and Shinozuka, M., 1994. Effects of large earthquake on the design of buildings in eastern united states. Proc. Fifth U.S. National Conference on Earthquake Engineering, Chicago, Illinois.

IBC., 2011. International Building Code. International Code Council, Inc., USA:ICC.

Ingle, R. K., 1999. Proportioning of columns for water tank supporting structures, The Indian Concrete Journal, pp. 255-257.

Jacobsen, L. S., 1949. Impulsive hydrodynamics of fluid inside a cylindrical tank and of fluid surrounding a cylindrical pier. Bulletin of the Seismological Society of America, Vol. 39, No. 3, pp. 189–203.

Jacobsen, L. S., and Ayre, R. S., 1951. Hydrodynamic experiments with rigid cylindrical tanks subjected to transient motions. Bulletin of the Seismological Society of America, 41(4): 313 - 346.

Joshi, S.P., 2000. Equivalent Mechanical Model for Horizontal Vibration of Rigid Intze Tanks", ISET Journal of Earthquake Technology, 37 (1-3), pp.39-47.

Kalani, M. and Salpekar, S. A., 1978. A comparative study of different methods of analysis for staging of elevated water tanks, Indian Concrete Journal, pp. 210-216.

Kianoush, M.R., and Chen, J.Z., 2006. Effect of vertical acceleration on response of concrete rectangular liquid storage tanks. Engineering Structures, 28(5), 704-715.

Kianoush, M.R., Mirzabozorg, H., and Ghaemian, M., 2006, Dynamic analysis of rectangular liquid containers in three-dimensional space, Canadian Journal of Civil Engineering, 33, 501-507.

Kim, J. K., Koh, H. M., and Kwahk, I. J., 1996. Dynamic response of rectangular flexible fluid containers. ASCE Journal of Engineering Mechanics, 122(9): 807–817.

Knoy, C. E., 1995. Performance of elevated tanks during recent California seismic events. AWWA Annual Conference & Exhibition.

Kobayashi, H., K. Seo and Midorikawa, S. 1986. Report on seismic micro zoning studies of the Mexico City earthquake of September 19, 1985, Part 2, Tokyo Institute of Technology, Yokohama, Japan.

Koh, H. M., Kim, J. K., and Park, J. H., 1998, Fluid-structure interaction analysis of 3D rectangular tanks by a variationally coupled BEM-FEM and comparison with test results, Earthquake Engineering and Structural Dynamics, 27: 109-124.

References

Krolicki, J. Maffei, G. and Calvi, M., 2011. Shear Strength of Reinforced Concrete Walls Subjected to Cyclic Loading, Journal of Earthquake Engineering, 15(S1):30–71.

Kuo, J.S.H, 1982. Fluid-structure interactions: Added mass computation for incompressible fluid, UCB/EERC-82/09 Report, University of California, Berkeley.

Kwak, H.G., Kim, S.P., 2002. Non-linear analysis of RC beams based on moment curvature relation. Comput Struct 80 7/8, pp. 615–628.

Labafzadeh, M.S.R. and Ziyaeifar M., 2008. Nonlinear behavior of RC dual ductility mode shear walls. Seismic Engineering International Conference, Italy, 1854-1862

Labafzadeh, M.S.R. and Ziyaeifar M., 2008. Seismic Behavior of RC Dual Ductility Mode Shear Walls. World Conference on Earthquake Engineering, Beijing, China.

Livaog˘lu. R., Dog˘angu¨n. A., 2005, Seismic evaluation of fluid-elevated tankfoundation/soil systems in frequency domain. Struct Eng Mech; 21(1):101–19.

Livaoğlu, R. and Doğangün, A., 2004. A simple seismic analysis procedure for fluid-elevated tank-foundation/soil systems. In Sixth International Conference on Advances in Civil Engineering (ACE 2004), İstanbul, Turkey, v1; pp.570-580.

Livaoglu, R. and Dogangun, A., 2006. Dynamic Behavior and Seismic Performance of Elevated Tanks Due To Ground Types Defined in EC-8 and TEC-06

Livaoğlu, R. and Doğangün, A., 2006. Simplified Seismic Analysis Procedures for Elevated Tanks Considering Fluid-Structure-Soil Interaction, Journal of Fluids and Structures, 22:3, 421-439.

Livaoglu, R. and Dogangun, A., 2006. The Effects of Local Site Classes on the Dynamic Behavior of Elevated Tanks with Frame and Shaft Supporting Structures

Livaoğlu, R., 2008. Investigation of Seismic Behavior of Fluid- Rectangular Tank-Soil/Foundation Systems in Frequency Domain, Soil Dynamics and Earthquake Engineering, 28:2, 132-146.

Livaoglua, R., and Dogangu, A., 2007. Effect of foundation embedment on seismic behaviour of elevated tanks considering fluid–structure-soil interaction. Soil Dynamics and Earthquake Engineering, 27 (9), pg. 855-863 963; 53(2):225–307.

Lu, X.L. and Wu, X.H., 2000. Study on A New Shear Wall System with Shaking Table Test and Finite Element Analysis. Earthquake Engineering and Structural Dynamics, 29(7), 1425-1440.

Malhotra, P. K., Wenk, T., and Weiland, M., 2000. Simple procedure of seismic analysis of liquid-storage tanks, J. Struct. Eng. Int., IABSE 10 (3), 197–201

Mander, J.B., Kim, J.H, and Dutta, A., 2001. Shear-Flexure Interaction Seismic Analysis and Design; pg. 369-383; Modeling of Inelastic Behavior of RC Structures under Seismic Loads: ASCE/SEI.

Mander, J.B., Priestley, M.J.N. and Park, R. 1988. Theoretical Stress-Strain Model for Confined Concrete, Journal of Structural Engineering. ASCE. 114(3). 1804-1826.

Manos, G. C., and Clough, R. W., 1982. Response of a Cylindrical Liquid Storage Tank to Static and Dynamic Lateral Loads. AMD-Vol. 53, American Society of Mechanical Engineers, New York, New York, Earthquake Ground Motion and Its Effect on Structures, presented at the Winter Annual Meeting, ASME, Phoenix, pages 77-90, 1982.

Marashi, E.S., Shakib. H., 1997. Evaluations of dynamic characteristics of elevated water tanks by ambient vibration tests. Proceedings of the 4th International Conference on Civil Engineering, Tehran, Iran,I, 367-73.

Menoni, S., Pergalani, F., Boni, M.P., Petrini, V., 2002, Lifelines earthquake vulnerability assessment: a systemic approach, Soil Dynamics and Earthquake Engineering 22, 1199-1208.

MacGregor, J.G., 1997. Reinforced Concrete Mechanics and Design. Third Edition. Prentice Hall.

Meslouris, K., 2000. Structural Dynamics; Models, Method and Experiment, Erst & Sohn.

Miao, et al., 2006. Nonlinear FE Model for RC Shear Walls Based on Multi-layer Shell Element and Microplane Constitutive Model. Computational Methods in Engineering and Science. EPMESC X, Aug. 21-23, 2006, Sanya, Hainan,China

Mickleborough NC, Ning F, Chan CM., 1999. Prediction of the stiffness of reinforced concrete shear walls under service loads. ACI Struct J 1999;96(6):1018–26.

Minowa, C., 1980. Dynamic analysis for rectangular water tanks. Recent Adv. Lifeline Earthquake Engineering Japan, Vol. 12, No. 3, pp. 135-142.

Miranda, E., and Bertero, V. V., 1994. Evaluation of strength reduction factors for earthquake resistant design. Earthquake Spectra, 10(2), 357–379.

Moses, F., 1974. Reliability of structural systems. J. Struct. Div., ASCE, 100(9), 1813–1820.

Moslemi M, Kianoush MR, Pogorzelski W. Seismic response of liquid-filled elevated tanks. Eng Struct 2011;33:2074–84.

Moslemi, M., Kianoush, M.R., and Pogorzelski, W., 2011, Seismic response of liquidfilled elevated tanks, Journal of Engineering Structures, 33(6), 2074-2084.

Mwafy, A.M. and Elnashai, A.S, 2002, Calibration of force reduction factors of RC building, Journal of Earthquake Engineering, 6(2), 239-273.

Mwafy, A.M. and Elnashai, A.S, 2002. Overstrength and force reduction factors of multistory reinforced-concrete buildings. Struct. Design Tall Build. 11, 329–351

Nazari, A., 2009. Seismic response of reinforced concrete elevated water towers, MASc Thesis, Ryerson University.

Newmark, N. M., and Hall, W. J. 1982. Earthquake spectra and design. Earthquake Engineering Research Institute, Oakland, Calif. Nassar AA, Krawinkler H. Seismic demands for SDOF and MDOF systems. Report No. 95.

Niwa, A., 1978. Seismic behavior of tall liquid storage tanks. UCB/EERC-78/04, Earthquake Engineering Research Center, University of California, Berkeley, 1978-02.

Olson, L.G., Bathe, K.J., 1983. A study of displacement-based fluid finite elements for calculating frequencies of fluid and fluid–structure systems. Nuclear Engineering and Design 76, 137–151.

References

Omidinasab, F., Shakib, H., 2008. Seismic vulnerability of elevated water tanks using performance based- design, The 14th World Conference on Earthquake Engineering, Beijing, China.

Omidinasab, F., Shakib, H., 2012. Seismic Response Evaluation of the RC Elevated Water Tank with Fluid-Structure Interaction and Earthquake Ensemble

Osteraas, J. D. and Krawinkler, H., 1990. Strength and Ductility Considerations in Seismic Design, John A. Blume Earthquake Engineering Centre, Report 90, Stanford University, California.

Papanikolaou, V.K., Elnashai, A.S. and Pareva, J.F., 2006. Evaluation of conventional and adaptive pushover analysis II: Comparative results. Journal of Earthquake Engineering, 10 (1), 127 – 151.

Park, J. H., Koh, H. M., and Kim, J., 1992. Liquid-structure interaction analysis by coupled boundary element-finite element method in time domain. Proceedings of the 7th International Conference on Boundary Element Technology, BE-TECH/92, Computational Mechanics Publication, Southampton, England. 89–92.

Park, R., 1988. Ductility evaluation from laboratory and analytical testing. Proceedings of the 9th World Conference on Earthquake Engineering. Tokyo - Kyoto, Japan , Vol. VIII, pp. 605 – 616 .

PEER, 2006a, PEER NGA Database, Pacific Earthquake Engineering Research Center, University of California, Berkeley, California, Available at http://peer.berkeley.edu/nga/.

Priestley, M. J. N., Wood, J. H. and Davidson, B. J., 1986. Seismic design of storage tanks. Bulletin of the New Zealand National Society for Earthquake Engineering, Vol. 19, No. 4, pp. 272-284.

Rajesh, M. N. and Prasad, S. K., 2014. Seismic performance study on RC wall buildings from pushover analysis. Vol. 3, No. 6, pp. 165-171.

Rai D. C., 2002. Review of Code design forces for shaft supports of elevated water tanks. In: Proceedings of 12th symposium on earthquake engineering. p. 1407–18.

References

Rai D.C., Narayan JP, Pankaj, Kumar A., 2002. Jabalpur earthquake of May 22, 1997: reconnaissance report. India: Department of Earthquake Engineering. University of Roorkee;

Rai, D. C., 2001. Performance of elevated tanks in Mw 7.7 Bhuj earthquake of January 26, 2001, Abstracts, International Conference on Seismic Hazard with Particular Reference to Bhuj Earthquake of January 26, 2001, Oct. 3–5, New Delhi.

Rai, D.C., 2002. Seismic retrofitting of R/C shaft support of elevated tanks. Earthquake Spectra, (18): 745-760.

Rai, D.C., Singh, B., 2004, seismic design of concrete pedestal supported tanks, 13th World Conference on Earthquake Engineering, Vancouver, B.C., Canada, Paper No. 230.

Ranjbar, M.M., Bozorgmehrnia, S. and Madandoust, R, 2013. Seismic Behavior Evaluation of Concrete Elevated Water Tanks

Reshidat, R.M. and Sunna, H., 1986. Behavior of elevated storage tanks during earthquake. Proceeding of the 3rd US National Conference on Earthquake Engineering, Charleston, South Carolina, 4, 2143-2154.

Rinne J. E., 1967. Oil storage tanks. The Prince William sound, Alaska, Earthquake of 1964 and aftershocks. vol II. Part A. Washington (DC, US): Coast and Geodetic Survey; 1967. p. 245–52.

Robert D. Cook, David S.Malkus, Michael E.Plesha, 1989. Concepts and Applications of Finite Element Analysis, 3rd edition, John Wiley & Sons, New York.

Sabouri J. and Ziyaeifar M., 2009. Shear walls with dispersed input energy dissipation potentialll. Asian journal of civil engineering (Building and housing), Vol. 10.

Sadjadi, R., 2009. Response of Reinforced Concrete Rectangular Liquid Containing Structures under Cyclic Loading. Doctor of Philosophy dissertation, Ryerson University, Toronto, Canada.

Saiidi M, Sozen MA., 1981. Simple nonlinear seismic analysis of R/C structures. Journal of the Structural Division, ASCE 1981;107(ST5):937–51.

Shakib, H., Omidinasab, F., Ahmadi M.T., 2010. Seismic Demand Evaluation of Elevated Reinforced Concrete Water Tanks. International Journal of Civil Engineering, 8: 3, 204-220.

Shepherd, R., 1972. Two mass representation of a water tower structure, J. Sound Vib. 23 (3), 391–196.

Shih, C. F., and Babcock, C. D., 1980. Scale Model Buckling Test of a Fluid Filled Tank under Harmonic Excitation. American Society of Mechanical Engineers, Paper 80-C2/PVP-66.

Shinde, D.N, Nair VV, Pudale YM, 2014. Pushover analysis of multy story building, International Journal of Research in Engineering and Technology, vol.3, pp.691-693.

Souli M., Benson D. J., 2010. Arbitrary Lagrangian-Eulerian and Fluid- Structure Interaction: Numerical Simulation. Wiley-ISTE. London. UK

Steinbrugge, K. V. and Rodrigo, F. A., 1963. The Chilean earthquakes of May 1960: A structural engineering viewpoint. Bulletin Seismology American, Vol. 53, No. 2, pp. 225-307.

Uang, C. M., 1991. Establishing R(or Rw) and Cd factor for Building Seismic provisions. Journal of Structural Engineering, ASCE, 117(1), pp. 19-28.

Veletsos, A.S., 1984. Seismic Response and Design of Liquid Storage Tanks, Guidelines for the Seismic Design of Oil and Gas Pipeline Systems. ASCE, New York, pp. 255–461.

Veletsos, A.S., and Kumar, A., 1984. Dynamic response of vertically excited liquid storage tanks. Proceedings of the Eighth World Conference on Earthquake Engineering, Vol. I, California, USA, pp. 453-459.

Veletsos, A.S., and Tang, Y., 1986. Dynamics of vertically excited liquid storage tanks. ASCE Journal of Structural Engineering, 112(6): 1228–1246.

Veletsos, A.S., and Tang, Y., 1990. Soil-structure interaction effects for laterally excited liquid-storage tanks. Journal of Earthquake Engineering and Structural Dynamics, Vol. 19, No. 4, pp. 473-496.

References

Veletsos, A.S., and Yang, J.Y., 1977. Earthquake response of liquid storage thanks. Proc. 2nd Adv. Civil. Eng. through Eng. Mech. Conf., ASCE, North Carolina, 1-24.

Villaverde, R, 2009. Fundamental concepts of earthquake engineering. Taylor and Francis group, 6000 Broken Sound Parkway NW, Suite 300

Virella, J.C., Godoy, L.A., and Suarez, L.E., 2006. Fundamental modes of tank-liquid systems under horizontal motions. Journal of Engineering Structures, 28, 1450-1461.

Wang, C.H., and Wen, Y.K. 2000, Evaluation of pre-Northridge low-rise steel buildings. II: Reliability. J. Struct. Eng., 126(10), 1169–1176.

Westergaard, H.M., 1931. Water pressures on dams during earthquakes. Proceedings of the ASCE 57, 1303.

Wilson, E.L., Khalvati, M., 1983. Finite elements for the dynamic analysis of fluid-solid systems. International Journal of Numerical Methods in Engineering 19, 1657–1668.

Yu, R., Zhou, X. and Yuan, M., 2012. The Practical Step-by-Step Procedure of High-order Dynamic Response Analysis for General Damped System. Advanced Materials Research Vols. 378-379, pp 161-165.

Zienkiewicz, O.C., Bettes, P., 1978. Fluid-structure dynamic interaction and wave forces; an introduction to numerical treatment. International Journal of Numerical Methods in Engineering 13, 1–16.

Ziyaeifar, M., 2001. Current R&D on Passive Energy Dissipation and Seismic Isolation Techniques in Iran. 7th International Seminar on Seismic Isolation, Passive Energy Dissipation and Active Control of Vibr a tion of Structures, Italy, 371-377.

Ziyaeifar, M., 2003. The Study of the Seismic Behavior of Shear Walls with Dual Ductility Behavior. IIEES Report, International Institute of Earthquake Engineering and Seismology, Tehran, Iran.

Appendix A

Data for the stress-strain models

A.1 Data for the stress-strain concrete models

Table A.1 Data for stress-strain concrete model

Strain (mm/mm)	Stress (N/mm^2)
-0.00383	-11.6885
-0.00267	-16
-0.00202	-18.4045
-0.00133	-20
-0.00105	-19.4221
-0.00065	-15.7655
-0.00013	-3.96039
0	0
9.28E-05	2.785068
0.001021	0

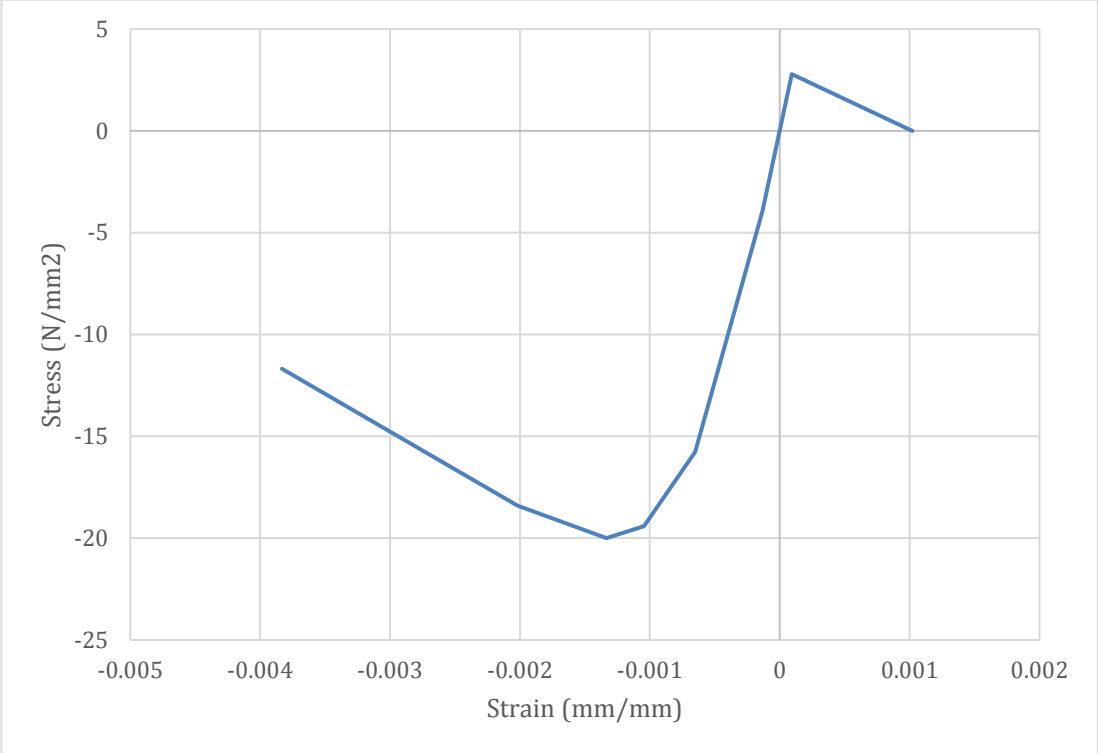

Figure A.1. The stress-strain concert model

A.2 Data for the stress-strain steel rebar model

Table A.2. Data for stress-strain steel rebar model

Strain (mm/mm)	Stress (N/mm^2)
-0.108	-260.6
-0.09	-620.5
-0.0456	-551.6
-0.0189	-482.6
-0.01	-413.7
-0.00207	-413.7
0	0
0.00207	413.7
0.01	413.7
0.0189	482.6
0.0456	551.6
0.09	620.5
0.108	260.6

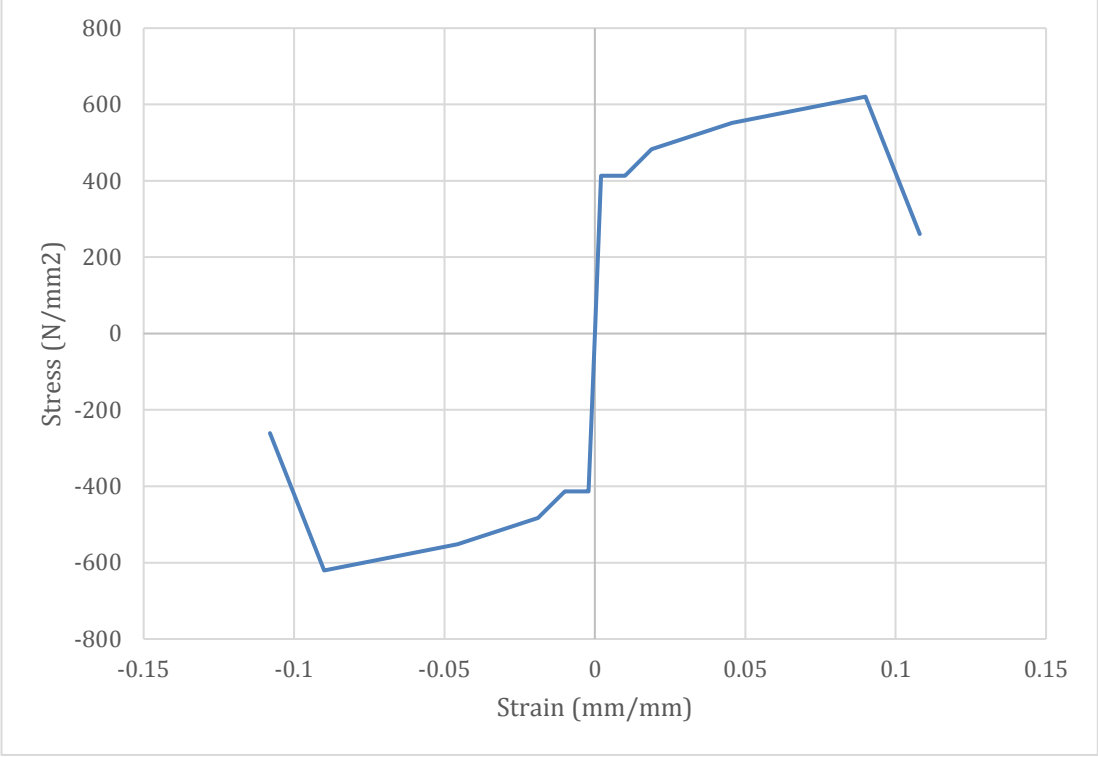

Figure A.2. The rebar stress-strain model

Appendix B

Results of modal analysis

B.1 Modal analysis

Table B.1. Modal analysis results for the M1 group FE models

FE model ID	Convective mode		Fundamental mode		2nd Impulsive mode		Total mass participation ratio (Ri)
	Period (s)	Mass participation ratio (Ri)	Period (s)	Mass participation ratio (Ri)	Period (s)	Mass participation ratio (Ri)	
M1	4.91	0.54	0.42	0.3	0.13	0.1	0.94
M1-50	4.92	0.55	0.48	0.33	0.16	0.03	0.90
M1-100	4.92	0.56	0.49	0.33	0.17	0.03	0.91
M1-200	4.92	0.57	0.51	0.33	0.17	0.02	0.92
M1-300	4.93	0.58	0.52	0.33	0.17	0.02	0.93
M1-500	4.93	0.59	0.55	0.32	0.18	0.02	0.94
M1-1000	4.93	0.61	0.61	0.31	0.19	0.02	0.94
M1-1500	4.94	0.64	0.67	0.28	0.19	0.03	0.95
M1-2000	4.95	0.68	0.78	0.24	0.21	0.04	0.96

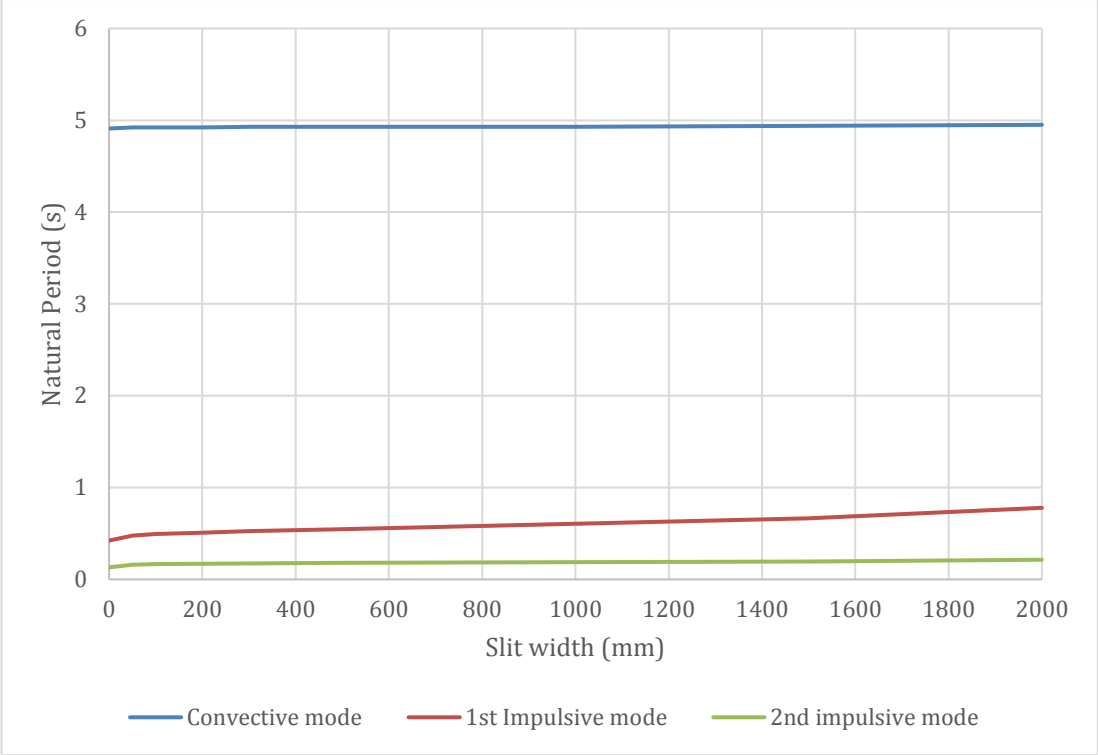

Figure B.1. Modal analysis results of M1 group FE models

B.2 Modal damping energy dissipation

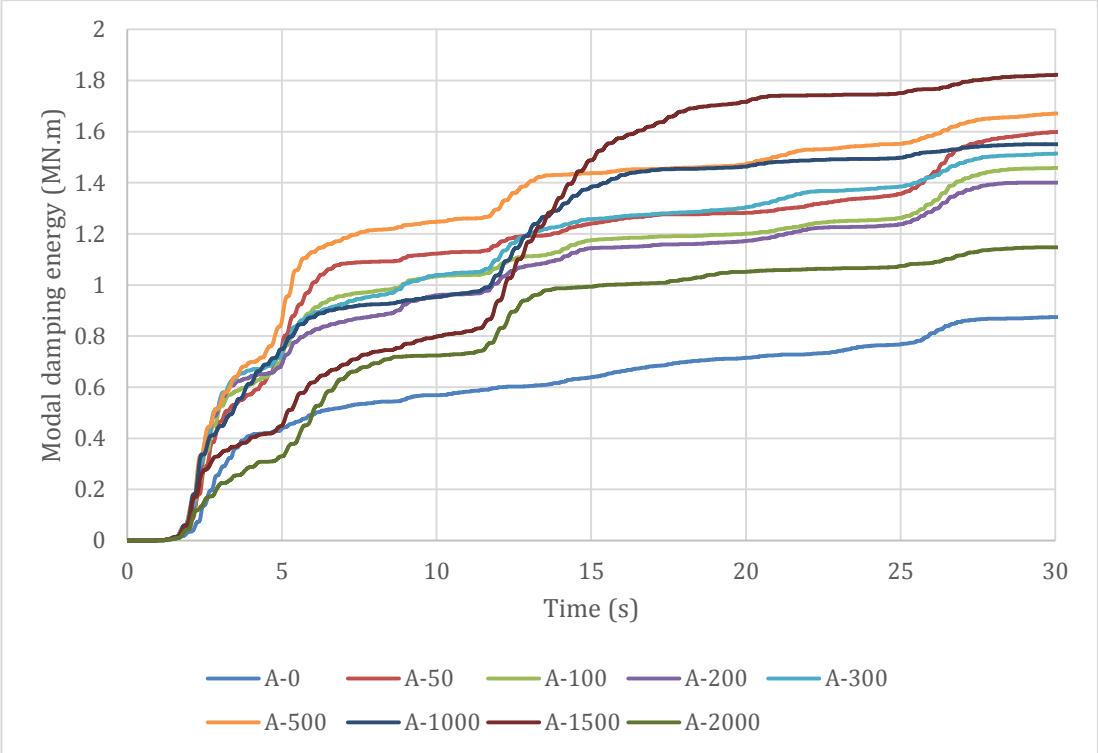

Figure B.2 Hysteretic energy dissipation of M1 group models at El-Centro 1940 earthquake, PGA = 0.4

Appendix C

Results of nonlinear static analysis

C.1 Response spectrums

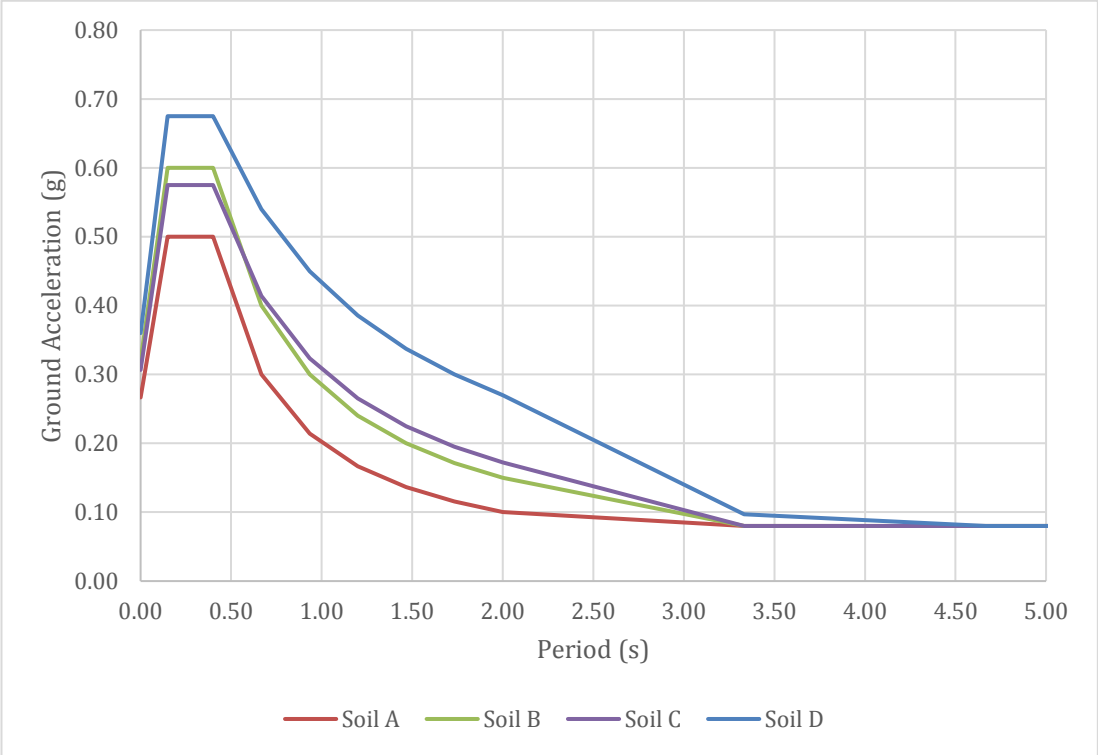

Figure C.1. Type 1 design response spectrums for peak ground acceleration equal to 0.4g for ground types A to D (5% damping) by Eurocode 8

Table C.1. Values for design type 1 design response spectrums for peak ground acceleration equal to 0.4g for ground types A to D (5% damping) by Eurocode 8

Period (s)	Spectral Acceleration (g)			
	Soil A	Soil B	Soil C	Soil D
0.00	0.27	0.32	0.31	0.36
0.05	0.34	0.41	0.40	0.47
0.10	0.42	0.51	0.49	0.57
0.15	0.50	0.60	0.58	0.68
0.40	0.50	0.60	0.58	0.68
0.67	0.30	0.40	0.41	0.54
0.93	0.21	0.30	0.32	0.45
1.20	0.17	0.24	0.27	0.39
1.47	0.14	0.20	0.23	0.34
1.73	0.12	0.17	0.20	0.30
2.00	0.10	0.15	0.17	0.27
3.33	0.08	0.08	0.08	0.10
4.67	0.08	0.08	0.08	0.08
6.00	0.08	0.08	0.08	0.08
7.33	0.08	0.08	0.08	0.08
8.67	0.08	0.08	0.08	0.08
10.00	0.08	0.08	0.08	0.08

C.2 Pushover analysis for full M1 group

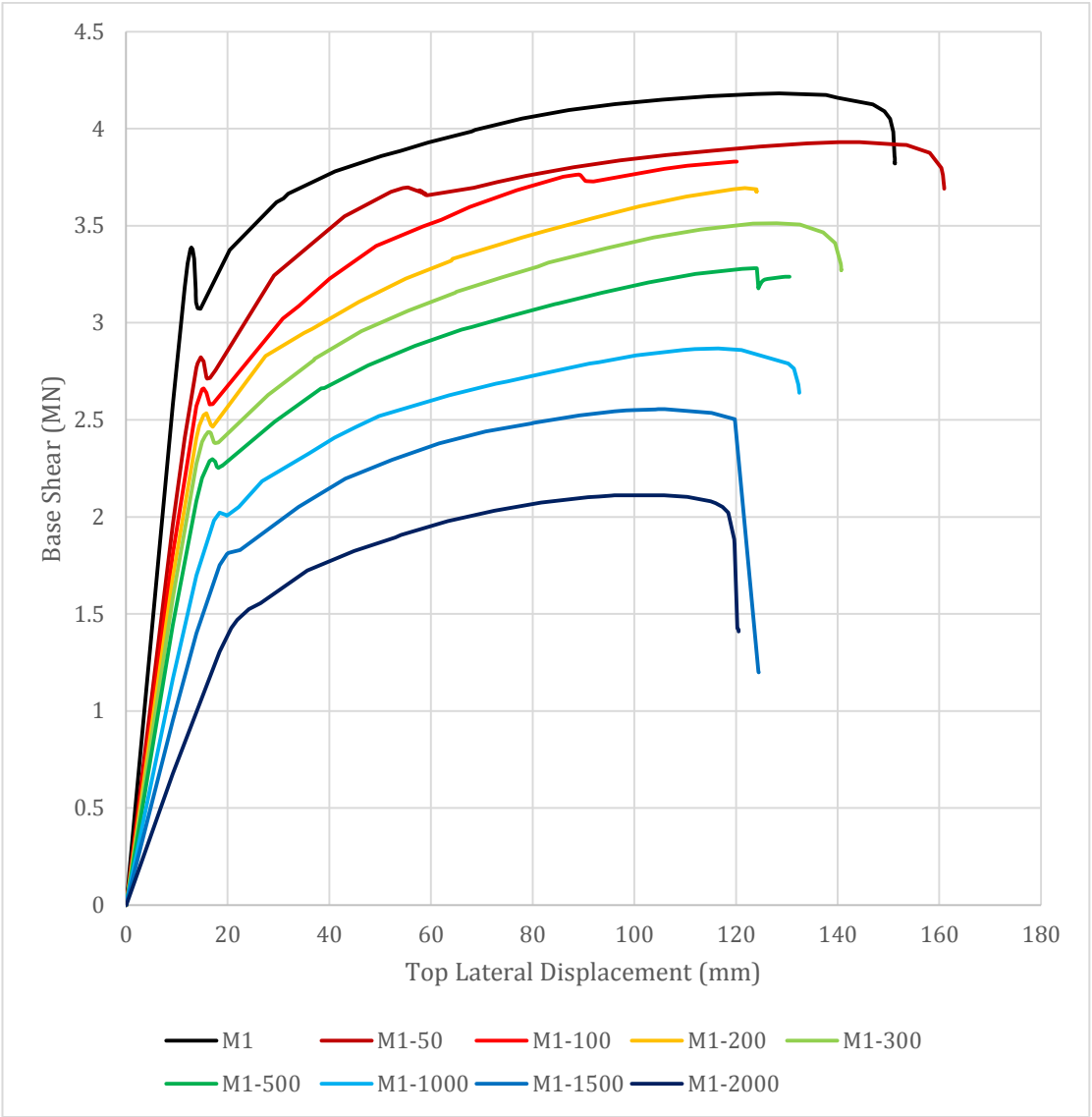

Figure C.2. Results of pushover analysis for full M1 group FE models

Table C.2. (a) Data for pushover curves for full M1 group

Model:	M1		Model:	M1-50		Model:	M1-100
Displacement	Base Shear		Displacement	Base Shear		Displacement	Base Shear
4.20E-02	0		4.20E-02	0		0.041729	0
9.242	2.577655		9.242	1.9607429		9.241729	1.810049
11.542	3.184469		11.542	2.4083724		13.84173	2.570672
12.117	3.305717		13.842	2.7681132		14.99173	2.657274
12.692	3.379177		14.129	2.7920005		15.27923	2.661664
12.835	3.387165		14.704	2.8216866		15.85423	2.638975
13.123	3.377473		15.279	2.8005293		16.42923	2.581306
13.41	3.329593		15.854	2.71872		16.46517	2.579126
13.698	3.165385		15.926	2.7123597		17.04017	2.580633
13.716	3.143222		16.501	2.7150456		30.84017	3.021477
13.788	3.103585		17.651	2.7556012		34	3.086097
14.075	3.075194		29.151	3.242851		40.04017	3.227244
14.65	3.071269		42.951	3.5490208		49.24017	3.395417
20.4	3.374749		52.151	3.6752013		58.44017	3.496926
29.6	3.621258		54.451	3.6943689		62	3.53068
31	3.641		55.457	3.697458		67.64017	3.597288
31.9	3.665656		59	3.662587		76	3.674
41.1	3.779133		57.757	3.6830162		76.84017	3.682822
50.3	3.859293		58.943	3.6588919		86.04017	3.752842
54	3.885		59.231	3.6569929		88.48392	3.762661
59.5	3.929697		68.431	3.6963002		89.09485	3.763326
68	3.986		73	3.724932		89.41829	3.761103
68.7	3.993714		78.781	3.757778		90.35267	3.732027
77.9	4.051992		87.981	3.801351		90.60423	3.730341
87.1	4.095637		97.181	3.8370679		91.75423	3.727501
96.3	4.126018		106.381	3.863561		91.8261	3.72745
105.5	4.149991		115.581	3.8876282		92.04173	3.727952
114.7	4.167374		124.781	3.9078939		105.8417	3.792786
123.9	4.178471		133.981	3.9235357		110.4417	3.809512
128.5	4.182242		140.306	3.9304896		119.6417	3.830136
137.7	4.173123		142.031	3.9312849		120.073	3.830836
140	4.159		144.331	3.9313116		120.1449	3.830627
146.9	4.125047		152	3.917252		120.1493	3.830633
149.2	4.090186		153.531	3.9152334			
150.35	4.049813		158.131	3.8761582			
150.925	3.983688		160.431	3.7973631			
151.213	3.857487		160.718	3.7604045			
151.222	3.848098		160.862	3.7262314			
151.226	3.823297		160.934	3.6967167			
151.226	3.823108		160.941	3.6904316			
151.226	3.823139						
151.231	3.82468						
151.236	3.822516						
151.238	3.820405						

Table C.2. (b) Data for pushover curves for full M1 group.

Model:	M1-200		Model:	M1-300		Model:	M1-500
Displacement	Base Shear		Displacement	Base Shear		Displacement	Base Shear
4.20E-02	0		4.20E-02	0		0.042	0
9.242	1.687494		9.242	1.5818424		9.242	1.4433153
13.842	2.408365		13.842	2.2727404		13.842	2.0821893
14.417	2.469218		14.992	2.3871506		14.992	2.200475
15.279	2.524552		15.567	2.4172581		16.429	2.287468
15.854	2.534279		16.142	2.4360418		17.004	2.2977461
16.717	2.474183		16.429	2.436334		17.579	2.2850301
17.076	2.464513		16.717	2.4321554		17.867	2.2591765
27.426	2.828318		17.292	2.3830108		18.154	2.2518004
35	2.947		17.579	2.3799349		18.729	2.2619905
36.626	2.967584		18.154	2.3830878		18.873	2.2625382
45.826	3.107731		27.929	2.6283551		29.223	2.4907474
55.026	3.227534		37	2.808		38.423	2.6625749
64	3.32		37.129	2.8142809		39	2.664
64.226	3.32887		46.329	2.9566383		47.623	2.7802572
73.426	3.403074		55.529	3.0620979		56.823	2.881511
78	3.44		64.729	3.1540432		66.023	2.9654307
82.626	3.473559		65	3.159		68	2.978
91.826	3.538376		73.929	3.233129		75.223	3.0318055
101.026	3.599569		81	3.289		84.423	3.0963773
110.226	3.650764		83.129	3.3093081		85	3.1
119.426	3.687933		94.629	3.3853112		93.623	3.1546288
121.726	3.694055		103.829	3.4398583		102.823	3.20766
124.026	3.688207		113.029	3.4797581		112.023	3.252456
124.031	3.676951		122.229	3.5078072		121.223	3.2784466
124.033	3.677169		123.379	3.5101694		123.523	3.2802692
124.034	3.677166		127.979	3.5125669		123.81	3.2803976
124.036	3.677201		132.579	3.5065781		123.819	3.2803892
124.037	3.67721		137.179	3.4663063		124.107	3.2802126
124.038	3.676981		139.479	3.4097389		124.111	3.2801759
124.038	3.676935		140.629	3.3036385		124.111	3.2801759
124.038	3.676891		140.701	3.2888629		124.399	3.1777479
124.038	3.676855		140.704	3.2719123		124.471	3.1843462
124.038	3.676801		140.704	3.2718317		125.046	3.209545
124.038	3.676785		140.709	3.2726603		125.333	3.2174174
124.038	3.676766		140.71	3.2726166		125.621	3.2222892
124.038	3.676768		140.711	3.2724091		126.196	3.2261309
			140.712	3.2720031		129.071	3.2353601
			140.713	3.2716696		129.646	3.2364102
			140.713	3.2715843		130.508	3.2372335
			140.713	3.2715844			

Table C.2. (c) Data for pushover curves for M1 group

	M1-1000			A-1500			M1-2000
Displacement	Base Shear		Displacement	Base Shear		Displacement	Base Shear
0.00E+00	0		0.00E+00	0		4.20E-02	0
9.242	1.164375		9.242	0.950992		9.242	0.677541
13.842	1.697896		13.842	1.400608		18.442	1.306579
17.292	1.981404		18.442	1.75113		20.742	1.426797
18.442	2.021948		19.879	1.808748		21.892	1.46938
19.592	2.010506		20.167	1.813926		24.192	1.524036
19.879	2.006178		22.467	1.829261		26.492	1.55521
22.179	2.050577		33.967	2.051637		35.692	1.724543
26.779	2.183923		43.167	2.196336		44.892	1.823711
35.979	2.325965		45	2.216831		53	1.894
41	2.408		52.367	2.293573		54.092	1.907083
45.179	2.463478		61.567	2.37868		63.292	1.977948
49.779	2.519693		70.767	2.439233		72.492	2.032099
63.579	2.625662		79.967	2.482703		81.692	2.074551
72.779	2.685836		80	2.48416		90.892	2.100897
75	2.6977		89.167	2.522645		93	2.104
81.979	2.738441		96.067	2.544198		95.492	2.110194
91.179	2.790477		98.367	2.548671		96.067	2.110949
93	2.797097		100	2.550027		96.642	2.111195
100.379	2.831434		104.117	2.554114		105.842	2.111666
109.579	2.85896		104.692	2.554454		110.442	2.103171
111.879	2.863831		105.123	2.554605		115.042	2.080652
116.479	2.86696		105.41	2.554634		116	2.07
121.079	2.859071		105.985	2.554667		117.342	2.051427
130.279	2.789442		115.185	2.536009		118.492	2.021377
131.429	2.763564		119.785	2.503282		119.642	1.88383
132.292	2.681083		124.385	1.202022		119.721	1.859386
132.435	2.642453		124.457	1.19996		119.723	1.859311
132.44	2.640376		124.471	1.19893		120.298	1.425199
132.44	2.640363		124.472	1.199077		120.495	1.418728
132.441	2.640291		124.472	1.198509		120.504	1.417904
132.441	2.639821		124.474	1.19873		120.507	1.41096
132.441	2.639627		124.475	1.198747		120.507	1.410172
132.441	2.639627		124.475	1.198729		120.507	1.409404
132.441	2.639632		124.476	1.198739		120.507	1.409407
132.441	2.639632		124.476	1.198688		120.509	1.409586
132.441	2.639632		124.476	1.198636			
132.441	2.639632		124.476	1.19859			
132.442	2.639575		124.477	1.198521			
132.443	2.639252		124.477	1.198401			
			124.477	1.198359			

C.3 Capacity spectrum analysis of full M1 group

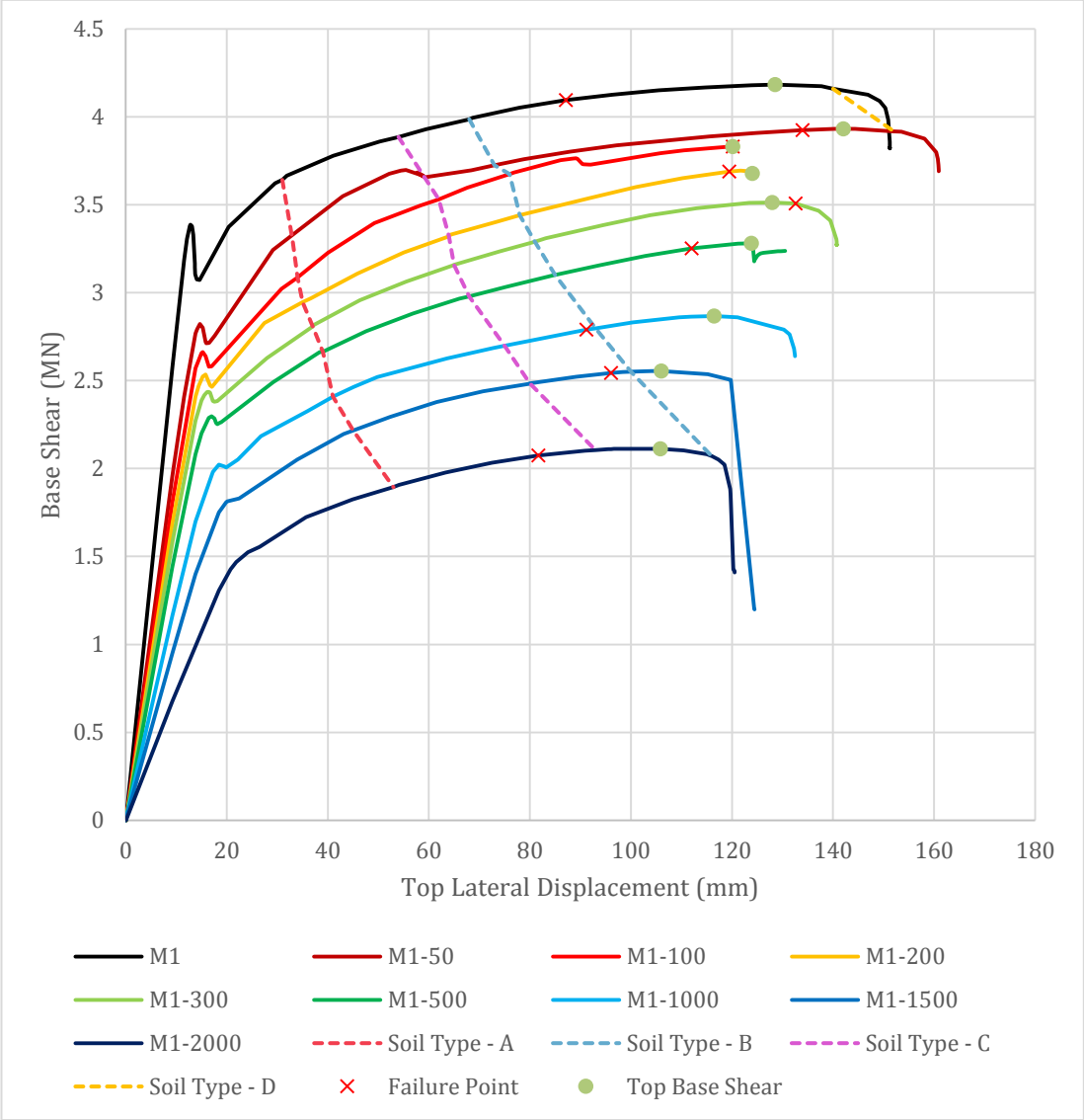

Figure C.3. Capability of A group models to withstand earthquake 0.4g with respect to soil types

Table C.3. Results of pushover analysis for full M1 group

FE model ID	Maximum Base Shear		Maximum Top Lateral Displacement	
	$V_{max}\ (MN)$	$\Delta_{V_{max}}\ (mm)$	$\Delta_{max}\ (mm)$	$V_{\Delta_{max}}\ (mm)$
M1-Solid	4.18	129	151	3.82
M1-50	3.93	142	161	3.69
M1-100	3.83	120	120	3.83
M1-200	3.68	124	124	3.68
M1-300	3.51	128	141	3.27
M1-500	3.28	124	131	3.24
M1-1000	2.87	116	132	2.64
M1-1500	2.55	106	124	1.20
M1-2000	2.11	106	121	1.41

Table C.4. Base shear at performance point of EC-8 0.5% damped response spectra of PGA = 0.4g for full M1 group

FE model ID	Base Shear (MN)			
	$Soil\ Type\ A$	$Soil\ Type\ B$	$Soil\ Type\ C$	$Soil\ Type\ D$
M1-Solid	3.64	3.89	3.99	3.99
M1-50	3.30	3.66	3.72	3.72
M1-100	3.09	3.53	3.67	N/A
M1-200	2.95	3.32	3.44	N/A
M1-300	2.81	3.16	3.29	N/A
M1-500	2.66	2.98	3.10	N/A
M1-1000	2.41	2.70	2.80	N/A
M1-1500	2.22	2.48	2.55	N/A
M1-2000	1.89	2.10	2.07	N/A

.

Model M1 – Soil Type A

Model M1 – Soil Type B

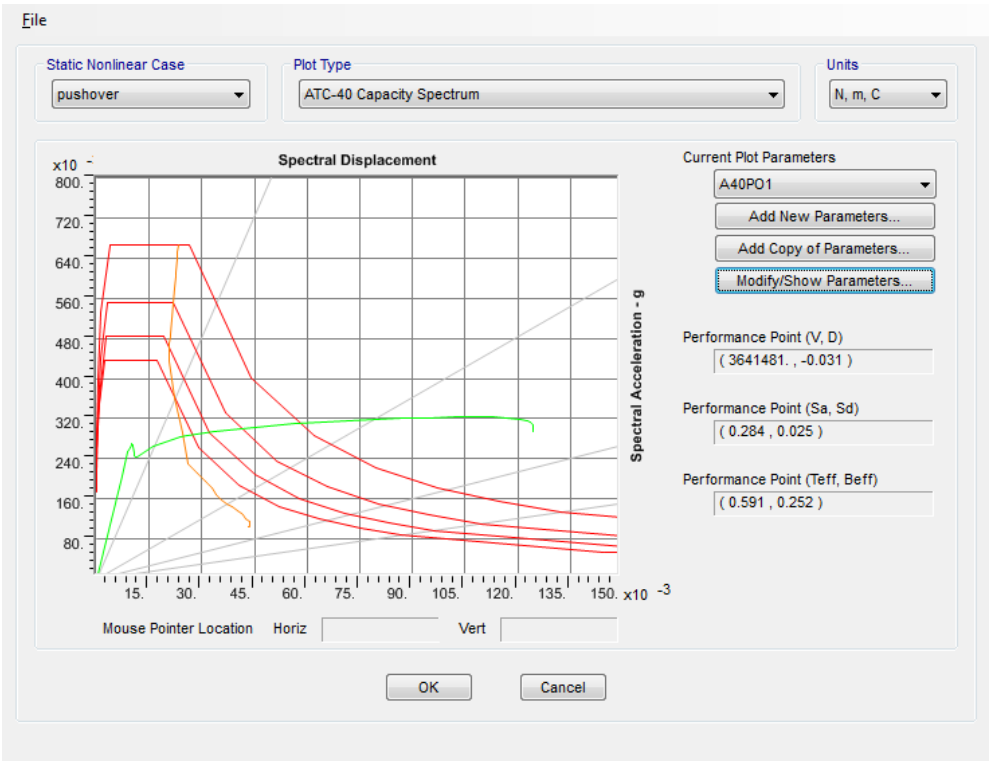

Figure C.4. (a) Performance point evaluation by capacity spectrum analysis for full M1 group.

Model M1 – Soil Type C

Model M1 – Soil Type D

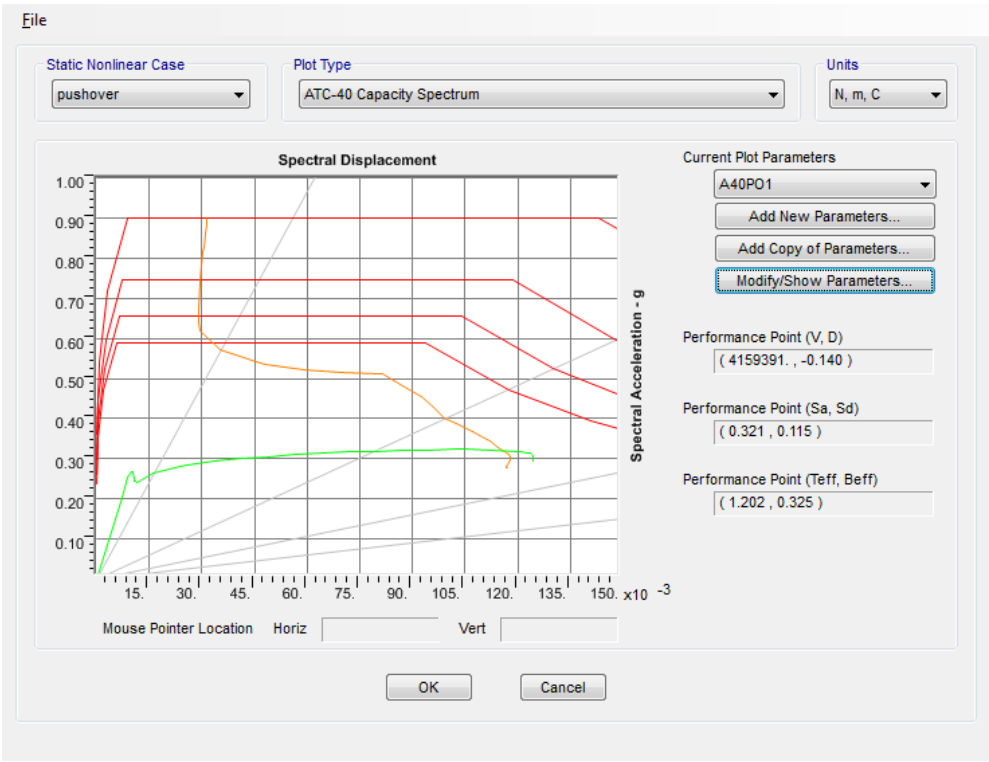

Figure C.4. (b) Performance point evaluation by capacity spectrum analysis of M1 group models.

Model M1-50 – Soil Type A

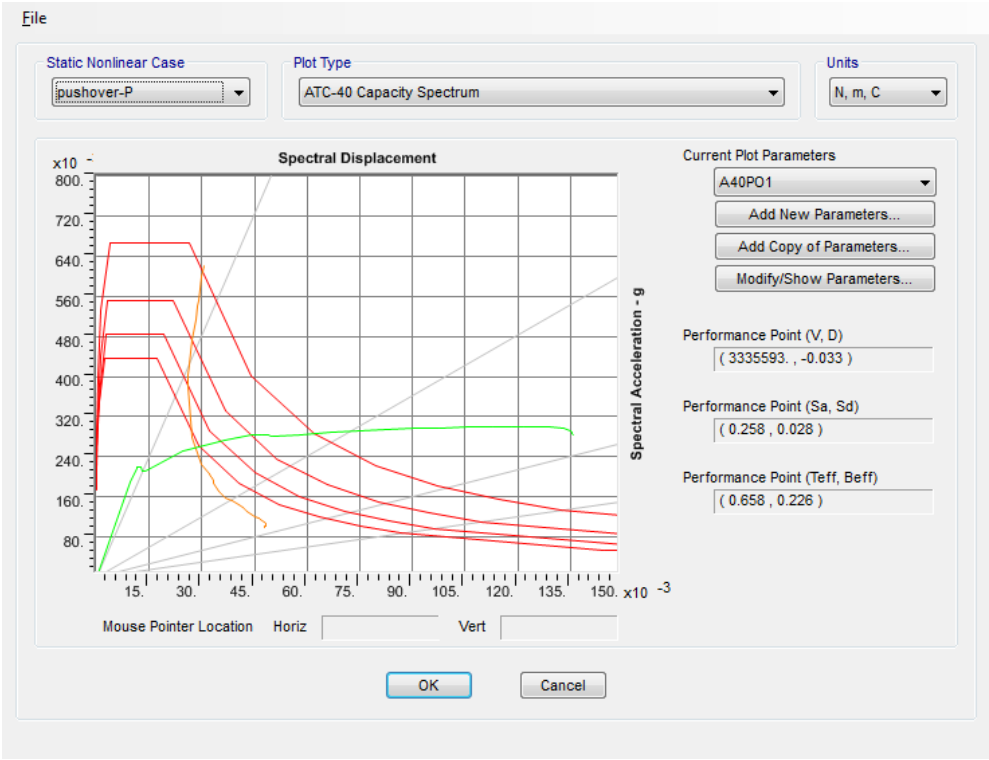

Model M1-50 – Soil Type B

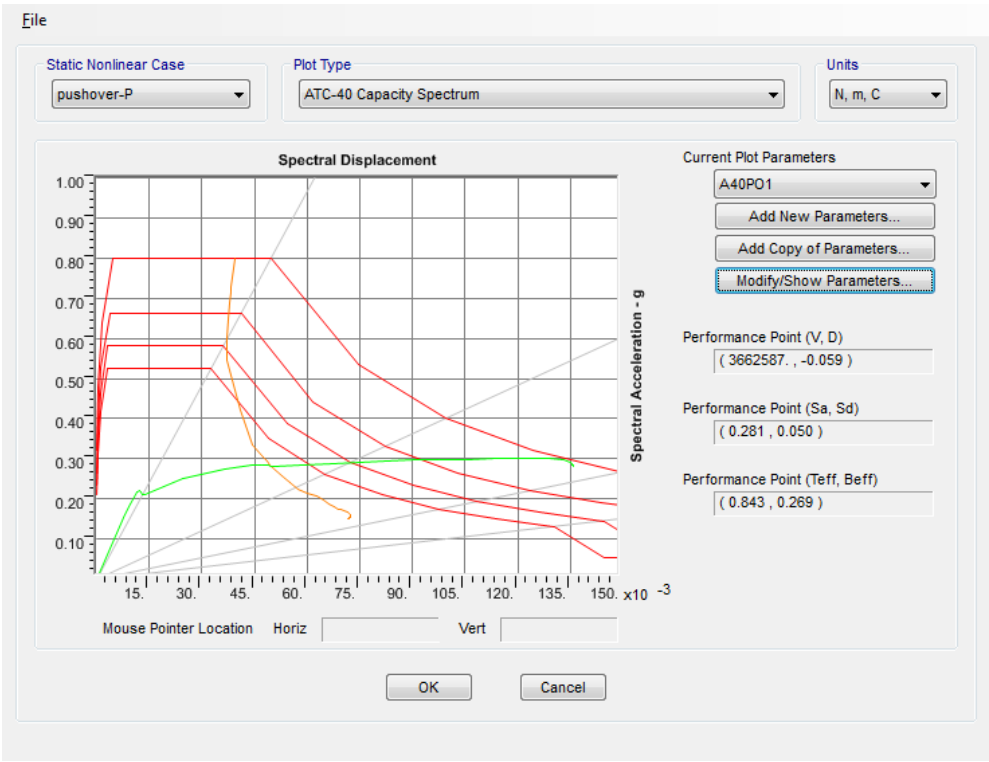

Figure C.4. (c) Performance point evaluation by capacity spectrum analysis of M1 group models.

Model M1-50 – Soil Type C

Model M1-50 – Soil Type D

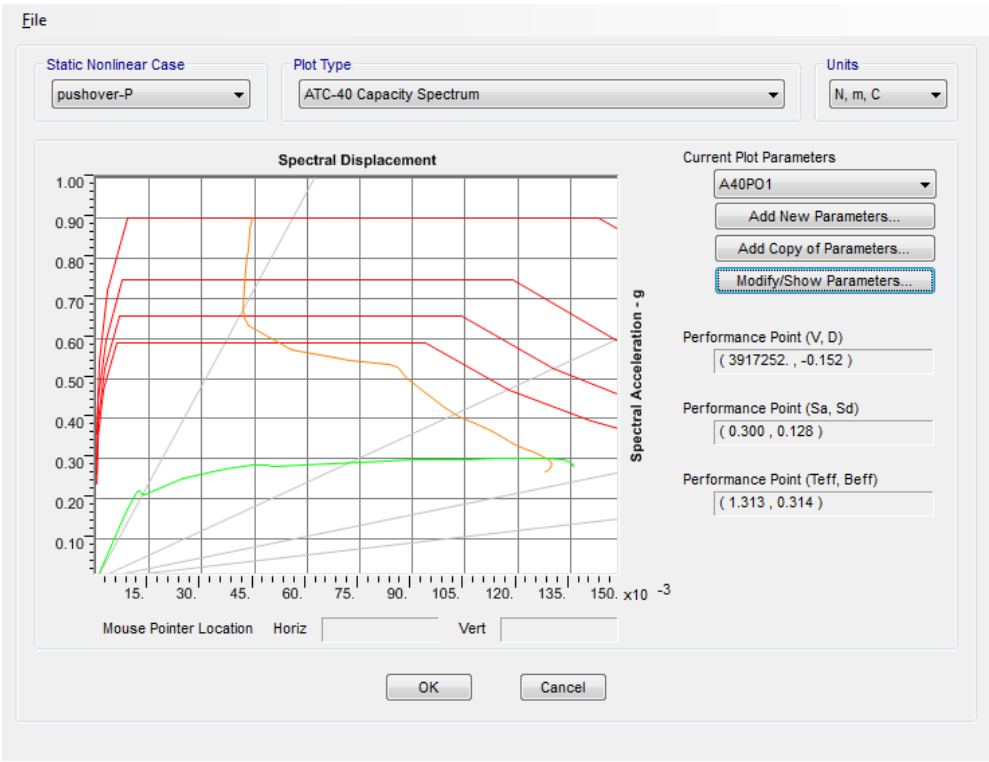

Figure C.4. (d) Performance point evaluation by capacity spectrum analysis of M1 group models.

Model M1-100 – Soil Type A

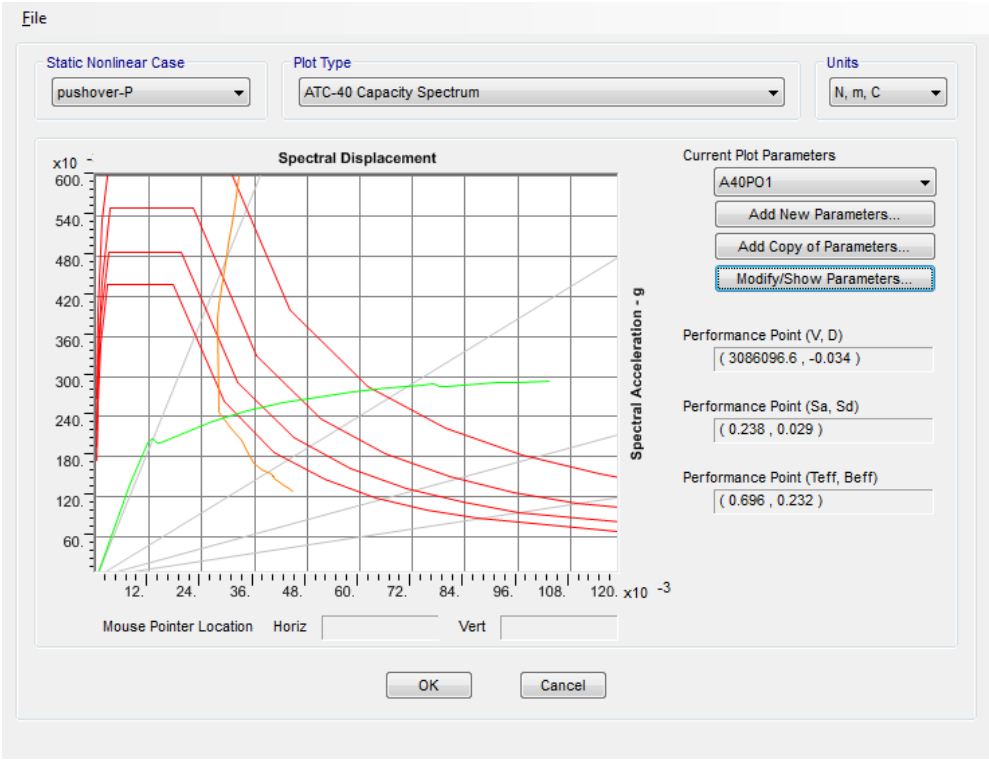

Model M1-100 – Soil Type B

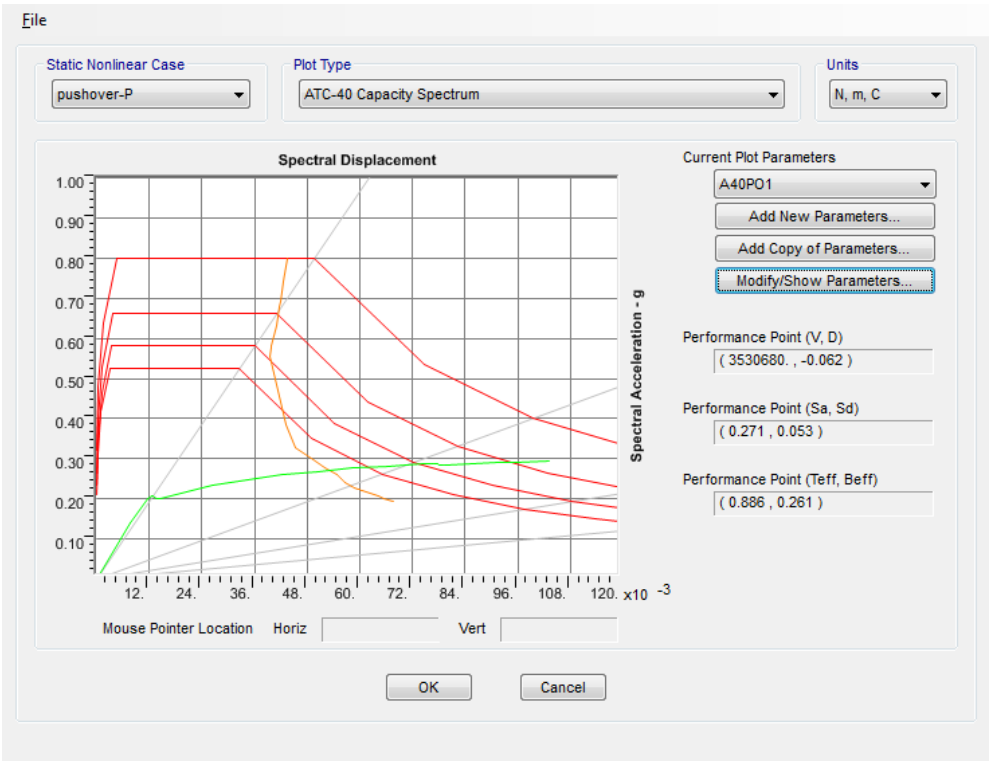

Figure C.4. (e) Performance point evaluation by capacity spectrum analysis of M1 group models.

Model M1-100 – Soil Type C

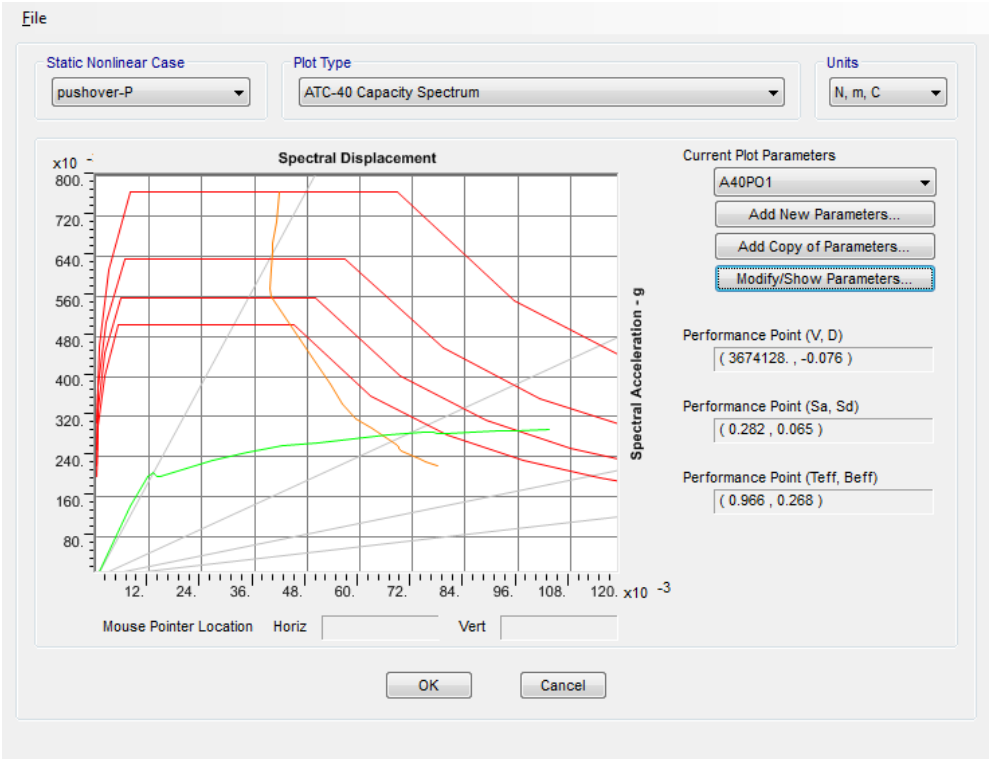

Model M1-100 – Soil Type D

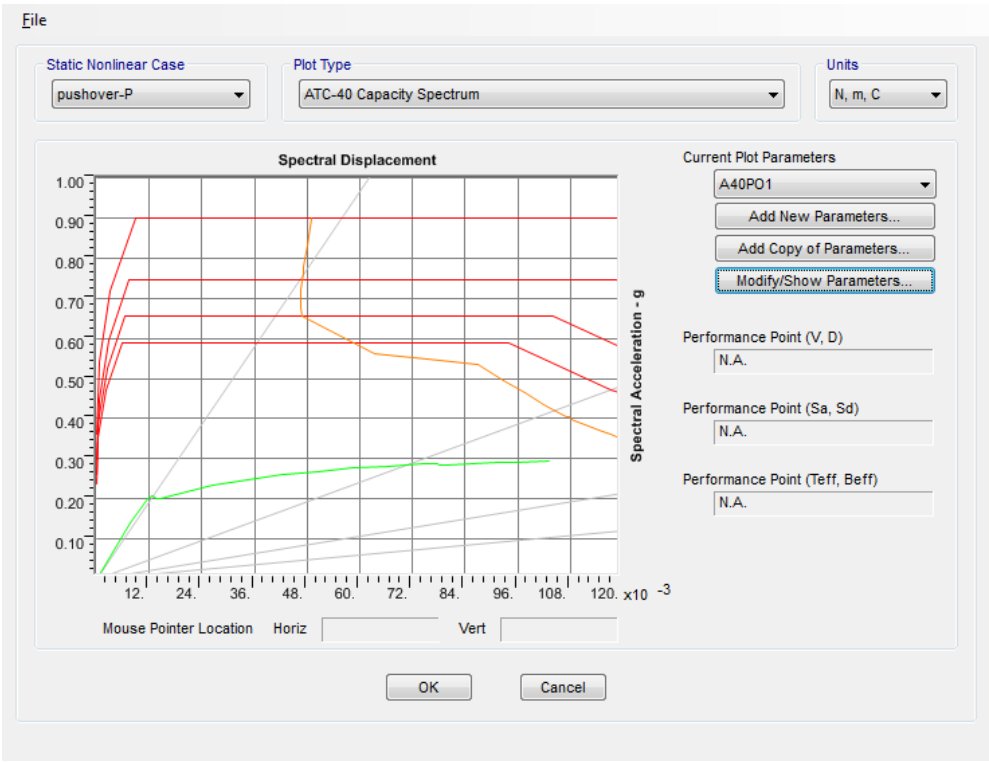

Figure C.4. (f) Performance point evaluation by capacity spectrum analysis of M1 group models.

Model M1-200 – Soil Type A

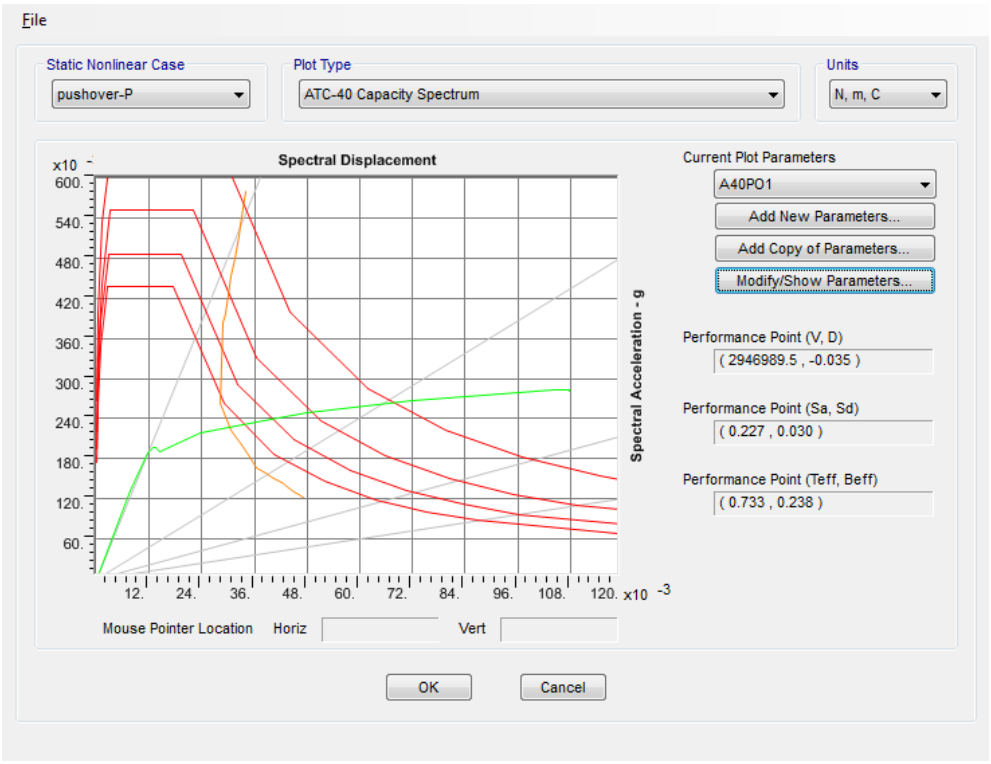

Model M1-200 – Soil Type B

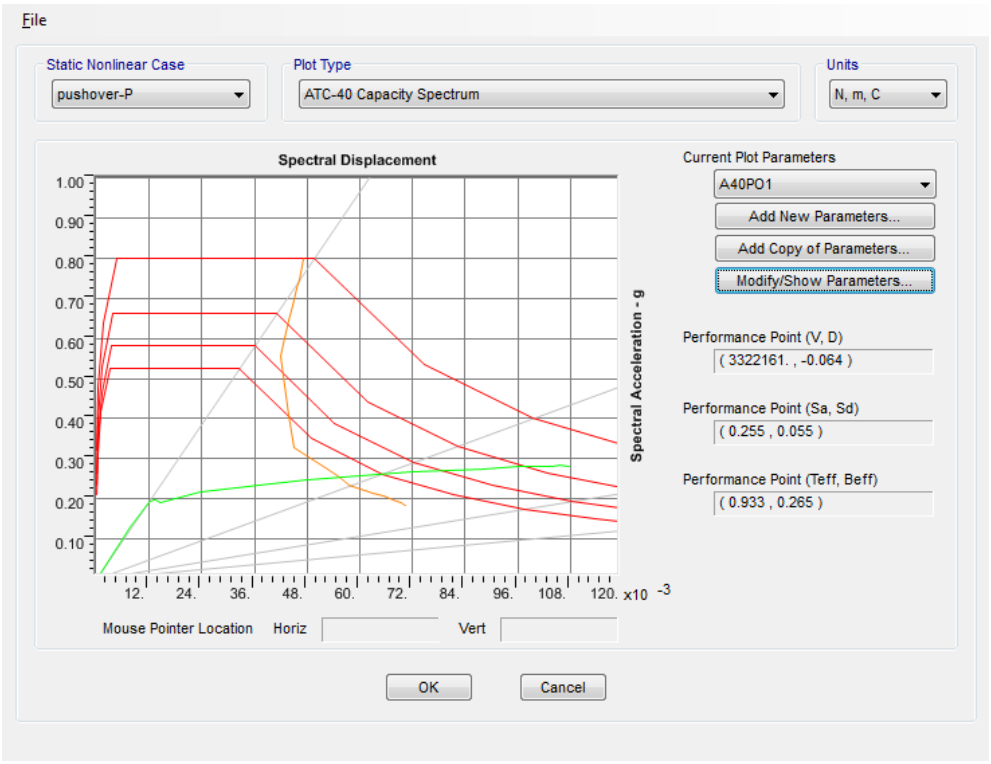

Figure C.4. (g) Performance point evaluation by capacity spectrum analysis of M1 group models.

Model M1-200 – Soil Type C

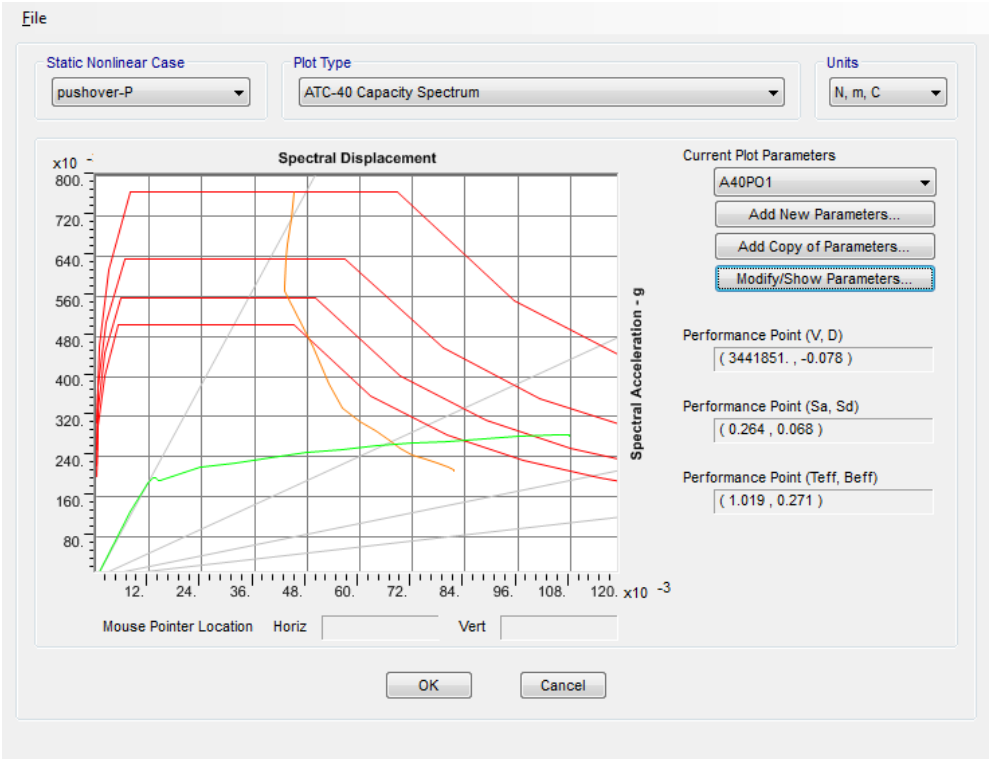

Model M1-200 – Soil Type D

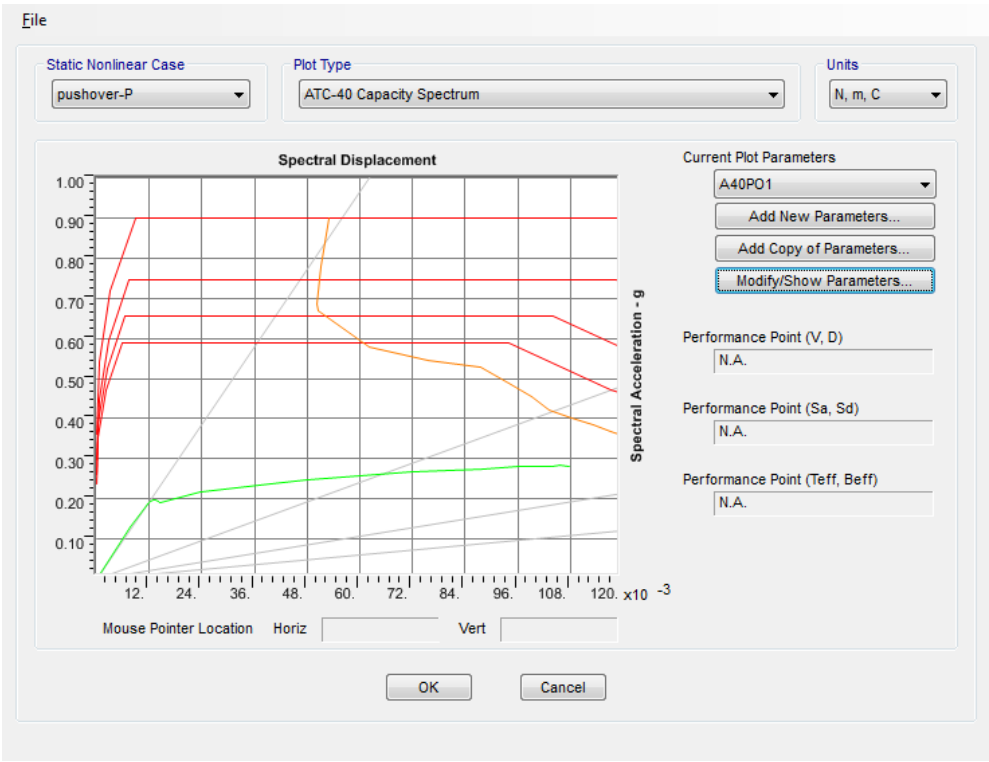

Figure C.4. (h) Performance point evaluation by capacity spectrum analysis of M1 group models.

Model M1-300 – Soil Type A

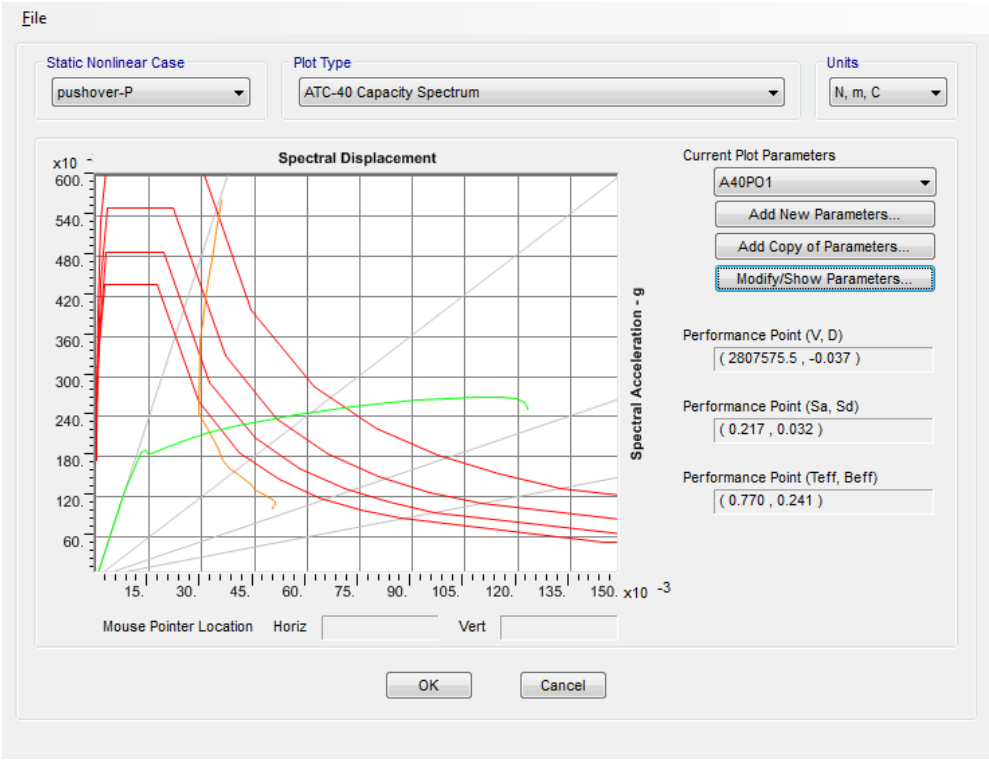

Model M1-300 – Soil Type B

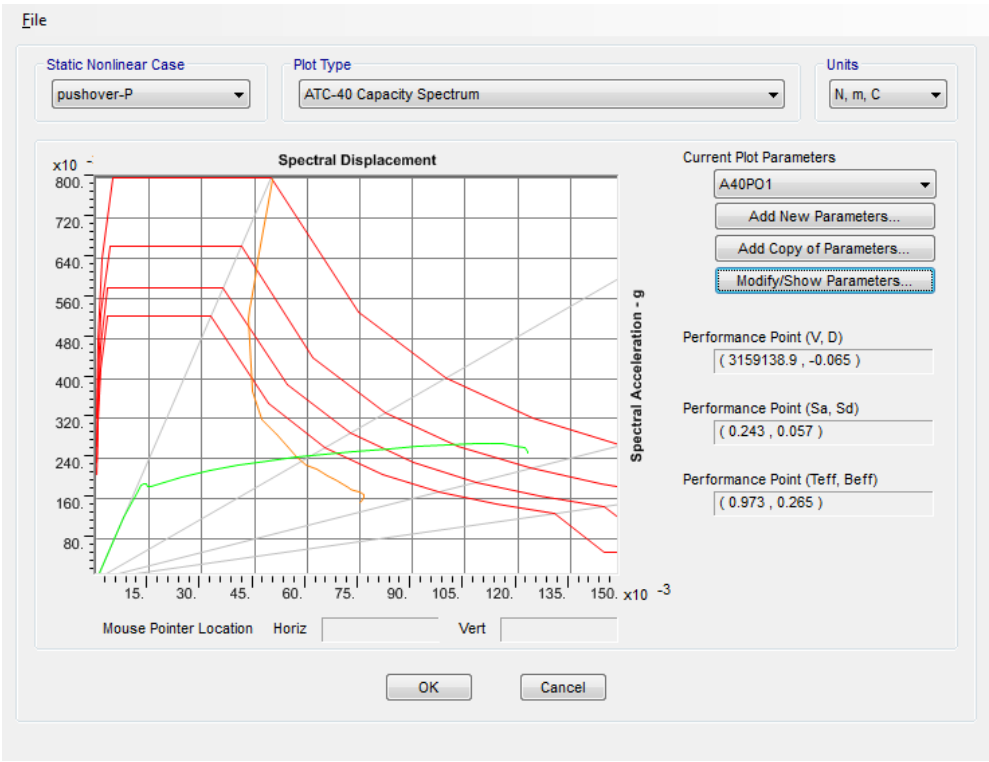

Figure C.4. (i) Performance point evaluation by capacity spectrum analysis of M1 group models.

Model M1-300 – Soil Type C

Model M1-300 – Soil Type D

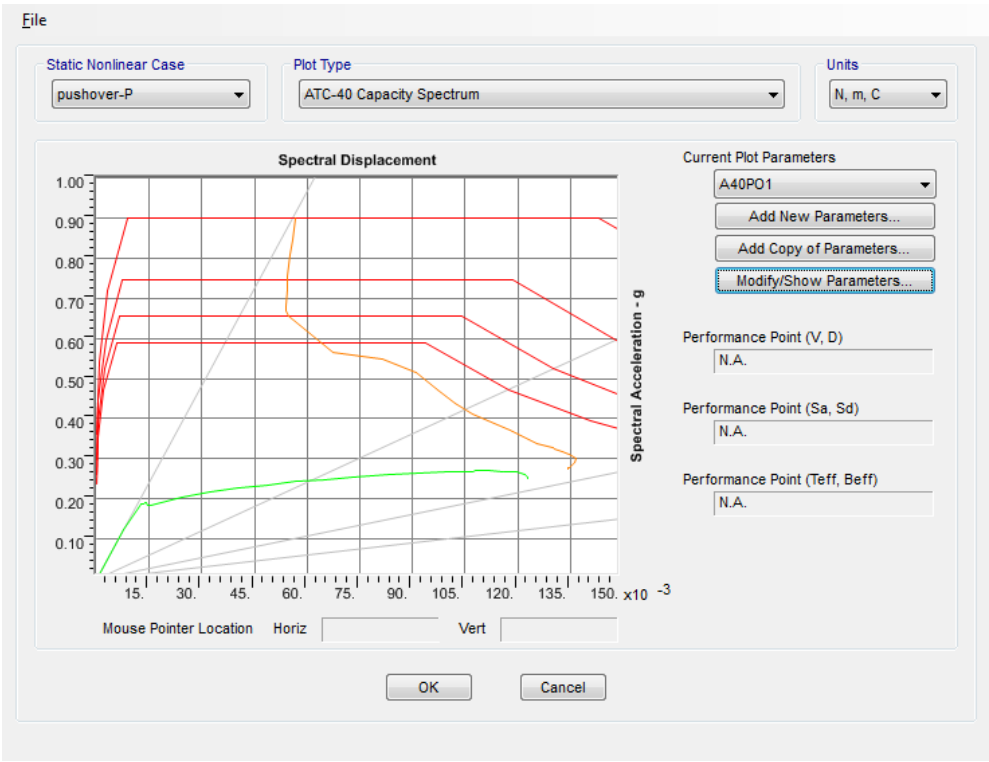

Figure C.4. (j) Performance point evaluation by capacity spectrum analysis of M1 group models.

Model M1-500 – Soil Type A

Model M1-500 – Soil Type B

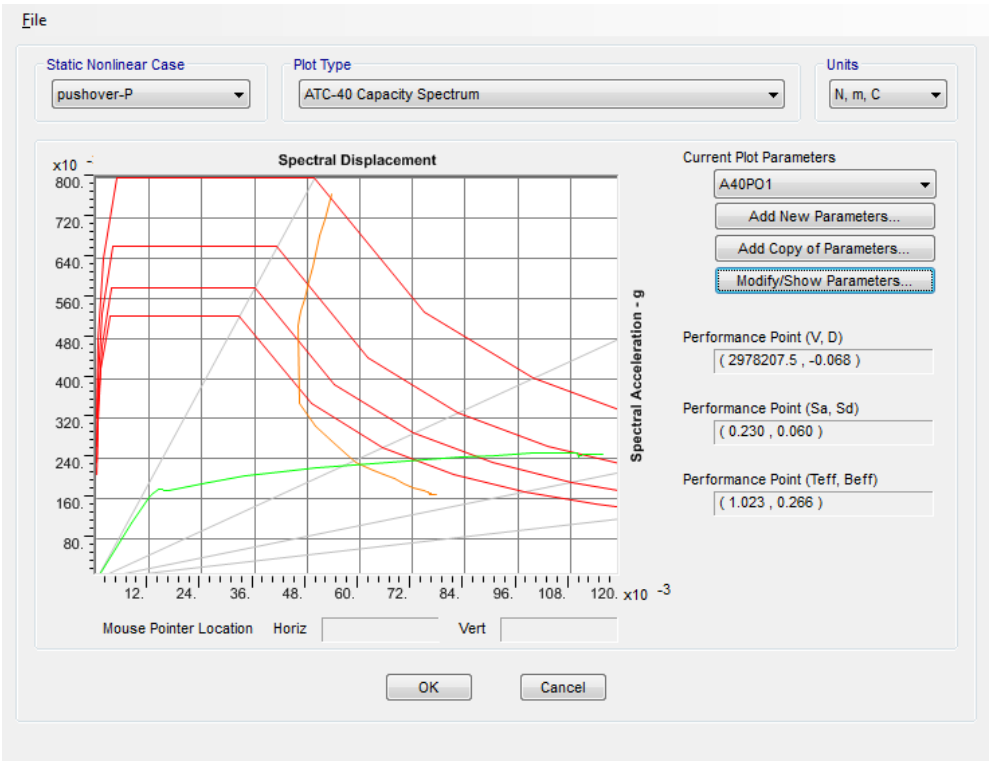

Figure C.4. (k) Performance point evaluation by capacity spectrum analysis of M1 group models.

Model M1-500 – Soil Type C

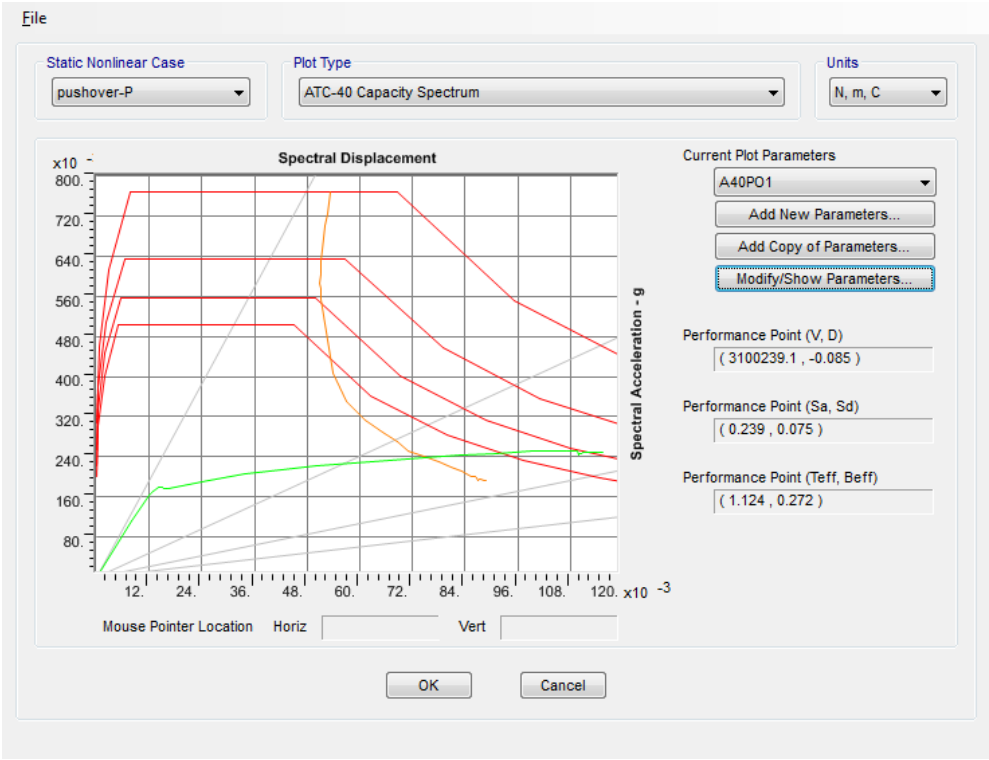

Model M1-500 – Soil Type D

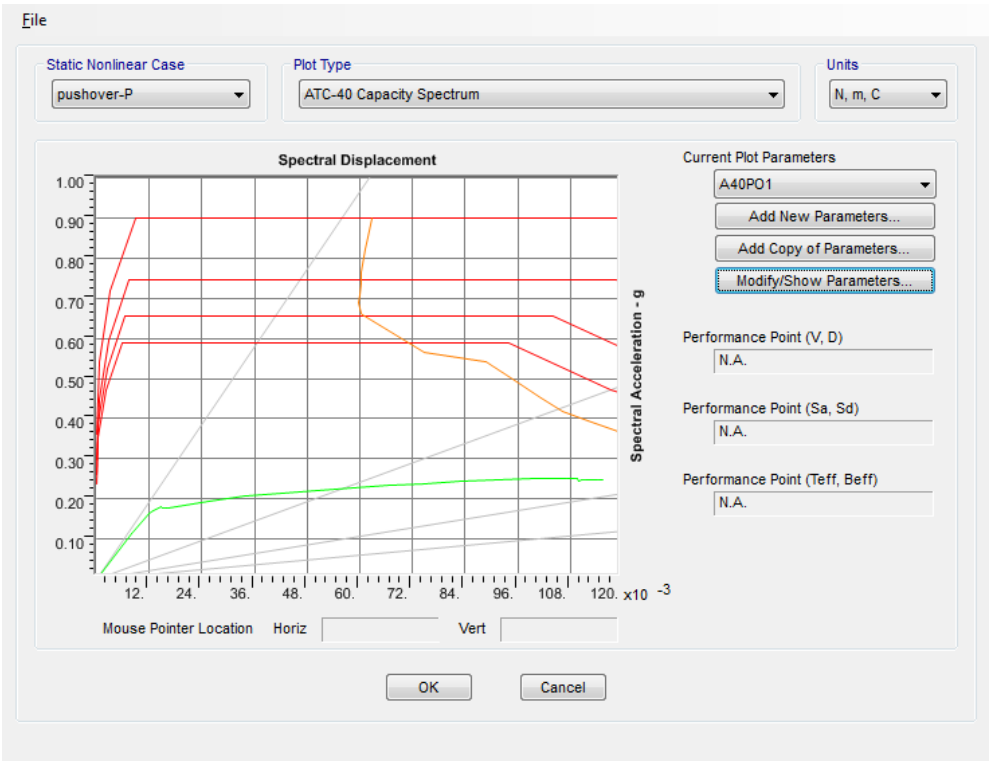

Figure C.4. (l) Performance point evaluation by capacity spectrum analysis of M1 group models.

Model M1-1000 – Soil Type A

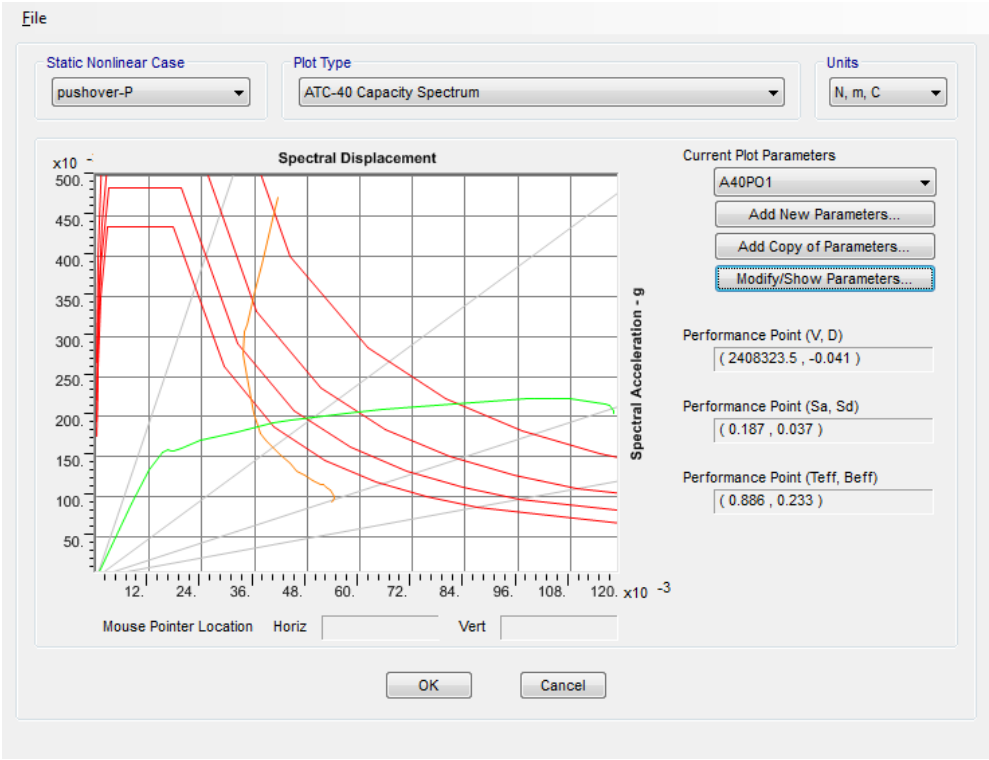

Model M1-1000 – Soil Type B

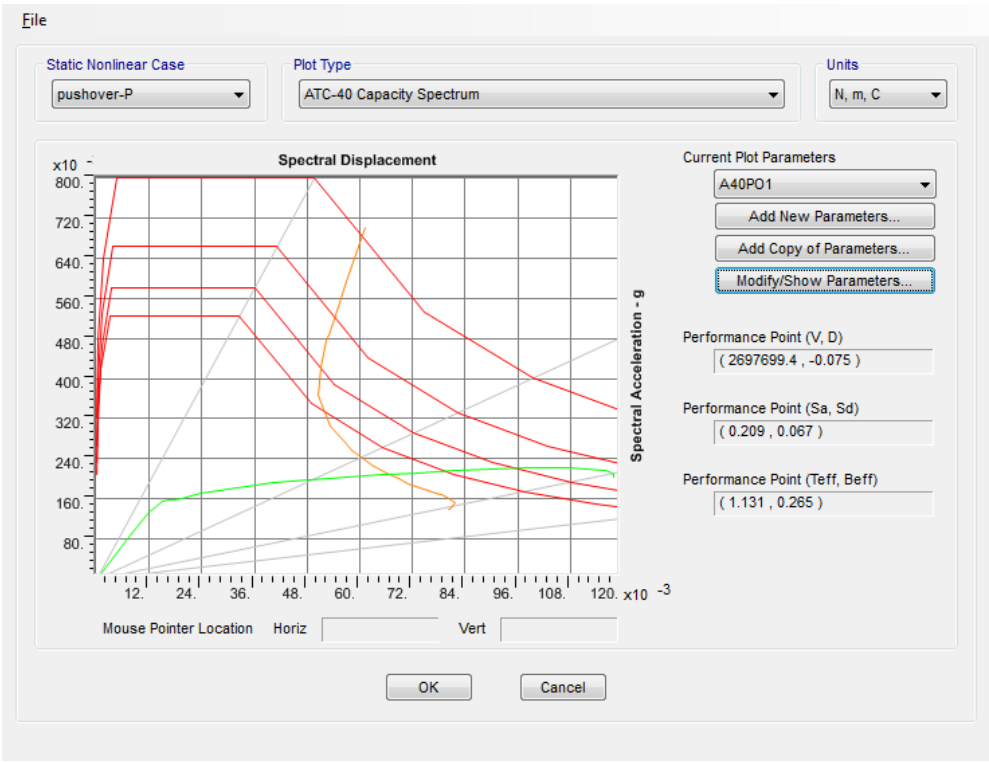

Figure C.4. (m) Performance point evaluation by capacity spectrum analysis of M1 group models.

Model M1-1000 – Soil Type C

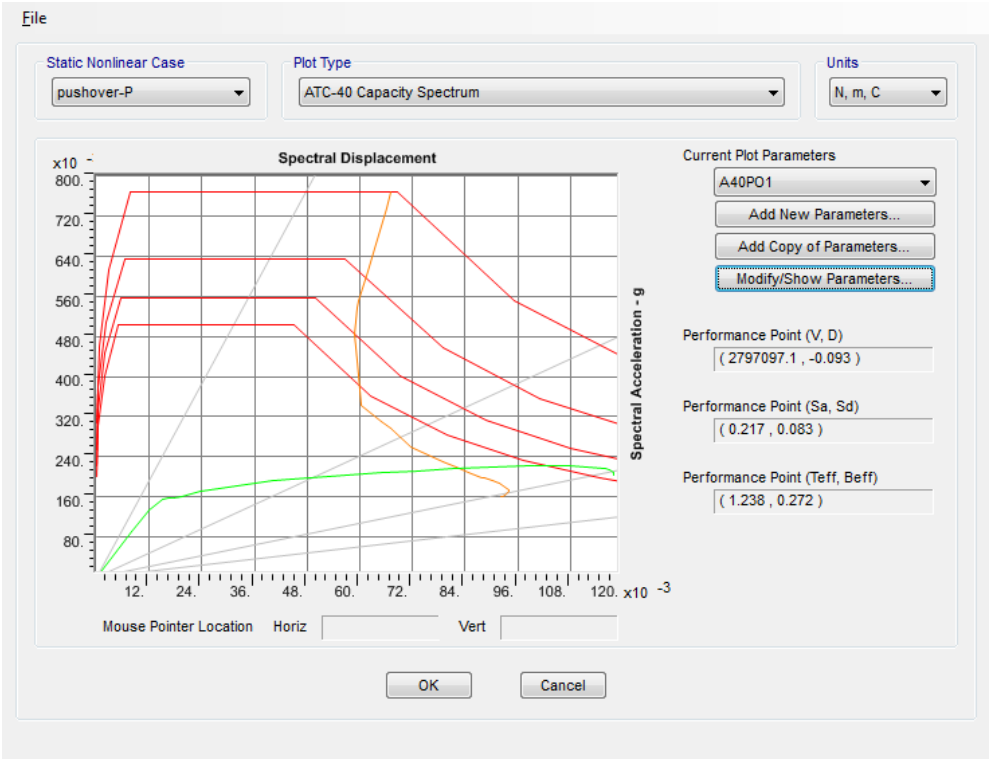

Model M1-1000 – Soil Type D

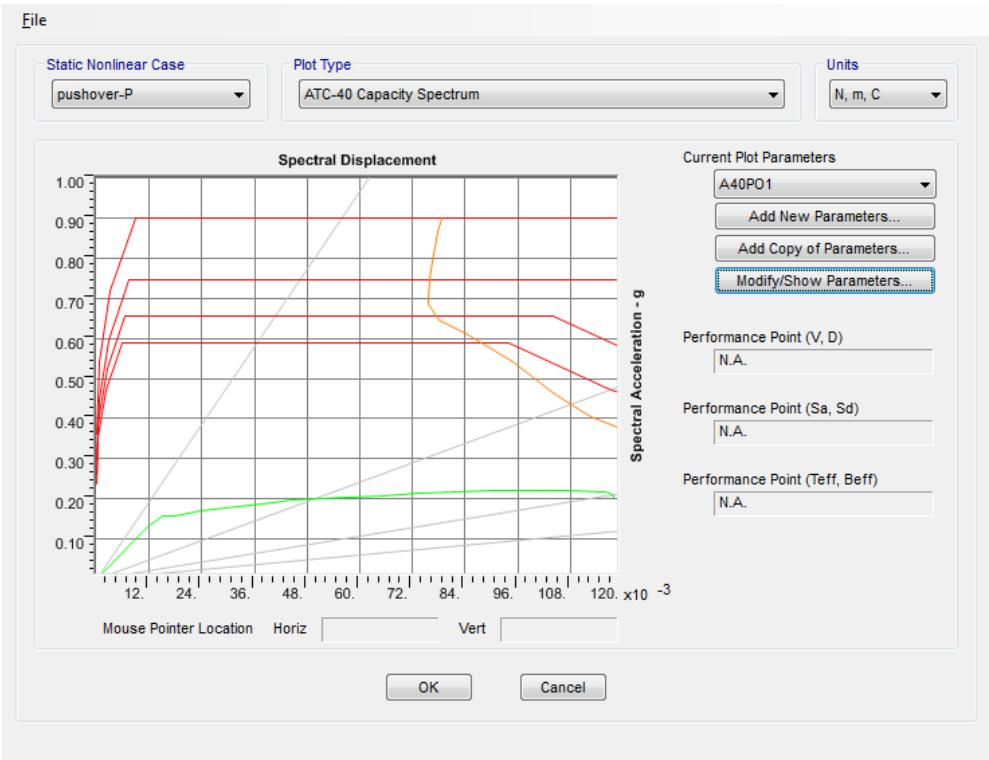

Figure C.4. (n) Performance point evaluation by capacity spectrum analysis of M1 group models.

Model M1-1500 – Soil Type A

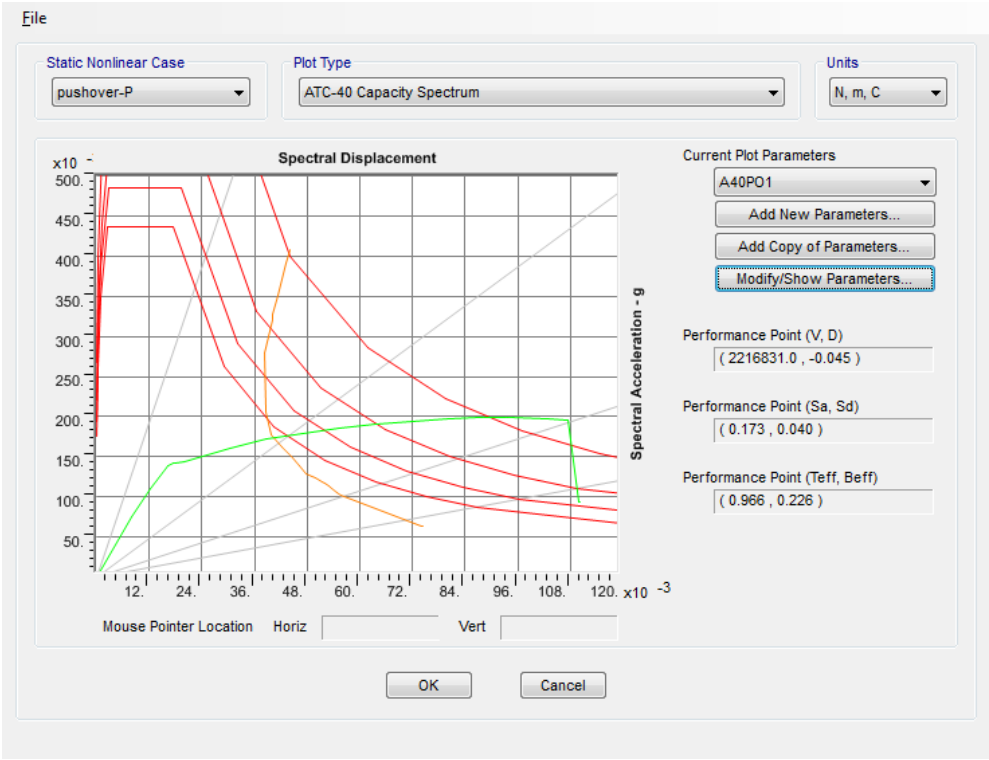

Model M1-1500 – Soil Type B

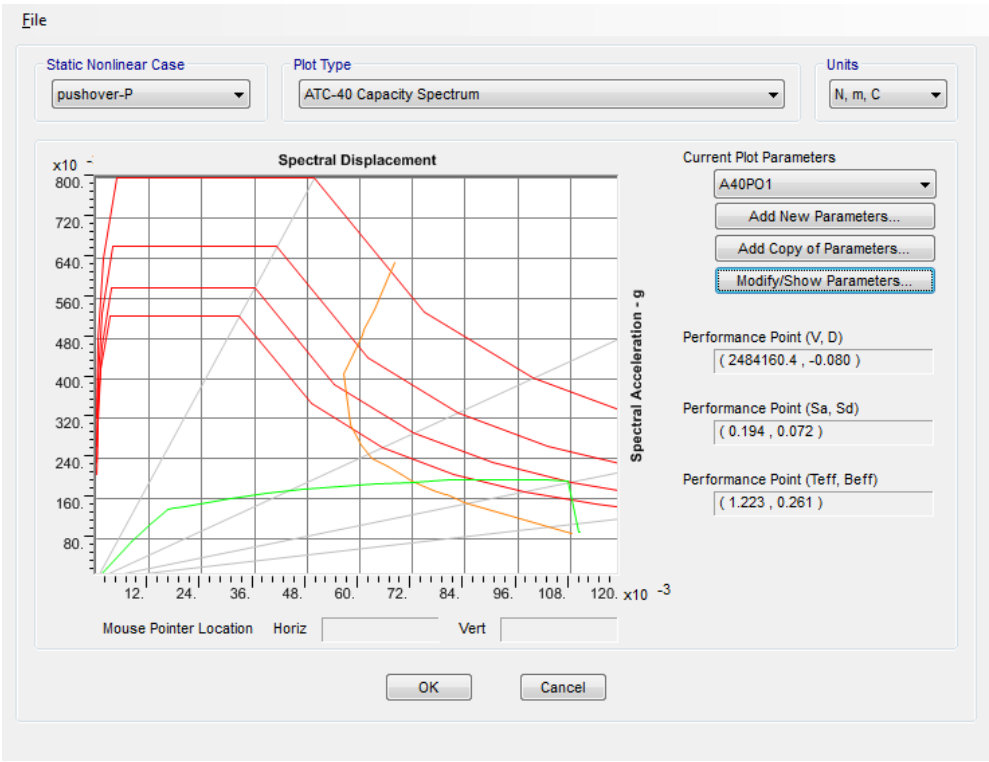

Figure C.4. (o) Performance point evaluation by capacity spectrum analysis of M1 group models.

Model M1-1500 – Soil Type C

Model M1-1500 – Soil Type D

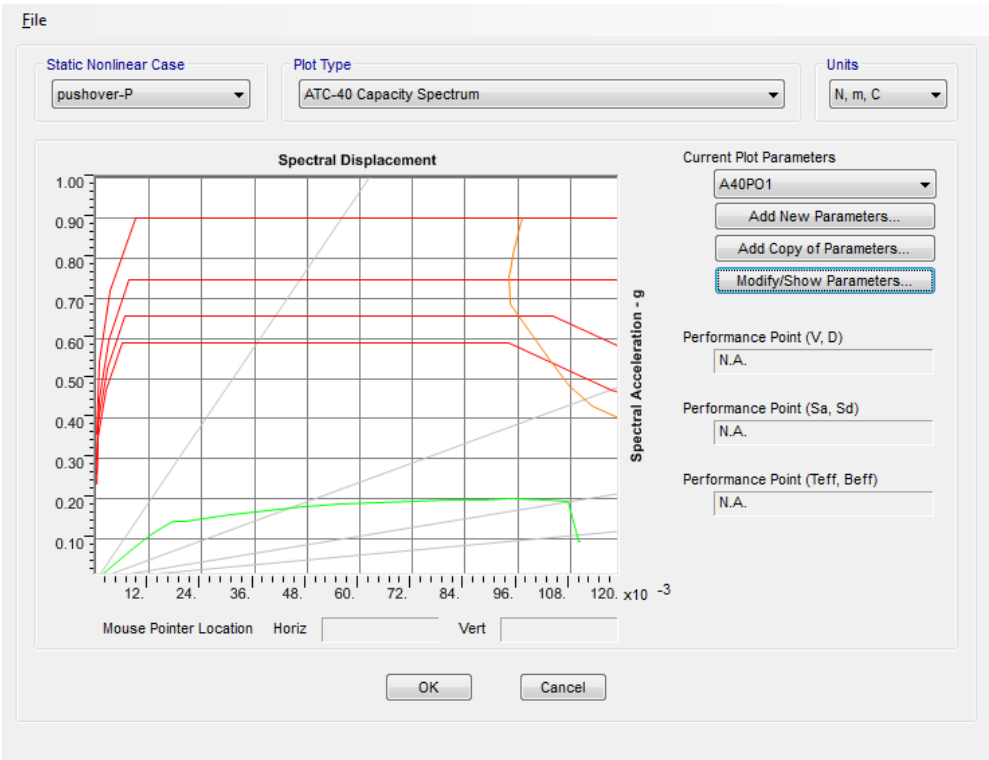

Figure C.4. (p) Performance point evaluation by capacity spectrum analysis of M1 group models.

Model M1-2000 – Soil Type A

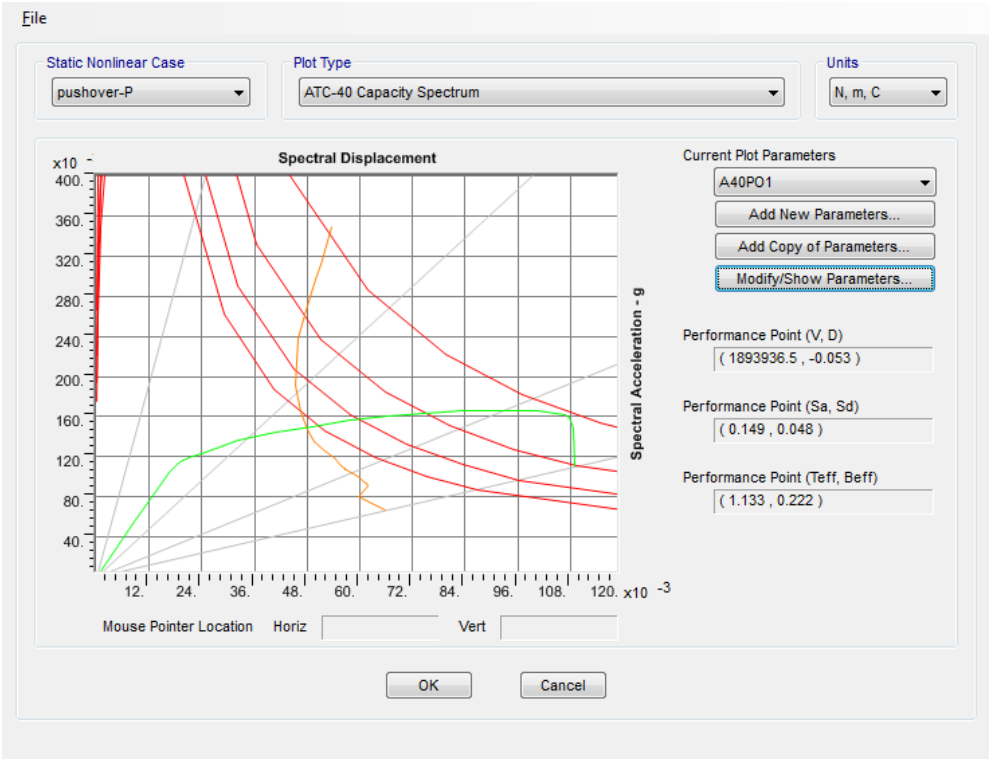

Model M1-2000 – Soil Type B

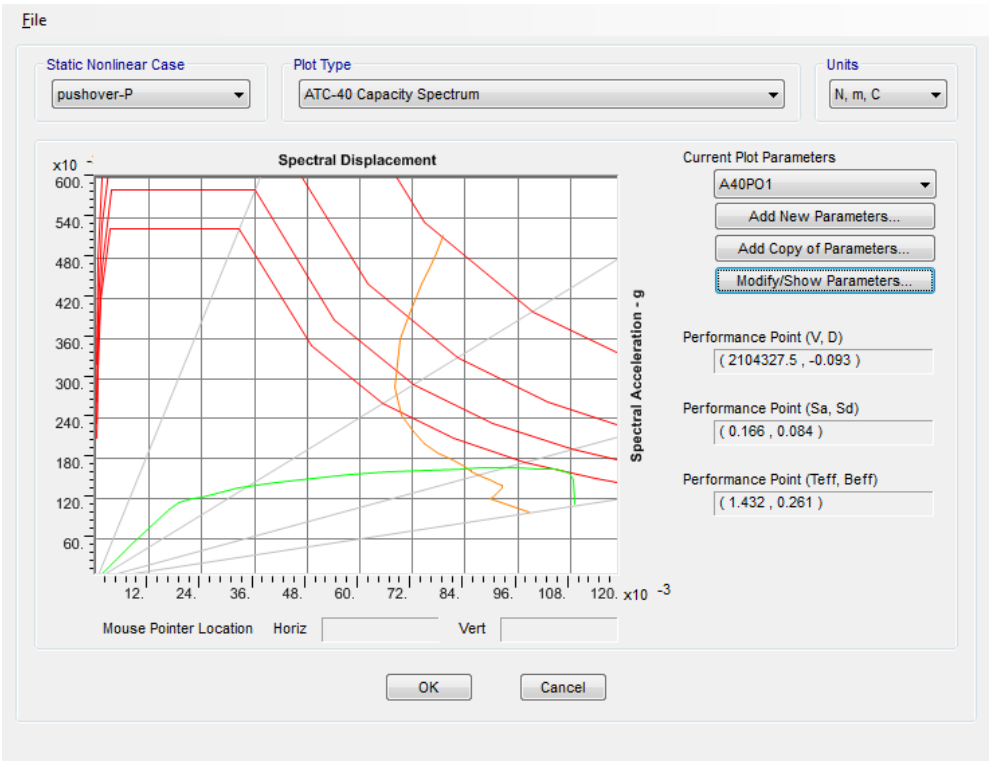

Figure C.4. (q) Performance point evaluation by capacity spectrum analysis of M1 group models.

Model M1-2000 – Soil Type C

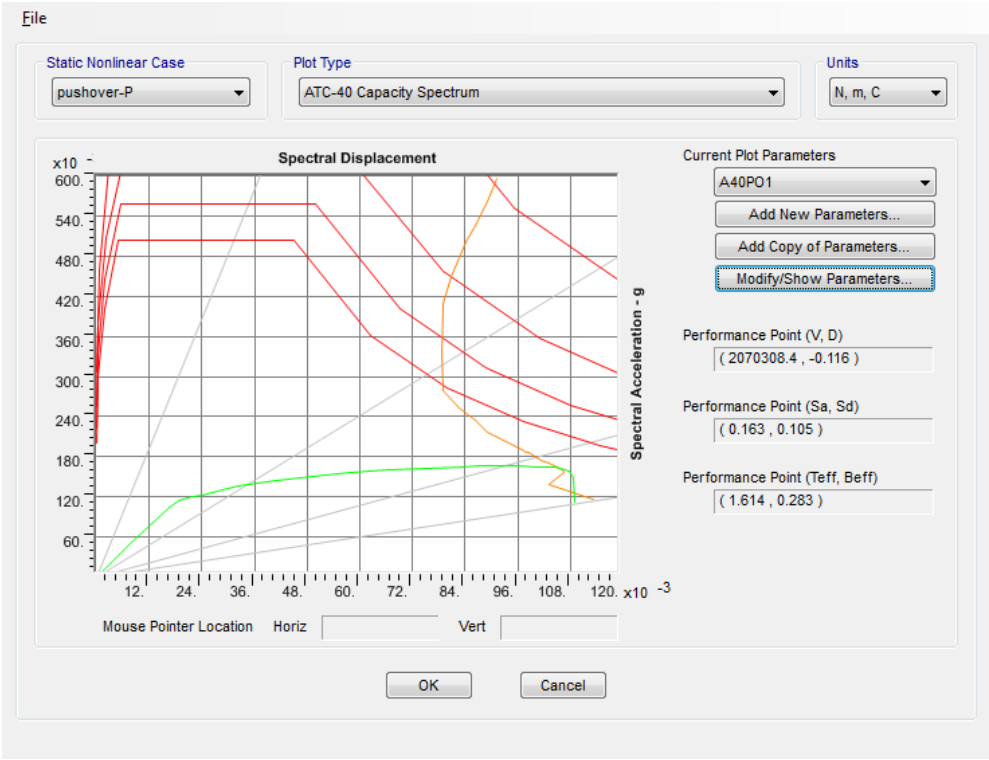

Model M1-2000 – Soil Type D

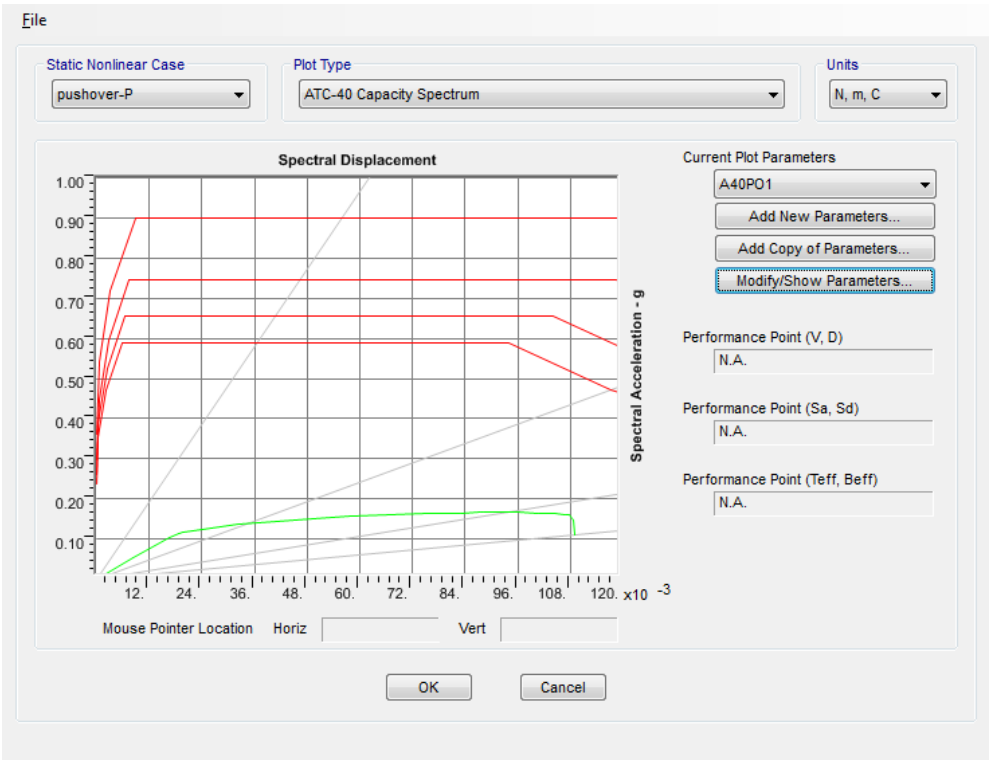

Figure C.4. (r) Performance point evaluation by capacity spectrum analysis of M1 group models.

C.4 Contours of top lateral displacement, maximum tension and compression stresses in RC shafts at peak base shear of pushover analysis

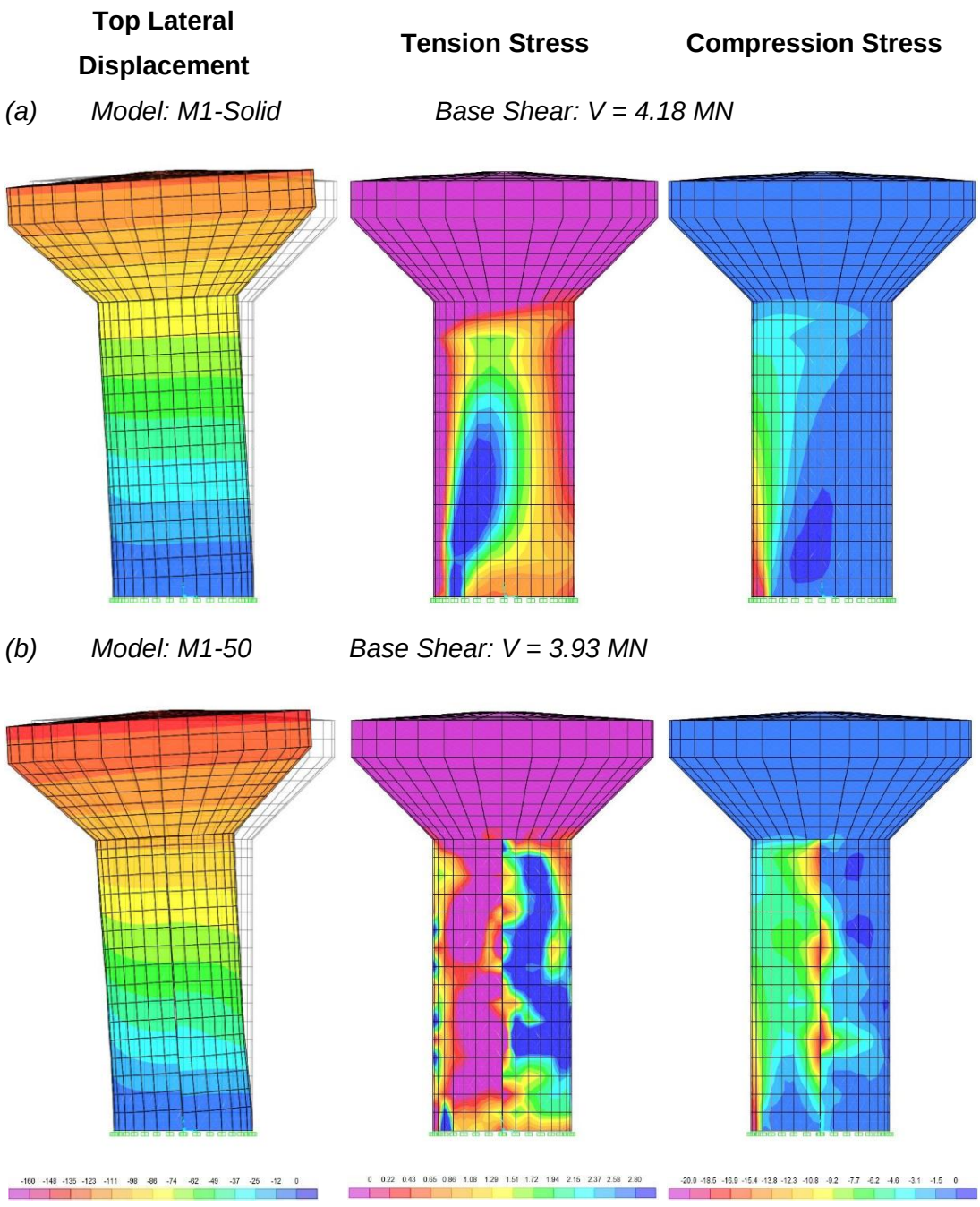

Figure C.5. (a) Contours of top lateral displacement, maximum tension and compression stresses in RC shafts at peak shear of pushover analysis

Top lateral Displacement	Tension Stress	Compression Stress
(c) Model: M1-100	*Base Shear: V = 3.83 MN*	
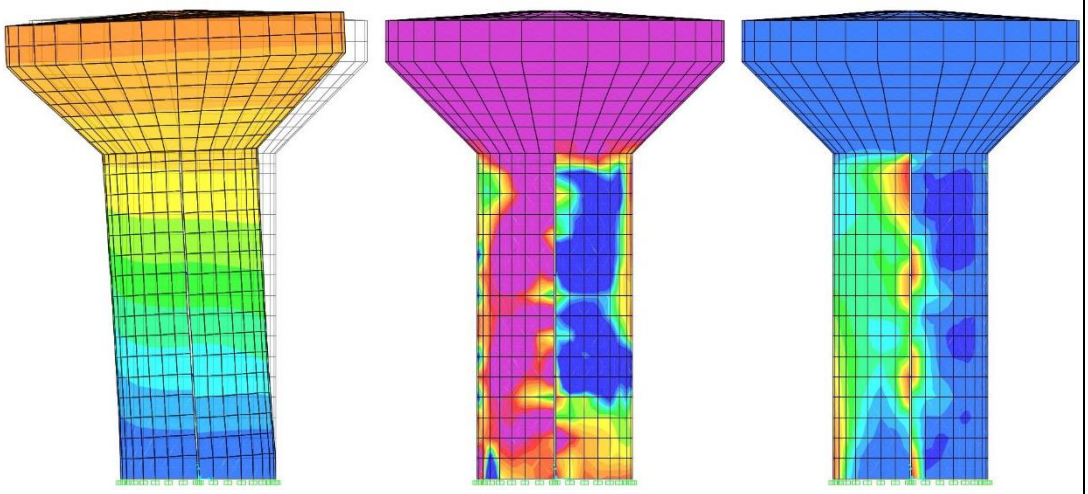		
(d) Model: M1-200	*Base Shear: V = 3.69 MN*	
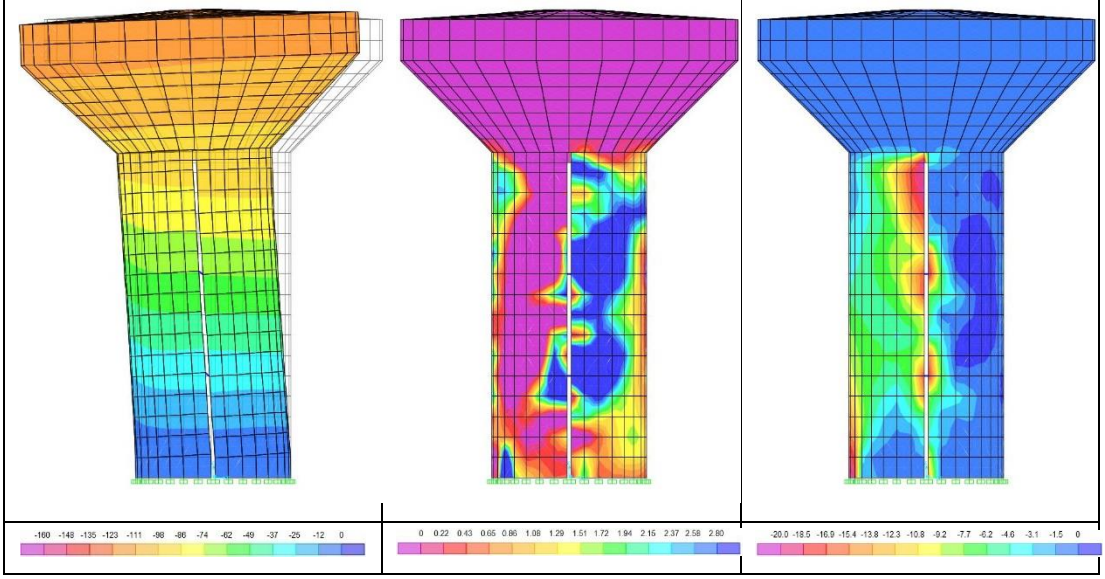		

Figure B.5. (b) Contours of top lateral displacement, maximum stress and minimum stress in RC shafts at peak shear of pushover analysis.

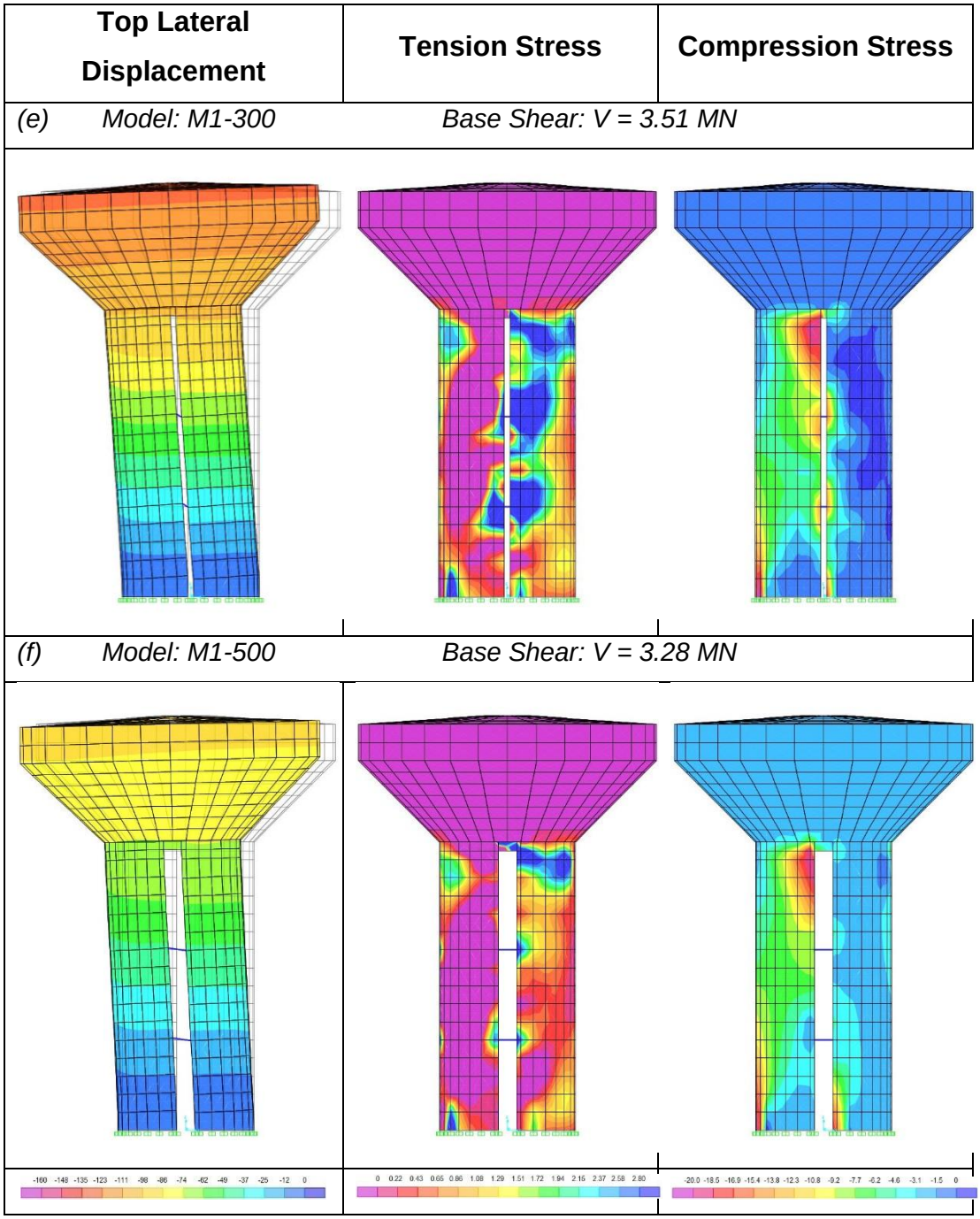

Figure B.5. (d) Contours of top lateral displacement, maximum stress and minimum stress in RC shafts at peak shear of pushover analysis.

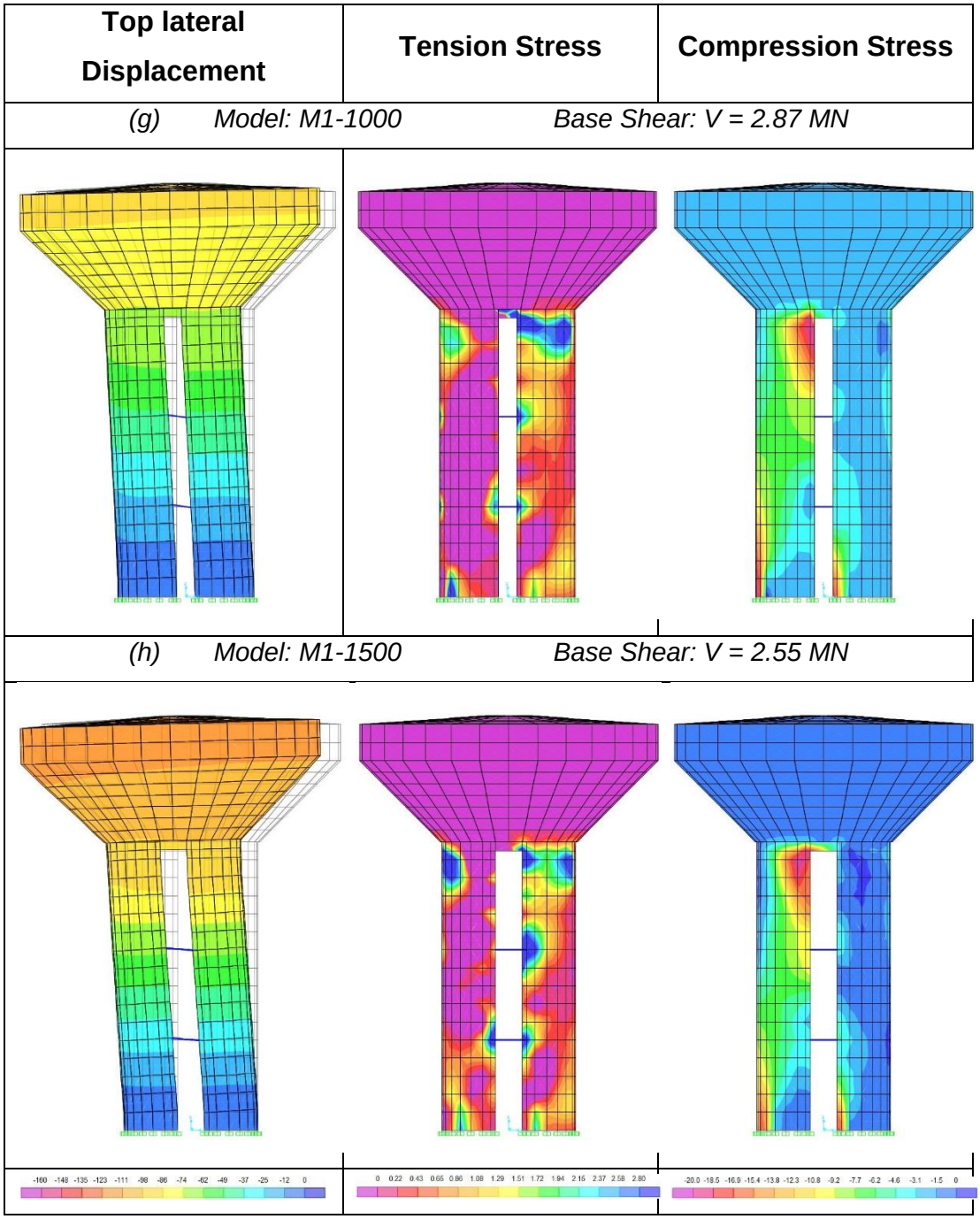

Figure B.5. (e) Contours of top lateral displacement, maximum stress and minimum stress in RC shafts at peak shear of pushover analysis

Top lateral Displacement	Tension Stress	Compression Stress
(i) Model: M1-2000	*Base Shear: V = 2.11 MN*	

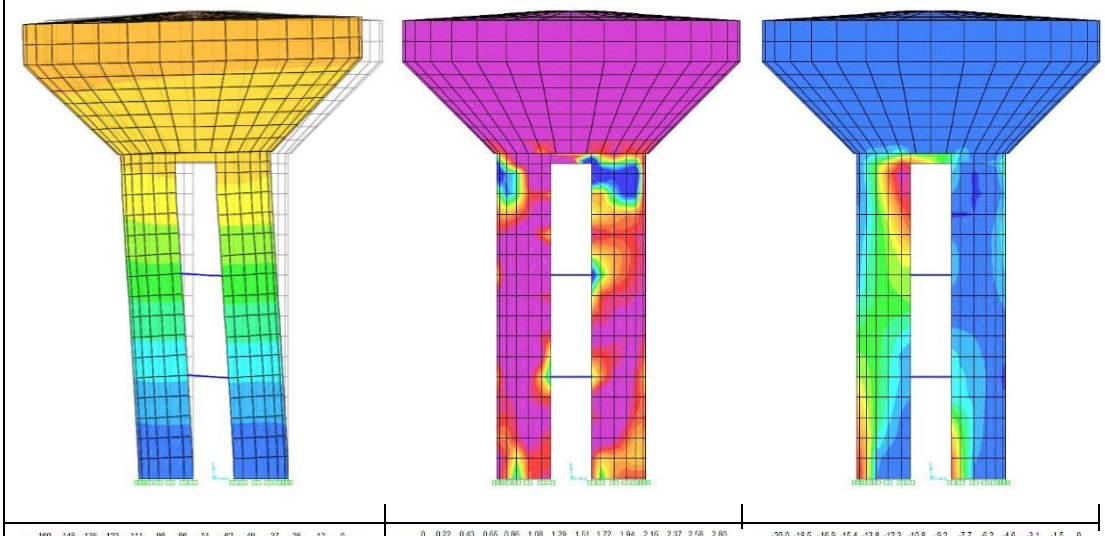

Figure B.5. (f) Contours of top lateral displacement, maximum stress and minimum stress in RC shafts at peak shear of pushover analysis.

Appendix D

Results of nonlinear dynamic analysis

D.1 1940 El-Centro ground motion, horizontal component (PGA=0.32g)

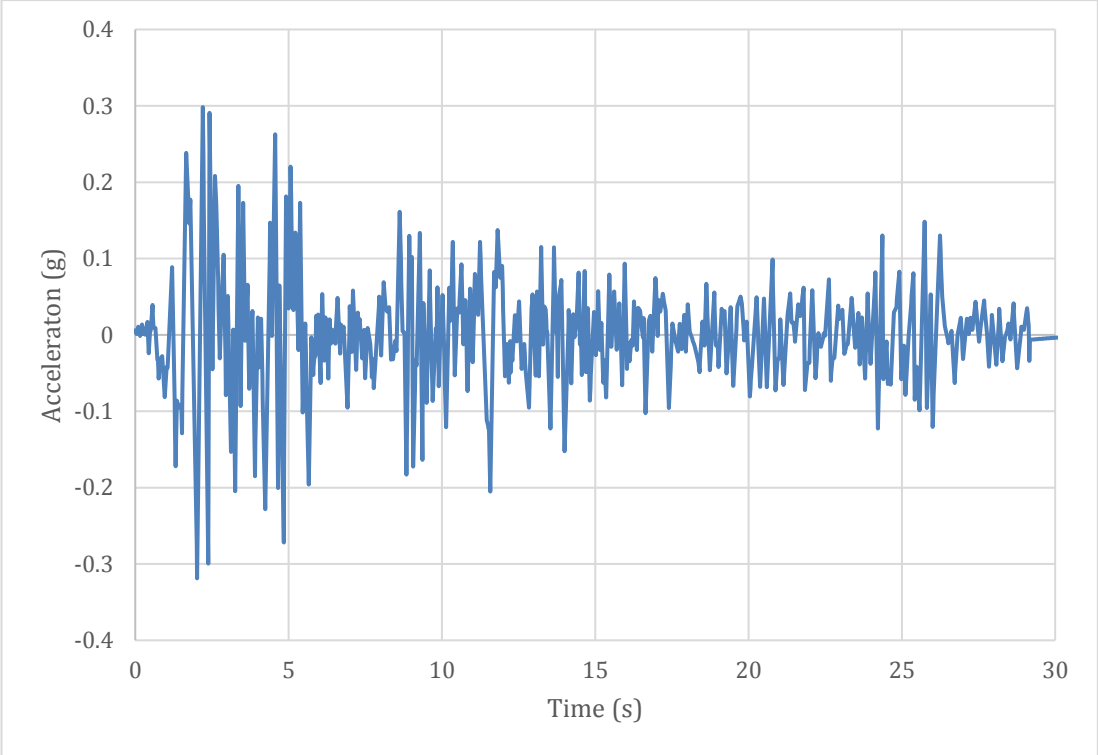

Figure D.1. 1940 El-Centro ground motion, horizontal component (PGA=0.32g)

Appendix D: Results of nonlinear dynamic analysis

Data for El Centro 1940 North South Component

1559 points at equal spacing of 0.02 sec

Points are listed 8 points across in a row with 5 decimal places

The units are (g)

Table D.1. Data for El Centro 1940 horizontal component

0.0063	0.00364	0.00099	0.00428	0.00758	0.01087	0.00682	0.00277
-0.00128	0.00368	0.00864	0.0136	0.00727	0.00094	0.0042	0.00221
0.00021	0.00444	0.00867	0.0129	0.01713	-0.00343	-0.024	-0.00992
0.00416	0.00528	0.01653	0.02779	0.03904	0.02449	0.00995	0.00961
0.00926	0.00892	-0.00486	-0.01864	-0.03242	-0.03365	-0.05723	-0.04534
-0.03346	-0.03201	-0.03056	-0.02911	-0.02766	-0.04116	-0.05466	-0.06816
-0.08166	-0.06846	-0.05527	-0.04208	-0.04259	-0.04311	-0.02428	-0.00545
0.01338	0.03221	0.05104	0.06987	0.0887	0.04524	0.00179	-0.04167
-0.08513	-0.12858	-0.17204	-0.12908	-0.08613	-0.08902	-0.09192	-0.09482
-0.09324	-0.09166	-0.09478	-0.09789	-0.12902	-0.07652	-0.02401	0.02849
0.08099	0.1335	0.186	0.2385	0.21993	0.20135	0.18277	0.1642
0.14562	0.16143	0.17725	0.13215	0.08705	0.04196	-0.00314	-0.04824
-0.09334	-0.13843	-0.18353	-0.22863	-0.27372	-0.31882	-0.25024	-0.18166
-0.11309	-0.04451	0.02407	0.09265	0.16123	0.22981	0.29839	0.23197
0.16554	0.09912	0.0327	-0.03372	-0.10014	-0.16656	-0.23299	-0.29941
-0.00421	0.29099	0.2238	0.15662	0.08943	0.02224	-0.04495	0.01834
0.08163	0.14491	0.2082	0.18973	0.17125	0.13759	0.10393	0.07027
0.03661	0.00295	-0.03071	-0.00561	0.01948	0.04458	0.06468	0.08478
0.10487	0.05895	0.01303	-0.03289	-0.07882	-0.03556	0.00771	0.05097
0.01013	-0.03071	-0.07156	-0.1124	-0.15324	-0.11314	-0.07304	-0.03294
0.00715	-0.0635	-0.13415	-0.2048	-0.12482	-0.04485	0.03513	0.1151
0.19508	0.12301	0.05094	-0.02113	-0.0932	-0.02663	0.03995	0.10653
0.17311	0.11283	0.05255	-0.00772	0.01064	0.029	0.04737	0.06573
0.02021	-0.0253	-0.07081	-0.04107	-0.01133	0.00288	0.01709	0.03131
-0.02278	-0.07686	-0.13095	-0.18504	-0.14347	-0.1019	-0.06034	-0.01877
0.0228	-0.00996	-0.04272	-0.02147	-0.00021	0.02104	-0.01459	-0.05022
-0.08585	-0.12148	-0.15711	-0.19274	-0.22837	-0.18145	-0.13453	-0.08761
-0.04069	0.00623	0.05316	0.10008	0.147	0.09754	0.04808	-0.00138
0.05141	0.1042	0.15699	0.20979	0.26258	0.16996	0.07734	-0.01527
-0.10789	-0.20051	-0.06786	0.06479	0.01671	-0.03137	-0.07945	-0.12753
-0.17561	-0.22369	-0.27177	-0.15851	-0.04525	0.06802	0.18128	0.14464
0.108	0.07137	0.03473	0.09666	0.1586	0.22053	0.18296	0.14538
0.1078	0.07023	0.03265	0.06649	0.10033	0.13417	0.10337	0.07257
0.04177	0.01097	-0.01983	0.04438	0.1086	0.17281	0.10416	0.03551
-0.03315	-0.1018	-0.07262	-0.04344	-0.01426	0.01492	-0.02025	-0.05543

-0.0906	-0.12578	-0.16095	-0.19613	-0.14784	-0.09955	-0.05127	-0.00298
-0.01952	-0.03605	-0.05259	-0.04182	-0.03106	-0.02903	-0.02699	0.02515
0.0177	0.02213	0.02656	0.00419	-0.01819	-0.04057	-0.06294	-0.02417
0.0146	0.05337	0.02428	-0.0048	-0.03389	-0.00557	0.02274	0.00679
-0.00915	-0.02509	-0.04103	-0.05698	-0.01826	0.02046	0.00454	-0.01138
-0.00215	0.00708	0.00496	0.00285	0.00074	-0.00534	-0.01141	0.00361
0.01863	0.03365	0.04867	0.0304	0.01213	-0.00614	-0.02441	0.01375
0.01099	0.00823	0.00547	0.00812	0.01077	-0.00692	-0.02461	-0.0423
-0.05999	-0.07768	-0.09538	-0.06209	-0.0288	0.00448	0.03777	0.01773
-0.00231	-0.02235	0.01791	0.05816	0.03738	0.0166	-0.00418	-0.02496
-0.04574	-0.02071	0.00432	0.02935	0.01526	0.01806	0.02086	0.00793
-0.00501	-0.01795	-0.03089	-0.01841	-0.00593	0.00655	-0.02519	-0.05693
-0.04045	-0.02398	-0.0075	0.00897	0.00384	-0.00129	-0.00642	-0.01156
-0.02619	-0.04082	-0.05545	-0.04366	-0.03188	-0.06964	-0.05634	-0.04303
-0.02972	-0.01642	-0.00311	0.0102	0.0235	0.03681	0.05011	0.02436
-0.00139	-0.02714	-0.00309	0.02096	0.04501	0.06906	0.05773	0.0464
0.03507	0.03357	0.03207	0.03057	0.0325	0.03444	0.03637	0.01348
-0.00942	-0.03231	-0.02997	-0.03095	-0.03192	-0.02588	-0.01984	-0.01379
-0.00775	-0.01449	-0.02123	0.01523	0.0517	0.08816	0.12463	0.16109
0.12987	0.09864	0.06741	0.03618	0.00495	0.0042	0.00345	0.00269
-0.05922	-0.12112	-0.18303	-0.12043	-0.05782	0.00479	0.0674	0.13001
0.08373	0.03745	0.06979	0.10213	-0.03517	-0.17247	-0.13763	-0.10278
-0.06794	-0.0331	-0.03647	-0.03984	-0.00517	0.0295	0.06417	0.09883
0.1335	0.05924	-0.01503	-0.08929	-0.16355	-0.06096	0.04164	0.01551
-0.01061	-0.03674	-0.06287	-0.08899	-0.0543	-0.01961	0.01508	0.04977
0.08446	0.05023	0.016	-0.01823	-0.05246	-0.08669	-0.06769	-0.0487
-0.0297	-0.01071	0.00829	-0.00314	0.02966	0.06246	-0.00234	-0.06714
-0.04051	-0.01388	0.01274	0.00805	0.03024	0.05243	0.02351	-0.00541
-0.03432	-0.06324	-0.09215	-0.12107	-0.0845	-0.04794	-0.01137	0.0252
0.06177	0.04028	0.0188	0.04456	0.07032	0.09608	0.12184	0.0635
0.00517	-0.05317	-0.03124	-0.0093	0.01263	0.03457	0.03283	0.03109
0.02935	0.04511	0.06087	0.07663	0.09239	0.05742	0.02245	-0.01252
0.0068	0.02611	0.04543	0.01571	-0.01402	-0.04374	-0.07347	-0.0399
-0.00633	0.02724	0.0608	0.03669	0.01258	-0.01153	-0.03564	-0.00677
0.0221	0.05098	0.07985	0.06915	0.05845	0.04775	0.03706	0.02636
0.05822	0.09009	0.12196	0.10069	0.07943	0.05816	0.03689	0.01563
-0.00564	-0.0269	-0.04817	-0.06944	-0.0907	-0.11197	-0.11521	-0.11846
-0.1217	-0.12494	-0.165	-0.20505	-0.15713	-0.10921	-0.06129	-0.01337
0.03455	0.08247	0.07576	0.06906	0.06236	0.08735	0.11235	0.13734
0.12175	0.10616	0.09057	0.07498	0.08011	0.08524	0.09037	0.06208
0.03378	0.00549	-0.02281	-0.05444	-0.0403	-0.02615	-0.01201	-0.02028
-0.02855	-0.06243	-0.03524	-0.00805	-0.04948	-0.03643	-0.02337	-0.03368
-0.01879	-0.00389	0.011	0.02589	0.01446	0.00303	-0.0084	0.00463
0.01766	0.03069	0.04372	0.02165	-0.00042	-0.02249	-0.04456	-0.03638

-0.02819	-0.02001	-0.01182	-0.02445	-0.03707	-0.04969	-0.05882	-0.06795
-0.07707	-0.0862	-0.09533	-0.06276	-0.03018	0.00239	0.03496	0.04399
0.05301	0.03176	0.01051	-0.01073	-0.03198	-0.05323	0.00186	0.05696
0.01985	-0.01726	-0.05438	-0.01204	0.03031	0.07265	0.11499	0.07237
0.02975	-0.01288	0.01212	0.03711	0.03517	0.03323	0.01853	0.00383
0.00342	-0.02181	-0.04704	-0.07227	-0.0975	-0.12273	-0.08317	-0.04362
-0.00407	0.03549	0.07504	0.1146	0.07769	0.04078	0.00387	0.00284
0.00182	-0.05513	0.04732	0.05223	0.05715	0.06206	0.06698	0.07189
0.02705	-0.01779	-0.06263	-0.10747	-0.15232	-0.12591	-0.0995	-0.07309
-0.04668	-0.02027	0.00614	0.03255	0.00859	-0.01537	-0.03932	-0.06328
-0.03322	-0.00315	0.02691	0.01196	-0.003	0.00335	0.0097	0.01605
0.02239	0.04215	0.06191	0.08167	0.03477	-0.01212	-0.01309	-0.01407
-0.05274	-0.02544	0.00186	0.02916	0.05646	0.08376	0.01754	-0.04869
-0.02074	0.00722	0.03517	-0.00528	-0.04572	-0.08617	-0.0696	-0.05303
-0.03646	-0.01989	-0.00332	0.01325	0.02982	0.01101	-0.00781	-0.02662
-0.00563	0.01536	0.03635	0.05734	0.03159	0.00584	-0.01992	-0.00201
0.01589	-0.01024	-0.03636	-0.06249	-0.0478	-0.03311	-0.04941	-0.0657
-0.082	-0.0498	-0.0176	0.0146	0.0468	0.079	0.0475	0.016
-0.0155	-0.00102	0.01347	0.02795	0.04244	0.05692	0.03781	0.0187
-0.00041	-0.01952	-0.00427	0.01098	0.02623	0.04148	0.01821	-0.00506
-0.00874	-0.03726	-0.06579	-0.026	0.0138	0.05359	0.09338	0.05883
0.02429	-0.01026	-0.0448	-0.01083	-0.01869	-0.02655	-0.03441	-0.02503
-0.01564	-0.00626	-0.01009	-0.01392	0.0149	0.04372	0.03463	0.02098
0.00733	-0.00632	-0.01997	0.00767	0.03532	0.03409	0.03287	0.03164
0.02403	0.01642	0.00982	0.00322	-0.00339	0.02202	-0.01941	-0.06085
-0.10228	-0.07847	-0.05466	-0.03084	-0.00703	0.01678	0.01946	0.02214
0.02483	0.01809	-0.00202	-0.02213	-0.00278	0.01656	0.0359	0.05525
0.07459	0.06203	0.04948	0.03692	-0.00145	0.04599	0.04079	0.03558
0.03037	0.03626	0.04215	0.04803	0.05392	0.04947	0.04502	0.04056
0.03611	0.03166	0.00614	-0.01937	-0.04489	-0.0704	-0.09592	-0.07745
-0.05899	-0.04052	-0.02206	-0.00359	0.01487	0.01005	0.00523	0.00041
-0.00441	-0.00923	-0.01189	-0.01523	-0.01856	-0.0219	-0.00983	0.00224
0.01431	0.00335	-0.0076	-0.01856	-0.00737	0.00383	0.01502	0.02622
0.01016	-0.0059	-0.02196	-0.00121	0.01953	0.04027	0.02826	0.01625
0.00424	0.00196	-0.00031	-0.00258	-0.00486	-0.00713	-0.00941	-0.01168
-0.01396	-0.0175	-0.02104	-0.02458	-0.02813	-0.03167	-0.03521	-0.04205
-0.04889	-0.03559	-0.02229	-0.00899	0.00431	0.01762	0.00714	-0.00334
-0.01383	0.01314	0.04011	0.06708	0.0482	0.02932	0.01043	-0.00845
-0.02733	-0.04621	-0.03155	-0.01688	-0.00222	0.01244	0.02683	0.04121
0.05559	0.03253	0.00946	-0.0136	-0.01432	-0.01504	-0.01576	-0.04209
-0.02685	-0.01161	0.00363	0.01887	0.03411	0.03115	0.02819	0.02917
0.03015	0.03113	0.00388	-0.02337	-0.05062	-0.0382	-0.02579	-0.01337
-0.00095	0.01146	0.02388	0.03629	0.01047	-0.01535	-0.04117	-0.06699
-0.05207	-0.03715	-0.02222	-0.0073	0.00762	0.02254	0.03747	0.04001

0.04256	0.04507	0.04759	0.0501	0.04545	0.0408	0.02876	0.01671
0.00467	-0.00738	-0.00116	0.00506	0.01128	0.0175	-0.00211	-0.02173
-0.04135	-0.06096	-0.08058	-0.06995	-0.05931	-0.04868	-0.03805	-0.02557
-0.0131	-0.00063	0.01185	0.02432	0.0368	0.04927	0.02974	0.01021
-0.00932	-0.02884	-0.04837	-0.0679	-0.04862	-0.02934	-0.01006	0.00922
0.02851	0.04779	0.02456	0.00133	-0.0219	-0.04513	-0.06836	-0.04978
-0.0312	-0.01262	0.00596	0.02453	0.04311	0.06169	0.08027	0.09885
0.06452	0.03019	-0.00414	-0.03848	-0.07281	-0.05999	-0.04717	-0.03435
-0.03231	-0.03028	-0.02824	-0.00396	0.02032	0.00313	-0.01406	-0.03124
-0.04843	-0.06562	-0.05132	-0.03702	-0.02272	-0.00843	0.00587	0.02017
0.02698	0.03379	0.04061	0.04742	0.05423	0.03535	0.01647	0.01622
0.01598	0.01574	0.00747	-0.0008	-0.00907	0.00072	0.01051	0.0203
0.03009	0.03989	0.03478	0.02967	0.02457	0.03075	0.03694	0.04313
0.04931	0.0555	0.06168	-0.00526	-0.0722	-0.06336	-0.05451	-0.04566
-0.03681	-0.03678	-0.03675	-0.03672	-0.01765	0.00143	0.02051	0.03958
0.05866	0.03556	0.01245	-0.01066	-0.03376	-0.05687	-0.04502	-0.03317
-0.02131	-0.00946	0.00239	-0.00208	-0.00654	-0.01101	-0.01548	-0.012
-0.00851	-0.00503	-0.00154	0.00195	0.00051	-0.00092	0.01135	0.02363
0.0359	0.04818	0.06045	0.07273	0.02847	-0.01579	-0.06004	-0.05069
-0.04134	-0.03199	-0.03135	-0.03071	-0.03007	-0.01863	-0.00719	0.00425
0.0157	0.02714	0.03858	0.02975	0.02092	0.02334	0.02576	0.02819
0.03061	0.03304	0.01371	-0.00561	-0.02494	-0.02208	-0.01923	-0.01638
-0.01353	-0.01261	-0.0117	-0.00169	0.00833	0.01834	0.02835	0.03836
0.04838	0.03749	0.0266	0.01571	0.00482	-0.00607	-0.01696	-0.0078
0.00136	0.01052	0.01968	0.02884	-0.00504	-0.03893	-0.02342	-0.00791
0.00759	0.0231	0.00707	-0.00895	-0.02498	-0.041	-0.05703	-0.0292
-0.00137	0.02645	0.05428	0.03587	0.01746	-0.00096	-0.01937	-0.03778
-0.02281	-0.00784	0.00713	0.0221	0.03707	0.05204	0.06701	0.08198
0.03085	-0.02027	-0.0714	-0.12253	-0.08644	-0.05035	-0.01426	0.02183
0.05792	0.094	0.13009	0.03611	-0.05787	-0.04802	-0.03817	-0.02832
-0.01846	-0.00861	-0.03652	-0.06444	-0.06169	-0.05894	-0.05618	-0.06073
-0.06528	-0.04628	-0.02728	-0.00829	0.01071	0.0297	0.03138	0.03306
0.03474	0.03642	0.04574	0.05506	0.06439	0.07371	0.08303	0.03605
-0.01092	-0.0579	-0.04696	-0.03602	-0.02508	-0.01414	-0.03561	-0.05708
-0.07855	-0.06304	-0.04753	-0.03203	-0.01652	-0.00102	0.00922	0.01946
0.0297	0.03993	0.05017	0.06041	0.07065	0.08089	-0.00192	-0.08473
-0.07032	-0.0559	-0.04148	-0.05296	-0.06443	-0.0759	-0.08738	-0.09885
-0.06798	-0.0371	-0.00623	0.02465	0.05553	0.0864	0.11728	0.14815
0.08715	0.02615	-0.03485	-0.09584	-0.071	-0.04616	-0.02132	0.00353
0.02837	0.05321	-0.00469	-0.06258	-0.12048	-0.0996	-0.07872	-0.05784
-0.03696	-0.01608	0.0048	0.02568	0.04656	0.06744	0.08832	0.1092
0.13008	0.10995	0.08982	0.06969	0.04955	0.04006	0.03056	0.02107
0.01158	0.0078	0.00402	0.00024	-0.00354	-0.00732	-0.0111	-0.0078
-0.0045	-0.0012	0.0021	0.0054	-0.00831	-0.02203	-0.03575	-0.04947

-0.06319	-0.05046	-0.03773	-0.025	-0.01227	0.00046	0.00482	0.00919
0.01355	0.01791	0.02228	0.00883	-0.00462	-0.01807	-0.03152	-0.02276
-0.01401	-0.00526	0.0035	0.01225	0.02101	0.01437	0.00773	0.0011
0.00823	0.01537	0.02251	0.01713	0.01175	0.00637	0.01376	0.02114
0.02852	0.03591	0.04329	0.03458	0.02587	0.01715	0.00844	-0.00027
-0.00898	-0.00126	0.00645	0.01417	0.02039	0.02661	0.03283	0.03905
0.04527	0.03639	0.0275	0.01862	0.00974	0.00086	-0.01333	-0.02752
-0.04171	-0.02812	-0.01453	-0.00094	0.01264	0.02623	0.0169	0.00756
-0.00177	-0.01111	-0.02044	-0.02977	-0.03911	-0.02442	-0.00973	0.00496
0.01965	0.03434	0.02054	0.00674	-0.00706	-0.02086	-0.03466	-0.02663
-0.0186	-0.01057	-0.00254	-0.00063	0.00128	0.00319	0.0051	0.00999
0.01488	0.00791	0.00093	-0.00605	0.00342	0.01288	0.02235	0.03181
0.04128	0.02707	0.01287	-0.00134	-0.01554	-0.02975	-0.04395	-0.03612
-0.02828	-0.02044	-0.0126	-0.00476	0.00307	0.01091	0.00984	0.00876
0.00768	0.00661	0.01234	0.01807	0.0238	0.02953	0.03526	0.02784
0.02042	0.013	-0.03415	-0.00628	-0.00621	-0.00615	-0.00609	-0.00602
-0.00596	-0.0059	-0.00583	-0.00577	-0.00571	-0.00564	-0.00558	-0.00552
-0.00545	-0.00539	-0.00532	-0.00526	-0.0052	-0.00513	-0.00507	-0.00501
-0.00494	-0.00488	-0.00482	-0.00475	-0.00469	-0.00463	-0.00456	-0.0045
-0.00444	-0.00437	-0.00431	-0.00425	-0.00418	-0.00412	-0.00406	-0.00399
-0.00393	-0.00387	-0.0038	-0.00374	-0.00368	-0.00361	-0.00355	-0.00349
-0.00342	-0.00336	-0.0033	-0.00323	-0.00317	-0.00311	-0.00304	-0.00298
-0.00292	-0.00285	-0.00279	-0.00273	-0.00266	-0.0026	-0.00254	-0.00247
-0.00241	-0.00235	-0.00228	-0.00222	-0.00216	-0.00209	-0.00203	-0.00197
-0.0019	-0.00184	-0.00178	-0.00171	-0.00165	-0.00158	-0.00152	-0.00146
-0.00139	-0.00133	-0.00127	-0.0012	-0.00114	-0.00108	-0.00101	-0.00095
-0.00089	-0.00082	-0.00076	-0.0007	-0.00063	-0.00057	-0.00051	-0.00044
-0.00038	-0.00032	-0.00025	-0.00019	-0.00013	-0.00006	0	

D.2 Peak time history response values considering to M1 group models

Table D.2. Peak time history response values for full M1 group

FE Model ID	Base Shear (MN)		Base Moment (MNm)		Tower Drift (mm)	
M1	4.64		93.08		44.74	
M1-50	4.33	**-6.76%**	83.06	**-10.76%**	58.46	**+30.67%**
M1-100	4.10	**-11.59%**	79.16	**-14.95%**	62.47	**+39.63%**
M1-200	3.95	**-14.95%**	76.79	**-17.50%**	65.17	**+45.66%**
M1-300	3.76	**-19.11%**	73.61	**-20.92%**	66.14	**+47.83%**
M1-500	3.53	**-23.89%**	69.96	**-24.84%**	67.66	**+51.23%**
M1-1000	3.10	**-33.33%**	62.60	**-32.75%**	70.34	**+57.22%**
M1-1500	2.74	**-40.93%**	56.09	**-39.74%**	71.74	**+60.35%**
M1-2000	2.26	**-51.36%**	46.29	**-50.27%**	78.99	**+76.55%**

D.3 Hysteresis loops of elevated water tank models M1 group

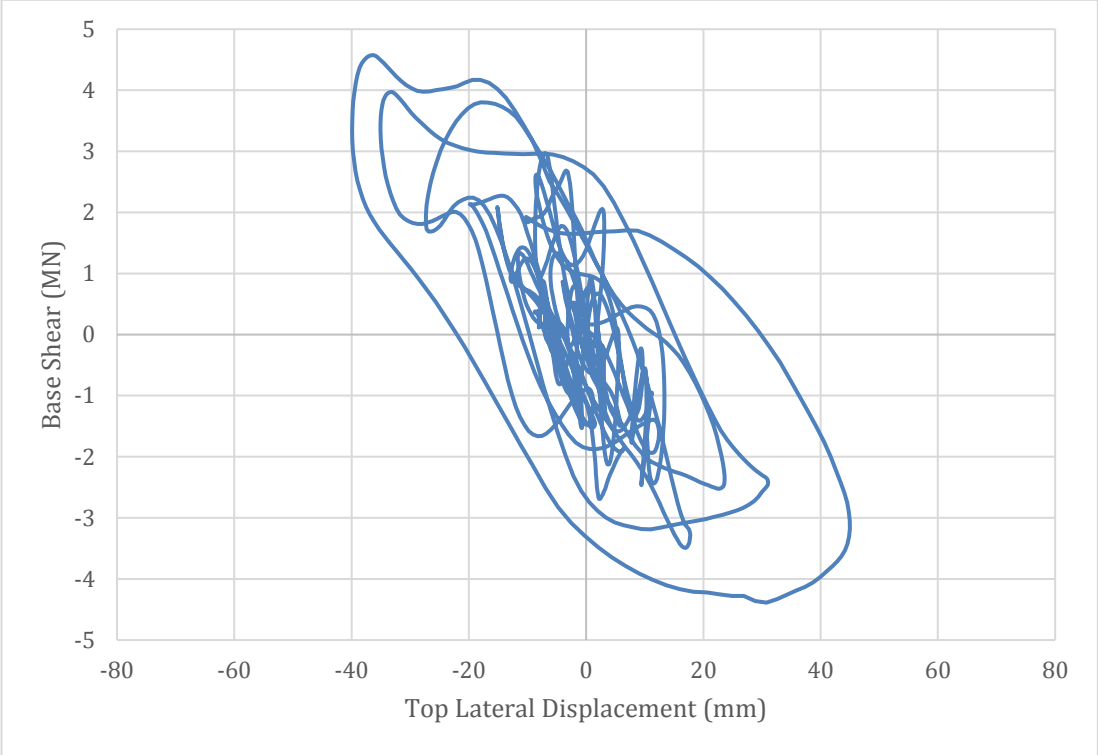

Figure D.2. Hysteresis behaviour of elevated water tank model M1-Solid

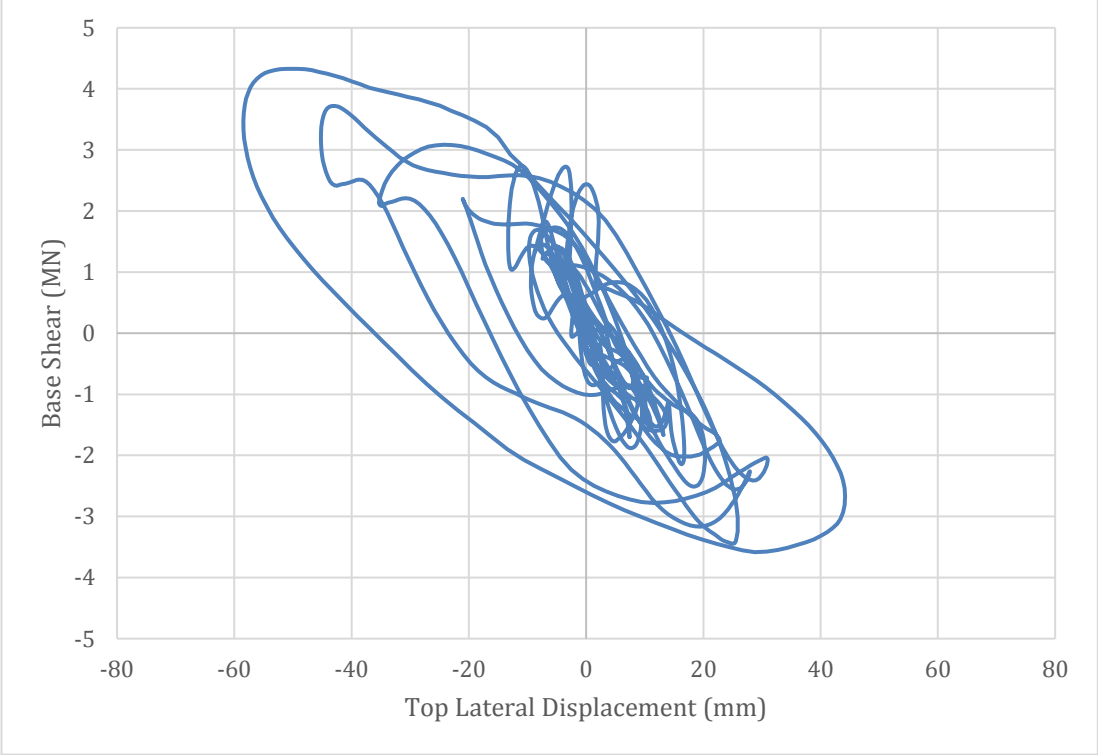

Figure D.3. Hysteresis behaviour of elevated water tank model M1-50

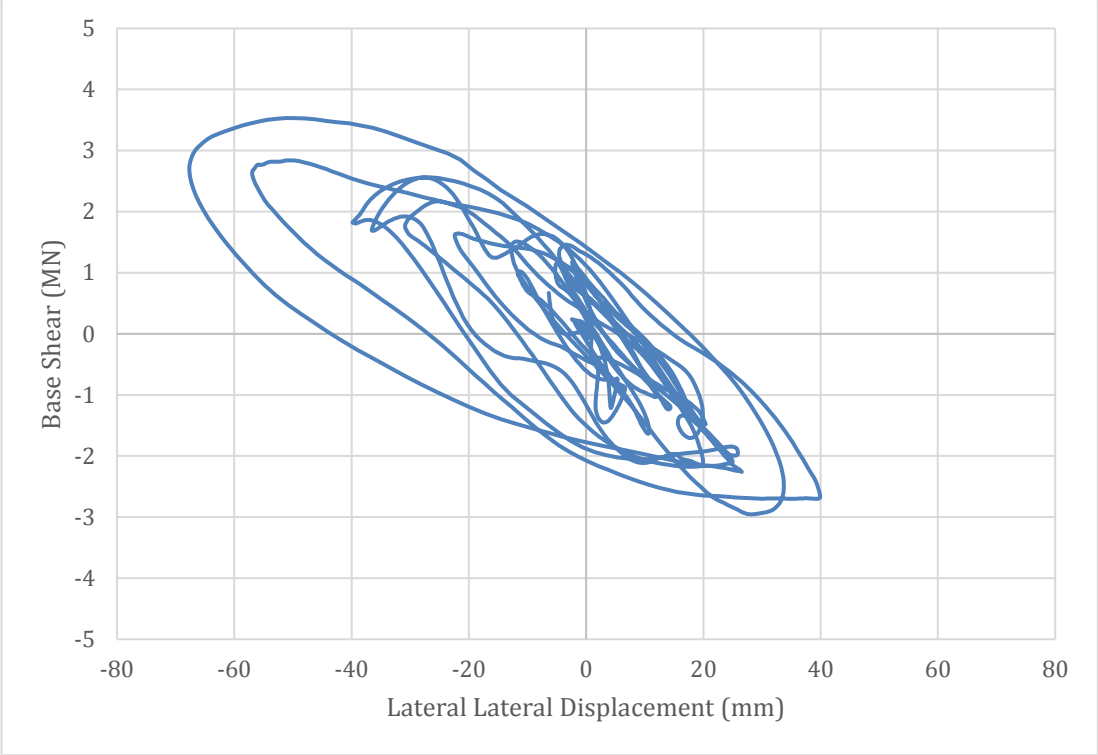

Figure D.4. Hysteresis behaviour of elevated water tank model M1-500

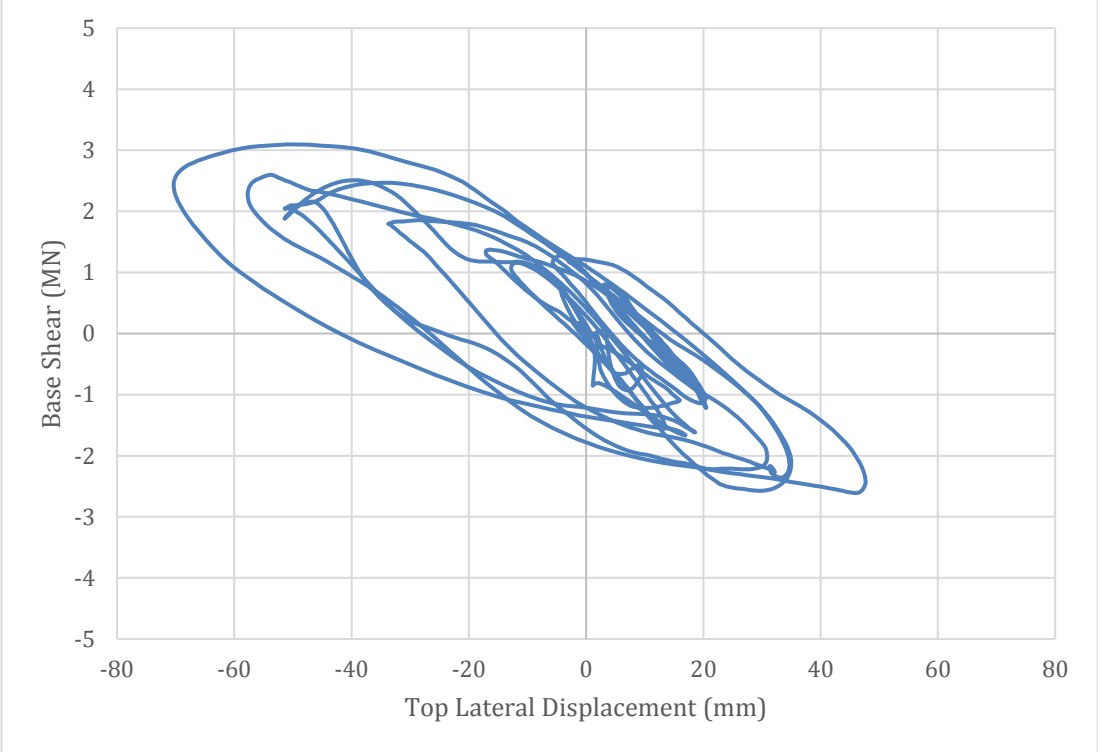

Figure D.5. Hysteresis behaviour of elevated water tank model M1-1000